

University of Nottingham
UK | CHINA | MALAYSIA

Polymeric Simvastatin-loaded Microsphere Delivery System for Bone Tissue Engineering

Nur Aliana Hidayah Mohamed

MMedSc in Pharmacology

Thesis submitted to the University of Nottingham in fulfilment of the

requirements for the Degree of Doctor of Philosophy

August 2019

TABLE OF CONTENTS

TABLE OF CONTENTS ..... **I**
LIST OF TABLES ..... **VIII**
LIST OF FIGURES ..... **X**
LIST OF ABBREVIATIONS ..... **XVI**
ABSTRACT ..... **XVIII**
DEDICATION ..... **XX**
ACKNOWLEDGEMENT ..... **XXI**
CONFERENCES ..... **XXII**
AWARDS ..... ERROR! BOOKMARK NOT DEFINED.

CHAPTER 1: INTRODUCTION TO BONE TISSUE ENGINEERING . 25
1.1 TISSUE ENGINEERING 25
1.2 PHYSIOLOGY OF BONE TISSUE 27
1.3 BONE ANATOMY 27
1.4 OSTEOGENESIS: THE DEVELOPMENT OF BONES 29
1.4.1 INTRAMEMBRANOUS OSSIFICATION 29
1.4.2 ENDOCHONDRAL OSSIFICATION 30
1.5 BONE REMODELING 31
1.5.1 OSTEOBLASTS AND BONE FORMATION 32
1.5.2 OSTEOCLASTOGENESIS 33
1.6 BIOMATERIALS USED FOR BONE TISSUE ENGINEERING APPLICATIONS ... 35
1.7 THE USE OF GROWTH FACTOR IN REGENERATIVE MEDICINE 35
1.8 THE USE OF STATIN IN REGENERATIVE MEDICINE 37
1.9 POLYMERS IN REGENERATIVE MEDICINE 41
1.9.1 NATURAL POLYMERS 42
1.9.2 SYNTHETIC POLYMERS 44
1.9.2.1 POLY LACTIC ACID (PLA) 48
1.9.2.2 POLY LACTIC-CO-GLYCOLIC-ACID (PLGA) 48
1.10 SOLID DISPERSION CONCEPT 48
1.10.1 PLGA MICROPARTICLES FORMULATION METHODS 48

1.10.2 Double Emulsion Solvent Evaporation Technique 49
1.11 Porosity 51
1.12 The Fundamental of Injectable SIM PLGA Microparticles as Bone Scaffold 53
1.3 Aim of The Studies 54
1.13.1 Specific Objectives 54

CHAPTER 2: FORMULATION OF NON-POROUS AND POROUS SIM PLGA MICROPARTICLES FOR BONE TISSUE ENGINEERING: OPTIMISATION OF PROTOCOL 56
2.1 Introduction 56
2.2 Materials and Methods 58
2.2.1 Materials 58
2.2.2 Methods 58
2.2.2.1 Preparation of Poly(vinyl alcohol) (PVA) 58
2.2.2.2 Preparation of Phosphate Buffer Saline (PBS) 58
2.2.2.3 Preparation of SIM stock solution 58
2.2.2.4 Formulation of Microparticles 59
2.2.2.4.1NonPorous Microparticles (NPMP) 59
2.2.2.4.2 Porous Microparticles (PMP) 60
2.2.2.5 Use of Porogen 61
2.2.2.5.1 Sodium Chloride (NaCl) as a porogen 61
2.2.2.5.2 Chilled Sodium Hydroxide for PMP 61
2.2.2.6 Encapsulation Efficiency and Drug Loading 61
2.2.2.7 Microparticles Characterization 62
2.2.2.7.1 Scanning Electron Microscope (SEM) . 62
2.2.2.7.2 Fourier Transform Imaging Resonance 63
2.2.3 Statistical Analysis 63
2.3 Results and Discussion 63
2.3.1 DCM-SIM Non-Porous Microparticles (NPMP) 64
2.3.2 DCM-SIM Porous Microparticles (PMP) 66
2.3.3 Factors that Contribute To Agglomeration Effects In The Microparticles Fabrication 69
2.3.4 Method Modification in Microparticles Preparation 72

2.3.4.1 DCM-SIM NPMP 72
2.3.4.2 DCM-SIM-PMP 74
2.3.4.2.1 Effect of Sodium Chloride As Poroen in PMP 75
2.3.4.2.2 Effect of Chilled NaOh in the PMP 76
2.3.4.2.3 Investigation of DCM-SIM with chilledNaOh % 0.5M NaOh : 70% EtOH protocol 78
2.3.5 Encapsulation Efficiency, Drug Loading and Percentage of Yield 81
2.3.6 FTIR Analysis 83
2.4 Conclusion 87

CHAPTER 3: HPLC METHOD DEVELOPMENT AND VALIDATION 89
3.1 Introduction 90
3.2 Method Development 90
3.2.1 General Introduction of HPLC System 90
3.2.2 Column Selection 93
3.2.3 Mobile Phases Composition and Elution Method 93
3.2.4 The Difference between Isocratic and Gradients 94
3.3 Materials and Methods 96
3.3.1 Materials 96
3.3.2 Methods 96
3.3.2.1 HPLC Methods Development 96
3.3.2.1.1 Instrumentation and Chromatographic 96
3.3.2.1.2 Preparation of Calibration and Validation Standard Solution 96
3.3.2.1.3 Preparation of SIM-Loaded PLGA 96
3.3.2.2 HPLC Method Validation 96
3.3.2.2.1 Specificities 96
3.3.2.2.2 Linearity 96
3.3.2.2.3 Precision 96
3.3.2.2.4 Accuracy 100
3.3.2.2.5 Recovery 100

3.3.2 LIMITS OF DETECTION AND QUANTIFICATION 10196
3.4 RESULTS AND DISCUSSION 102
3.4.1 SELECTIVITY AND SYSTEM SUITABILITY 102
3.4.1.1 MOBILE PHASE SELECTION 102
3.4.2 HPLC METHOD VALIDATION 106
3.4.2.1SPECIFICITY 106
3.4.2.2 DETECTION OF SIM FROM THE EXTRACTION IN MICROPARTICLES 107
3.4.2.3 LINEARITY 108
3.4.2.4 ACCURACY 109
3.4.2.5 PRECISION 112
3.4.2.6 RECOVERY 106
3.5 CONCLUSION 115

CHAPTER 4: VARIATIONS IN THE REACTION PARAMETERS DURING THE SYNTHESIS OF SPHERICAL MICROPARTICLES .. 116

4.1 INTRODUCTION 116
4.2 MATERIALS AND METHODS 117
4.2.1 MATERIALS 117
4.2.2 ANALYTICAL METHODOLOGY 118
4.2.2.1 Encapsulation Efficiency and Cumulative Study 118
4.2.2.2 Scanning Electron Microscopy (SEM) and Size Analysis 118
4.2.2.3 Preparation of SIM-Loaded Biodegradable Microparticles 118
4.2.2.4 Evaluation of Process and Formulations Variables 119
4.2.2.4.1 Effect of homogenization speed 121
4.2.2.4.2 Effect of evaporation time 122
4.2.2.4.3 Effect of surfactant concentration 122
4.2.2.4.4 Effect of polymer molecular weight 122
4.2.2.4.5 Effect of polymer amount and different size of stir bar 123
4.2.2.4.6 Effect of drug amount 123
4.2.2.5 Characterization of SIM-Loaded Microparticles 123

4.2.2.5.1 Determination of encapsulation efficiency 123
4.2.2.5.2 Determination of in-vitro drug release kinetics 123
4.2.3 DATA ANALYSIS 119
4.3 RESULTS AND DISCUSSION 124
4.3.1 CHARACTERIZATION OF SIM-LOADED BIODEGRADABLE POLYMERIC MICROPARTICLES 124
4.3.1.1 Effect of Homogenization Speed 125
4.3.1.2 Effect of Evaporation Time 126
4.3.1.3 Effect of Surfactant Concentration 129
4.3.1.4 Effect of Polymer Molecular Weight 135
4.3.1.5 Effect of Polymer Concentration 136
4.3.1.6 Effect of Stir Bar Size on the Emulsification Evaporation Process 138
4.3.1.7 Effect of Drug Amount 141
4.4 CONCLUSION 142

CHAPTER 5: PHYSICOCHEMICAL CHARACTERIZATION OF SIM-LOADED POLY(DL-LACTIC-CO-GLYCOLICACID) MICROSPHERES 145
5.1 INTRODUCTION 145
5.2 MATERIAL AND METHODS 148
5.2.1 MATERIALS 148
5.2.2 METHODS 148
5.2.2.1 X-ray Powder Diffractometry (XRD) 148
5.2.2.2 Differential Scanning Calorimetry (DSC) 148
5.2.2.3 Fourier Transformation Infrared Spectroscopy (FTIR) ... 149
5.2.2.4 Scanning Electron Microscopy (SEM) and Size Analysis 149
5.2.2.5 Laser Diffraction Analysis 149
5.2.2.6 Atomic Force Microscopy 149
5.3 RESULTS AND DISCUSSION 150
5.3.1 XRD ANALYSIS 150
5.3.2 FTIR ANALYSIS 154

5.3.3 Differential Scanning Calorimetry (DSC) Analysis 157
5.3.4 Evaluation of Surface Characteristics Using Scanning Electron Microscopy (SEM) and Atomic Force Microscopy (AFM). 158
5.3.4.1 Scanning Electron Microscopy (SEM)…… …..159
5.3.4.2 Atomic Force Microscopy 159
5.4 Conclusion 168

CHAPTER 6: PHYSICO-MECHANICAL PROPERTIES OF SINTERED SCAFFOLDS FORMED FROM SIM-LOADED POLY (PLGAMICROSPHERES FOR BONE TISSUE ENGINEERING. 169
6.1 Introduction 169
6.2 Materials and Methods 171
6.2.1 Materials 171
6.2.2 Methods 172
6.2.2.2 Scanning Electron Microscopy (SEM) and Size Analysis 172
6.2.2.3 Differential Scanning Calorimetry (DSC) 173
6.2.2.4 Encapsulation Efficiency of SIM Within Microspheres.. 173
6.2.2.5 Preparation of 3D Scaffolds……...174
6.2.2.6 Characterization of 3D Scaffolds..... 174
6.2.2.7 Release of SIM from Microspheres and Scaffolds 175
6.2.2.8 Mechanical Testing..... 175
6.2.2.9 Statistical Analysis..... 175
6.3 Results and discussion 175
6.3.1 Microstructure and Size Analysis of Porous and Non-Porous PLGA microspheres 175
6.3.2 Microstructure and Porosity of Scaffolds 181
6.3.3 Sintering of Microspheres into Scaffolds and Compressive Strength of Scaffolds 185
6.3.4 Release of SIM from Non-Porous Microspheres 187
6.3.5 Release of SIM from Scaffolds 188

6.4 CONCLUSIONS 191

CHAPTER 7: *IN-VITRO* TESTING OF PLGA COMPOSITE MICROSPHERES AND SCAFFOLDS 193

7.1 INTRODUCTION 193

7.2 MATERIALS AND METHODS 197

7.2.1 MATERIAL 197

7.2.2 METHODS 197

7.2.2.1 Preparation of Non-Porous and Porous Microspheres 198

7.2.2.2 Cell Culture and Seeding onto Scaffolds 198

7.2.2.3 Cell Viability Assay 199

7.2.3.4 Inverted Microscopy Imaging 199

7.2.2.5 Environmental Scanning Electron Microscope (ESEM) Imaging 199

7.3 RESULTS AND DISCUSSION 200

7.3.1 VIABILITY ASSAY 200

7.3.2 CELL MORPHOLOGY AND PROLIFERATION 207

7.3.2.1 Observation of MG 63 Cells with Scaffold using inverted Microscope .....

7.3.2.2 Observation of MG 63 Cells with Scaffold via Environmental Scanning Electron Microscopy (ESEM) . 208

7.4 CONCLUSION 215

CHAPTER 8: FINAL CONCLUSIONS AND FUTURE WORK 218

8.1 FINAL CONCLUSIONS 217

8.2 LIMITATION OF THE WORK 219

8.3 FUTURE WORK 220

REFERENCES 223

LIST OF TABLES

No	Table	Page
2.1	Mean diameters and size ranges of NPMP prepared using varying concentrations of SIM diluted in DCM	66
2.2	Mean diameter of (PMP) in prepared using varying concentrations of SIM diluted in the DCM	69
2.3	Mean diameter ± SD of NPMP prepared with varying concentrations of SIM using the modified method	74
2.4	Mean diameter of PMP prepared using varying concentrations of SIM diluted in the dichloromethane	81
2.5	The difference percentage of yield, drug loading and encapsulation efficiency of NPMP and PMP of different SIM amount	83
3.1	SIM serial dilution for HPLC validation analysis	99
3.2	Comparison of studies using different mobile phases	103
3.3	The linearity, quantification, and detection limits observed for the HPLC method outlined in Section 3.4.2.3	108
3.4	Accuracy studies of the standard SIM dilution in HPLC validation protocol	110
3.5	Accuracy studies of SIM in non-porous microparticles (NPMP) in HPLC validation protocol	111
3.6	Analysis of intraday and interday precision of HPLC method	113
3.7	Analysis of intraday and interday precision of HPLC method	114
4.1	Effect of formulation variables on the preparation of SIM-loaded biodegradable microparticles	120
4.2	Comparison of particle size, encapsulation efficiency, and cumulative amount of drug released from SIM loaded biodegradable polymeric microparticles using various process and formulation variables	134

5.1	Particle size of the various preparations of microparticles determined using Image J software	160
5.2	AFM mean roughness values for various preparations of microparticles. 5 different points were taken for the analysis	161
5.3	AFM skewness of surface height distribution (Ssk) and kurtosis of surface height distribution (Sku)	162
6.1	Polydispersity index of different types of microparticles	180
6.2	Glass transition temperatures (T_g) of porous PLGA microspheres pre- and post-ethanolic-NaOH treatment	183
6.3	Cumulative release of different scaffolds for 35 days	190
7.1	Previous studies on pleotropic effects of SIM with various cell lines	196

LIST OF FIGURES

No	Figure	Page
1.1	Type of bone	28
1.2	The steps in the intramembranous ossification in the bone	30
1.3	The Schematic diagram showing the process of endochondral ossification	31
1.4	The osteoblast (OB) differentiation from mesenchymal stem cells (MSC) with indication of typical stage-dependent markers	33
1.5	Osteoclastogenesis process	35
1.6	Function of statin as HMG-CoA reductase inhibitor and its pleotropic effects	38
1.7	The structure of SIM	39
1.8	Hydrolysis of PLGA	46
1.9	The preparation of double emulsion microparticles	50
2.1	SEM images of NPMP prepared using the double emulsion solvent extraction as described in section 2.2.4.1 with varying concentration of SIM	65
2.2	SEM images of PMP prepared using the double emulsion solvent extraction as described in section 2.2.4.2 with varying concentration of SIM	68
2.3	A schematic diagram showing the surfaces of PLGA nanoparticles interacting with PVA in its highly hydrolyzed form	71
2.4	SEM images of PLGA NPMP using the modified method with varying concentrations of SIM	73
2.5	SEM images of PLGA microparticles prepared with (a) 250 µl sodium chloride and (b) 500 µl sodium chloride as a porogen in a pH-controlled environment	75
2.6	SEM images of PMP prepared using the double emulsion solvent extraction method followed by	77

	treatment with 30% 0.5 M sodium hydroxide and using PBS as a porogen	
2.7	The distribution of PMP size of varying concentration of SIM	80
2.8	Comparison of EE in NPMP and PMP made with varying SIM concentrations	82
2.9	Fourier-transform infrared (FT-IR) spectra of SIM. The small figure representing the previous study by Tandale *et al*., 2011	84
2.10	Fourier-transform infrared (FT-IR) spectra of poly(D,L-lactic-co-glycolide) (PLGA)	84
2.11	Fourier-transform infrared (FT-IR) spectra of and SIM-NPMP	85
2.12	Fourier-transform infrared (FT-IR) spectra of and SIM-PMP	86
3.1	Schematic diagram of HPLC system	890
3.2	Online Transfer calculator outputs which can calculate the expected flow rate, injection volume, analysis time of the new column	97
3.3a	HPLC chromatogram of SIM of acetonitrile and 50mM potassium di-hydrogen phosphate buffer (65:35, v/v)	105
3.3b	HPLC chromatogram of SIM using a mobile phase of ACN70:30 v/v and water (containing 0.2% acetic acid pH 4.0)	106
3.4a	HPLC chromatogram of NPMP containing SIM using the method described in Section 3.4.1.1	107
3.4b	HPLC chromatogram of blank NPMP using method described in section 3.1.1.4	107
3.5	An example of chromatogram obtained for standard solution of 5 µg/mL	109
4.1	Effect of homogenization speed on in-vitro drug release kinetics of SIM-loaded biodegradable microparticles	126

4.2	Effect of time on in-vitro drug release kinetics of SIM-loaded biodegradable microparticles	128
4.3a	Scanning electron micrographs of the SIM degraded biodegradable microparticles made with (a) 1 % PVA (b) 0.6 % PVA and (c) 0.06 % PVA	130
4.3b	Effect of surfactant concentration on in-vitro drug release kinetics of SIM loaded biodegradable polymeric microparticles	130
4.4	Effect of polymer type on in-vitro drug release kinetics of SIM loaded biodegradable polymeric microparticles	136
4.5	Effect of polymer concentration on in-vitro release kinetics of SIM-loaded biodegradable polymeric microparticles	138
4.6	Scanning electron micrographs of SIM loaded degraded biodegradable microparticles for (a) Formulation D1 (0.5 cm) (b) Formulation D2 (1.0 cm) and (c) Formulation D3 (1.5 cm)	140
4.7	Effect of stir bar on in-vitro release kinetics of SIM-loaded biodegradable polymeric microparticles	141
4.8	Effect of drug amount on in-vitro release kinetics of SIM-loaded biodegradable polymeric microparticles	144
5.1	Analytical methods applied to the microsphere samples	147
5.2a	X-ray diffraction spectra of (A) SIM; (B) blank microspheres	151
5.2b	X-ray diffraction spectra of (a) blank microspheres; (b) blank microspheres; (c) SIM-loaded PLGA microspheres (depicted as 3c SIM for HMW-SIM NPMP and 4ca SIM for IMW-SIM NPMP)	152
5.2c	Schematic representation of the structure of an amorphous and a crystalline solid	153
5.3a	FTIR of HMW-NPMP blank	154
5.3b	FTIR of HMW- NPMP with SIM	1454
5.3c	FTIR of IMW- NPMP Blank	156

5.3d	FTIR of IMW- NPMP SIM	156
5.4	DSC thermogram of SIM, pure PLGA and optimized formulations of solid dispersions of IMW-NPMP and HMW-NPMP, pure IMW PLGA and HMW PLGA	158
5.5a	The pure SIM crystalline structure observed under SEM	159
5.5b	SEM images of different preparations a=IMW-BLANK-NPMP, b= IMW-SIM NPMP, c =HMW-BLANK-NPMP, d= HMW-SIM NPMP	160
5.6a	a) Atomic force microscopy (AFM) analysis of IMW-BLANK NPMP. b) the histograms of depth and surface roughness	164
5.6b	a) Atomic force microscopy (AFM) image of IMW-SIM NPMP. b) the histograms of depth and surface roughness	165
5.6c	Atomic force microscopy (AFM) analysis of HMW-BLANK NPMP. b) the histograms of depth and surface roughness	166
5.6d	Atomic force microscopy (AFM) analysis of HMW-SIM NPMP . b) the histograms of depth and surface roughness	167
6.1	SEM images of porous (A-B) and non-porous microspheres (D-F) formulated with IMW (A,C) and HMW (B,D) PLGA	177
6.2	Size distribution for NPMP (A) and blank (B), (C) and (D) with SIM, and PMP (E) and (F) as a function of PLGA molecular weight	179
6.3a	Analysis of size distribution for IMW of (a) IMW – PMP (b) IMW – NPMP Blank (c)IMW - NPMP SIM	181
6.3b	Analysis of size distribution for HMW. (a) HMW – PMP (b) HMW– NPMP Blank (c) HMW – NPMP SIM	181

6.4	DSC thermal profiles of (A) IMW PLGA and (B) HMW PLGA porous microspheres pre- and post-ethanolic-NaOH treatment.	183
6.5	SEM images of sintered scaffolds with various SIM loadings A-C=IMW PLGA, D-F= HMW PLGA (1 mg/g, 2 mg/g and 3 mg/g)	184
6.6a	Percentage of porosity of porous PLGA scaffolds loaded with various SIM concentrations;1 mg/g, 2 mg/g and 3 mg/g	185
6.6 b	The scaffolds after 24 hours sintering	185
6.7	Compressive strengths of scaffolds of various SIM loadings: 1 mg/g, 2 mg/g and 3 mg/g; * indicate $p \leq 0.05$	187
6.8	SIM release from microspheres as a function of PLGA molecular weight (IMW and HMW)	189
6.9a	SIM release profiles from 1 mg SIM/g loadings. Data points represent the mean ± standard deviation. * $p < 0.05$	191
6.9b	SIM release profiles from 2 mg SIM/g loadings. Data points represent the mean ± standard deviation. * $p < 0.05$	192
6.9c	SIM release profiles from 3 mg SIM/g loadings. Data points represent the mean ± standard deviation. * $p < 0.05$	193
7.1	In-vitro toxicity of SIM in MG63 cell line. Growth of MG63cell was valuated after 48 hours exposure to a wide range of SIM concentrations (0.4-100 μg/ml) in comparison to control cell (blank) which was treated with solvent alone	200
7.2a	Viability of MG63 responding to different concentrations IMW-SIM NPMP for different days.	202

	Values are the mean ± SE (three parallel samples for each concentration)	
7.2b	Viability of MG63 responding to different concentrations HMW-SIM NPMP for different days	202
7.3a	Comparison between IMW and HMW MG63 viability responding to different concentrations for 24 hours treatment	204
7.3b	Comparison between IMW and HMW MG63 viability responding to different concentrations for 48 hours treatment	205
7.3c	Comparison between IMW and HMW MG63 viability responding to different concentrations for 72 hours treatment	206
7.4a	Inverted microscope image of MG 63 cells treated with different concentration of IMW SIM-NPMP for 24 hours incubation	210
7.4b	Inverted microscope image of MG63 cells treated with different concentration of HMW SIM-NPMP for 24 hours incubation	211
7.4c	Inverted microscope image of MG 63 cells treated with different concentration of IMW SIM-NPMP for 48 hours incubation	212
7.4d	Inverted microscope image of MG 63 cells treated with different concentration of HMW SIM-NPMP for 48 hours incubation	213
7.5	5ESEMimages after cell MG 63 proliferation on a) IMW-BLANK b) IMW porous, c) IMW SIM-NPMP, d) HMW BLANK and HMW SIM-NPMP scaffold after 3 days	215

LIST OF ABBREVIATIONS

(KBr)	Potassium bromide
(Rq)	Root mean square roughness
(Sku)	Kurtosis of surface height distribution
(Ssk)	Skewness of surface height distribution
3D	3 Dimension
ABC	Ammonium bicarbonate
Acp5	Acid phosphatase 5
ACS	Absorbable collagen sponges
AFM	Atomic force microscope
ALP	Alkaline phosphatase
BET	Brunauer–Emmett–Teller
BMP-2	Bone morphogenetic protein-2
CP	Calcium phosphate
CS	Calcium sulfate
CSF-1	Colony stimulating factor 1
Ctsk	Cathepsin K
DBM	Decalcified bone matrix
DCM	Dichloromethane
DES-E	Double emulsion solvent evaporation
DL	Drug loading
DMSO	Dimethyl sulfoxide
DNA	Deoxyribonucleic acid
DSC	Differential Scanning Colorimetry
ECM	Extracellular matrix
EHD	Electrohydrodynamic
FDA	Food and drug administration
FTIR	Fourier-transform infrared spectroscopy
GC/MS	Gas chromatography–mass spectrometry
HA	Hydroxyapetite
HMW-SIM NPMP	SIM encapsulated non-porous microparticles for high molecular weight

HPLC	High-performance liquid chromatography
IGF-1	Insulin growth factor 1
IMW-SIM NPMP	SIM encapsulated non-porous microparticles for intermediate molecular weight
LC/MS	Liquid chromatography–mass spectrometry
LDL	Low density lipoproteins
MC3T3-E1	Non-transformed osteoblastic cells
MITF	Microphthalmia-associated transcription factor
MP	Microparticles
MSC	Mesenchymal cells
NaCl	Sodium chloride
NaOH	Sodium hydroxide
NFkB	Nuclear factor kB
NIR	Near-infrared spectroscopy
NMR	Nuclear magnetic resonance
O/W	Oil-in-water
PBS	Phosphate buffered saline
PCL	Poly(ε-caprolactone)
PDI	Polydispersity index
PGA/ PLGA	Polylactic acid/polyglycolic acid copolymer
PLA	Poly lactic acid
PLGA	Poly(lactic-co-glycolic acid)
PU.1	Transcription factor
PVA	Poly-vinyl-alcohol
RANKL	Receptor activator of NF-B ligand
SDS	Sodium dodecyl sulfate
SEM	Scanning electron microscope
SF	Silk fibroin
Simvastatin	SIM
TRAF6	TNF receptor associated factor 6
TRAP	Tartrate-resistant acid phosphatase
w/o/w	Water-in-oil-in-water
XRD	X-ray powder diffractometry

ABSTRACT

Bone graft are useful in the treatment of musculoskeletal injuries/diseases including trauma, bone fractures, painful vertebrae, missing teeth, osteosarcoma, and birth defects. The gold standard for bone graft therapies must be osteoconductive, osteogenic and osteoinductive. Different synthetic and natural biomaterials are being investigated for this purpose. The need to find less sophisticated and more patient-friendly alternatives to the bone graft procedure is a driving force behind recent advances in bone tissue engineering.

In this study, our main aim was to develop a porous, SIM-loaded microsphere delivery system with the capability of sintering *in situ*. Poly (lactic-co-glycolic acid) (PLGA) was used for this formulation due to its biodegradability, biocompatibility, controllable mechanical properties and good processing capabilities. In order to increase the encapsulation of the drug within the PLGA microparticles, we studied different variables that influenced the stability of the SIM and facilitate controlled and sustained release of it. An optimised procedure for formulating porous and non-porous (SIM-loaded) microspheres was established and the microspheres were extensively characterised.

The relationship between the molecular weight of the PLGA and both SIM release and compressive strength showed significant results for intermediate molecular weight (53 kDa) variety of PLGA thus it was chosen for further work based on balancing the need for retaining sufficient compressive strength and higher release profile. The simvasatain-loaded and porous microspheres were combined as a paste and found to sinter at body temperature (37°C) into scaffolds. Mechanical testing was carried out as to rule the possibility of the scaffold to mimic the bone.

The biocompatibility and osteogenic potential of the scaffolds were investigated using MG-6. Despite SIM gave antiproliferative effect to the cells, MG-63 was chosen as it can give faster results as compared to normal bone cells. Overall studies indicate IMW SIM-NPMP has higher release and increase the

MG 63 suppression in the viability studies, whilst the HMW SIM-NPMP showed delay particularly in the viability assay.

The composite PLGA/SIM and porous microspheres combine both porosity and the ability to load and sustain the release of the drug into one system. Moreover, their ability to sinter at body temperature and the possibility to use it as injectable scaffold or applied as a paste demonstrates the dual functionality of the system. This represents a novel approach to delivering SIM for tissue regeneration as presently, there has been no report of the combination of PLGA/SIM microspheres with porous PLGA microspheres as a system that is able to sinter, both post-injection and when packed as a paste, at 37°C. Therefore, the formulation presented in this thesis shows potential for further *in vitro* and *in vivo* testing to determine its suitability for bone tissue engineering applications.

DEDICATION

In the memory of my loving mum..

Hasnah Abu Bakar

May Allah SWT in his infinite mercy forgive her sins and grant her a place in Jannah.

ACKNOWLEDGEMENT

I would like to first and foremost thank and praise Allah for allowing me to carry out this research, which without His assistance and guidance, would have been impossible.

My huge thanks and appreciation go to my all supervisors, Professor Andrew Morris, Professor Kevin Shakesheff and Professor Nashiru Billa, who were always patient and supportive throughout the whole process. I thank them for always being available to answer my questions, even when they were very busy. Thank you for the endless help and support.

I would like to sincerely thank Dr Omar Qutachi for his encouragement, motivation, invaluable help and friendship. My appreciation goes to Dr Yamina Boukari, Dr Rayan Sabra, and Dr Enas Alkader for all their help and technical expertise throughout this project. I would also like to acknowledge the Islamic Development Bank for funding this work.

I am especially thankful to my amazing family for supporting me throughout this journey. To my late mum and my dad – I thank you both for your unwavering support throughout my life, endless encouragement and love; I am forever grateful to you both. Thank you to both my daughters (Mia and Hana) for being so understanding and the sacrifice that you have had made to allow me to complete this journey. To my siblings, Amalina, Khairul, Aimi, Izyan and Haaziq, Thank you for your support. My deep appreciation also goes to my labmate, Janet, Rajesh and all the technical staff.

Finally, to the best life partner I could ask for – my husband Mohd Zurix Mohamed, thank you for your patience, love, guidance and encouragement, all of which were invaluable throughout this PhD journey.

CONFERENCES

1. Effect of process and formulation variables on the preparation of SIM loaded poly DL-lactic-co-glycolic acid (PLGA) microspheres for injectable scaffold in tissue regeneration. 6th International Conference on Functional Materials & Devices 2017 (ICFMD - 2017). Bayview Hotel Melaka, MALAYSIA. 15th – 18th August 2017.
2. MG63 human osteoblast tumour cells exhibit different behaviour when treated with encapsulated SIM PLGA microspheres: A morphological studies International Conference on Drug Discovery and Translational Medicine 2018 (ICDDTM '18), The Everly Hotel, Putrajaya, Putrajaya, Malaysia. 3rd -6th December 2018.
3. The effect of molecular weight on poly (lactic-co-glycolic acid) microparticles and scaffolds in tissue engineering In: International Post Graduate Research Award Seminar 2017, University of Nottingham. 1st June -3rd June 2017.

CHAPTER 1

INTRODUCTION TO BONE TISSUE ENGINEERING

1.1 TISSUE ENGINEERING

Tissue engineered scaffolds or synthetic scaffolds are designed to influence the physical, chemical and biological environment surrounding a cell population. Cells, scaffolds and growth factors are regarded as the three important factors in tissue engineering (Park *et al.,* 2012). Apart from that, in our population, there is a rapid increase in musculoskeletal conditions particularly due to aging in the population and diseases such as fractures, osteoporosis and bone metastases (Agarwal *et al.,* 2015). Therefore tissue-engineered bone holds a significant impact to that. In addition, tissue engineering seems to alleviate the demand arising from the shortage of suitable autograft (patient's own tissue) and allograft (tissues taken from another person) for augmenting bone healing. The field of tissue engineering is concerned with the regeneration of new tissue following damage or injury (Wang *et al.,* 2009) and can be applied to various tissue types.

Controlled release of therapeutic agents from biodegradable polymeric microspheres can be accomplished by physically or chemically adsorbing the drug onto the surface (Rice *et al*., 2013) of the material matrix (scaffold), encapsulating the drug directly within the scaffold, or by incorporating drug delivery systems onto the scaffold (Krebs *et al*., 2009; Jeon *et al*, 2011; Vikingsson *et al.*, 2015). The subsequent release of the drug occurs either by diffusion or due to degradation of the scaffold or encapsulating material. The focus of this strategy is the creation of a microenvironment that can facilitate the growth, recruitment, adhesion, proliferation, and differentiation of cells. The scaffold should therefore be able to act as a mechanical support to the transplanted cells until the regenerated tissue is able to support itself.

Scaffolds that secure and deliver therapeutic ingredients like signaling molecules and stem cells hold great promise for drug delivery and tissue engineering. Employing a core–shell design for scaffolds provides a promising

solution (Perez *et al.*, 2015). Thus, an ideal scaffold must resemble the extracellular matrix of the tissue later. The scaffolds have to act as a 3D template whereby the cells can attach, multiply, migrate and function. The most important criteria for ideal scaffolds used for bone regeneration are; biocompatibility, the surface texture that promotes cell adhesion and sufficient mechanical properties, the inclusion of adequately large pore volumes to accommodate and deliver a cell mass sufficient for tissue repair. The necessity to have an appropriate large pore sizes is to allow continuous tissue growth and sufficient fluid diffusivity and transport properties to allow for transport of nutrients and waste products to and from the implant), and the provision of adequate mechanical strength (Freyman *et al*., 2016; Hench, 1997; Barrere *et al*., 2008; Reichert *et al*., 2009; Hing, 2005).

Porosity is an important factor to consider in the application of tissue regeneration via the scaffold route (Cochran *et al.,* 1999). The porous matrix for tissue engineering should have high porosity to be able to accommodate a large number of cells, as well as large interconnected pores to facilitate a uniform distribution of cells and the diffusion of oxygen and nutrients to them (Krebs *et al*., 2009; Jeon *et al*., 2011; Vikingsson *et al*., 2015). It has also been found that increased porosity can promote cell adhesion, migration, proliferation and extracellular matrix formation (Jeon *et al.,* 2011). Therefore, scaffolds with a high degree of porosity and a network of interconnecting pores are preferential, whilst at the same time maintaining a suitable degree of mechanical strength that matches with the requirement of the specific tissue in question (Vikingsson *et al.,* 2015; Naga *et al.,* 2015). In this context, it would be advantageous for designing and optimizing extracellular matrices to be able to study the proliferation, viability, and function of cells in well-characterized matrices.

Bone regeneration, following fracture and other orthopedic damage that may be associated with traumatic, surgical or degenerative events, is also another important tissue engineering application (Hing, 2005). The bone graft procedure can involve taking autologous bone harvested from various sites in the patient (the current ‘gold standard’ therapy) allograft bone from donors or cadavers, or xenograft bone from non-human sources and then implanting it into the injury site. However, there are drawbacks for all three sources for example there is a

limited supply of autologous bone, the usage of which can result in complications at the donor site and issues with graft resorption, whereas allograft and xenograft bone is associated with issues such as incompatibility with the host and transmission of disease and infection (Wang *et al.,* 2009; Hing, 2009). In addition, all three presents with high surgical costs and therefore tissue regeneration is seen as an attractive strategy for the repair of bone.

1.2 PHYSIOLOGY OF BONE TISSUE

The skeletal system is important to the body both biomechanically and metabolically. It is made up of individual bones and the connective tissue that joins them. Bone is a mineralized connective tissue that exhibits four types of cells: osteoblasts, bone lining cells, osteocytes, and osteoclasts (Downey, 2006). The rigidity and hardness of bone allow the skeleton to maintain and support the shape of the body; to protect internal organs such as of the cranial, thoracic, and pelvic cavities (Clarke *et al*., 2008) and to transmit the load transmission between muscle and bone (Duda, 2008). The mineral content of bone particularly calcium, magnesium and posphorous, contribute to the regulation of extracellular fluid composition (Hrafnkelsson *et al.,* 2010). In addition, bone has capability to self-repairing constantly undergoes renewal and repair (Sims *et al.,* 2014), able to withstand high loads and properties to changes in mechanical requirements and endures voluntary physical activity for life without breaking or causing pain (Compston, 2002; Warden, 2010; Roberts *et al*., 2012; Ralston, 2017).

1.3 BONE ANATOMY

The skeleton consists of two main structural types of bone (Figure 1.1). The adult human skeleton is composed of 80% cortical bone (also known as compact bone) and 20% trabecular bone (also known as cancellous or spongy bone (Ralston, 2013; Akter, 2016). Cortical bone is dense with a low surface area and forms an envelope around the marrow cavity. It is formed from Haversian systems, which consist of concentric lamellae of bone tissue surrounding a central canal that contains blood vessels (Baron, 2000). Trabecular or cancellous bone (also known as spongy bone) has a lower density and larger surface area than cortical

bone. Trabecular bone fills the center of the long bones, flat bones and vertebrae; it consists of an interconnecting meshwork of bony trabeculae, separated by spaces filled with bone marrow (Burr *et al.,* 2013).

Figure 1.1 illustrates the anatomy of the bone tissue. Compact bone makes up the outer layer of the bone while spongy bone is found mostly at the ends of bones and contains red marrow. Bone marrow is located at the center of most bones and has many blood vessels. There are two types of bone marrow: red and yellow. Red marrow contains blood stem cells that can become red blood cells, white blood cells, or platelets. Yellow marrow is made mostly of fat (Burr *et al*., 2013).

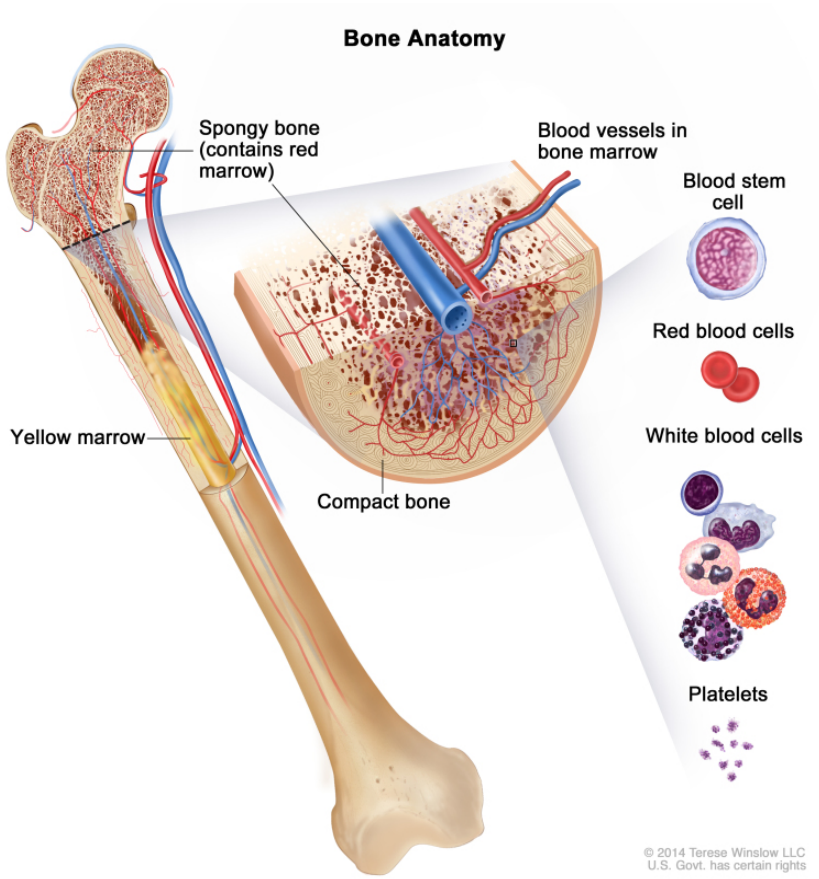


Figure 1.1: Type of bone. Image courtesy of PDQ cancer information summary for health professionals, National Institutes of Health (NIH).

1.4 OSTEOGENESIS: THE DEVELOPMENT OF BONES

Bone formation is made via two major modes. The direct conversion of mesenchymal tissue into bone is called intramembranous ossification. This process occurs primarily in the bones of the skull. Secondly, bone may also be formed from endochondral ossification where the mesenchymal cells differentiate into cartilage, and this cartilage is later replaced by bone (Gilbert, 2000).

1.4.1 INTRAMEMBRANOUS OSSIFICATION

Intramembranous ossification is achieved by direct transformation of mesenchymal progenitor cells differentiating directly into osteoblasts, (not on cartilage as in endochondral ossification). It occurs in healing of bone fractures and the initial formation of the flat bones of our skull. This process is also responsible for forming our jaw and clavicles, or collar bones (Akter *et al*., 2016). Figure 1.2 shows the steps in intramembranous ossification which started with (a) mesenchymal cells (MSC) group into clusters, and ossification centers form. (b) Secreted osteoid traps osteoblasts, which then become osteocytes. (c) Trabecular matrix and periosteum form. (d) Compact bone develops superficial to the trabecular bone, and crowded blood vessels condense into red marrow (Bone, 2012).

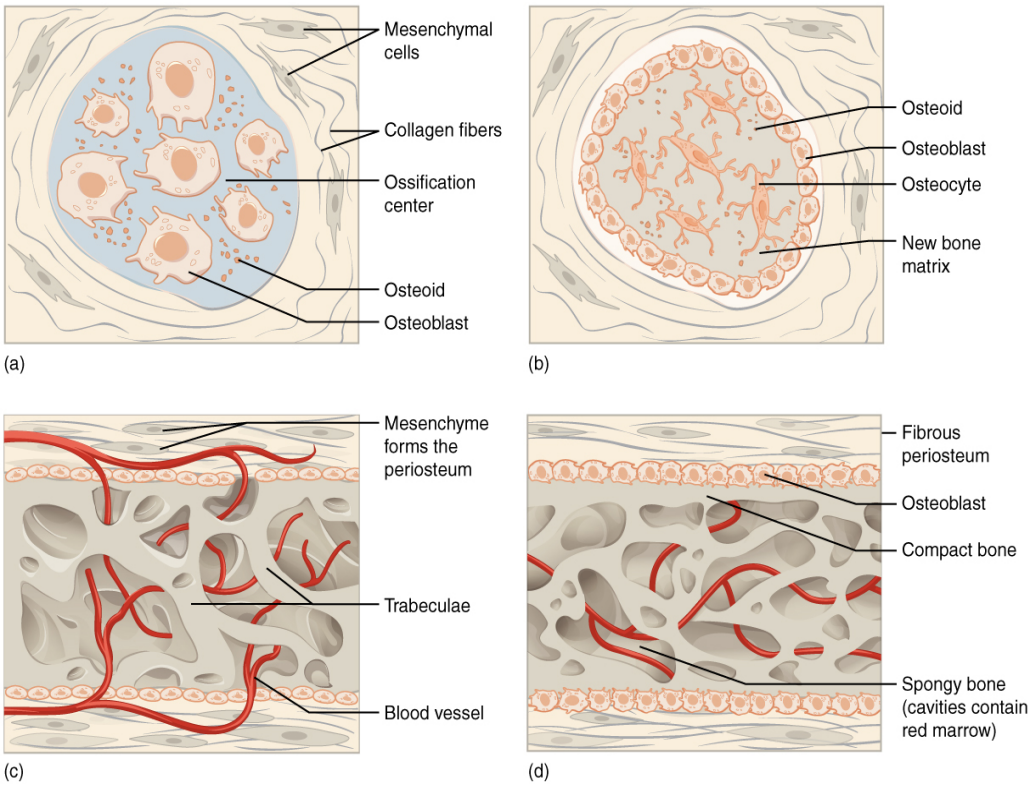


Figure 1.2: The steps in the intramembranous ossification in the bone. (http://olivero.info/bari/e/endochondral-ossification-diagram/)

1.4.2 ENDOCHONDRAL OSSIFICATION

Endochondral ossification involves the formation of cartilage tissue from aggregated MSCs, and the subsequent replacement of cartilage tissue by bone (Olsen, 1990). The process of endochondral ossification can be divided into five stages. Figure 1.3 illustrates the steps involved in the endochondral ossification. The mesenchymal cells differentiate into chondrocytes (cartilage cells) that form the cartilaginous skeletal precursor of the bones. As more matrix is produced, the chondrocytes in the center of the cartilaginous model grow in size. Upon matrix calcifies, nutrients can no longer reach the chondrocytes and this lead to disintegration of the surrounding cartilage and death. Blood vessels carrying osteogenic cells invade the resulting spaces and enlarged the cavities which many of them will become osteoblasts and eventually combined to become the medullary cavity (Bone, 2012).

As the cartilage grows, capillaries penetrate it. This penetration initiates the transformation of the perichondrium into the bone-producing periosteum. Here, the osteoblasts form a periosteal collar of compact bone around the

cartilage of the diaphysis. While these changes are occurring, chondrocytes and cartilage continue to grow at the ends of the bone (the future epiphyses), which increases the bone's length at the same time bone is replacing cartilage in the diaphyses (Akter *et al.,* 2016). By the time the fetal skeleton is fully formed, cartilage only remains at the joint surface as articular cartilage and between the diaphysis and epiphysis as the epiphyseal plate, the latter of which is responsible for the longitudinal growth of bones (Horton, 1990).

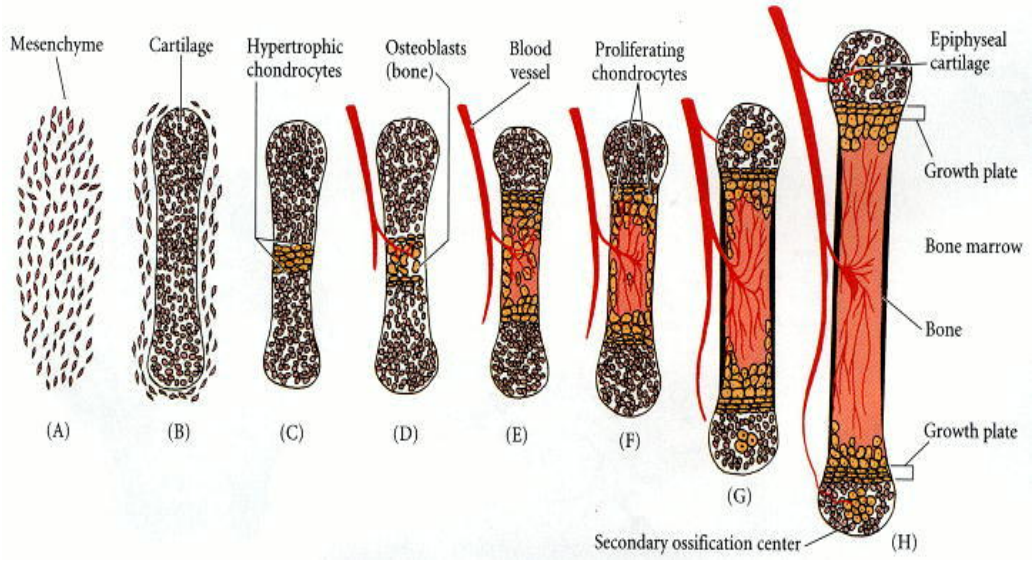


Figure 1.3: The Schematic diagram showing the process of endochondral ossification (Horton, 1990).

1.5 BONE REMODELING

Bone is a dynamic tissue that continuously undergoes two key activities to maintain its homeostasis, first the influence of skeletal mass and composition where mature bone tissue is removed from the skeleton, known as bone removal (resorption) by osteoclasts and secondly, the bone formation by osteoblasts (Sims *et al*., 2015, Choi *et al*., 2015). In short, bone is constantly being remodeled in a dynamic process where osteoblasts are responsible for bone formation and osteoclasts for its resorption (Caetano-Lopes *et al*., 2007). This process, called bone remodeling, is a prerequisite for normal skeletal homeostasis throughout life. Bone remodeling is regulated by a variety of factors, such as cytokines, chemokines, hormones, and biochemical stimuli (Kajita *et al*., 2018).

1.5.1 OSTEOBLASTS AND BONE FORMATION

Osteoblasts, specialized bone forming cells, develop from mesenchymal stem cells (MSCs), which are abundantly found in the periosteum and in the bone marrow. During oseteoblast differentiation, MSCs differentiate through pre-osteoblasts, transited osteoblasts, and finally into mature secretive osteoblasts (Zhang *et al*., 2015, Amini *et al*., 2012). Pre-osteoblasts and transited osteoblasts are mitotically active, expressing alkaline phosphatase (ALP), but do not secrete bone matrix (Choi *et al.,* 2015).

Osteoblast lineage cells include osteoprogenitors, osteoblasts, and osteocyte are derived from mesenchymal progenitor cells commonly referred to as mesenchymal stem cells (MSCs) (Roberts *et al.,* 2012). MSCs are originated from bone marrow, periosteum, and other sources are capable of differentiating along the osteoblastic, chondrogenic, adipogenic, and/ or myogenic cell lineages (Tare *et al.,* 2008; Augello *et al.,* 2010). These differentiation processes are tightly governed by intricate networks of regulatory molecules in a spatially and temporally controlled manner (Hartmann, 2009; Long, 2012) (Figure 1.4). The mesenchymal progenitor cells differentiated into chondrogenic and osteogenic lineages starts with the expression of Sox9 (Akiyama *et al.,* 2005). In bones, the development is through the endochondral ossification, a stage of bipotency of osteo-chondroprogenitors is recognized before the cells specify in either the chondrocyte or the osteoblast lineage. Early osteoblast progenitors express Runx2, encoding a Runt domain containing transcription factor that is absolutely required for the differentiation of osteoblasts as well as for the appropriate functioning of mature osteoblasts. Runx2 is viewed as the master controller of osteoblastogenesis (Rojas *et al*., 2015). Its deletion in mice resulted in a cartilaginous skeleton with absence of osteogenic differentiation and bone formation (both intramembranous and endochondral) (Komori, 2010). A similar phenotype was observed in mice with inactivation of the Sp7 gene encoding Osterix (Osx), a second transcription factor expressed in osteoprogenitors that is essential for osteoblast differentiation and function (Nakashima *et al*., 2002; Dirckx *et al.,*2013).

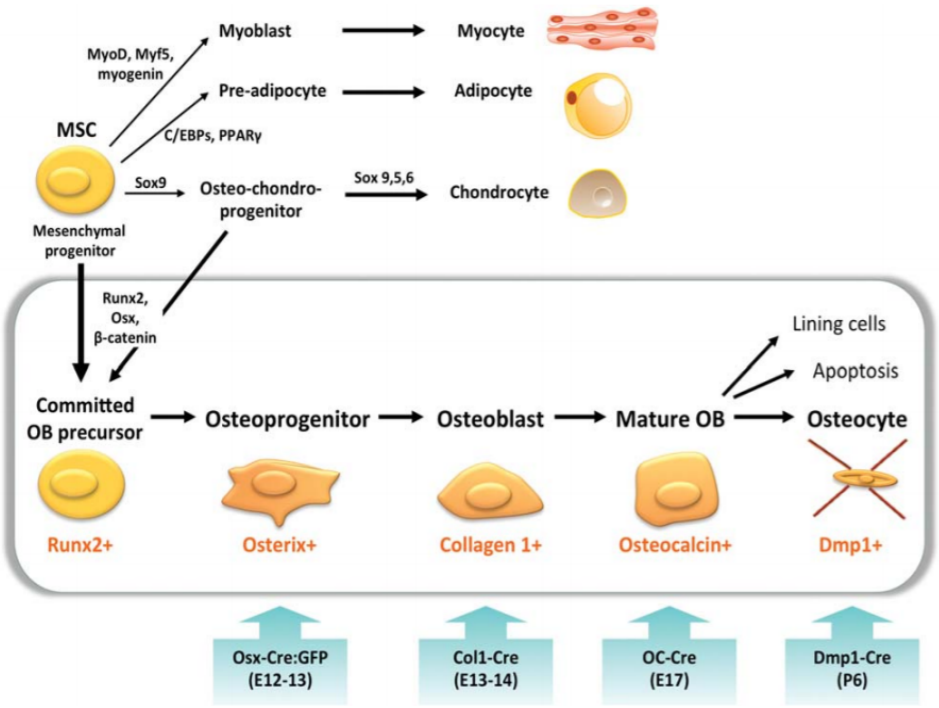


Figure 1.4: The osteoblast (OB) differentiation from mesenchymal stem cells (MSC) with indication of typical stage-dependent markers (Dirckx *et al.,* 2013)

Since MSCs is able to expand in culture and differentiate into multiple cell types, this suggests that they are potentially useful as therapeutic agents for the repair of tissues by engrafting and differentiating to replace damaged tissue cells. MSCs are the ideal seed cells for osteogenesis for bone regeneration due to their unique features: easy isolation from different adult tissues; high proliferative potential and ability to withstand freezing storage conditions allowing *in vitro* expansion to obtain clinically relevant cell numbers; pre-differentiation into the osteogenic lineage before implantation to enhance the efficacy of bone regeneration for repair; and no evidence of deleterious changes or malignant transformation of implanted MSCs (Goff *et al.,* 2008; Bina *et al.,* 2010; Dirckx *et al.,*2013; Chen *et al.,* 2016).

1.5.2 OSTEOCLASTOGENESIS

Osteoclasts and the bone-forming cells, osteoblasts, play reciprocal roles in the bone remodeling as is important to maintain the structural integrity by replacing effete bone that has a compromised structure with new bone. This further

prevents weak bone from accumulating, and prevents the development of fractures (Sharma *et al*., 2007).

Osteoclasts are derived from committed myeloid progenitors that differentiate into highly specialized multinuclear cells and tartrate-resistant acid phosphatase (TRAP)-positive cells, formed by the fusion of multiple mononuclear hematopoietic precursors (Martin *et al.,* 1992; Väänänen *et al., 2*008) which is capable of bone resorption in response to the action of colony stimulating factor 1 (CSF-1) and receptor activator of NF-B ligand (RANKL) (Roodman, 1992; Boyle *et al.*, 2003). It then secretes acid and lytic enzymes that degrade it in a specialized, extracellular compartment. The differentiation and survival of developmentally unrelated cell types, including osteoclasts, melanocytes, and pigmented retinal epithelial cells are associated with the transcription factor MITF (microphthalmia-associated transcription factor), a basic helix-loop-helix-leucine zipper protein. MITF and PU.1 collaborate to increase expression of target genes like cathepsin K (Ctsk) and acid phosphatase 5 (Acp5) during osteoclast differentiation (Luchin *et al*., 2001). However, MITF and PU.1 are expressed in macrophages and osteoclasts and in the common mononuclear precursor for both cell types (Matsumoto *et al*., 2004). This poses a general question concerning how gene regulation patterns are maintained in closely related cell lineages.

Figure 1.5 illustrates briefly on the osteoclastogenesis process in the bone. Early nonspecific differentiation along the osteoclast pathway is dependent on PU.1 and the MITF family of transcription factors, as well as the macrophage proliferation and survival cytokine M-CSF. Activation of RANK by osteoblast-expressed RANK ligand (RANKL) commits the cell to the osteoclast fate, which is mediated by signaling molecules such as AP-1 transcription factors, TNF receptor associated factor 6 (TRAF6), nuclear factor kB (NFkB), c-Fos, and Fra-1 leading to development of mature osteoclast (Sims *et al*., 2015; Choi *et al*., 2015). RANKL-stimulated osteoclastogenesis is inhibited by the RANKL decoy receptor OPG. Committed osteoclasts express the fusogenic genes DC-STAMP and Atp6v0d2 (Choi *et al.,* 2015; Yuan *et al.,* 2018) allowing formation of the multinucleated cell.

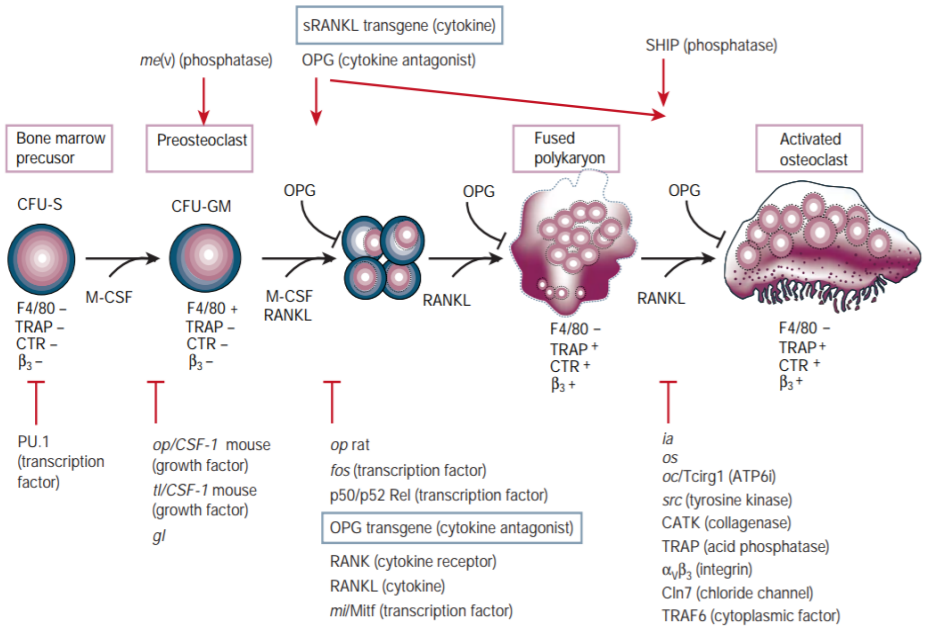


Figure 1.5: Osteoclastogenesis process. The Regulation of osteoclast formation and function is supported by different pathways (Boyle *et al*., 2003).

1.6 Biomaterials Used for Bone Tissue Engineering Applications

Biomaterials are a crucial component of the bone tissue engineering approach as they provide the means to form scaffolds. Scaffolds, as mentioned previously, are needed in order to provide multidimensional support to growing cells and, furthermore, to encourage their attachment, proliferation and differentiation. The chosen biomaterials must meet certain criteria, which include mechanical and physical properties that are suitable for the particular area, the ability to undergo sterilization without a loss in structure, biocompatibility and the appropriate degradation time. Materials used at the defect sites must be specifically capable of withstanding compressive loads that are common in this type of tissue. A variety of materials are being investigated in this field and there is an increasing demand for them to be bioactive rather than inert. The material should be osteoconductive and osteoinductive.

1.7 The Use of Growth Factor in Regenerative Medicine

Synthetic polymeric scaffolds, which can be used as surrogates of autologous bone grafts, should not only have suitable physicochemical and mechanical

properties, but it must also have some properties that facilitate the tissue growth. The formation and remodeling of bone structures result from coupling subsequent deposition of bone matrix by osteoblasts with balanced bone resorption by activated osteoclasts (Roberts *et al*., 2012; Yu *et al*., 2017; Gaihre *et al*, 2017). The advances in strategies for growth factors to mimic the body's normal physiological pattern, both spatially and temporally (Luginbuehl *et al*., 2004; Devescovi *et al.,* 2008) is a technique that is showing promise in the field of regenerative medicine, including bone defect repair due to fractures, diseases or surgical procedures. The formation of functional tissue requires coordinated cell processes, for example; proliferation, differentiation and angiogenesis, which is achieved by the release of a complex series of different growth factors (Kajita *et al*., 2018; Choi *et al*., 2016). This allows the transfer of information between the extracellular matrix (ECM) and the cells. The type of growth factor varies between different tissues, but it has become apparent that in order to facilitate tissue regeneration the controlled release of growth factors must play a part in any cell scaffold system (Aravamudhan *et al*., 2013).

Growth factors are key components of biological molecules that are able to promote or prevent cell processes such as proliferation, differentiation, migration, motility and adhesion (Luginbuehl *et al.,* 2004; Khan *et al.,* 2005; Devescovi *et al*., 2008). They often work in a concentration dependent manner, which in turn determines whether there will be an up or down regulation in the synthesis of various components e.g. proteins, other growth factors or receptors. Growth factors can be produced in a recombinant form, as well as extracted from cells. It has also been possible for their production to be induced locally using gene therapy. For example, in Alzheimer's patients, targeted injection of the nerve growth factor gene into the patients' brains rescued dying cells around the injection site, enhancing their growth and inducing them to sprout new fibers (Tuszynski *et al.,* 2015).

The delivery of growth factors to the site of injury is an important aspect of the tissue engineering approach and needs careful consideration as they have very short half-lives (Whitaker *et al*., 2001) and can diffuse away from the wound site. It is also important as the should also be noted that growth factors

which are delivered may elicit other undesirable effects elsewhere in the body (WHO Report, 1998).

1.8 THE USE OF STATIN IN REGENERATIVE MEDICINE

Statins are commonly used to treat several forms of hypercholesterolemia. They have potent cholesterol-lowering effects and further significantly reduce morbidity and mortality associated with coronary heart disease (Stancu *et al*., 2001; Lennernäs *et al.,* 1997; Koch, 2012; Whitten, *et al.,* 2014). The beneficial effects of the HMG CoA reductase inhibitors are usually attributed to their capacity to reduce the endogenous cholesterol synthesis, by competingly inhibiting the principal enzyme involved (Kazi *et al.,* 2018). Since mevalonate, the product of HMG CoA reductase reaction, is the precursor not only for cholesterol, but also for many other nonsteroidal isoprenoidic compounds, inhibition of this key enzyme may result in pleiotropic effects. They have been divided into two categories, involving: directly lipids, or intracellular signaling pathways. The first category includes: inhibition of cholesterol biosynthesis, increased uptake and degradation of low density lipoproteins (LDL), inhibition of the secretion of lipoproteins, inhibition of LDL oxidation, and inhibition of the scavenger receptors expression. Figure 1.6 illustrates the usage of statin including its potential pleotropic effects; angiogenesis, osteogenesis, anti-resorption and anti-inflammation.

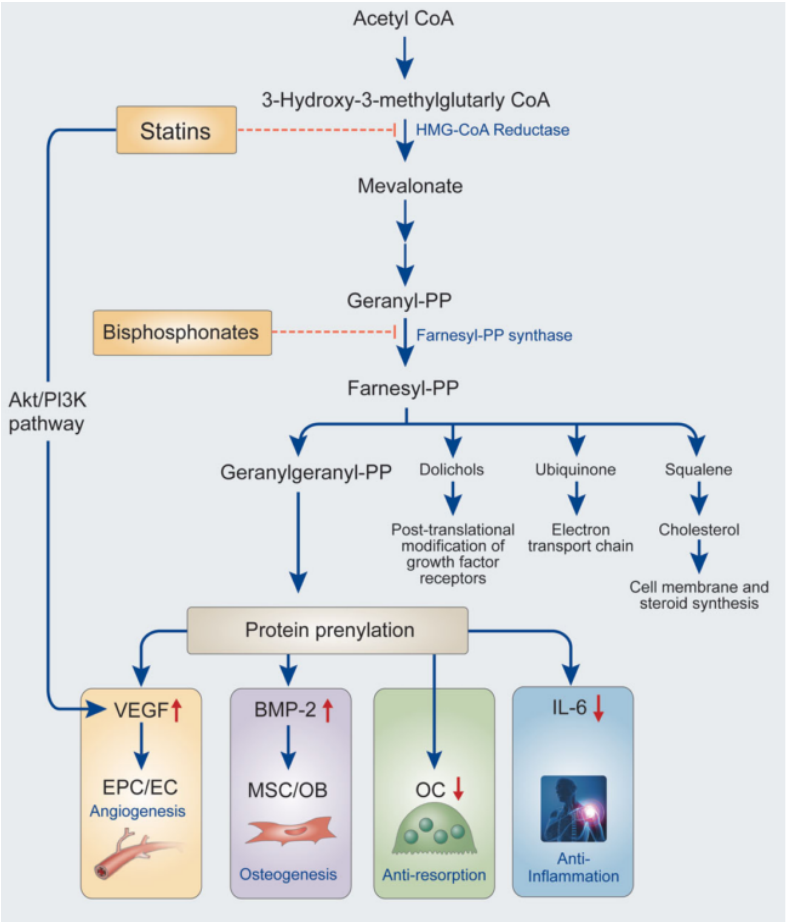


Figure 1.6: Function of statin as HMG-CoA reductase inhibitor and its pleotropic effects. (Whitten *et al.,* 2018)

Simvastatin (SIM) is a lipophilic statin derived from fungal metabolites and has elimination half-life of 1–3 h. Lipophilic statins are more susceptible to metabolism by the cytochrome P (450) system. The chemical structure (Figure 1.7) of SIM governs its water solubility, which in turn influences its absorption, distribution, metabolism, and excretion. It is not well absorbed, and less than 5% of an oral dose reaches the systemic circulation (Schachter, 2005; Kheirallah *et al*., 2016). The molecular weight is 418.66 Da with the formula of $C_{25}H_{38}O_5$. (Aceves-Hernández *et al*., 2011).

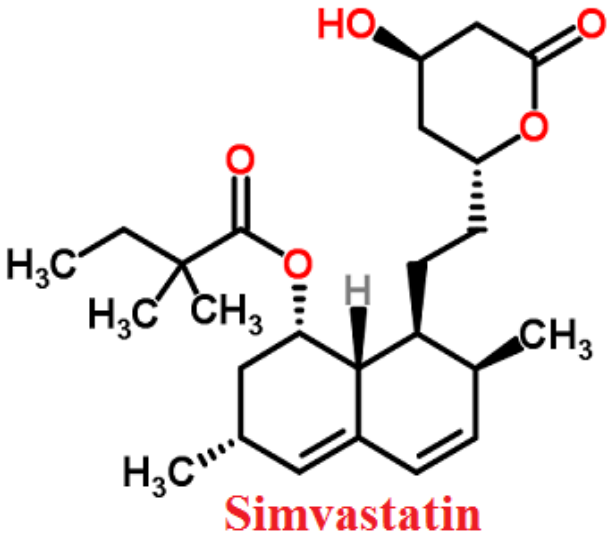


Figure 1.7: The structure of SIM. (Kheirallah *et al.,* 2016)

SIM has been reported to increase osteoblastic activity and inhibits osteoclastic activity. Mundy *et al*. (1999), first reported that statins stimulate *in-vivo* bone formation in rodents and suggested that this effect was associated with the increased expression of the bone morphogenetic protein-2 (BMP-2) in osteoblasts, implicating a possible beneficial role for statins in promoting anabolic effects (Lee *et al*, 2008; Liu *et al*., 2009) on bone, however substantial challenge of *in vivo* studies and clinical applications are still controversial. Several studies have also shown the effects of SIM on human osteosarcoma cells, bone marrow cells, and non-transformed osteoblastic cells (MC3T3-E1) (Garrett *et al*., 2001; Maeda *et al.,* 2004).

Locally applied statin promoting bone formation *in vivo* is only achieved on a high local concentration (Wu *et al.,* 2008). Local administration can bypass hepatic degradation of statins to achieve therapeutic concentrations in bone and avoid the side effects caused by its systemic administration (Pradeep *et al*., 2010; Pradeep *et al.,* 2012). There have been continuous efforts to find an appropriate delivery system to increase the circulating concentrations of this drug (Wu *et al*., 2008; Ezirganli *et al*., 2014). Eliminating this disadvantage using the SIM seems to be an alternative. SIM also has pleiotropic effects, including bone stimulation, promotion of vasculogenesis, and anti- inflammatory effects (Liao *et al*., 2009; Wang *et al*., 2010; Moon *et al*., 2011; Kheirallah *et al*., 2016). There is evidence

that statins promote osteoblast differentiation and enhance BMPs in mouse bone marrow stromal cells (Song *et al.,* 2003) and SIM increased alkaline phosphatase activity and osteocalcin expression levels in human bone marrow stem cells (Baek *et al*., 2008). According to *in vitro* and *in vivo* studies, SIM is considered a statin suitable for bone growth activation (Garrett *et al.,* 2001). Several studies have demonstrated that high concentrations of SIM increase bone formation and decrease bone resorption (Maritz *et al.,* 2001). This include the finding from the osteoporosis patients treated with SIM for low bone mass (Moshiri *et al.,* 2016). SIM presents local and systemic anti- inflammatory activity but may cause clinical symptoms (inflammation) when applied locally in high concentrations (Thylin *et al.,* 2002; Kheirallah *et al.,* 2016). Several studies reported the effect of locally administered SIM in various concentrations (Thylin *et al*., 2002; Wong & Rabie, 2005; Nyan *et al*., 2007; Ma *et al*., 2008; Moriyama *et al*., 2008; Kheirallah *et al.,* 2016; Moshiri *et al*., 2016). Some of them are the ACS (absorbable collagen sponges) (Boyne *et al.,* 1997; Howell *et al.,* 1997), the DBM (decalcified bone matrix) (Toriumi *et al*., 1991; Sigurdsson *et al*., 1996), hyaluronate (hyalorunan) (Hunt *et al.,* 2000), the inorganic bovine bone graft (deproteinized bovine bone matrix) (Jang *et al.,* 2003; Wong & Rabie, 2003), hydroxyapatite (HA) (Koempel *et al*., 1998), calcium phosphate (CP) (Wikesjo *et al.,* 2002), calcium sulfate (CS) (Nyan *et al.,* 2007), PGA/ PLGA (polylactic acid/polyglycolic acid copolymer) (Boyne *et al*., 2001).

A cautiously positive trend in favour of the use of statins in prevention of osteoporosis can be found in the current literature. Bisphosphonates are a class of drugs that are used currently to prevent the loss of bone mass. bisphosphonates inhibit an enzyme in the mevalonate pathway downstream of HMG-CoA reductase, giving rise to the hypothesis that statins could also be beneficial in pathologies related to loss of bone mass, such as osteoporosis, while reducing the potential for later osteonecrosis. Uzzan B. et al., in his meta analysis studies suggested statistically significant beneficial effects of statins on hip BMD should promote large double-blind randomized controlled trials on

their bone effects (20).Increased accumulated statin use was found to corresponded to a subsequent decrease in the risk of fracture (Shah, S. R. *et al.,* 2015). A study from Lupattelli, G. et al., stated 40mg/day SIM was given to 40 subjects as compared to diet only in postmenopausal women and showed higher spine and femoral hip bone mineral density (BMD) after 2 years (Lupattelli, G. et al., 2004).

1.9 POLYMERS IN REGENERATIVE MEDICINE

Recent regenerative medicine strategies are based on three primary components: a scaffold, cells and biomolecules. Biomolecules include all the signals required for informational function, e.g., material containing growth factors sequence which facilitates cell attachment, proliferation (Malafaya *et al*., 2007). Moreover, the solid phase must be biocompatible and promote cell adhesion and growth (Karageorgiou *et al.,* 2005; Cui *et al*., 2011). Over time, as the cells produce their own natural extracellular matrix, the synthetic matrix should degrade into non-toxic components that can be eliminated from the body (Cui *et al*., 2011). Biocompatible materials form the basis of the scaffolds used in regenerative medicine, in general consist of bioactive ceramics, bioactive glasses, biological or synthetic polymers, and composites of these. Natural polymers, for example the proteins collagen and silk fibroin, and polysaccharides such as chitosan and alginate have also been used in tissue engineering scaffolds (Hench, 1997; Jianhua *et al*., 2016). The synthetic polymer group includes biodegradable polyesters such as poly (α-hydroxyacids) (Krebs *et al*., 2009). Examples of this group of polymers include poly (D- or DL- lactic acid), poly (glycolic acid) and a co-polymer of the two, poly (lactic-co-glycolic acid) (PLGA) (Lee *et al.,*2008). Synthetic biodegradable polymers, such as PLA, PLGA and PCL, are more prevailing materials for the construction of nanofibrous scaffolds because of their good process ability (Gentile *et al.,* 2016).

1.9.1 NATURAL POLYMERS

Chitosan, is a popular choice in the field of regenerative medicine as it is a biodegradable, naturally occurring polymer, has drawn considerable attention in recent years as a scaffolding material in tissue engineering and regenerative medicine. It is a linear cationic polysaccharide that is derived from the N-deacetylation of chitin and has a similar structure to hyaluronic acid, a component of the ECM (Perez, 2011; Mathews, 2011; Raftery, 2013). Chitosan is especially attractive as a bone scaffold material because it supports the attachment and proliferation of osteoblast cells as well as formation of mineralized bone matrix (Raftery, 2013). Its surface is hydrophilic, which promotes the adhesion, differentiation and proliferation of cells (Krebs *et al.,* 2009). Chitosan has been applied in various forms including porous film-like structures (either pure Chitosan or composite materials), films and gel (Perez, 2011). It has been shown to promote the differentiation and mineralization of osteoblasts by the up-regulation of genes that are responsible for controlling these processes and so has promising applications in bone tissue engineering.

The silk of the silkworm is composed of a fibrous protein called silk fibroin (SF), along with a glue-like protein called sericin that holds the fibroins together (Puppi *et al.,* 2010). Fibroin is a natural protein extracted from silk cocoons of *Bombyx mori* silkworm that can be processed to create a variety of materials such as hydrogels, ultrathin and thick films, 3D porous matrices, and fibers with controllable diameters (Omenetto, 2010). This protein is also a potential candidate material for biomedical applications because it has several attractive properties, including good biocompatibility, good oxygen and water vapor permeability, and biodegradability (Altman *et al.,* 2003; Wang *et al.,* 2006) that can be controlled by functionalization of fibroin or changing the processing methods

Collagen is a natural protein that is found in the extracellular matrix of many tissues and provides structural and mechanical support to tissues (Wang *et al.,* 2006). It is biocompatible, has low antigenicity and is able to bind cells (Glowacki *et al.,* 2008). It has been shown, when fashioned in a sponge form, to promote cell and tissue attachment as well as growth, and has also been combined with other materials such as the bioactive ceramic, b-tricalcium

phosphate and an osteoinductive growth factor, bone morphogenetic protein (BMP-2) to enhance bone regeneration (Huss *et al.,* 2010). A PLGA knitted mesh has been combined with collagen to provide the mechanical strength, for application in cartilage regeneration (Dai *et al.,* 2010).

Potential of statins to promote bone regeneration has spurred an interest to deliver the statin in a different delivery strategies. Statins that is given via local delivery is of interest for a number of reasons. First, systemic administration of statins can result in rare but serious side effects, most notably liver toxicity, myositis, and rhabdomyolysis. Second, local delivery allows an adequate dosage to be delivered to the desired area without relying on systemic administration, which depending on the situation may be hindered by impaired vascularity. Local administration may lessen the possibility of widespread muscle and liver damage and obviate any unintended effects of statin usage given its pleiotropic effects while providing therapeutic benefit to the delivery area (Shah, S. R. *et al*., 2015)

Hydrogels have been used for local delivery of SIM in bone applications. Hydrogels has three dimensional, hydrophilic, cross-linked polymeric networks are a heterogeneous group of biomaterials and can be either naturally derived or synthesise (Deligkaris, K. *et al*., 2010). They are able to swell without disintegrating and can absorb up to several times their dry weight in water (Liu, M. et al., 2017). Examples of hydrogels include collagen, gelatin, and poly(ethylene glycol) which have the distinct advantage of being able to swell with water, making them very easy to load with drugs (Hoffman, A. S. *et al.,* 2016). In addition, modifications can be performed in order to impart desired characteristics, such as degradation or retention of bioactive factors. Benoit *et*

al. synthesized a novel fluvastatin-releasing hydrogel with fluvastatin covalently tethered via lactic acid linkages into a poly(ethylene glycol) hydrogel and released by degradation of lactic acid into the surrounding area (Benoit D.S.W.*et al.,* 2006). However, several disadvantages of hydrogel include non-biocompatible properties of hydrogel, batch to batch variation which causes differences in final formulation (Pillai, O. et al., 2001) and generally suffer from weak mechanical properties, lack of a sustained supply of nutrients or simulants to maintain the cell functions, which severely limits their further practical applications (Wang, N. *et al*., 2018).

Ceramics and synthetic polymers are also being investigated as carriers for statins which demonstrate good mechanical properties and osteoconductiveness. Ceramic bone cements are readily available in FDA-approved to provide a framework upon which bone can grow. In some cases, it is resorbable, allowing native bone to slowly replace it, and has been well characterized as a delivery vehicle for other small molecule drugs such as antibiotics. Nevertheless, the scaffolds fabricated from ceramics usually demonstrate poor integration with surrounding bone tissues (Wu S. *et al*., 2014).

1.9.2 SYNTHETIC POLYMERS

1.9.2.1 POLY LACTIC ACID (PLA)

Poly (lactic acid) (PLA) is a biodegradable synthetic polymer that has attracted massive interest as an effective substitute material in regeneration medicine due to its good biodegradability and biocompatibility (Abdal-Hay, 2016). Specifically, poly(lactic acid) (PLA) is one of the most widely used synthetic polymers in this field due to the non-toxicity of lactic acid, which is naturally present in the human body, and is FDA-approved (Chen *et al*.,2010; Wang *et al*.,

2010; Puppi *et al.,* 2010). It is a poly (α-hydroxyacid) and can exist in 3 different forms, PLA, PLA and a racemic mixture, P_{DL}LA (Puppi *et al.,* 2010). It is degraded by hydrolysis of the ester linkage to form lactic acid, a normal metabolic breakdown product, however the increase in acidity than can ensue following the degradation of PLA can lead to inflammation and swelling (Niu *et al.,* 2008). There are some major limitations such as the hydrophobic nature and poor ductility of PLA which hinder its practical use as substitute materials in tissue regeneration. It is known that the surface wettability reflects the adhesion, growth of cells, and protein absorption on the surface of the material (Abdal-Hay *et al.*, 2013). Some researchers noticed that the porous scaffolds fabricated from PLA floats on cell culture medium (Sarapirom *et al*., 2015). Thus, the hydrophobic nature of PLA is a serious problem in a predominantly hydrophilic bioenvironment where the cells fail to have initial attachment to the implanted scaffolds. This means PLA suffers from high hydrophobicity due to the lack of hydrophilic groups on its surface, which lends to its poor affinity for cell (Niu *et al*., 2008). PLA is often modified with other compounds or combined with other bioactive materials in order to deal with some of the issues above. Composite materials have also been produced, such as the electrospinning of hydroxyapatite (HA) nanoparticles, one of the major inorganic components of bone (Sui *et al.,* 2007). HA is often used due to its osteoconductivity and bioactivity (Jaiswal, 2013). The composite membrane showed enhanced osteoblast cell growth in comparison to a membrane composed of PLA alone, a higher elastic modulus and lower strain at failure, in addition to slowing down the degradation rate of the membrane (Sui *et al.,* 2007). Jaiswal *et al.* (2018) blended PLA with gelatin to form nanofibrous scaffolds and then mineralized the scaffolds with HA. They found that the mineralized scaffolds exhibited higher ALP activity leading them to conclude that HA increases the osteogenic capacity of the scaffold. The inclusion of HA also leads to increased surface roughness, which is important for protein absorption, cell attachment and proliferation. With regards to the degradation rate the addition of the gelatin appeared to increase the degradation rate of the scaffolds, and the HA switched the mechanism from bulk to gradual degradation.

1.9.2.2 POLY (LACTIC-CO-GLYCOLIC ACID) PLGA

Poly(lactic-co-glycolic acid) (PLGA) is one of the most successfully used biodegradable polymers because its hydrolysis leads to metabolite monomers, lactic acid and glycolic acid (Figure 1.8). Because these two monomers are endogenous and easily metabolized by the body via the Krebs cycle, minimal systemic toxicity is associated with the use of PLGA for drug delivery or biomaterial applications (Avgoustakis, 2005; Danhier *et al*., 2012). PLGA is an FDA approved biosynthetic polymer, belonging to the poly (α-hydroxyacids) which is one of the most commonly used synthetic materials for preparing fibrous scaffolds in tissue engineering (Keiser *et al.,* 2010; Ho *et al*., 2013; Gentile *et al.,* 2014; Masaeli *et al.*, 2016). PLGA is approved by the US FDA and European Medicine Agency (EMA) in various drug delivery systems in humans. The polymers are commercially available with different molecular weights and copolymer compositions. The degradation time can vary from several months to several years, depending on the molecular weight and copolymer ratio (Danhier *et al.,* 2012). The forms of PLGA are usually identified by the monomers ratio used. For example, PLGA 50:50 identifies a copolymer whose composition is 50% lactic acid and 50% glycolic acid. Poly(lactic acid) (PLA) has also been used to a lesser extent than PLGA due to the lower degradation rate (Bret *et al.,* 2011, Li *et al.,* 2017).

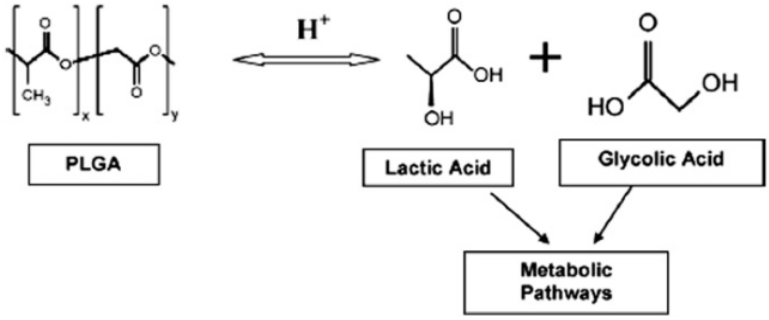


Figure 1.8: Hydrolysis of PLGA (Gentile *et al.,* 2014)

PLGA has been used to create microparticles, which are generally considered to fall within the size range of 1-100 μm (Lee, 2008), for use in tissue engineering applications, including for the delivery of growth factors (Barrere, 2008) and also plasmid deoxyribonucleic acid (DNA). PLGA microparticles loaded with insulin growth factor 1 (IGF-1) have also been incorporated into

PVA hydrogel structures in order to facilitate cartilage regeneration (Vikingsson *et al.,* 2015).

An important consideration when using a polymer in regenerative medicine is its degradation (Agrawal *et al*., 2015). The rate at which this occurs should be compatible with the rate at which the tissue regenerates and the products of the degradation must be acceptable within the body. Lactic acid and glycolic acid are the break down products that are formed by ester hydrolysis of PLGA. These products are involved in the normal metabolism of cells and hence are non-toxic and water-soluble (Milella *et al*., 2001; Spiller *et al.,* 2012).

The four important processes involved in the biodegradation of PLGA; hydration, initial degradation, further degradation and solubilization (Albertsson, 1993; Pişkin *et al*., 2002; Makadia *et al*., 2011). The aqueous medium first penetrates the polymer and relaxes the structure, reducing its glass transition temperature (Tg) (Park *et al.*, 2006). It is in these hydrated regions that the initial degradation begins, with the hydrolysis of the ester bonds within the polymer backbone structure (Gentile *et al*., 2014). As the backbone is degraded the molecular weight of the polymer is reduced and the PLGA maintains its integrity but loses mechanical strength. As it moves onto the next degradation step, the molecular weight is reduced to such an extent that the polymer loses its integrity. Finally, the smaller fragments are broken down into the monomer molecules leading to solubilization of the PLGA (Wang *et al*., 2000) PLGA degradation is also known to auto-accelerate due to the formation of acidic breakdown products (Liechty *et al.,* 2010) this phenomenon is known as autocatalysis.

The ratio of lactic acid to glycolic acid in the PLGA has an impact on the rate of polymer degradation. A study by Bible *et al.* (2009) used 85 (lactic acid): 15 (glycolic acid) PLGA in order to formulate microparticles that would reside in the tissue for up to 5 months (Bible *et al*., 2009). Other factors which influence the degradation rate of the microparticles are the porosity, molecular weight, geometry and the nature of the aqueous environment. As mentioned in the following section 1.11, a desirable feature of these systems is the retention of porosity whilst at the same time being able to withstand mechanical stresses. With the adequate selection of polymers an additional factor that needs to be

considered is the type of scaffolds used. Microparticles are particularly useful in this field and will be discussed in the following chapter 2.

1.10 SOLID DISPERSION CONCEPT

The term 'solid dispersion' has been utilized mainly to describe a family of dosage forms whereby the drug is dispersed in a biologically inert matrix. The dispersion of one or more active ingredients in an inert carrier matrix at solid-state can be prepared by the melting (fusion), solvent or melting-solvent method' (Chiou *et al*., 1971). Solid dispersion technique has been used for a variety of poorly aqueous soluble drugs such as nimesulide, ketoprofen, tenoxicam, nifedipine, nimodipine and SIM (Kavitha *et al*., 2012; Murtaza, 2012).

1.10.1 PLGA MICROPARTICLES FORMULATION METHODS

Various methods have been used to produce PLGA microparticles including the spray-drying, phase separation, the 'syringe infusion pump' method, double emulsion solvent evaporation (DES-E), and electrohydrodynamic (which include electrospraying and electrospinning).

The spray-drying technique involves transforming liquid feed into a dried powder by spraying the feed into a hot drying medium (air, inert gas such as nitrogen), which can be divided into three steps: (i) atomization of the feed into small droplets via an atomizer; (ii) leading to the rapid evaporation of the organic solvent and the formation of microparticles (iii) separation of the dry particles from the drying medium (Wan *et al.,* 2016). The electrospraying method involves dissolving the polymer, along with the agent to be incorporated (e.g. drug or growth factor), in a solvent and then forcing it through a nozzle which has a voltage applied across it (Nath *et al*., 2013; Liu, 2016). Nath *et al* formulated SIM encapsulated microparticles with a size range of 2-8 μm, and when tested on human MG-63 osteoblast cells microparticles were found to be non-cytotoxic and to enhance cell proliferation (Nath *et al*., 2013).

The 'syringe infusion pump' method involves the polymer solution, e.g. PLGA in dichloromethane (DCM), being pushed through a syringe into a perpendicular flow of PVA solution acting as the continuous phase (Dahlberg, C., 2010). The size of the MPs can be reduced by reducing the size of the needle

used to inject the polymer solution and also by increasing the speed at which the continuous phase is pumped in (Chen & Kawazoe, 2016).

Electrohydrodynamic (EHD) techniques is a procedure that utilize electrostatic forces as the driving force to fabricate fibers or particles of different shapes with sizes in the nanorange to a few microns through electrically charged fluid jet (Zamani *et al.,* 2013). The shape, size, morphology, and composition of micro/nanostructures can be modulated through process parameters and material choice, which can consequently customize the drug-release profile.

Various polymers have been electrospun, ranging from natural polymers like collagen, gelatin, chitosan, silk fibroin, and hyaluronic acid to synthetic polymers such as poly(lactic acid) (PLA), poly(ε-caprolactone) (PCL), polyethylene oxide, and copolymers, such as poly (L-lactide-co-caprolactone) and poly(lactic-co-glycolic acid) (PLGA), to fabricate scaffolds with desired properties for specific tissue regeneration and drug-delivery applications (Ma *et al.,* 2012).

1.10.2 DOUBLE EMULSION SOLVENT EVAPORATION TECHNIQUE

The oil-in-water (O/W) emulsion method has been widely used in encapsulation of active pharmaceutical ingredients into microparticles (Ye, 2010). This method generally forms microparticles with a spherical shape and a broad size distribution, which may cause a lack of good reproducibility (Bock *et al.,* 2010). The advantages include the relative ease with which the procedure can be carried out the lack of complicated instruments required. In addition, the parameters can be changed (Levengooda *et al*., 2014), hence it was the chosen method in work.

Figure 1.9 illustrates the preparation of microparticles via double emulsion technique. To produce a water in oil in water (w/o/w) emulsion, PLGA polymer is first dissolved in an organic solvent, often dichloromethane (DCM), and then emulsified with an aqueous phase to produce a w/o primary emulsion. It is in this first aqueous phase that proteins or drugs can be incorporated if required. This primary emulsion is then transferred to a second aqueous phase, often containing poly (vinyl alcohol) (PVA) functioning as a surfactant, to create a w/o/w emulsion. The DCM acts as a barrier between the two aqueous phases

in order to prevent the escape of any drug/protein that was dissolved in the first aqueous phase (Puppi *et al.,* 2014). The removal of DCM is then the next step and occurs by either the application of heat, vacuum, or extraction (Lee *et al.,* 2010). The resultant microparticles are then centrifuged, washed to remove any remaining porogen or surfactant, and then freeze-dried work (Levengooda *et al.,* 2014).

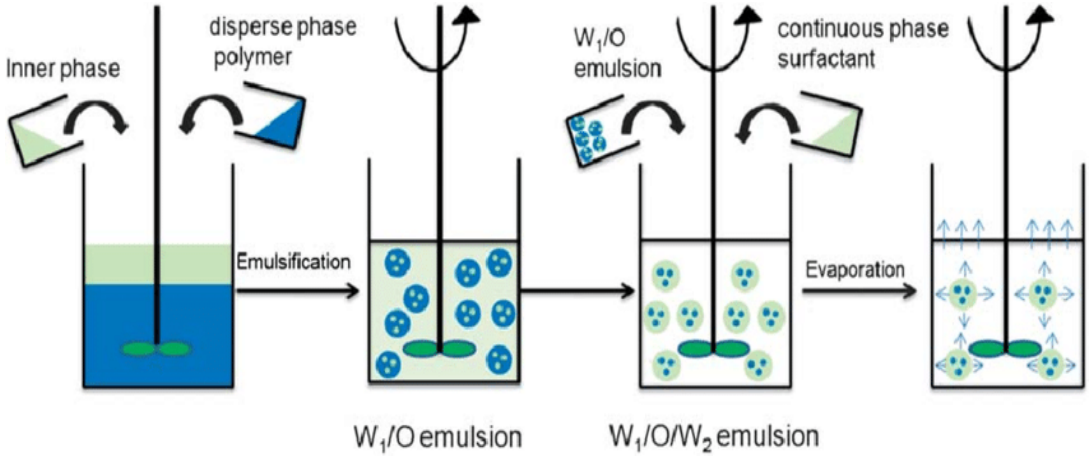


Figure 1.9: The preparation of double emulsion microparticles

The advantageous of this technique is likely due to the manipulation of the parameter at ease (Yang *et al*., 2009; Boukari, 2016) for example by changing the type and concentration of stabilizer employed in the system, versatile with respect to different oils and emulsifiers being employed, different speed of homogenization, different polymers, stabilizers, surfactants and drugs encapsulated and average particle size can be obtained in different studies via this technique (Iqbal *et al.,* 2015; Han *et al.,* 2016).

1.11 POROSITY

As mentioned in section 1.1 porosity is an important structural requirement of a scaffold in the tissue engineering field, especially when the method of tissue regeneration relies solely on host cells being recruited to the defect site. Apart from that scaffold serves as a template for cell interactions and the formation of bone-extracellular matrix to provide structural support to the newly formed tissue (Karageorgiou *et al.,* 2005; Khoda, 2010; Mallick *et al*., 2013).

Porous microspheres have external pores on the surface or internal pores in the core (usually interconnective), and active substances can be dissolved or dispersed on the surface or in the core of the microspheres (Cai *et al.,* 2013). In order to regulate porosity of this scaffold to a larger extent, porous microspheres were considered for using as the matrix for the fabrication of microsphere sintered scaffold (Low *et al*., 2006). Therefore, there are two kinds of pores on the scaffolds: which the first type is the larger pores among microspheres, where it facilitates blood vessel and bone tissue ingrowth; whilst the second type is the smaller pores on the microspherical surface which enhance nutrition transmission (Wang *et al.,* 2008). At the same time, the increased surface roughness resulting from smaller pores on the microspherical surface would promote cellular attachment and proliferation (Zareidoost *et al*., 2012).

Tevlin *et al*. (2014) proposed that the pore size should be at least 100 μm in diameter for successful diffusion of essential nutrients and oxygen for cell survivability. Bose *et al.* (2012) however, indicated that scaffolds should possess multi-scale porosity involving both micro-porosity and macro-porosity, with pore diameters ranging from <20 μm to >100 μm. Optimum pore sizes for bone tissue in-growth are found in the range of 200–350 μm (Murphy *et al*., 2010). Furthermore, recent studies have indicated that multi-scale porous scaffolds involving both micro and macro porosities can perform better than only macro porous scaffolds (Woodard *et al.,* 2007). The versatility of chemically synthesized polymers such as PLGA is an advantage in this respect, as it enables the fabrication of scaffolds with different porosities and mechanical properties. Unfortunately, porosity reduces mechanical properties such as compressive strength, and increases the complexity for reproducible scaffold manufacturing. Researchers have explored porous scaffolds using polymers, ceramics,

composites and metals. Strength of dense bioceramic materials matches close to the cortical bone, and different polymers to that of cancellous bone, however ceramic–polymer composite scaffolds are typically weaker than bone (Bose *et al*., 2012).

It is thought that the kinetics of the polymer precipitation step is important as if the polymer precipitates rapidly then it will harden while there are still solvent droplets present leading to a porous structure (Luan *et al.,* 2007). At a slower rate of polymer precipitation, the solvent is more likely to have been removed and this results in denser microparticles. Various methods can be used to increase the porosity of the microparticles, for example the incorporation of gas forming salts, e.g. ammonium bicarbonate (ABC) (Yoo *et al.,* 2011) and porogen leaching using sodium chloride (NaCl) (Ahmed *et al.,* 2009; Tran *et al*., 2012). Sodium oleate, an anionic surfactant, has also been used as a porogen as extraction from the microsphere structure to PVA solution is relatively easy (Sun *et al.,* 2009).

In the preparation of PLGA microparticles the ammonium bicarbonate works is by the liberation of carbon dioxide and ammonia, which forms pores when the primary water in oil emulsion comes into contact with the second water phase. Gas is liberated throughout the early stage of formation of the PLGA microparticles, leading to droplet volume expansion and the stabilization of enlarged inner phase aqueous droplets from coalescence during the phase of solvent evaporation. This maintains a macroporous structure until the microparticles solidify (Gupta *et al.,* 2018).

A study carried out by Mittal et al., examined the porosity of microparticles produced by varying the amount of ammonium bicarbonate (ABC). As the concentration of ammonium bicarbonate increased from 0% to 15% the microparticle size increased from 200µm to 357µm, with the maximum porosity of 81.2% attained when 15% of ammonium bicarbonate was used. ABC produced highly-porous structures in the PLGA particles as it escaped as ammonia and carbon dioxide (Qutachi *et al.,* 2014). Another observation was that microparticles containing less ammonium bicarbonate degraded more rapidly. This was attributed to the degradation products being trapped within the

MP structure, as there were more closed pores, which then served as an autocatalyst for further degradation (Mittal *et al*., 2014).

Sodium chloride functions as a porogen by its incorporation into the polymer and then leaching during various aqueous washing steps. An example of its use was in the formation of microparticles loaded with oligonucleotide (Ahmed *et al*., 2009). Varying amounts of sodium chloride were added, from 0-100mg/1ml of water, to PLGA solutions of varying molecular weights and lactide content. The resulting microparticles were porous and it was observed that as the sodium chloride concentration increased the microparticles became larger in size. Porosity was seen to increase as the molecular weight and lactide content increased. This was attributed to the precipitation of the polymer occurring more rapidly (Roy *et al.,* 2016). Treatment with ethanolic sodium hydroxide for 2 min was found to increase surface porosity without causing the microsphere structure to disintegrate. This surface treatment also enabled the microspheres to fuse together at 37 °C to form scaffold structures (Boukari *et al.,* 2015).

1.12 THE FUNDAMENTAL OF INJECTABLE SIMVASTATIN PLGA MICROPARTICLES AS BONE SCAFFOLD

The use of polymer scaffolds has gained attention to deliver cells for regenerative medicine and potentially overcome poor cell engraftment and improve cell survival (Qutachi *et al*., 2014). With challenges due to presence of complex and complicated physiological structures, injectable scaffold involving polymers looks promising looks promising (Gaihre *et al.,* 2017). With substantial limitations of the allografts usage, which include delayed in vascular penetration, slow bone formation, and possibility of disease transmission, injectable scaffold is the latest avenue in the tissue engineering (Garbuz *et al*., 1998; Amini *et al.,* 2012). Injectable scaffold aims to develop functional substitutes for damaged or diseased tissues through complex constructs of living cells, bioactive molecules in three-dimensional porous scaffolds, which will further support the cell attachment, proliferation and differentiation. Such constructs can be formed either by seeding cells within a pre-formed scaffold or through injection of a solidifiable precursor and cell mixture to the defective

tissue. Statin particularly the SIM, as described in sectioned 1.8 have been seen to improve bone metabolism via a number of pathways. The most interesting is Yamashita *et al*. (2010) have demonstrated that SIM inhibits BMP-induced osteoclast differentiation by regulating the RANKL/BMP-to-MAPK/AKT/Src pathway, suggesting a potential role of SIM in improving bone damage related to excessive bone resorption (Garrett *et al.,* 2002; Yamashita *et al*., 2010; Yuan *et al.,* 2018). Analysis of the literature search did not get similar match for injectable SIM scaffold in bone tissue engineering. Therefore, injectable scaffolds containing SIM as the drug carrier is appealing, particularly from the clinical point of view, because they offer the possibility of homogeneously distributing cells and molecular signals throughout the scaffold and can be injected directly into cavities, even of irregular shape and size, in a minimally invasive manner.

1.3 AIM OF THE STUDIES

From the literature, it is apparent that bone tissue engineering has the potential to have a significant clinical impact in defective bone growth. The injectable delivery route is an attractive strategy in bone tissue engineering as it would circumvent the need for invasive bone graft procedures. Therefore, the overall aim of this project was to develop a porous, SIM-loaded microparticulate scaffold system for potential use in bone regeneration.

1.3.1 SPECIFIC OBJECTIVES

The project is described in five chapters, each with specific objectives, as highlighted below.

Chapter 2

To successfully reproduce an established protocol for the formulation of porous and non-porous microparticles.

To analyze the properties of the microparticles using scanning electron microscopy, and Fourier Transform Infrared (FTIR).

Chapter 3

To develop and validate a High-Performance Liquid Chromatography (HPLC) method for the determination of SIM in loaded microparticles.

Chapter 4

To study the release profiles of SIM in loaded microspheres prepared with various variables parameters.

Chapter 5

To characterize the SIM-loaded microparticles system as a potential scaffold for bone tissue and determine its injectable potential.

Chapter 6

To develop a dual-application scaffold system comprising of both porous and SIM-loaded microspheres. This formulation was designed to form porous scaffolds at body temperature which has potential for tissue regeneration purposes. Porous (PMP) and non-porous (SIM-loaded) PLGA microspheres (NPMP) were formulated with IMW PLGA (53 kDa) HMW PLGA (84-109 kDa).

Chapter 7

To investigate the attachment, proliferation and differentiation of MG63 (Osteosarcoma bone cells) as the model of bone cell proliferation treated with SIM-loaded PLGA microsphere sintered scaffolds.

CHAPTER 2

FORMULATION OF NON-POROUS AND POROUS SIM PLGA MICROPARTICLES FOR BONE TISSUE ENGINEERING: OPTIMISATION OF PROTOCOL

2.1 INTRODUCTION

Tissue engineering scaffolds has been useful to serve as the three-dimensional (3D) template and must be designed to have a suitable matrix microenvironment with respect to cell adhesion, proliferation and differentiation as this is important for the formation of bone-extracellular matrix to provide structural support for the newly formed tissue (Huang *et al*., 2014; Costa, 2015; Rambhia *et al*., 2015). Scaffolds for bone regeneration should meet certain criteria to serve this function, including the possession of mechanical properties similar to those at the bone repair site and also biocompatibility and biodegradability at a rate commensurate with remodelling. To increase the capability of the scaffold promoting cell adhesion and proliferation, effort has focused on the development of 3D porous scaffolds to support and guide the new cells. This will allow the growth of tissues and nerve endings which enable the union of the bone (Kumaresan *et al*., 2015). Generally, to prepare porous scaffolds, it requires preparation of porous microparticles and usually, the scaffold is added together with growth factors, peptide (López-Noriega *et al*., 2015) or drugs (Sultana, 2017). As mentioned in Chapter 1, it has been found that SIM has pharmacological actions which are beneficial to bone regeneration. The combination of bone scaffolds with osteogenic induction factors such as SIM might be potentially an effective strategy to facilitate bone healing processes.

Porosity is a crucial parameter in scaffold engineering as it affects not only the structural and fluidic performance of the scaffold, but it also affects the release kinetics of encapsulated drugs (Karageorgiou, 2005; Klose, 2006; Mao *et al.,* 2007; Huang *et al.,* 2014; Vysloužil *et al*., 2014; Costa, 2015; Rambhia *et al*., 2015). In such scaffolds, porosity is defined as the percentage of the void

volume (the porous structure) to the total volume of the scaffold. Porosity and pore size are estimated usually using gas porosimetry which commonly analysed by Brunauer-Emmett-Teller (BET) surface area and pore size distribution analyser or using the quantitative 3D evaluation program which is included in the micro computed tomography (CT) software package. In BET analyser, nitrogen and mercury gases are commonly used for the analysis. BET analysis provides precise specific surface area evaluation of materials by gas multilayer adsorption measured as a function of relative pressure using a fully automated analyser. The technique encompasses external area and pore area evaluations to determine the total specific surface area. Several techniques have been used to produce porous 3D scaffolds such as porogen leaching (Mikos *et al*., 1994), gas foaming (Harris *et al.,* 1998), phase separation (Zhang *et al*., 1999) and solid free form fabrication technologies (Zein *et al*., 2002). Porous microspheres have drawn much attention in the last two decades in determining the capacity efficiency and release kinetics for applications in many fields. It is known that scaffold pore size affects both cell migration and diffusion of factors within the local scaffold environment. Eventually, this porous scaffold are important carriers for interconnectivity within the proximity of of tissue regeneration (Taek *et al*., 2006; Aronin *et al.,* 2009; Cai *et al*., 2013).

Porogens, also known as pore-forming agents, are widely used in solvent evaporation methods to fabricate porous microspheres. Their mechanism of action involves solvent casting and particulate leaching, in which porogen is added as an unreactive agent to the formulation used for porous microsphere preparation. Once the porogen particulates are removed via washing, the spaces they previously occupied become the pores, which may be internal or on the surface (Lin *et al*., 2002; Yang *et al*., 2009, Duncanson *et al*., 2012).

This chapter focuses on the preparation of SIM-containing porous and non-porous microparticles. Being porous will enhance the scaffold's ability to act as a reservoir for SIM and it will also facilitate cell attachment and proliferation within the 3D structure. However, it is anticipated that the encapsulation of SIM in PMP and NPMP might lead to two different encapsulation profiles. This is mainly come from the preparation protocols of these two types of microparticles. The protocol from Boukari *et al*. (2017) was

adapted for the preparation for both PMP and NPMP and the encapsulation efficiency derived using both protocols was analysed.

2.2 MATERIALS AND METHODS

2.2.1 MATERIALS

Poly (vinyl alcohol) (CAS: 9002-89-5), fully hydrolysed and 87-89% hydrolysed, was obtained from Sigma-Aldrich (city, country). Poly (lactic-co-glycolic acid) (CAS: 26780-50-7) 85:15 ratio was obtained from Lakeshore Biomaterials (manufactured by Evonik Degussa Corporation, Birmingham Laboratories, country). Sodium chloride, NaCl (CAS:7647-14-5), AR grade was obtained from Sigma-Aldrich (Merck, USA) . Dichloromethane, DCM (methylene chloride) (CAS: 75-09-2) HPLC and AR grade was obtained from Fisher Scientific (UK). Phosphate buffered saline (PBS) tablets (0.01 M phosphate buffer, 0.0027 M potassium chloride and 0.137 M sodium chloride, pH 7.4 at 25 °C) was obtained from Sigma-Aldrich (Merck, USA). Sodium hydroxide, NaOH (CAS: 1310-73-2) was obtained from Sigma-Aldrich (Merck, USA). Acetonitrile (HPLC grade) and 0.1 % acetic acid buffer were obtained from R&M chemicals, UK.

2.2.2 METHODS

2.2.2.1 PREPARATION OF POLY (VINYL ALCOHOL) (PVA)

3.0 g of PVA was added to 1 litre of distilled water (to make 3% w/v) and stirring speed (4000 rpm) using (15 mm length x 4mm) magnetic stirring bar and was maintained overnight at room temperature until the poly (vinyl alcohol) had dissolved. The resulting solution was then cooled and filtered under vacuum conditions using 500 ml Nalgene Rapid-Flow filter, 0.2 µm pore sizes and 75 mm diameter with a water suction pump (Eyela, A-1000s).

2.2.2.2 PREPARATION ON PHOSPHATE BUFFER SALINE (PBS)

PBS solution was prepared by dissolving 1 tablet in 200 ml of Ultra-pure deionised (DI) water from a Milli-Q plus system, EMD millipore, (Merck, USA) and agitate on a magnetic stirrer at 180 rpm until both tablets were fully dissolved. The final pH obtained using a Sartorius, PB-10 pH-meter was 7.4 for each of the solutions..

2.2.2.3 PREPARATION OF SIMVASTATIN STOCK SOLUTION

Preparation of SIM stock solution was carried out by dissolving the SIM crystalline powder in organic solvent particularly the DCM (Nandagiri, V. K. *et al*., 2012). At this point, our attempt is to observe and analyse the potential of double emulsion evaporation technique in encapsulating SIM into the microparticles. Four concentrations were chosen; 0.1 mg/ml, 0.5 mg/ml, 1.0 mg/ml and 5.0 mg/ml.

2.2.2.4 FORMULATION OF MICROPARTICLES: DOUBLE EMULSION SOLVENT EVAPORATION METHOD

The protocol for the preparation of both non-porous and porous microparticles, was adapted from Boukari, *et al.* (2015) and Boukari *et al.* (2017). The improved double emulsion solvent evaporation technique was used to prepare the SIM encapsulated microparticles. Generally, this technique is the most common method used to produce biodegradable microspheres aimed at drug and protein delivery. In addition, several studies supported this technique with regards to the formulation of SIM encapsulated microparticles with the aim for bone regeneration (Nandagiri *et al.,* 2012; Nath *et al*., 2013). Outcome of the protocol will be further discussed in Section 2.3.

2.2.2.4.1 NON-POROUS MICROPARTICLES (NPMP)

NPMP using PLGA of intermediate molecular weight (IMW) were prepared using the double emulsion solvent evaporation method as previously described by Qutachi *et al*. (2013). Briefly, a 100 µl aliquot of distilled water was added to a 20% w/v PLGA solution in DCM and homogenized at 4000 rpm using a Silverson L5M homogenizer to form the primary emulsion. SIM of different concentrations (0.1 mg/ml, 0.5 mg/ml, 1.0 mg/ml and 5.0 mg/ml) was then added

to 200 ml of 0.3 % w/v PVA solution and homogenized at 2000 rpm to form the secondary emulsion. Blank however indicates SIM is not added in the preparation of microparticels and substitute with distilled water. The emulsion was then stirred for 4 hours at 300 rpm to allow the DCM to evaporate and the microspheres to precipitate. The microspheres were washed with distilled water three times prior to centrifugation. Immediately after washing, the microparticles were subjected for centrifugation at 5000 rpm for 2 minutes. All microspheres were freeze-dried using a Thermofisher Scientific FR-Drying Digital Unit for 48 hours and stored at -20 °C until use.

2.2.2.4.2 POROUS MICROPARTICLES (PMP)

Porous PLGA microspheres using intermediate molecular weight (IMW) were prepared using the double emulsion solvent evaporation method as previously described by Qutachi *et al*. (2014). Briefly, 250 µl PBS (Ph 7.4) was added to a 20 % w/v PLGA solution in DCM and homogenized at 9000 rpm using a Silverson L5M homogeniser to form the primary emulsion. SIM of different concentrations (0.1 mg/ml, 0.5 mg/ml, 1.0 mg/ml and 5.0 mg/ml) was then added to 200 ml of 0.3 % w/v PVA solution and homogenized at 4000 rpm to form the secondary emulsion, which was then stirred for 4 hours at 300 rpm to allow the DCM to evaporate and the microspheres to precipitate with magnetic stirrer (15 mm x 4mm). Blank however indicates SIM is not added in the preparation of microparticels and substitute with distilled water. The microspheres were washed three times with distilled water. Immediately after washing, the microparticles were subjected for centrifugation at 5000 rpm for 2 minutes. All microspheres were freeze-dried using a Thermofisher Scientific FR-Drying Digital Unit for 48 hours and stored at -20 ºC until use.

2.2.2.5 USE OF POROGENS

2.2.2.5.1 SODIUM CHLORIDE (NACL) AS A POROGEN IN MICROPARTICLE PREPARATION

Microparticles were produced using the protocol detailed in Section 2.2.4.2 however we attempted to substitute PBS with NaCl. The objective of the substitution was to see whether using NaCl as a porogen increased the size of the pores in the microparticles. NaCl solution was prepared by dissolving 1 g of NaCl in 10 ml of distilled water to give a concentration of 1.71 mol/litre. 250 µl of the NaCl solution was then added to the PLGA/DCM solution. This primary emulsion was subsequently added to the PVA aqueous phase and stirred for 4 hours, centrifuged and freeze dried as detailed in the procedure above (section 2.2.2.4.1 and 2.2.2.4.2).

2.2.2.5.2 CHILLED SODIUM HYDROXIDE (NAOH) FOR POROUS MICROPARTICLES (PMP)

Microparticles were treated with NaOH to further open up any pores present. A 0.50 M NaOH and 96% ethanol (EtOH) solution was prepared in a ratio of 30:70 respectively. Upon completion of 4 hours stirring as described in the section 2.2.4.2.2, the microparticles were collected into 15 ml tube. 10 ml of 30% 0.25 M NaOH:70% absolute ethanol (EtOH) was added rapidly into the tube and vortexed (VELP, model F20220176) for 2 minutes. The sample was then poured into a 40 µm cell strainer (BD Falcon 40 µm Nylon) and washed with deionized water for 3 minutes. Excess water was removed from the cell strainer by placing it on the blue roll as it acts to absorb the excess water from the cell strainer. Subsequently, the microparticles were freeze-dried for 72 hours.

2.2.2.6 ENCAPSULATION EFFICIENCY AND DRUG LOADING OF THE PMP ENCAPSULATED WITH SIMVASTATIN

10 mg of SIM-encapsulated microparticles was determined by using a HPLC method as described by Micheal *et al*. (2013). Briefly, the chromatographic procedure used is as follows: HPLC analysis was performed with an Agilent Series 1120 HPLC (Agilent Technologies, Wilmington, DE), Agilent 1120

Infinity LC pump, USA equipped with UV/Vis detector (Agilent Series 1120 HPLC, USA) with Agilent EZChrom Elite Compact software. The chromatographic separations were performed using a ThermoScientific® 100 C18, 5 µ, 150 mm × 4.6 mm column, at 45 ºC, eluted with mobile phase at a flow rate of 1.0 mL/min. The mobile phase consisted of acetonitrile and 0.1 % acetic acid buffer (60:40, v/v). Mobile phase components were filtered through a 0.45 µm nylon filter and degassed in an ultrasonic bath prior to use. The column was equilibrated for 5 min following each sample each run. Prior to analysis each sample filtered through a 0.22 mm poly tetra fluoroethylene (PTFE) membrane filter and then analysed in triplicate with the results being reported as an average of the three. The calibration curve for the quantification of SIM was prepared using samples in the range of 0.001-100 µg/mL and the correlation coefficient of R^2 was 0.9994.

SIM encapsulation efficiency was determined by Equation 1 whilst the percentage of drug loading (DL) in non-porous and porous microparticles was determined using Equation 2. The percentage (%) of yield was calculated from the prepared microspheres and weighed from different formulations as in Equation 3.

$$\% \text{ EE} = \frac{\text{Actual mass of SIM in 10 mg of microspheres}}{\text{Mass of SIM used for 10 mg of microspheres}} \times 100 \quad \text{..... Equation 1}$$

$$\text{DL\%} = \frac{\text{Amount of SIM found in microparticles}}{\text{Total amount of microparticles in the system}} \times 100 \quad \text{..... Equation 2}$$

$$\% \text{ yield} = \frac{\text{Actual weight of microspheres}}{\text{Total weight of drug and polymer}} \times 100 \quad \text{..... Equation 3}$$

2.2.2.7 MICROPARTICLES CHARACTERIZATION

2.2.2.7.1 SCANNING ELECTRON MICROSCOPY (SEM)

Samples were mounted on metal stubs and viewed under a scanning electron microscope (FE-SEM, Quanta 400F, FEI, USA). Images were analysed with image J software (version ImageJ/Fiji 1.49) which is a public domain, Java-based image processing program developed at the National Institutes of Health. This software was used to count and determine the size distribution of the microparticle images obtained from the SEM.2.2.2.7.2 Fourier Transform imaging Resonance (FTIR)

The IR spectrum of each drug was recorded using a Perkin Elmer FTIR Spectrometer Spectrum RX-I. 5 mg of sample was mixed thoroughly with 100 mg Potassium Bromide IR powder and compacted using a hydraulic press at a pressure of about 100-150 kg/cm^2 for 3 minutes. The resultant disc was mounted in a suitable holder in the spectrophotometer and the IR spectrums were recorded from 4000 cm^{-1} to 625 cm^{-1}.

2.2.3 STATISTICAL ANALYSIS

Statistical analysis was performed using SPSS (Version 22) software. ANOVA analysis was used for all statistical testing, performed on data from between 3-6 repeat experiments. Analysis is considered significant, and the * designation is assigned, if $p>0.05$ *, $p>0.01$ **, $p>0.001$ ***, $p>0.0001$ ****. Bar graphs represent the mean of 3-6 individual repeats, with associated error bars to show the standard error in the mean (SEM). Details of individual statistical tests (ie. one way or two-way ANOVA, number of repeats) are provided in the figure caption for each graph.

2.3 RESULTS AND DISCUSSION

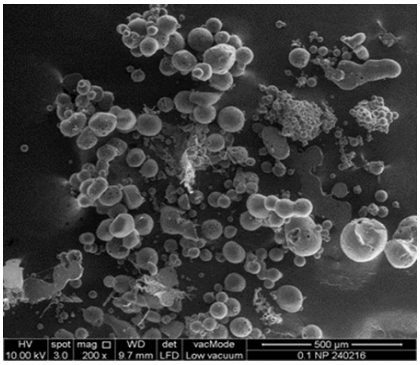
In order to stabilize the emulsion formed between polymer and drug solution with water, polyvinylalcohol (PVA) was used as emulsifier (Assessment, 2004; Baptista *et al*., 2016). Following the evaporation of the organic solvent from the surface of droplets, the concentration of the polymer increased, reaching a critical point at which the polymer concentration exceeded its solubility in the

organic phase and then precipitated to produce microspheres (Vysloužil *et al*., 2014; Iqbal *et al*., 2015).

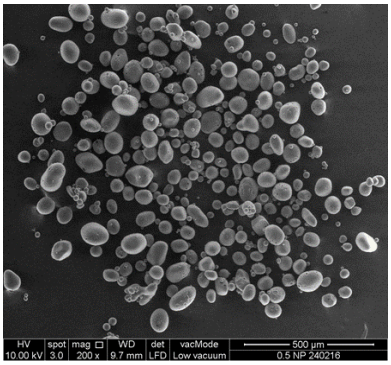
2.3.1 DCM-SIM NON-POROUS MICROPARTICLES (NPMP)

SEM images of these samples can be seen in Figure 2.1 below. From the images it is apparent that the resulting microparticles are non-porous with a varied size distribution. However, agglomeration occurred immediately after the centrifugation where the jelly like structure was observed. This agglomeration prevented any microparticles from being collected and we unable to measure the size of the microparticles.

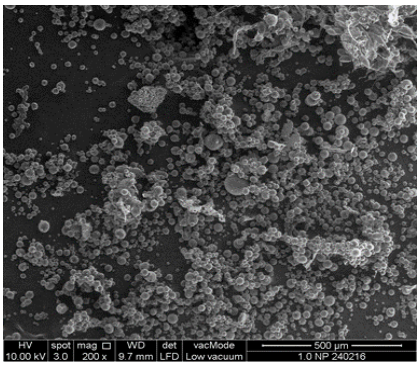
The size range of the microparticles (mean ± SD) was described in Table 2.1. Due to agglomeration effects, some of the microparticles were in an oval shape rather than being spherical. The 1.0 mg/ml SIM formulation showed particularly bad agglomeration which could be due to a plasticising effect as a result of the PVA or it is possibly due to inefficient removal of DCM (Boukari *et al*., 2017). However, the microparticle size in the blank preparation were observed to be almost similar in size as compared to all SIM-encapsulated NPMP. More debris polymer was present between the microparticles in this preparation.



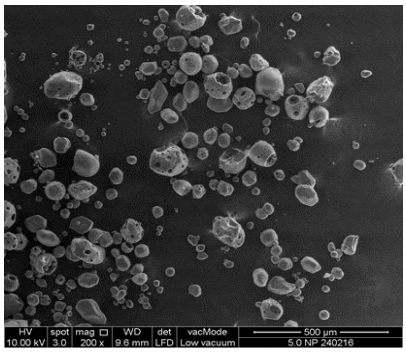
a



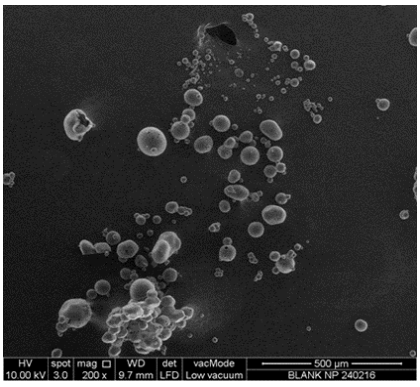
b



c



d



e

Figure 2.1: SEM images of NPMP prepared using the double emulsion solvent extraction as described in section 2.2.4.1 with varying concentration of SIM. (a: 0.1 mg/ml, b: 0.5 mg/ml, c: 1.0 mg/ml, d: 5.0 mg/ml, e: blank)

Table 2.1: Mean diameters and size ranges of NPMP prepared using varying concentrations of SIM diluted in DCM

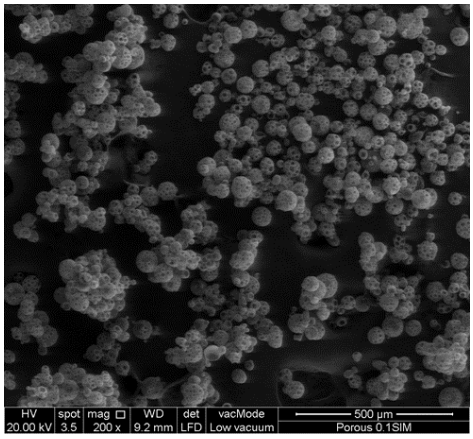
SIM-DIC Stock solutions (mg/ml)	Mean microparticles diameter (µm)	Microparticles range (µm)
0.1	35.45 ± 20.52	13.54-107.5
0.5	31.29 ± 28.78	8.19-86.96
1.0	33.51 ± 17.99	6.29-118.38
5.0	36.45 ± 21.31	11.10-83.51
Blank	35.96 ± 30.92	11.1-39.39

The results obtained clearly showed agglomeration effects between the particles. Theoretically, the developments of droplet microfluidics should enable the generation of monodisperse and size-controlled emulsion droplets. At this point, the protocol that we adapted failed to fabricate spherical microparticles with a smooth surface, resulting production of microparticles of lower quality. We speculated that this effect resulted from the final step of microparticle preparation which involved centrifugation prior to freeze drying. The form of mechanical agitation from the centrifugation, can disturb the droplet templates and distort the shape and size uniformity of the resultant solid particles. Therefore, we further demonstrate additional steps as to get sphere and round shape with little form of debris in the fabrication process. These additional steps were further discussed in the section 2.3.3.1.

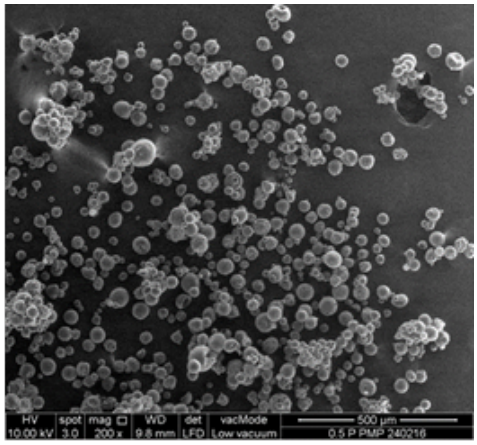
2.3.2 DCM-SIM POROUS MICROPARTICLES (PMP)

Microparticles were prepared using the general method detailed in section 2.2.4.2. SIM with different concentration was added (0.1 mg/ml, 0.5 mg/ml, 1 or 5 mg/ml) into the primary emulsion. PBS was added in the primary emulsion with the aim to create pore at the surface of the microparticles. The average particle diameter was measured from the images in Figure 2.2 using Image J software and the mean plus standard deviation (SD) was calculated as in Table 2.2. The particle size measured here are almost similar with the size of microparticles that was fabricated in the NPMP in the section 2.3.1. Here, again,

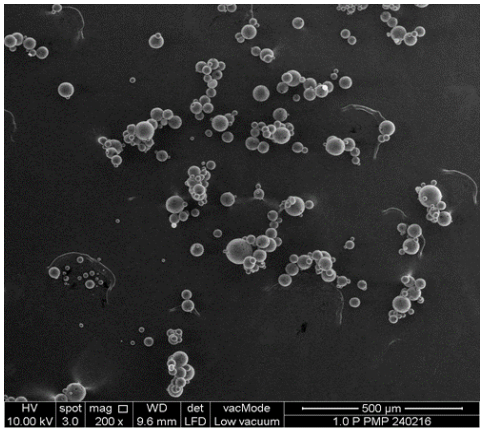
the resulting PMP fabricated showed aggregation using this protocol. However, it is important to point out that, although agglomeration effects still can be observed here, the formation of porous microspheres was achieved with the addition of PBS in the protocol. Despite the achievement in the pore formations, the pore sizes contributed to important feature in tissue regeneration. As described by other researchers, porous microspheres exhibit a greater surface area, with lower mass density, improved cell attachment and proliferation, increased the drug absorption and drug release kinetics compared to bulk microspheres (Cai *et al*., 2013). In addition, these microspheres can be assembled into three-dimensional (3D) porous scaffolds (Cai *et al.,* 2013; Li *et al.,* 2010; Perez *et al.,* 2011). Since the pores observed in PMP here can be further widen up, we prompted to investigate other porogens as to substitute PBS as the porogen agent.



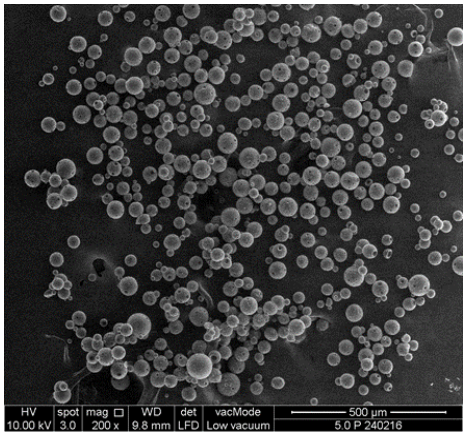
a



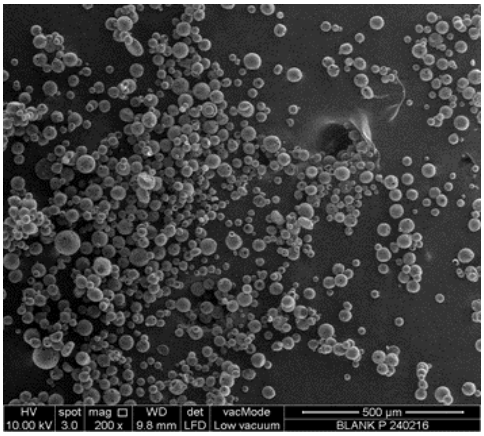
b



c



d



e

Figure 2.2: SEM images of PMP prepared using the double emulsion solvent extraction as described in section 2.2.4.2 with varying concentration of SIM (a: 0.1 mg/ml, b: 0.5 mg/ml, c: 1.0 mg/ml, d : 5.0 mg/ml, e: blank

Table 2.2: Mean diameter of (PMP) in prepared using varying concentrations of SIM diluted in the DCM.

SIM-DIC Stock solutions (mg/ml)	Mean microparticles diameter (µm)	Microparticles range (µm)
0.1	35.93 ± 22.88	22.81-67.7
0.5	30.09 ± 29.12	14.64 -58.67
1.0	37.99 ± 25.65	13.19 - 61.75
5.0	36.32 ± 30.12	10.61- 67.14
Blank	30.53 ± 31.79	12.45- 69.84

2.3.3 FACTORS THAT CONTRIBUTE TO AGGLOMERATION EFFECTS IN THE MICROPARTICLES FABRICATION

Figure 2.1 and Figure 2.2 show particles which appear to be partly collapsed and agglomerated. Based on the results observed, both NPMP (section 2.3.1) and PMP (Section 2.3.2) showed a lack of reproducibility, which means the amount of microparticles collected with the general protocol, primarily as a result of microparticles becoming agglomerated which could not then be re-dispersed. Two important factors that would account for the agglomerated effects; the properties belong to PVA and also the DCM.

PLGA as mentioned earlier, are dissolved in DCM and emulsified into an aqueous drug solution to form an emulsion. The primary emulsion is reemulsified into PVA solution (an aqueous emulsifier solution) to produce multiple water-oil-water (w/o/w) dispersion. In this study, as for organic solvent, DCM was chosen following the studies by Naito *et al*. (2014), and Nath *et al*. (2013), where a given amount of SIM was diluted in DCM for microparticle preparation. DCM, a polar organic solvent, is able to dissolve PLGA and SIM in high amounts (Oh *et al*., 2007). DCM is the most common solvent used for encapsulation using the solvent evaporation technique. This is because of its high volatility, low boiling point and high immiscibility with water (Yang *et al.,* 2000a). Its high saturated vapour pressure which is 47.4 at 21ºC (Muhaimin *et al*., 2013) as compared to other solvents (at least two times higher compared to ethyl acetate or ethyl formate which is 10 and 25.6 at 21ºC respectively

(*PubChem*) promises a high solvent evaporation rate, which shortens the duration of microsphere fabrication (Li *et al*., 2008). For the emulsifier, the semi hydrolysed PVA was chosen instead of fully hydrolysed PVA. Here, DCM acts as a barrier between the two aqueous phases, preventing the diffusion of the SIM toward the external aqueous phase.

In a normal circumstances, solidified microparticles can be collected by ultracentrifugation and washed with distilled water to remove additives such as surfactants and finally, the product is lyophilized. However, in this study, we postulated a premature polymer layer was formed instead of powdery microparticles which lead to a solid and clumped microparticles after the freeze dried process. This is true if the DCM is not completely removed (Boukari *et al*, 2016). The cause of this effect was attributed to DCM having a plasticizing effect on the polymer. The glass transition temperature of pure PLGA is 49ºC, whereas with 10% DCM present it reduces to 25°C (Li *et al*., 2002). Excess residual of DCM as a result from uncomplete washing procedure could lead to the aggregation of microparticles during the solvent evaporation stage (Murakami *et al*., 1999).

Apart from that, it is also possible that the PVA solution could be impeding the diffusion of DCM through the aqueous phase leading it to be trapped both in, and in close proximity to the organic phase. This could then lead to the lowering of the glass transition temperature of PLGA and altering its viscoelastic behaviour. This could then make it more prone to adherence to neighbouring microparticles resulting in the agglomerated mass that was observed.

Another possible explanation also involves the PVA itself playing a role in the aggregation of the microparticles. PVA is water-soluble and its degradability is enhanced through hydrolysis because of the presence of hydroxyl groups on the carbon atoms (Gaaz *et al*., 2015). Although PVA is solubilize in water, the hydrogen bonding that occurs between the hydroxyl groups in the PVA structure and water being weaker than those that form between the molecules of PVA (Sui *et al*., 2007). Therefore, as the degree of PVA hydrolysis increases its hydrophilicity decreases. A study into the effect of the degree of PVA hydrolysis on the formation of PLGA nanoparticles

postulated that hydrophobic portions of the PVA molecule are adsorbed onto the surface of the microparticles (Jaiswal *et al*., 2013), as shown in Figure 2.3. The hydration of the PVA molecules on the surface of the microparticles, which results in a stable dispersion, are more likely to be hindered when the level of hydrolysis of the PVA is high as there is a greater inclination for hydrogen bonds to form inter- and intra-molecularly rather than with water molecules. This in turn leads to the agglomeration of the particles. When the degree of hydrolysis is lower in the acetoxyl group provides steric hindrance which reduces the amount of intra and inter-molecular hydrogen bonding hence creating a dispersion which is more stable.

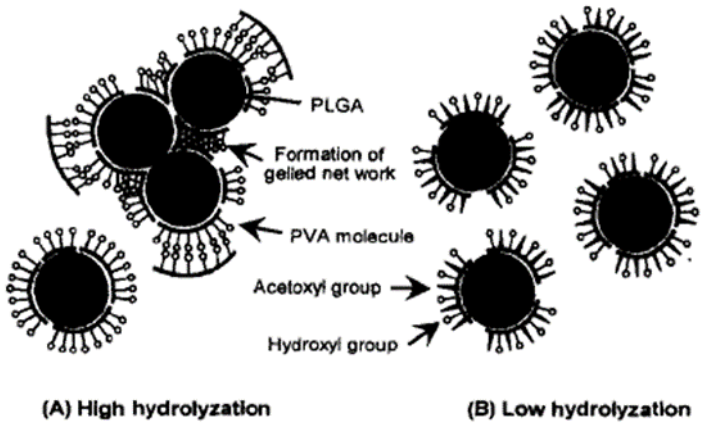


Figure 2.3: A schematic diagram showing the surfaces of PLGA nanoparticles interacting with PVA in its highly hydrolyzed form (a) and reduced hydrolysis (b) Image courtesy of Jaiswal *et al.* (2013).

To address the issue of agglomeration, we then changed the preparation method by taking into consideration of the interaction of DCM and PVA. This approach is done by eliminating the effect of uncomplete removal of PVA by adding additional washing step in the centrifugation steps.

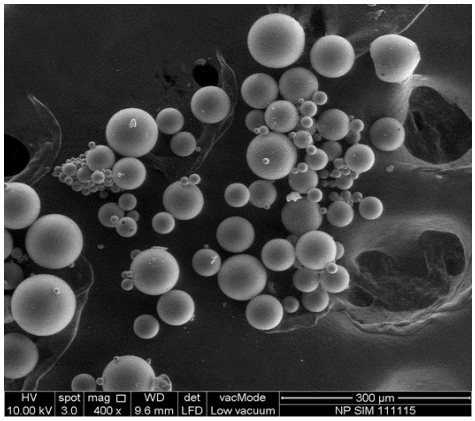
2.3.4 METHOD MODIFICATION IN MICROPARTICLES PREPARATION

2.3.4.1 DCM-SIM NPMP

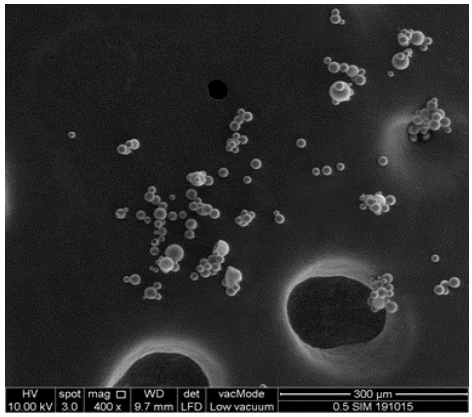
The problem of microparticle aggregation manifested in the unmodified DCM-SIM NPMP formulation is a great challenge, hence we proposed some modification to the protocol. As to collect the solidified microparticles, this is done by centrifugation and washed with distilled water to remove the PVA. Briefly, the microparticles were collected into a 20 ml tube and to this, 10 ml distilled water was added. This mixture was then centrifuged for 5 minutes at 4500 rpm, 21 °C. Upon completion, the supernatant was removed from the tube and a further 10 ml distilled water was added and the resultant mixture was centrifuged for 5 minutes at 4500 rpm.

In the previous method, we incorporated the washing steps for three times upon centrifugation. Here in the modified method, the washing steps were repeated 5 times to remove the remaining PVA from the preparation before the microparticles were subjected to drying. The sample was then poured into a 40 µm cell strainer (BD Falcon 40 µm Nylon), which was not described elsewhere, as the strainer is usually used for the preparation of porous microparticles. Sieving the microparticles in this way was found to be an effective method for collecting them and preventing agglomeration. The microparticles were stored at -20ºC for 24 hours and freeze-dried for 72 hours.

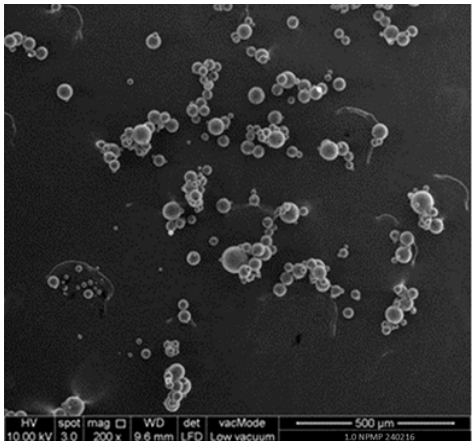
In this modification, the aim was to optimise the preparation of the microparticles that would result in a spherical shape. This can be obtained by reducing the agglomeration effect. Failure to achieve this would be indicative of a failure in microparticle fabrication. The SEM images observed (Figure 2.4) in this phase clearly showed formation of spherical morphology with very little debris formation.



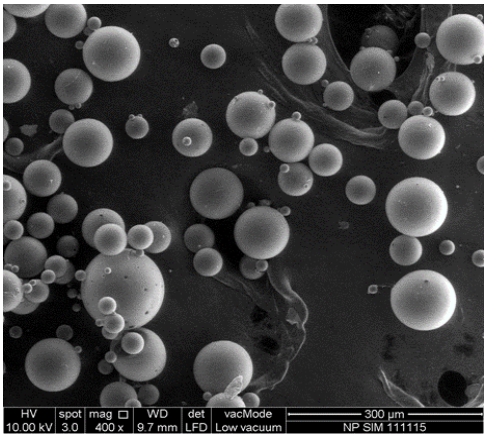
a



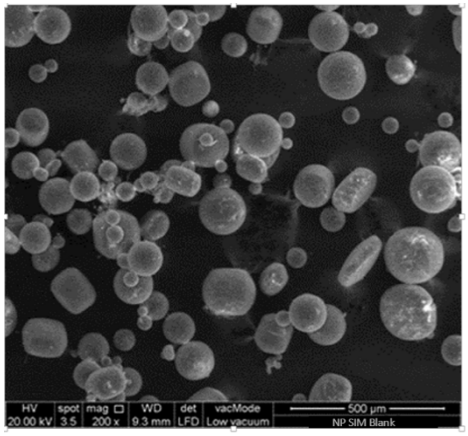
b



c



d



e

Figure 2.4: SEM images of PLGA NPMP using the modified method with varying concentrations of SIM (a: 0.1 mg/ml, b: 0.5 mg/ml, c: 1.0 mg/ml, d : 5.0 mg/ml, e: blank)

Table 2.3: Mean diameter ± SD of NPMP prepared with varying concentrations of SIM using the modified method

SIM-DIC Stock solutions (mg/ml)	Average Mean ± SD diameter (µm)	Microparticles range (µm)
0.1	25.49 ± 19.46	4.38-82.32
0.5	37.91 ± 30.08	5.69-101.31
1.0	38.97 ± 26.47	11.27-115.56
5.0	40.97 ± 20.93	11.18-124.683
Blank	50.63 ± 25.01	12.82 -129.83

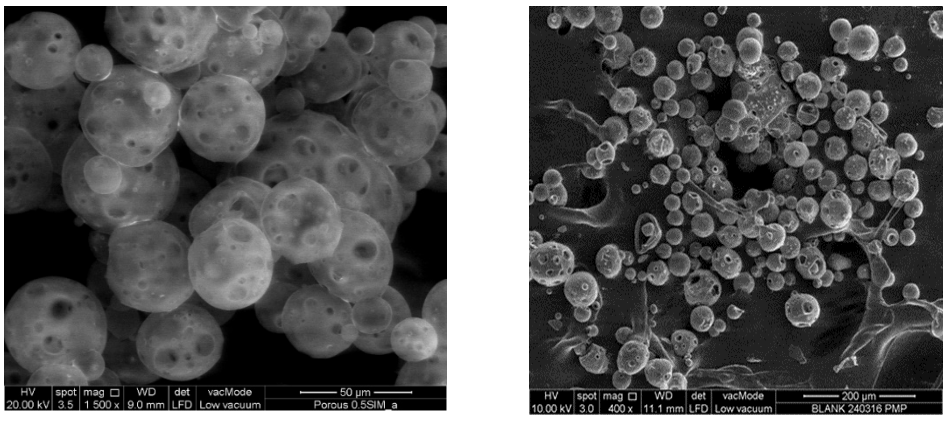
The comparatively larger average diameter recorded amongst the NPMP as compared to PMP can be attributed to the lower homogenisation speed used during the formation of the secondary emulsion: 2000 rpm for the NPMP as opposed to 4000 rpm for the PMP (Table 2.3). Interestingly, the modified method observed seems to increase in size when the concentration of SIM is added gradually from 0.1 mg/ml to 5.0 mg/ml. This prompted us to understand that the variation in particle size could also be attributed via incorporation of SIM within the NPMP. This phenomenon of variation in particle size has been observed too by other studies with regards to drug encapsulation (Chung *et al*., 2006; Ohba *et al.,* 2012). With this variation to the protocol, the agglomeration effects seemed to be reduced (Figure 2.4).

2.3.4.2 DCM-SIM PMP

The main objective of the work carried out in this section was to reduce the agglomeration effects and to increase the visibility of the pores at the surface of the microparticles. The original protocol employed PBS as a porogen which subsequently leached from the microparticles leaving the pores. Since controlling the pore structure and improving surface properties including the surface topography and chemistry, are of importance, two other porogens were identified as the substitutes for PBS; which is sodium chloride (NaCl) and sodium hydroxide (NaOH).

2.3.4.2.1 EFFECT OF SODIUM CHLORIDE (NACL) AS A POROGEN IN PMP PREPARATION

The addition of NaCl (1.71 mol/litre) 250 µl (a) and 500 µl (b) as a substitute for PBS solution as the internal aqueous phase was found to form more porous structure as compared to the microparticles treated with the PBS alone. To conserve the SIM, only the blank preparation was used to test the effect of NaCL as a porogen. It is important to note that a high porosity will be responsible for the loss of drug (Witschi *et al*., 1998; Li *et al*., 2008) whereby the drugs can escape from the polymeric matrices through the pores and cracks that were formed during the microparticle fabrication process (Yeo *et al.,* 2004). From the SEM images in Figure 2.5, the microparticles appear relatively fragile with more polymer debris present between the microparticles.



a b

Figure 2.5: SEM images of PLGA microparticles prepared with (a) 250 µl sodium chloride and (b) 500 µl sodium chloride as a porogen in a pH-controlled environment

Microparticles that were prepared with PBS as the inner aqueous phase (unmodified protocol) were found to be less porous than those prepared with NaCl solution (NaCl also act as the inner aqueous phase) when examined under SEM (Figure 2.5). This could be attributed to the lack of osmotic gradient between the inner and outer aqueous phases. However, when the inner aqueous phase was replaced with 1.71 M NaCl solution an osmotic gradient is created that favours the inflow of water into the internal droplets causing them to swell

in size and hence create pores (Figure 2.5a). When NaCl solution of the same concentration, was used along with an external aqueous phase that was composed of PVA and water, the microparticles that resulted had larger pores and were more irregular in shape. The reason behind this pore size variation could be that the osmotic gradient created by PVA in water and the inner aqueous phase is now even greater; hence an increased amount of water is encouraged to penetrate through the polymer causing the internal droplets to swell to a greater degree and create larger pores (Ahmed *et al*., 2006; Cai *et al*., 2013.

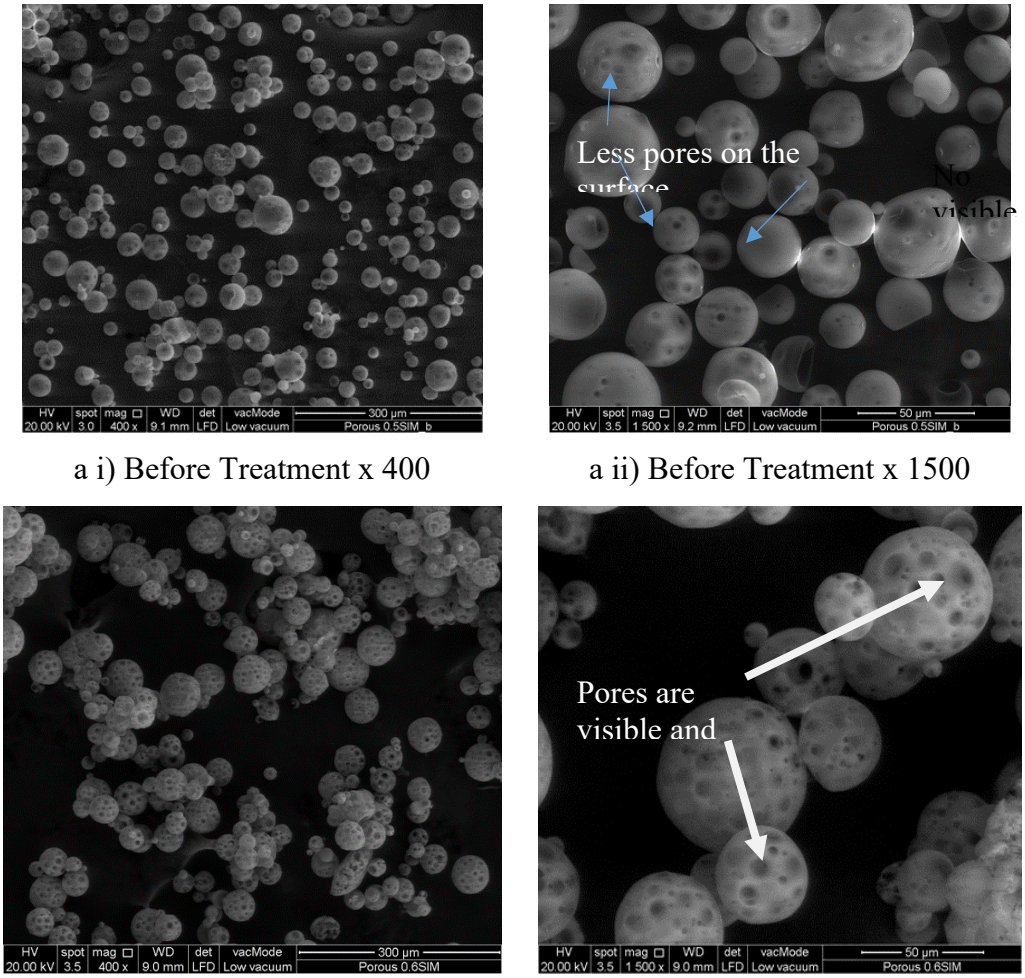
2.3.4.2.2 EFFECT OF CHILLED SODIUM HYDROXIDE (NAOH) IN THE PMP AS POROGENS

The use of PBS and NaCl in the internal aqueous phase have generated hollow microspheres with surface pores as described in Section 2.3.3.2.1. We further tested the next method in order to widen up the pores by using EtOH–NaOH. Here, the preparation is similar as explained in Section 2.2.4.2.2 which means, we still used PBS in the primary emulsion however in the final part after the washing step, the microparticles were treated with chilled EtOH-NaOH. A treatment time of 2 min was identified as optimal for increasing porosity without compromising the structural integrity of the microspheres. According to Qutachi O. *et al*., 2014, increasing the time of the treatment to 3.5 and 5 min would compromise the structural integrity of the microspheres, as surface of the microparticles cracks and induce structural damage to the microspheres

Upon 4 hours stirring, the microparticles were allowed to settle for 10 minutes, and the supernatant was removed. The microparticles were then collected into 1.5 ml tubes and washed with chilled distilled water and vortexed for 1 minute at 1000 rpm. Following that, 10 ml of chilled 30% 0.25 M NaOH :70% (EtOH) was added to observe if the pores could be effectively opened up. The mixture was vortexed at 1000 rpm for 1 minute.

From the SEM observations (Figure 2.6), the microparticles that were treated with NaOH-EtOH possessed significantly larger pores than microparticles prepared with PBS alone which was added in the primary emulsion. The pores diameters were enlarged through treatment with EtOH–NaOH and the pores seems not too hollow which make the microparticles less

fragile as compared to the treatment with NaCl (Section 2.3.3.2.1). In comparison with non-treated EtOH-NaOH, it was observed that the surface of the microparticles were less porous and some of the microparticles are with neither pore formation on their surface.



a i) Before Treatment x 400 a ii) Before Treatment x 1500

b i) After treatment x 400 b ii) After treatment x1500

Figure 2.6: SEM images of PMP prepared using the double emulsion solvent extraction method followed by treatment with 30% 0.5 M sodium hydroxide and using PBS as a porogen (a = before treatment, b = after treatment).

From the results using NaCl and chilled NaOH:EtOH, it was found that treatment with chilled 30% 0.5M NaOH:70% EtOH solution precipitated increased porosity in the microparticles as compared to NaCl treatment (Figure 2.6). In the following section 2.3.4, we next evaluated the encapsulation

efficiency of SIM in the porous microparticles using 30% 0.5M NaOH:70% EtOH solution (a modified protocol for the preparation of porous microparticles formulation).

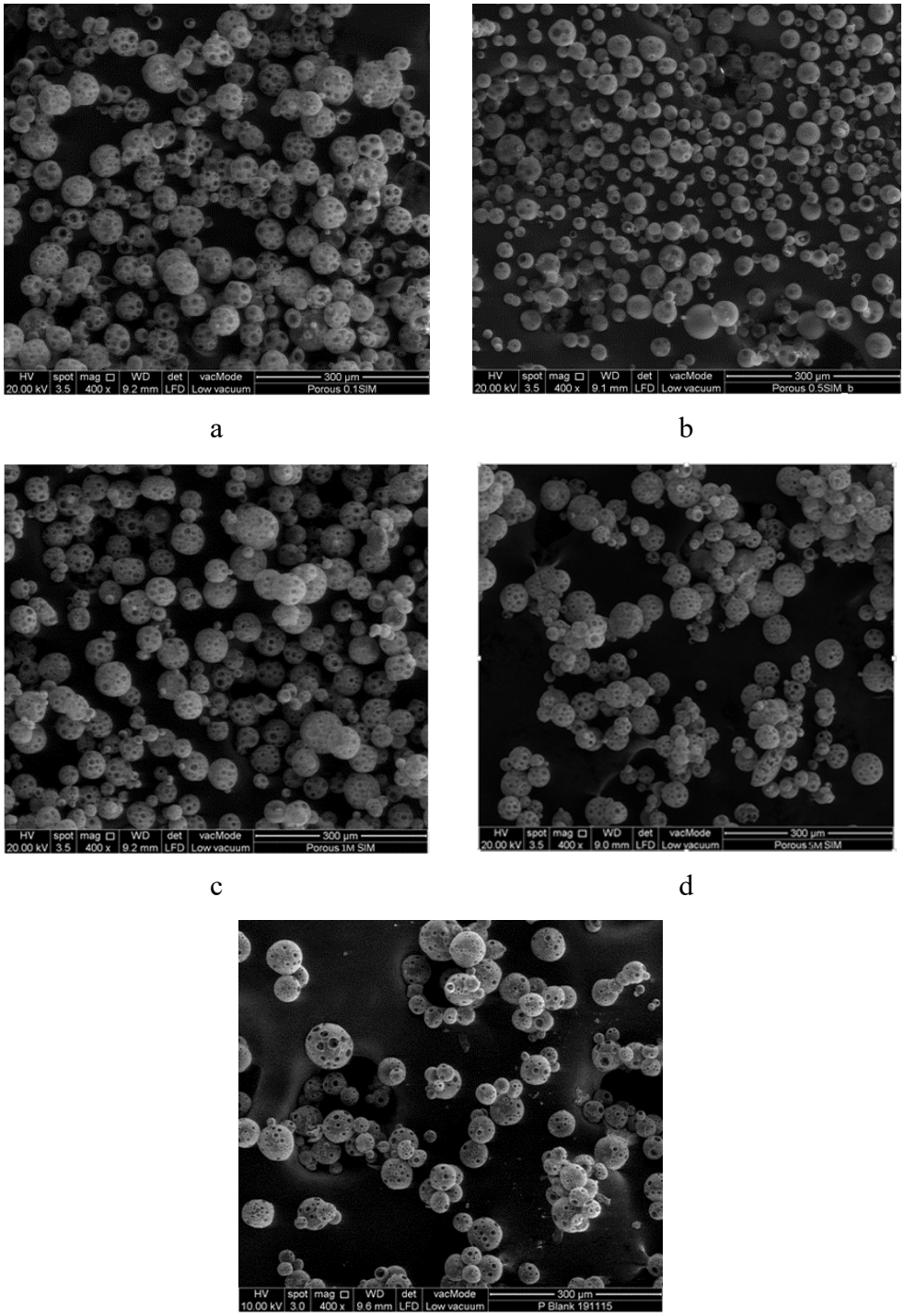
It is important to emphasise pore size in the formation of scaffolds from microparticles. The feature of scaffolds must not only have the mechanical properties, but also the porosity and appropriate pore diameter to support the formation of new tissue (Taek *et al*., 2006; Wang *et al*., 2009). In the current study, porous PLGA microspheres were fabricated with different sizes above 30 μm. This size is inacceptable for the use in scaffold preparation. Treatment with chilled NaOH-EtOH solution for 2 min was observed to increase surface porosity without causing the microsphere structure to disintegrate. This is in line with the work of Qutachi *et al*. (2014), who used a similar approach for fabricating porous PLGA microspheres. In their experiment, they used similar porous microparticles preparation in order to form a solid porous scaffolds at body temperature which capable of supporting NIH-3T3 cell attachment and proliferation in vitro. For this section, the original protocol was modified using PBS, NaCl and chilled NaOH-EtOH and it was concluded the best approach to produce porous microparticles was with chilled 30% 0.5M NaOH:70% EtOH solution.

2.3.4.2.3 INVESTIGATION OF DCM-SIM PMP-WITH CHILLED 30% 0.5M SODIUM HYDROXIDE:70% ETHANOL PROTOCOL

As we have finalised the formulation of PMP, we tested the particles size distribution of the PMP with different SIM concentration. 0.1 mg, 0.5 mg, 1.0 mg and 5.0 mg of SIM was added to the primary emulsion respectively and then the protocol outlined in Section 2.3.2 was followed. The microparticles were further washed with chilled 30% 0.5M NaOH 70% EtOH solution (Section 2.3.3.2.2). The average particle diameter was measured from the images in Figure 2.7 using Image J software and the mean and standard deviation was calculated (Table 2.4).

It was found that the overall size range of these microparticles was much lower than the unmodified method (Figure 2.7) particularly with the 0.1mg/ml and 0.5 mg/ml. The range of sizes is comparatively smaller here as compared to

the NPMP microparticles. Increase in the homogenization speed delivers greater energy to the system, resulting in an increased breakdown of the forming microparticles (Mao *et al*., 2008; Vysloužil *et al*., 2014). In addition, increasing SIM concentration in the formulation was observed to increase the range of microparticles size too which this effect was not observed in the original protocol. This could be due to increased in PVA concentration will further stabilize the system against coalescence (Mainardes *et al.,* 2008) of the emulsion and therefore led to formation of smaller microparticles when low concentration of SIM was added.



a b

c d

e

Figure 2.7: The distribution of PMP size of varying concentration of SIM (a: 0.1 mg/ml, b: 0.5 mg/ml, c: 1.0 mg/ml, d : 5.0 mg/ml, e: blank) in modified protocol treated with chilled 30% 0.5M NaOH 70% EtOH solution

Table 2.4: Mean diameter of PMP prepared using varying concentrations of SIM diluted in the dichloromethane

SIM-DIC Stock solutions (% w/v)	Mean microparticle diameter (µm)	Microparticles range (µm)
0.1	15.17 ± 9.374	4.02-38.22
0.5	27.27 ± 12.49	8.26-55.91
1.0	31.64 ± 26.47	14.12-65.89
5.0	32.75 ± 14.50	11.09-61.74
Blank	30.54 ± 16.99	10.85-67.75

2.3.5 Encapsulation Efficiency, Drug Loading and Percentage of Yield

To determine the amount of SIM that successfully encapsulated in the microspheres, the encapsulation efficiency (EE) for both PMP and NPMP was measured. EE ranged from 5.69% to 82.33% for NPMP and 1.77% to 29.87% for PMP were observed. The results clearly showed that the amount of encapsulated SIM in the NPMP was significantly higher than for the PMP. The results disclosed a maximum in NPMP could possibly be attributed to the hydrophobicity of SIM (SIM is a water insoluble drug). During fabrication process, the SIM is covalently bound to the NPMP whilst in PMP, it tends to have lower affinity due to the presence of pores within it. (Rashidi *et al.,* 2010). Secondly, it may be due to the loss of SIM during preparation to the PMP formulation (Nandagiri *et al*., 2012). The 0.1 mg and 0.5 mg SIM PMP were found to contain almost no SIM as a result of loss during fabrication as the amount used was little. However, the 1 mg/ml and 5 mg/ml SIM PMP showed an improved EE. Nevertheless, the overall EE was found to be higher in the preparation of NPMP as compared to PMP. As for PMP, SIM release was driven by the large concentration gradient of SIM between the inner cores and outer layers of the microspheres. Therefore, the NPMP exhibited advantages over the PMP in properties of encapsulation efficiency and loading capacity.

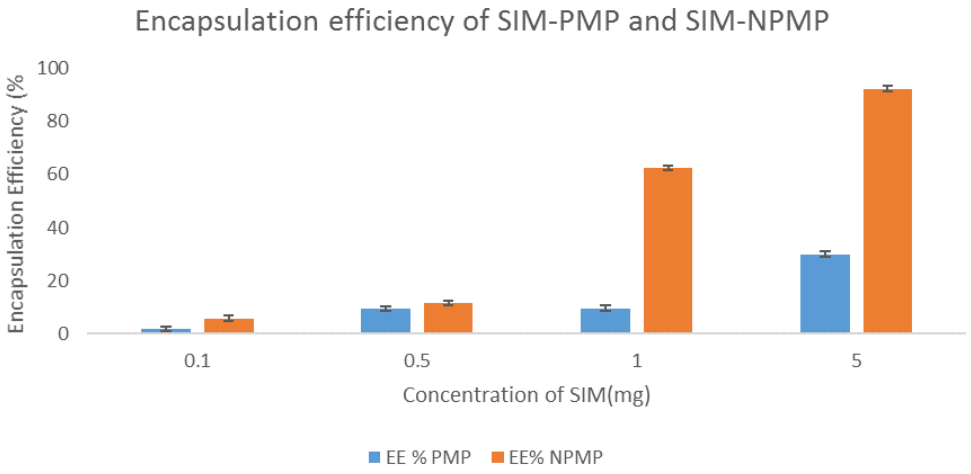


Figure 2.8: Comparison of EE in NPMP and PMP made with varying SIM concentrations

The percentage of drug loading (DL) was calculated based upon the Equation 2. In terms of drug loading, SIM loading within PLGA microparticles was increased with an increase in the initial amount of the formulation. Maximum encapsulation of SIM of above 82% was observed in 1:20 drug polymer specifically the NPMP. The ratio 1:20 was obtained from the total amount of SIM used (5 mg) and the average microparticles produced (100 mg) per single preparation. The results clearly indicate significant different in drug loading in respect to ratio of drug to polymer during the microparticles preparation. However, this correlation is true, as the amount of polymer increased, the EE will also increase. This is attributed from the viscosity of the polymer which would further delays the drug diffusion within the polymer droplets and therefore increase the encapsulation efficiency in the microparticles. The 0.1 mg/ml concentration seems too low to be encapsulated in the microparticles for both NPMP and PMP.

In terms of % of yield, microparticle formulations had high yields (Equation 3) with respect to the initial amounts of polymer and the SIM used. Overall, the PMP yield was lower that the NPMP. Although the amount of fabricated microparticles can be collected based on the % of yield calculated, it must correlate with the amount of SIM encapsulated in the microparticles. Here, it can generally explain the drug load of 0.1 mg/ml and 0.5mg/ml were too low for the encapsulation process to take place and this further affected the EE.

Table 2.5: The difference percentage of yield, drug loading and encapsulation efficiency of NPMP and PMP of different SIM amount

SIM (mg)	**% yield Mean ± SD**		**% drug loading (DL) Mean ± SD**		**%encapsulation efficiency (EE)Mean ± SD**	
	NPMP	PMP	NPMP	PMP	NPMP	PMP
5.0	75.66 ± 3.32	66.97 ± 15.60	1.36 ± 0.01	0.39 ± 0.04	82.33± 5.33	29.87 ± 0.34
1.0	64.07 ± 5.25	61.88 ± 16.40	0.86 ± 0.02	0.29 ± 0.14	62.47± 8.64	9.54 ± 0.07
0.5	62.87 ± 10.29	58.14 ± 17.13	0.02 ± 0.03	0.16 ± 0.05	11.59± 1.16	9.49 ± 0.20
0.1	60.01± 9.23	54.37 ± 5.10	-	-	5.69± 0.98	1.77 ± 0.01

2.3.6 FTIR ANALYSIS

FTIR spectroscopy was used to study the possible interactions between SIM and the polymer. There is no significant difference in the FTIR spectra of SIM (Figure 2.9) for PLGA (Figure 2.10), the SIM-loaded NPMP PLGA (Figure 2.11) and SIM-loaded PMP PLGA (Figure 2.11).

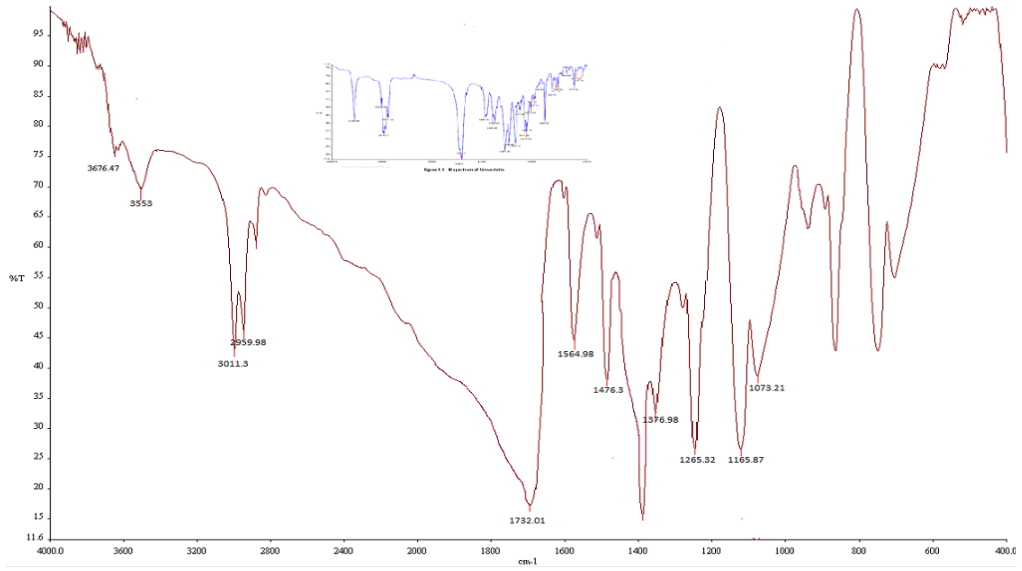


Figure 2.9: Fourier-transform infrared (FT-IR) spectra of SIM. The small figure representing the previous study by Tandale *et al*., 2011. All major peaks of SIM were observed at wave numbers 3553 cm^{-1} (free O–H stretching vibrations); 3011.3 cm^{-1} and 2999.98 cm^{-1} (C–H stretching vibrations); and 1782.01 cm^{-1} (stretching vibration of ester and lactone carbonyl functional groups) as previously observed by Tandale *et al*., 2011

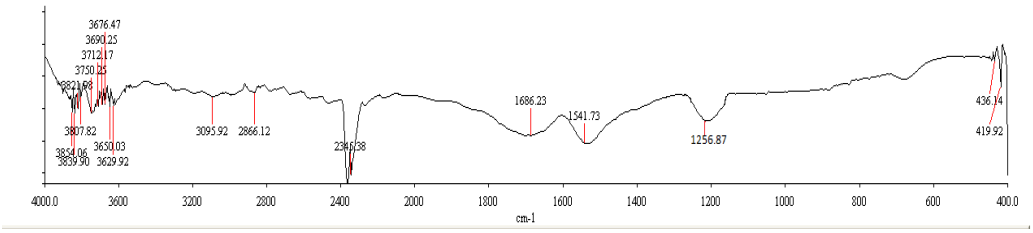


Figure 2.10: Fourier-transform infrared (FT-IR) spectra of poly(D,L-lactic-co-glycolide) (PLGA)

The PLGA spectrum (Figure 2.10) show the peaks at 3650.03 cm^{-1}, which indicate the OH stretching vibrations (3200–3600 cm^{-1}), 3095.92 cm^{-1}, 2866.12 cm^{-1} and 2345.38 cm^{-1} which indicate the CH, CH2, CH3 stretching vibrations (2850–3000 cm^{-1}). Absorption bands at 1686.23 cm^{-1} and 1541.73 cm^{-1} indicate the carbonyl C = O stretching vibrations (1900–1500 cm^{-1}) (Erbetta *et al*., 2012), and the band at 1256.87 cm^{-1} indicates the C–O stretching vibrations (1050–1250 cm^{-1}).

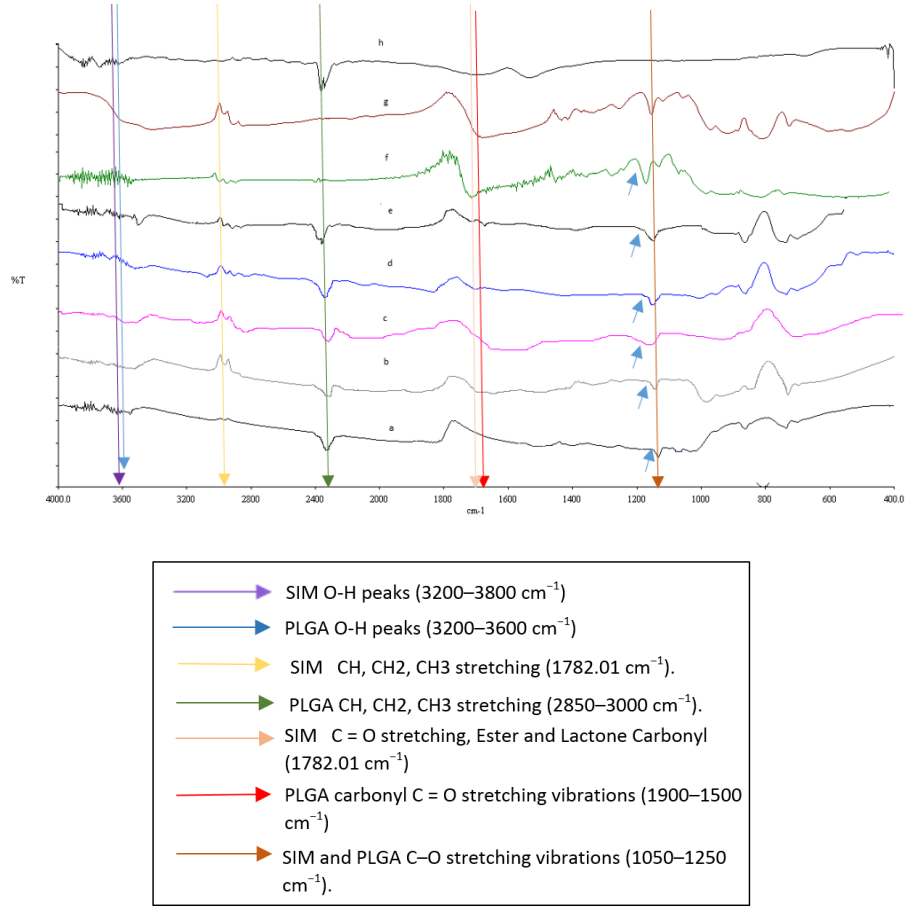


Figure 2.11: Fourier-transform infrared (FT-IR) spectra of and SIM-NPMP. a= blank, b= 5.0mg, c= 1.0mg, d=0.5, e=Blank, f= SIM, g=polyvinyl alcohol (PVA), h= poly(D,L-lactic-co-glycolide) (PLGA)

Figure 2.11 shows the spectra of the NPMP. The profile of the spectra presented are practically identical. All the major absorption bands presented in PLGA and SIM were found in the microparticles preparation. The major SIM peaks for O−H stretch vibration found between 3500- 3800 cm^{-1}. The C−H stretch vibration was found between 3000- 2700 cm^{-1} and stretch vibration of −C−O and −C=O carbonyl functional group was found between 1900-1500 cm^{-1}.

The PLGA peaks observed here are the hydroxyl OH stretching vibrations (3200–3500 cm^{-1}), the CH, CH_2, CH_3 stretching vibrations (2850–3000 cm^{-1}), the carbonyl C = O stretching vibrations (1900–1500 cm^{-1}). The absence of absorption bands between 3600 and 3400 cm^{-1} in the spectra presented in blank, which suggest the characteristic of the hydroxyl group, indicates that the blank microparticles are anhydrous.

Similarly, in PMP preparation, there is no significant difference in the FTIR spectra of pure drug, PLGA, PVA and the porous microparticles (Figure 2.12). All major peaks of SIM were observed at wavenumbers 3553 cm^{-1} (free O–H stretching vibrations); 3011, 2959, and 2872 cm^{-1} (C–H stretching vibrations); and 1714 cm^{-1} (stretching vibration of ester and lactone carbonyl functional groups) were retained in the microparticles, which clearly indicate that no interaction exists between pure drug and the polymer. The small arrow ( ) in the figure 2.11 indicates the peaks observed in the SIM spectrum which were also found in the PMP and observed between 1165.17-1170.09 cm^{-1} which indicate the presence of C- O- C asymmetric stretching (Klee *et al.,* 2007; Shinde *et al.,* 2011; Tandale *et al*., 2011).

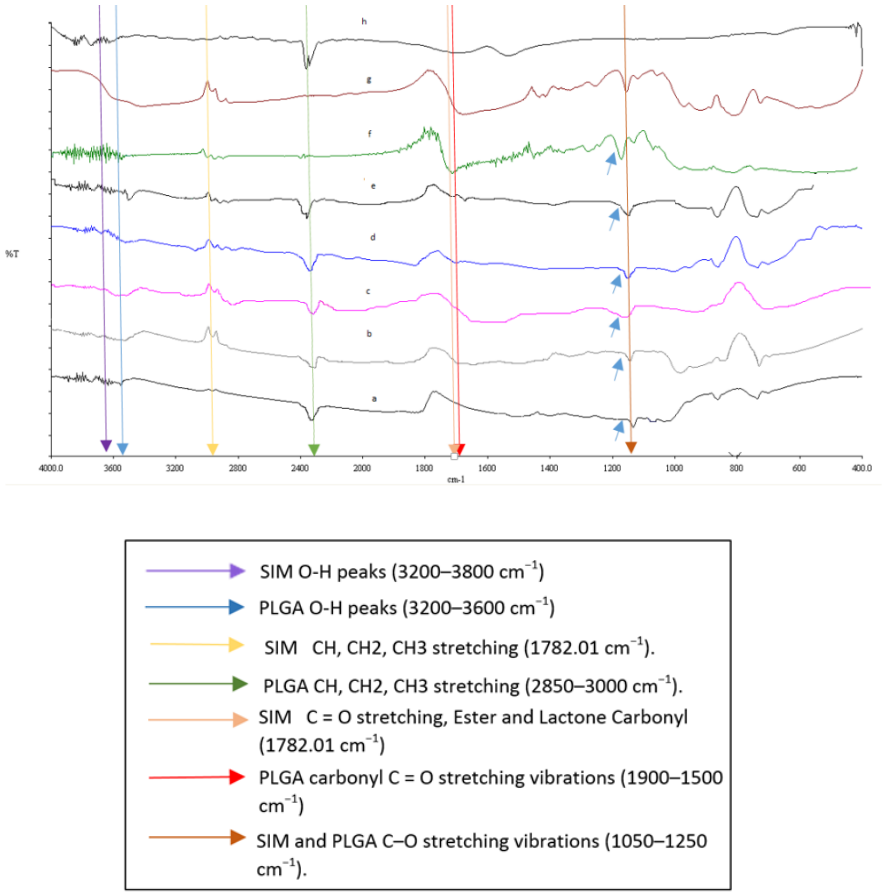


Figure 2.12: Fourier-transform infrared (FT-IR) spectra of and SIM-PMP. a= blank, b= 5.0mg, c= 1.0mg, d=0.5, e=Blank, f=SIM (SIM), g=polyvinyl alcohol (PVA), h= poly(D,L-lactic-co-glycolide) (PLGA).

IR spectroscopy has a great potential in elucidating the molecular structure of the microparticles. The IR spectrum of an organic substance is like

a fingerprint which facilitates its identification by the comparison with previously recorded reference spectra. It can also be used to identify the important structural parts of the molecules with intense vibration bands even if the substance is in mixtures or complexes (Shinde *et al.,* 2011; Shinde *et al.,* 2014; Masaeli *et al.,* 2016).

FT-IR studies were performed to detect the possible interactions between SIM and PLGA. The FT-IR spectra of pure SIM presented characteristic peak at 3552 cm^{-1} and 3749 cm^{-1} (O−H stretch vibration), 2960 cm^{-1} (C−H stretch vibration) and 1730 cm^{-1}, and 1164 cm^{-1} and 1066 cm^{-1} (stretch vibration of −C−O and −C=O carbonyl functional group).

The spectrum of PLGA showed important bands between 3800-3600 cm^{-1} (O−H stretch vibration) that were attributed to the presence of water. The absorbance at 3095.92 cm^{-1} and 2866.12 cm^{-1} indicate the CH, CH_2, CH_3 stretching vibrations (2850–3000 cm^{-1}), The 1686 cm^{-1} band indicate carbonyl group (−C=O) stretch vibration which suggest the ester and acid bond formation (Chung *et al.,* 2006; Manoochehri *et al.,* 2013).

The FT-IR spectra of the physical mixture seemed only to be a summation of drug and carrier. For both NPMP and PMP preparation, it was clearly seen from the results that there were no interactions between the drug and carrier and SIM maintained its crystallinity. If the drug and carrier interact, then the functional groups in the FT-IR spectra will show major band shifts and broadening compared to the spectra of drug and carrier.

2.4 CONCLUSION

It has been possible to prepare microparticles using modified versions of the double emulsion solvent evaporation technique. The adaptations employed involved increasing the washing time and the addition of a sieving stage after washing procedure (to produce both porous and non-porous microparticles). The possible explanation for the agglomeration that was experienced centred around plasticization of PLGA due to the inefficient removal of DCM. Secondly, it could also be due to the adsorption of hydrolyzed PVA onto the surface of microparticles and subsequent hydrogen bonding between the OH groups of adjacent PVA molecules. It was postulated that this contributed to the

agglomeration effect. This agglomeration effect was obvious and was totally resolved after the washing steps were increased (to five times instead of two times). With the increase of the washing steps and using the sieving method, the collection of microparticles was improved significantly. This can be observed during particle size measurement as there was no debris formation within the particles. More importantly, the characteristics of oval and sphere shapes of microparticles were enhanced through this method modification.

For PMP formulation, NaCl and PBS were compared as porogens. When prepared in the absence of a pH-controlled environment, NaCl led to larger pores but a more irregular microparticle shape. This characteristic may not be ideal for regenerative medicine applications due to the lack of control of microparticle shape. Thus, the future work for scaffold preparation will continue with PBS being employed as a porogen and treated with chilled NaOH-EtOH to open up the pores.

SIM, being the drug of choice in this study, can be incorporated into both NPMP and PMP. Incorporation of SIM play roles in the variation of particle size. Since 5 mg/ml concentration can achieve the maximum EE, further analysis will further incorporate this concentration as the model drug for tissue regeneration study.

Adding SIM in the PMP is thought to be realistic as the porous microparticles would act as the carrier for SIM. However, the EE found in the PMP is low as compared to EE in the NPMP. FTIR studies showed no evidence of interaction between the drug and carrier. The SEM studies revealed better images in modified methods for both NPMP and PMP preparation.

CHAPTER 3

HPLC METHOD DEVELOPMENT AND VALIDATION

3.1 INTRODUCTION

Validation is an essential part to confirm that the analytical equipment, method, or system for a specific test is suitable for its intended use. The suitability of all test methods used should always be verified under the actual conditions of use and should be well documented. Methods should be validated to include consideration of characteristics included in the International Conference on Harmonization (ICH) guidelines addressing the validation of analytical methods.

Among the analytical methods currently available, high performance chromatography (HPLC) coupled with ultraviolet (UV) detection represents one of the most common methods used for the characterization of pharmaceuticals. HPLC-UV offers a quick, sensitive and accurate method to separate and identify drugs or other analytes used in pharmaceutical nanoparticulate formulations (Fuster, 2015). In this chapter, the primary focus is on general approaches and the considerations towards the development of chromatographic methods for the separation, identification, and quantification of SIM compound, both before and after encapsulation in the microparticles.

Since the highest encapsulation efficiency was ultimately found in NPMP-SIM as compared to PMP-SIM from Chapter 2, we highlight the HPLC development and validation method in SIM-NPMP formulation.

3.2 METHOD DEVELOPMENT

3.2.1 GENERAL INTRODUCTION OF HPLC SYSTEM

A schematic of an HPLC system is shown in Figure 3.1, with emphasis on the flow path of the solvent (solid arrows) as it proceeds from the solvent reservoir to the detector (the solvent is usually referred to as the mobile phase or eluent). Upon injection of the sample, a separation will takes place within the column, and separated sample components leave (are eluted or washed from) the column—with detection in most cases is either by ultraviolet absorption (UV) or mass spectrometry (MS). The fundamental nature or ‘‘mode’’ of the separation is determined mainly by the choice of column, as summarized in Table 3.3. For sample analysis, the predominant HPLC mode in use today is reversed-phase chromatography (RPC), which features a nonpolar column in combination with a (polar) mixture of water plus an organic solvent as mobile phase.

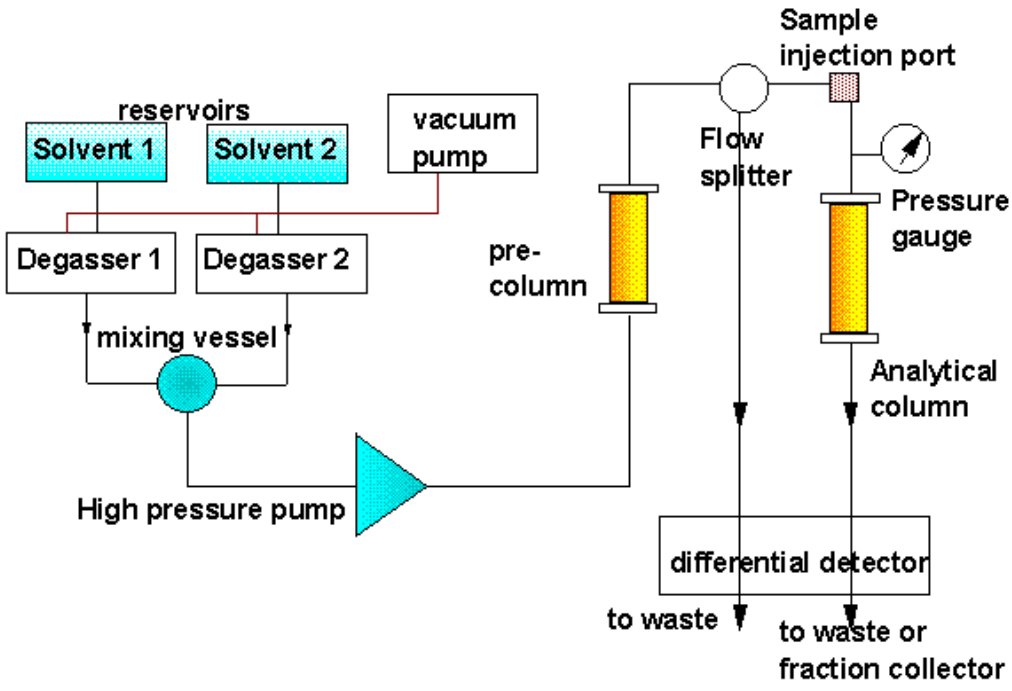


Figure 3.1: Schematic diagram of HPLC system. Image is adapted from http://elchem.kaist.ac.kr/vt/chem-ed/sep/lc/hplc.htm

An understanding of the physical and chemical characteristics of a drug allows one to select the most appropriate HPLC method development approach from the vast array of literature. Information concerning the sample, for example, molecular mass, structure and functionality, pK_a values, UV spectra and the solubility of the compound should all be compiled. The requirement for the removal of insoluble impurities in samples is important as this can suddenly render the diluent ineffective. To avoid that, it would be prudent to use a sample diluent capable of solubilizing compounds having a range of polarity. In addition, the sample should undergo different common protocols for example filtration, centrifugation, dilution or concentration to control the concentration, extraction (liquid or solid phase) and derivatization for detection should be checked (ICH Harmonised Guideline, 1997). For pure compounds, the relative solubility in water and organic solvents should be determined as this helps to select the best mobile phase and column to be used in HPLC method development. Method development in HPLC can be a laborious and time-consuming process and chromatographers may spend many hours trying to optimize a separation method. Even among reverse-phase columns, there is astonishing diversity, owing to differences in both the base silica and bonded phase characteristics. Many of these columns show unique selectivity. The objective of validation of an analytical procedure is to demonstrate that it is suitable for its intended purpose. and this validation is required mainly by regulatory agencies at certain stages of the drug approval process.

SIM which is detailed in Chapter 1, is a drug that belongs to the statin family; these are prescribed to lower cholesterol in patients with hypercholesterolemia. This semi synthetic drug undergoes hepatic first-pass metabolism by inhibiting 3-hydroxy- 3- methylglutaryl coenzyme-A reductase (HMG- CoA) and reduces low-density lipoproteins (Guan *et al.,* 2015; Lennernas *et al.,* 1997).

Various methods such as HPTLC (Rosegay *et al.,* 1990) electrokinetic chromatography and voltammetry (United States Pharmacopoeia, 2002) have been reported. Based on different techniques several methods such as high performance liquid chromatography/mass spectrometry (LC/MS) (Patel *et al.*, 2008; Nirogi *et al.*, 2007), gas chromatography/mass spectrometry (GC/MS)

(Sirén *et al*., 2014; Alakhali, 2013) and HPLC (Reddy *et al*., 2014; Silva *et al*., 2012; Dixit *et al*., 2010; Guzik *et al*, 2010; Nováková *et al*, 2008; Kromidas, 2006) have all been developed for the analysis of SIM. Due to the availability of equipment the analytical methods involving LC/ MS and GC/MS were discounted and SIM method development continued with an Agilent 200 Series HPLC instrument.

The USP method for SIM tablets (30-NF25) employs HPLC with UV detection at 238 nm. SIM elutes at about 10 min on a 250 mm×4.6 mm L1 column with an isocratic mobile phase containing 35:65 (v/v)38 mM phosphate buffer (pH 4.5): acetonitrile flowing at 1.5 mL/min. The USP method requires the chromatographic performance to meet the following criteria: Asymmetry < 2.0; Precision (Peak area %RSD, n = 3),2.0%. (United States Pharmacopeia 30). With this data, we outlined the development of the HPLC analytical methods specifically for SIM detection in the microparticles.

In this study, the development of the HPLC analytical method comprised of the following four steps described below. Step 1, selection of the preliminary HPLC method based on the data available in the literature for the particular analyte. In this stage, the basic parameters are chosen, such as how the sample is prepared, the mode of chromatographic retention time, the type of elution (gradient / isotonic) and the type of detector employed (Guidelines, 2017). Step 2 entails the selection of chromatographic conditions to retain the drug, in this case SIM. These conditions include the mobile phase (MP) composition and the flow rate that is used (Shabir *et al.,* 2004). Step 3 aims to achieve the optimum resolution within the minimum run time; hence parameters such as column dimensions, packing particle size, run time, and flow rate are optimized in this step (ICH Guidelines, 2017). Finally, step 4, is the method validation stage which is performed to ascertain the reliability and reproducibility of the analytical method (Shabir *et al.,* 2004; Al-Khadeer *et al*., 2018; WHO, 2017).

3.2.2 COLUMN SELECTION

The physical properties of the target molecules (analytes) determine the most suitable HPLC column for a given separation. The molecular characteristics that impact HPLC column selection include hydrophobicity/hydrophilicity, intermolecular forces (particularly dipole-dipole), intramolecular forces (ionic), and size. HPLC column separations can often exploit multiple differences in the molecular properties of the target molecules. Generally, the structure and chemistry of the HPLC column packing (stationary phase) determines the analyte elution profile. The use of smaller-diameter beads generally results in improved separation sensitivity due to the increased surface area. However, column pressure increases as bead diameter is reduced for a given flow rate, placing a practical lower limit on bead size. A 250 mm column containing 5 μm particles is the most common column that has been regularly used in normal HPLC analysis for SIM. However, some other studies used the 150 mm column in their SIM analysis study (Table 3.3).

3.2.3 MOBILE PHASES COMPOSITION AND ELUTION METHOD

HPLC analytical methods should ideally be simple, utilize common stationary phases and MP. The mobile phase in reversed phase HPLC usually consists of water/aqueous solution (commonly an aqueous buffer) and an organic modifier. When ionizable compounds are analysed, buffer and other additives may be present in the aqueous phase to control retention and peak shape. (http://www.chromacademy.com/index.html).

The elution order of solutes in HPLC is governed by polarity. For a normal-phase separation, solutes of lower polarity spend proportionally less time in the polar stationary phase and are the first solutes to elute from the column. Given a particular stationary phase, retention times in normal-phase HPLC are controlled by adjusting the mobile phase's properties. For example, if the resolution between two solutes is poor, switching to a less polar mobile phase keeps the solutes on the column for a longer time and provides more opportunity for their separation. In reversed-phase HPLC the order of elution is the opposite of that in a normal-phase separation, with more polar solutes eluting first. Increasing the polarity of the mobile phase leads to longer retention times.

Shorter retention times require a mobile phase of lower polarity (https://chem.libretexts.org)

Different buffers such as potassium phosphate, sodium phosphate and acetate were evaluated for system suitability parameters and overall chromatographic performance. Effect of pH is also another important parameter in separating the analytes. If analytes are ionisable, the proper MP pH must be chosen based on the analyte pKa so the target analyte is in one predominate ionization state.

3.2.4 THE DIFFERENCE BETWEEN ISOCRATIC AND GRADIENTS

Isocratic elution is the term used when the composition of a mobile phase system in an HPLC analysis remains constant throughout the separation of the analytes. That means, it is a separation that employs a single solvent or solvent mixture of constant composition. Gradient elution is whereby two or more solvent systems that differ significantly in polarity are employed. After elution is begun; the ratio of the solvents is varied in a programmed way, sometimes continuously and sometimes in a series of steps. Separation efficiency is greatly enhanced by gradient elution (Barkovich, 2015). The advantage of gradient elution is that is that the run time can often be reduced and improved resolution can be obtained. Maintaining the same proportion of solvents in a mobile phase system for HPLC analysis of compounds with different solvent solubilities requires a long run time, sufficient to allow the interaction of hydrophobic analytes with the stationary phase prior to their elution or partitioning back into the mobile phase. Conversely, by changing the ratio of the organic modifier and the gradient shape various compounds of differing polarities can interact faster with the stationary phase producing shorter retention times.

In general, isocratic or gradient elution can be used for separating a mixture of analytes and provided that all other conditions are optimal, peak resolution can be maintained through both approaches. This choice of whether to use an isocratic or a gradient method can therefore be based upon the results from preliminary studies as well as an assessment of the polarity range of the analytes in question. In reverse-phase HPLC non-polar compounds interact strongly with the stationary phase resulting in long retention times; gradient

elution is therefore often a better choice for the analysis of polar and non-polar compounds since this has the ability of allowing for a shorter run time while also ensuring that the peaks are well resolved. In this study, we used isocratic method in determining the SIM in the microparticles. Further detail of this method will be described in Section 3.3.

3.3 MATERIALS AND METHODS

3.3.1 MATERIALS

Materials that are required for validation of HPLC include Acetonitrile and Methanol (HPLC grade) and asolute alcohol purchased from R&M chemicals, UK. Acetic Acid and SIM (analytical grade) purchased from Sigma Aldrich (St.Louis, USA), These materials are mainly used as the mobile phases in the validation HPLC process. The ratio of each solvent was further described in the section 3.4.

3.3.2 METHODS

3.3.2.1 HPLC METHOD DEVELOPMENT

3.3.2.1.1 INSTRUMENTATION AND CHROMATOGRAPHIC CONDITIONS

The HPLC analysis were performed on the Agilent HPLC system (Series 200 auto-sampler, Series 200 UV/VIS detector, Waltham, MA, USA) configured to TotalChrom® Navigator software was used for sample validation. A Hypersil gold® C18 (150 x 4.6 mm, 5 μm) column (Thermo Scientific, USA) with temperature at 45°c was employed.

The method of Nandagiri *et al*. (2012) was first adopted as a starting point in validating SIM. Maximum wavelengths for SIM is 238 nm (Alakhali K.M. 2014) therefore in the optimization process, the detection was set at 238 nm. Selection of columns were carried out as to choose the best column to use for the entire studies. Table 3.2 depicted previous studies with regards to different type of columns that had been used to analyse SIM encapsulated microparticles. In order to confirm the performance of the C18 (150 x 4.6 mm, 5 μm), we calculated the HPLC transfer using the software adapted from Guillarme *et al*. (2008) which is also known as USP method. The method transfer calculator outputs the transferred column flow rate and transferred column injection volume; it also calculates the expected improvements in separation efficiency and analysis time. Figure 3.2 displays the inputs and outputs for the USP method, with the outputs backhanded in light blue. This calculator served

as the guideline for us for the selection of flow rate, injection time and expected analysis time for the C18 (150 x 4.6 mm, 5 µm) column from the commonly used C18 (250 x 4.6 mm, 5 µm) column in SIM analysis.

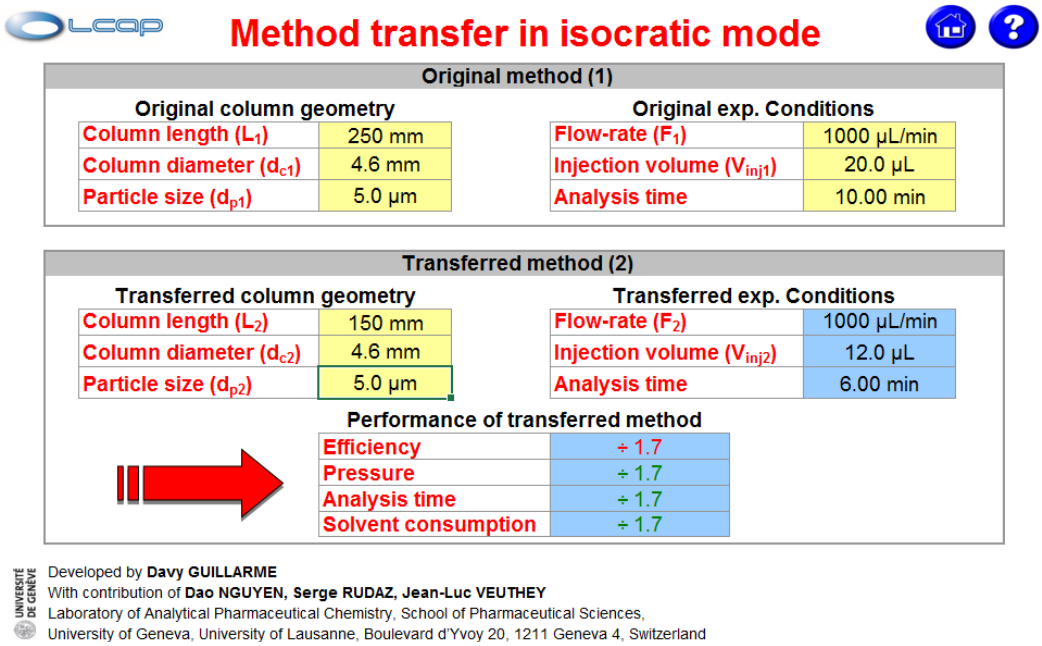


Figure 3.2: Online Transfer calculator outputs which can calculate the expected flow rate, injection volume, analysis time of the new column.

For the mobile phase, we tested two types of solvents which was either methanol (MeOH) or acetonitrile (ACN) to 0.25 acetic acid diluted in water in ratio based. These solvents were prepared according to ratio as to find the best resolution peak. The ratio tested were 60:40, 70:30 and 80:20 based on the previous study in Table 3.3. A flow rate of 1 mL/min in isocratic mode was used and the sample volume was 50 µl with the UV /VIS detector set at a wavelength of 238 nm. The flow rate of 1 mL/min was chosen based on the USP method. Retention times were calculated as mean values of three replicate determinations. The column was flushed with methanol at a flow rate of 3 mL/min for 15 min prior to the analysis of each set of three samples.

3.3.2.1.2 PREPARATION OF CALIBRATION AND VALIDATION STANDARD SOLUTIONS

A stock solution of SIM (0.1 mg/mL) was prepared by dissolving 1 mg of SIM in 1000 mL of methanol. Calibration curves were constructed by diluting the stock solution with water to eight final concentrations 4, 8, 10, 20, 40, 60, 80 and 100 μg/mL constituting the calibration standard solutions. These eight dilutions were prepared in triplicate to obtain three independent series of calibration standard solutions.

3.3.2.1.3 PREPARATION OF SIM-LOADED PLGA MICROPARTICLES

In Chapter 2, the encapsulation efficiency was found to be the highest in preparation of SIM-NPMP microspheres loaded with 5 mg of SIM. In order to measure the exact amount of SIM in the microparticles as compared to the theoretical SIM that has been added in the microparticles HPLC analysis need to be carried out. 1 mg NPMP-SIM was accurately weighed and dissolved in 1 mL of methanol in a 1 ml centrifuge tube and centrifuged for 10 minutes (mins) at the speed of 10,000 RPM. The samples were filtered and diluted to (100 μg/mL) and subjected to HPLC for quantification.

3.3.2.2 HPLC METHOD VALIDATION

All the HPLC methods that were developed for the SIM were validated according to ICH guidelines (ICH, 1994). The validation criteria includes measures of linearity, precision, accuracy and limits of detection and quantification. The number of replicates for both interday and intraday analysis was five. Each method validation criterion is detailed in following subsections.

3.3.2.2.1 SPECIFICITIES

The specificities of the analytical methods were based on individual observations of the chromatograms obtained for the analytes in different solvents. The peaks for SIM must ideally be sharp. Specificity studies are crucial in excluding peak interferences from other substances which were present in the microparticles, ascertaining that the drug in the microparticles elute similarly as pure drug solutions and that the co-elution or other substances of the drug is not affected by the mobile phases or other interference.

3.3.2.2.2 LINEARITY

The linearity of response was assessed over the range 100–10µg/mL. A stock solution of SIM was prepared using methanol. The stock solution was further diluted with methanol yielding concentrations of 100, 50, 25, 10, 8, 6, 4, and 2 µg/mL (Table 3.1). Three individually prepared replicates at each concentration were analysed The resultant area under the curve (AUC) on the chromatograms were plotted against the sample concentration. The linearity was confirmed by calculating the coefficient of regression on five consecutive days , with three runs each day.

Table 3.1: SIM serial dilution for HPLC validation analysis.

SIM dilution	S	D1	D2	D3	D4	D5	D6	D7
Concentration (µg/ml)	1000	800.00	600.00	400.00	200.00	100.00	10.0	5.0

*S=Stock solution.

3.3.2.2.3 PRECISION

Intraday and interday precision was determined with three quality control (QC) drug concentrations (n=3), representing high, medium and low concentrations. The AUC was determined, to inspect the precision of the method at high, medium and low drug concentration. Results were presented as relative standard deviation (%).

$$\% \text{ RSD} = \frac{\text{Mean Concentration}}{\text{Standard deviation}} \times 100\% \quad \text{.....Equation 3.1}$$

3.3.2.2.4 ACCURACY

Accuracy is defined as the closeness of the agreement between the result of a measurement and a true value. Both intraday and interday accuracy were determined. As with the precision determination, high, medium and low QC drug concentrations were analysed for intraday (n=3) and interday (n=3) accuracy. Results were calculated and presented as percentage relative error, %.

$$\text{Absolute Error} = \text{Measured value} - \text{Actual value} \quad \ldots\ldots \text{ Equation 3.2}$$

$$\text{Relative Error} = \frac{\text{Mean absolute error}}{\text{True concentration}} \times 100\% \quad \ldots\ldots \text{ Equation 3.3}$$

3.3.2.2.5 RECOVERY

The recovery of an analyte in an assay is actually refer to the detector response obtained from an amount of the analyte added to or extracted from the matrix, compared to the detector response for the true concentration of the pure authentic standard. In his study, the recovery of SIM which was retrieved from the microparticles was investigated by comparing the peak signal of pure SIM. Investigation were carried out in three individual validation concentrations. Each validation consisted of five replicates and data was presented as % recovery and calculated as follows:

$$\% \text{ Recovery} = \frac{\text{Mean concentration of drug in microparticles}}{\text{Mean of concentration of pure drug solution}} \times 100\%. \text{ ..Equation 3.4}$$

3.3.2.2.6 LIMITS OF DETECTION AND QUANTIFICATION

For a linear calibration curve, it is assumed that the instrument response y is linearly related to the standard concentration x for a limited range of concentration. It can be expressed in a model using this equation; y = a +bx. With this model, it can also be used to compute the sensitivity b and the limit of detection (LOD) and limit of quantification (LOQ) (Shrivastava, A.*et al*., 2011).

The detection limit of an individual analytical procedure is the lowest amount of analyte in a sample which can be detected but not necessarily quantitated as an exact value. The sensitivity of the SIM analysis was assessed in terms of the LOD, the lowest amount of the analyte in a sample that can be detected but not necessarily quantified. The detection limit is determined by the analysis of a sample of known concentration of analyte and by establishing the lowest concentration level at which the analyte can be calculated based on peak height to the baseline ratio. LOD can be calculated as follows:

$$\text{LOD} = \frac{3 \times \text{SD of the LC}}{\text{Slope of the concentration}} \qquad \text{…….. Equation 3.5}$$

The LOQ is the amount of analyte in a sample that can be quantified with acceptable precision and accuracy under the stated operational. The LOQ is determined by the analysis of samples with known concentrations of analyte and by establishing the minimum level at which the analyte can be quantified with acceptable accuracy and precision. The LOQ can be calculated as in Equation 3.5.

$$\text{LOQ} = \frac{10 \times \text{SD of the LC}}{\text{Slope of the concentration (S)}} \qquad \text{……. Equation 3.6}$$

3.4 RESULTS AND DISCUSSION

3.4.1 SELECTIVITY AND SYSTEM SUITABILITY

The proposed analytical methodology was developed to provide a simple, reproducible and rapid RP-HPLC-UV method for the simultaneous detection and quantification of SIM in biodegradable PLGA microparticles. During the development of the analytical procedure, several chromatographic parameters were investigated such as composition, pH and flow rate of mobile phase, as well as the chromatographic column and temperature of analysis. The aim was to develop a system that obtained peaks with baseline separation, symmetry and shape, together with acceptable retention times.

3.4.1.1 MOBILE PHASE SELECTION

In HPLC method development, one of the most important criteria is choosing the elution mode, isocratic or gradient elution. Table 3.1 shows previous studies which have used HPLC to quantify SIM in microparticles or nanoparticles.

Gradient elution is usually used for the analysis of multi-component samples of wide-ranging polarities (Alkhader, 2018) to enable separation over shorter run times (Barkovich, 2017). However, isocratic elution can be simpler, easier to transfer between columns, instruments and laboratories (Schellinger *et al.,* 2006), maintain constant flow rate and provides better reproducibility (Alkhader, 2018).In this study, samples will contain only one component, thus, an isocratic elution method was selected. A majority of the analytical methods listed in Table 3.3 are also isocratic in nature.

Table 3.2: Comparison of studies using different mobile phases

Column	*Mobile Phase*	*Elution*	*Additional compound in the particles*	*Flow rate (ml/min)*	*Wavelength (nm)*	*Temperature °C*	*Retention time (min)*	*Reference*
C 8, 5µm, 3.9 mm 150 mm	MeOH: Water (80: 20 v/v), pH adjusted to 5.5 using H_3PO_4 1 M	Gradient	Q10	1.5	238 (SIM) 275 (Q10)	45	3.84 (SIM) 8.72 (Q10)	Clementino A. *et al*.,(2018).
Phenomenex AQUA C18 150 mm × 4.6 mm, 5 mm	ACN:H20 + 0.1% Acetic acid (60:40 v/v)	Isocratic	NS	1.0	248	NIL	NIL	Rashidi, H. *et al.,* (2010)
Phenomenex ® 100 C18, 5 mm, 250 mm × 4.6 mm.	Acetonitrile:50 mM potassium di-hydrogen phosphate buffer (65:35, v/v), pH adjusted to 4.5 ± 0.1 with phosphoric acid solution.	Isocratic	PLGA	1.0	NIL	45		Nandagiri, V. K., Muttu et al. (2012) Gentile, P et al. (2016)
C18 NS	Acetonitrile: water with 0.1% trifluoroacetic acid (70:30 v/v)	Isocratic	PLGA	1.0	240	NS	NS	Edalat, F. *et al*., (2012).
C12 Phenomenex, USA 150 × 4.6 mm, 300 Å,	0.05 mM phosphate buffer at pH 3.0/acetonitrile (30:70 v/v)	Isocratic	fibroin/alginate beads	1	238	NS	NS	Ungaro, F. *et al*. A (2017)

NIL	NS	NS	NS					Tai, I. C *et al* .,(2013)
Zorbax C18 analytical column 200 × 4.6 mm	Acetonitrile: 25 mM sodium dihydrogen phosphate solution (70/30%, v/v)	Isocratic	silica/sucrose composite	1	NS	40	NS	Zhang, Y. *et al*., (2013)
C18-Hypersil 100 mm x id × 3.9 mm	Acetonitrile: Formic acid 3 Mm (51: 49% v/v)	Isocratic	NS	1	238	25	NS	Alakhali K. M. *et el.,* (2014)

NS = Not stated, °C = degree celsius, mins=minutes, v/v= volume per volume.

As explained in the method section 3.3.2.2, The method of Nandagiri *et al.* (2012) was first adopted as a starting point in validating SIM. Here, the mobile phase consisted of Acetonitrile (ACN) and 50 mM potassium di-hydrogen phosphate buffer (65:35, v/v). Maximum wavelengths for SIM is 238 nm (Alakhali, 2014). Figure 3.3 a show the chromatogram for SIM (100 µg/ml), under the chromatographic conditions as described above. The chromatogram shows a broad, unsymmetrical SIM peak therefore this analytical method was not further optimized. We tried to improve the chromatogram by adopting Rashidi H. *et al.* (2010) (Table 3.1) however the chromatogram was slightly broadened (Figure 3.2). We further modified the composition with the mobile phase ratio was set at 70:30 v/v ACN and water (0.2% acetic acid, pH 4.0), flow rate 1.0 ml/min. Upon optimization, the chromatogram in Figure 3.3 b clearly shows a sharp and fairly symmetrical SIM peak eluting at 2.967 min, however, validation of the analytical method was necessary and will be further discussed in the validation method under section 3.4.2.

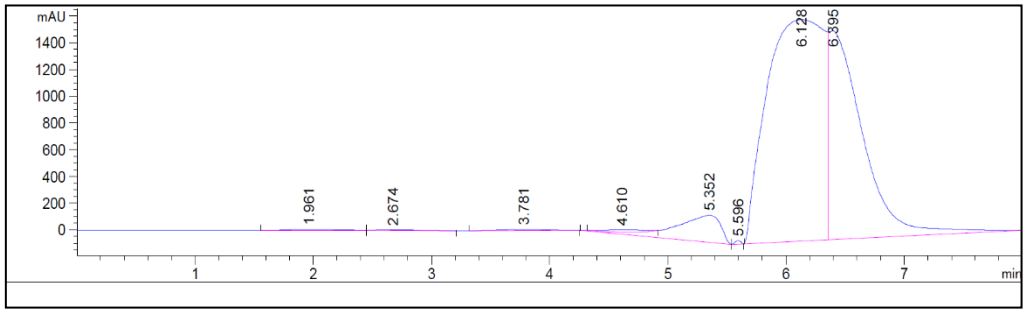


Figure 3.3 a: HPLC chromatogram of SIM of acetonitrile and 50mM potassium di-hydrogen phosphate buffer (65:35, v/v).

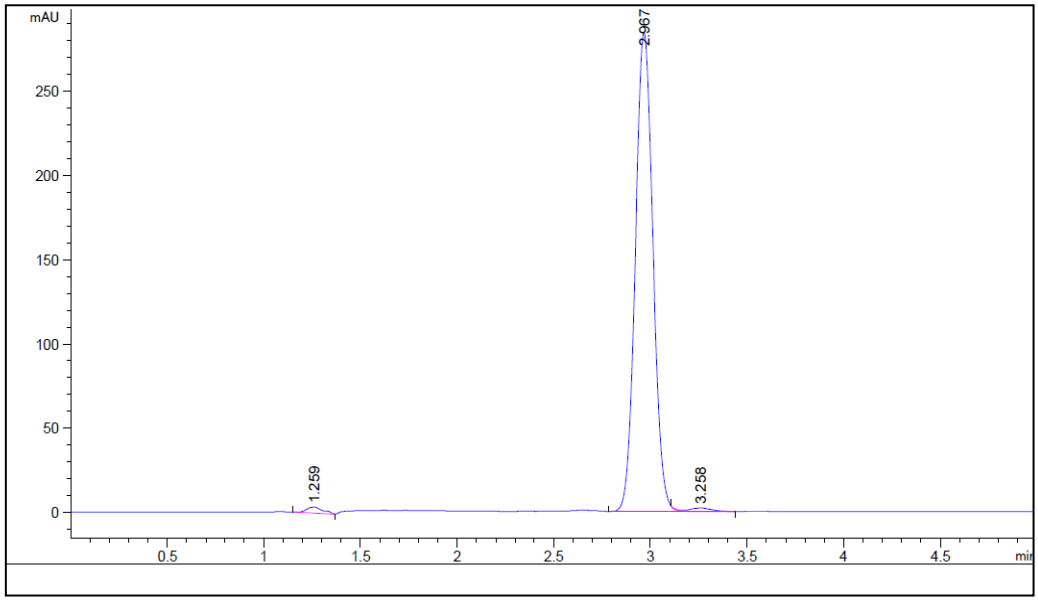


Figure 3.3 b: HPLC chromatogram of SIM using a mobile phase of ACN70:30 v/v and water (containing 0.2% acetic acid pH 4.0).

3.4.2 HPLC METHOD VALIDATION

The present method which was developed in section 3.3.2.1, (ACN : H_2O 0.2% acetic acid, pH 4.0 ((70:30 v/v)) into the mobile phase composition), flow rate 1.02 ml/min. and validated in accordance with ICH guidelines determining the following parameters: selectivity/specificity, linearity, detection and quantification limits, repeatability and intermediate precision and accuracy. The method was then applied to the quantification of SIM released from the microparticles and further used for encapsulation efficiency in the SIM-NPMP.

3.4.2.1 SPECIFICITY

Specificity is crucial in analytical method development and validation to ascertain that the analyte in question is actually the one that is being quantified. In this regard, SIM was dissolved in methanol (MeOH) and injected onto the HPLC system to obtain the individual retention time. To optimize the peak shape and separation between compounds, a stationary Thermo-scientific column (C18, 150 mm x 4.6 mm, 5 µm). A water and acetonitrile mobile phase was used with the pH adjusted to 4.0 acetic acid 0.2% (from 30:70 % v/v) while methanol was used as the diluent for the sample standards. To confer a desirable peak shape, with reduced tailing, the chromatographic column the analysis was

performed at 40 °C. Figure 3.3 b illustrates the chromatogram obtained when pure drug solution containing 100.0 µg/ml were injected. The SIM retention time was at 2.67 min.

3.4.2.2 DETECTION OF SIM FROM THE EXTRACTION IN THE MICROPARTICLES

SIM were extracted from microparticles as described in Section 2.2.6. A similar chromatographic protocol was employed in order to determine the retention time and peaks that appeared as explained in section 3.3.2.1. Obtain peaks is depicted in Fig. 3.4 a for 5 mg of SIM-NPMP and Figure 3.4 b for blank microparticles. A well-resolved and symmetrical peak with a retention time of approximately 3 minutes was observed using this method. . Under the proposed chromatographic conditions, no interference was observed at the retention time corresponding to SIM.

A

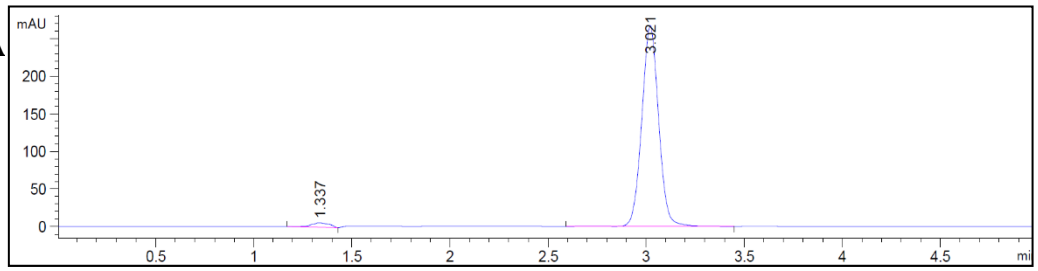


Figure 3.4 a: HPLC chromatogram of NPMP containing SIM using the method described in Section 3.4.1.1.

B

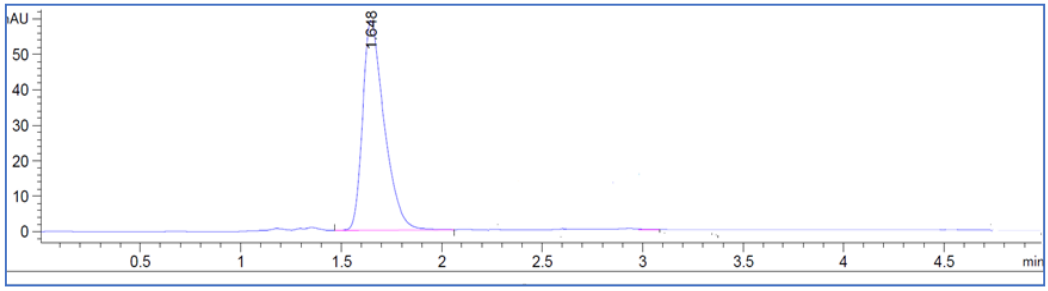


Figure 3.4 b: HPLC chromatogram of blank NPMP using method described in section 3.1.1.4

3.4.2.3 LINEARITY AND RANGE

For the determination of linearity, the response function was firstly used. The linearity was constructed by plotting the AUC of the main peak versus SIM concentration. Sample solutions were dissolved in MeOH and subsequently were injected in duplicate. A calibration curve was plotting using average AUC versus known SIM concentrations in a range of 4 to 50 µg/ml. The resulting regression equation was $y = 7.44x + 56.89$; $R^2 = 0.9994$. A R^2 of 1 indicates that the regression predictions perfectly fit the data. The linearity results revealed that the drug concentration was directly proportional within the specific concentration interval. The square of correlation coefficient (R^2) values over the acceptance criteria (> 0.9994) indicate a very high level of correlation between the concentration of the analyte and the peak area response provided by the detector. Thus, this HPLC method can be considered to show adequate linearity over the concentration range for quantitative analysis of SIM under the expected experimental conditions. Table 3.4 depicted the details of linearity studies in this work.

Table 3.3: The linearity, quantification, and detection limits observed for the HPLC method outlined in Section 3.4.2.3

Range of Linearity (µg/mL)	Peak area (mean, n=3) *
50	429.36
40	359.632
30	272.332
20	206.348
10	133.48
5	92.64
2	85.14
1	79.122
Equation	y= 7.44x + 56.89
r^2	0.9994,
Slope	7.44
Intercept	56.89

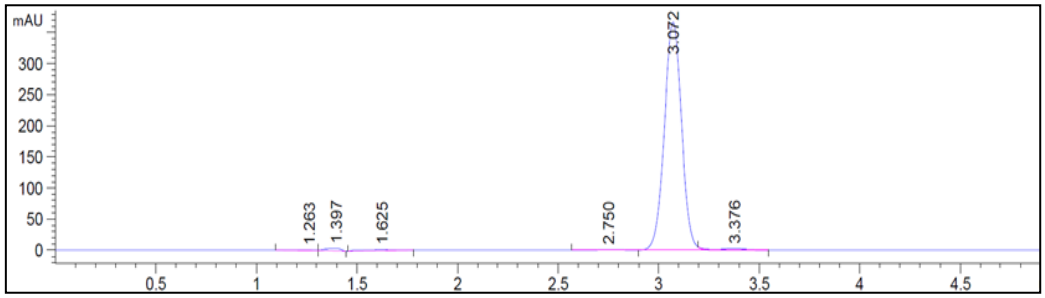


Figure 3.5: An example of chromatogram obtained for standard solution of 5 µg/mL.

3.4.2.4 ACCURACY

To determine the accuracy of the HPLC method described in Section 3.3.2.4 were employed with three quality control samples (1 µg/ml, 20µg/ml, and 50 µg/ml) were used. The samples chosen were such to represent the entire range of the standard curve i.e. lower, middle and higher concentrations of the analyte. Table 3.5 showed the accuracy studies obtained for standard SIM dilution.

In addition to the accuracy test, SIM that was extracted from the microparticles were determined. This was done by following the method in section 3.3.2.1, however the amount of SIM added in the microparticles were prepared individually (10mg, 5 mg and 1mg). Results for the accuracy studies are depicted in Table 3.5. The deviation of mean from the true value served as the measure of accuracy.

Table 3.4: Accuracy studies of the standard SIM dilution in HPLC validation protocol.

Concentration of standard solution (µg/ml)	Amount recovered (µg/ml)	% Recovery	Accuracy (%) ± RSD
1	1.09	112.23	
1	1.57	114.00	112.23 ± 2.26
1	1.35	114.00	
20	28.34	141.71	
20	21.42	107.09	101.95 ± 0.17
20	21.30	106.51	
50	50.141	100.28	100.18 ±
50	50.061	100.12	0.076
50	50.061	100.12	

The accuracy of an analytical method expresses the concordance degree between the measurement value and the true value of a sample. Percentage recoveries (Table 3.5) varied from 100.18 ± 0.038 % to 112.23 ± 0.83, with relative standard deviation (RSD), ranging from 0.0765 to 2.26 indicating acceptable accuracy. According to Ribani *et al*, (2004) and Hong, L. *et al*, (2017) acceptable recovery range is between 70% to 120%, that depending on the sample preparation and analytical process.

The overall results for SIM encapsulated microparticles show recovery values (Table 3.5) between 98.99 ± 1.425 (upper concentration level) and 113.11 ± 0.07 (lower concentration level). For all individual samples, at the three concentrations tested, the recovery was within the 100 ± 1% limit with RSD values lower than 2%. Therefore, this method can be considered accurate for quantifying SIM present in encapsulated microparticles as the experimental percentage recovery and RSD values obtained are within an acceptable proximity to the theoretical results (Shabir, 2003). The results obtained in this

validation study are superior to those obtained by Birari (2015) whereby their average recovery was 99.84% for all three different concentrations i.e: high, middle and low concentrations. The RSD values reported in the literature were in the range of 0.01 and 0.488 for SIM standard solution (Birari, 2015; Raju *et al*, 2012) respectively. Therefore, in comparison with our data, the HPLC method in our study showed better accuracy then the published research before for the pure SIM detection in standard dilution. However, there is slight differences in RSD value when comparing the accuracy study for SIM detection extracted from the microparticles but overall has better recovery value than the accuracy results obtained from Birari (2015).

Table 3.5: Accuracy studies of SIM in non-porous microparticles (NPMP) in HPLC validation protocol

Amountof drug (mg)	**Amount of drug (mg)**	**% Recovery**	**Accuracy (%) ± RSD**
1	1.097	109.734	
1	1.231	123.083	113.11 ± 0.07
1	1.0652	106.520	
5	4.938	98.753	
5	5.106	102.110	99.9 ± 1.56
5	4.942	98.836	
10	10.04	100.425	
10	9.948	99.487	98.99 ± 1.425
10	9.707	97.075	

3.4.2.5 PRECISION

Precision reflects the closeness of individual measures of an analyte when the analytical method is applied. It is usually represented as percentage coefficient of variation (% CV) (WHO, 2017). However, some articles use relative standard deviation as the measurement to indicate precision. The RSD was analysed in the validation protocols on drug encapsulated studies by several authors (Clementino *et al.*, 2018; Furman *et al.*, 2017; Oliveira *et al.*, 2015; Bhadra *et al.*, 2013; Urban *et al.*, 2009). Both coefficient of variation and the RSD are the same thing. Precision study of the method was carried out for the pure standard SIM concentration. As we also wanted to see the precision of this HPLC method on SIM-NPMP, thus we carried out the precision study on the extracted SIM from the microparticles.

The values of %RSD for intraday and interday precision are given in Table 3.7. The %RSD values were found to be well within the 2% limit, indicating that the current method is repeatable (Furman *et al*, 2017). Precision was measured using six replicates at three concentrations: 50µg/ml, 20µg/ml and 1 µg/ml.

Table 3.6: Analysis of intraday and interday precision of HPLC method for SIM stock solution.

Serial Number	Concentration of standard solution (µg/ml)	Intra-day precision (concentration recovered) (µg/ml)	Inter-day precision (concentration recovered) (µg/ml)
1	50	50.063	51.541
2	50	50.161	51.639
3	50	50.048	51.479
4	50	50.073	51.461
5	50	50.060	51.240
6	50	50.075	51.350
Mean		50.08	51.452
SD		0.037	0.128
%RSD		0.074	0.249
1	20	20.088	20.339
2	20	20.047	20.325
3	20	20.046	20.325
4	20	20.053	20.338
5	20	20.051	20.338
6	20	20.042	20.337
Mean		20.05	20.334
SD		0.014	0.006
%RSD		0.073	0.029
1	1	1.033	1.103
2	1	1.107	1.223
3	1	1.212	1.253
4	1	0.962	1.127
5	1	0.965	1.159
6	1	1.009	1.159
1	1	1.033	1.128
Mean		1.048	1.1650
SD		0.087	0.0501
%RSD		8.392	4.307

The intra-day precision assessment gave values of 0.074 to 8.392 % for SIM in the standard concentration. On the other hand, the inter-day evaluation is 0.249 to 4.307. The precision must ideally be less than 15% at all concentrations except for the LC where it should not exceed 20% (WHO, 2017). Based on the aforementioned data, the maximum precision value was 8.392 %, which indicates an acceptable degree of variation in both analytical methods.

We then proceed the precision analysis on the SIM that was extracted from the microparticles. The RSD of the SIM was found in a range of 1.067 to 2.479 for intra-day precision and 1.464 to 1.677 for inter-day precision. This result shows that the RSD is small which further indicate the data is tightly clustered around the mean. Table 3.8 depicts the RSD obtained for intra and inter-day precision of the drug matrix particles.

Table 3.7: Analysis of intraday and interday precision of HPLC method SIM-NPMP

Drug-matrix (mg)	**Intra-day precision (concentration recovered) (mg)**	**Inter-day precision (concentration recovered) (mg)**
10	10.778	10.222
10	10.127	10.082
10	10.992	10.654
10	10.660	10.317
10	10.651	10.370
10	10.765	10.320
Mean	**10.662**	**10.328**
SD	**0.264**	**0.173**
%RSD	**2.479**	**1.677**
5	5.002	5.120
5	5.031	5.167
5	4.868	4.979
5	5.003	5.137
5	5.001	5.120
5	5.002	5.131
Mean	**4.984**	**5.109**
SD	**0.053**	**0.060**
%RSD	**1.067**	**1.178**
1	1.097	0.951
1	1.127	0.984
1	1.065	0.969
1	1.073	0.942
1	1.07	0.974
1	1.08	0.963
Mean	**1.086**	**0.964**
SD	**0.020**	**0.014**
%RSD	**1.890**	**1.464**

3.4.2.6 RECOVERY

The limits of detection and quantification are determined by establishing the lowest concentration level at which the analyte can be reliably detected and quantified. Specifically, the limit of quantification is the concentration of analyte in a sample that can be quantified with acceptable precision and accuracy under the stated operational conditions. In this study the LOD and LOQ were 0.07 µg/ml and 0.22 µg/ml respectively.

3.5 CONCLUSION

The HPLC method using in this study was developed in accordance with ICH guidelines. The method was shown to be rapid, sensitive, and accurate in simultaneously detecting and quantifying SIM either alone or in the presence of microparticle excipients, such as PLGA. This implied that the analytical method would be valid for the quantification of the SIM drug loading and drug release experiments in the subsequent chapters.

CHAPTER 4

VARIATIONS IN THE REACTION PARAMETERS DURING THE SYNTHESIS OF SPHERICAL MICROPARTICLES

4.1 INTRODUCTION

Cells, scaffolds and growth factors are regarded as the three critical factors in tissue engineering. Tissue engineering scaffolds are designed to influence the physical, chemical and biological environment surrounding a cell population and to act as a structure for cell attachment and subsequent tissue development (Hollister, 2005; Chan *et al*., 2008; O'Brien 2011; Lyles *et al*., 2015; Misra, 2017).

In this study, poly (lactic-co-glycolic acid) (PLGA) has been used to entrap the hydrophobic drug SIM. The microparticles from which the scaffold is prepared are made using the double emulsion solvent evaporation method (Liu *et al*., 2012). The process follows two steps: firstly, the conversion of the solvents and aqueous phase into a coarse emulsion. This step is also known as physiochemical method, which primarily based on spontaneous assembly of molecules or colloidal particles into larger particles. Preparation of microparticles usually followed by the mechanical methods which is the use of processing equipment specifically designed to create small particles from the larger particles (McClements *et al*., 2017). In this study, we opt for double emulsion evaporation technique through which the final fine emulsion dispersion was obtained via a high-pressure system.

High pressure system also known as high pressure homogenizer, consist of high pressure pump and homogenizing nozzle. It is a purely mechanical process, which is evoked by forcing a fluidic product through a narrow gap which is usually the homogenizing nozzle, at high pressure (150-200 MPa) (Dumay *et al*., 2013). The liquid product is subjected to very high shear stress causing the formation of very fine emulsion droplets. Origin of this shear is the sudden restriction of flow under high pressure through a restrictive valve.

Several factors of formulation design may influence the size of the final microparticles. These include the selection of the solvent phase, the water phase, the choice of emulsifier and the size of the stirring bar used during the emulsion process (Ma *et al.,* 2001; Wu *et al*., 2008; Ezirganli *et al.,* 2014). In this study, we show the effects of various formulation variables that were optimised in order to develop microparticles which were the optimal diameter and possessed high encapsulation efficiency and appropriate in-vitro drug release kinetics.

In this chapter, the aim is to evaluate how variations in the parameters during the synthesis of spherical microparticles impact upon the outcome. Since the encapsulation efficiency of porous microspheres (PMP) was low compared to non-porous microspheres (NPMP) as described in section 2.3.4, the work in this chapter is focusing on the manipulation of NPMP formulation. The morphology and the particle size of microparticles are important determinants which will affect the release of SIM in the carrier system. The variables of homogenization speed, evaporation time, stir bar size and surfactant concentration were evaluated in the preparation of non-porous-SIM-loaded biodegradable PLGA microparticles (NPMP) using a modified solvent evaporation technique. The NPMP were then characterised according to particle size, encapsulation efficiency and in-vitro drug release kinetics.

4.2 MATERIALS AND METHODS

4.2.1 MATERIALS

PLGA (lactic acid: glycolic acid ratio, 85:15) of intermediate (53 kDa) and high (92-109 kDa) molecular weight was purchased from Evonik (USA). Dichloromethane (DCM) was acquired from Fisher (UK) and phosphate buffered saline (PBS) was procured from Gibco (UK). Poly vinyl alcohol (PVA) 100% hydrolysed) and sodium hydroxide (NaOH) pellets were both obtained from Sigma Aldrich (UK). Dimethyl sulfoxide (DMSO) and sodium dodecyl sulfate (SDS) were bought from Fisher Scientific (UK). SIM was purchased from Merck (USA).

4.2.2 ANALYTICAL METHODOLOGY

4.2.2.1 ENCAPSULATION EFFICIENCY AND CUMULATIVE STUDY

The encapsulation efficiency of PLGA microparticles containing 5 mg of SIM was determined using a modified HPLC method as described by B.D Micheal *et al*, 2013. Briefly, the chromatographic procedure was as follows: an Agilent Series 1120 HPLC (Agilent Technologies, Wilmington, DE) was used with a ThermoScientific® 100 C18, 5 µm, 150 mm × 4.6 mm. column, at 45 ºC. The mobile phase consisted of acetonitrile and 0.2% acetic acid buffer, pH 4 (70:30, v/v) and the flow rate of 1.0 mL /min as depicted on section 3.3.2. The mobile phase was filtered through a 0.45 µm nylon filter and degassed in an ultrasonic bath prior to use. Each sample was passed through a 0.22 micronpolytetrafluoroethylene (PTFE) membrane filter before HPLC analysis and then each sample was analyzed in triplicate and subsequent results were reported as the mean of three readings. The range of the SIM standards used for the calibration curve was 0.001-100 µg/mL and this gave a correlation coefficient (R^2)= 0.9994. The encapsulation efficiency was calculated based on the percentage ratio of the amount in mass (mg) of SIM loaded into microspheres to the initial amount used.

4.2.2.2 SCANNING ELECTRON MICROSCOPY (SEM) AND SIZE ANALYSIS

Samples were mounted on metal stubs and viewed under a scanning electron microscope (FE-SEM, Quanta 400F, FEI, USA). Images were analysed with image J software, version ImageJ/Fiji 1.49. Image J is a public domain, Java-based image processing program developed at the National Institutes of Health. This software was used to count and determine the size distribution of the microparticle images obtained from the SEM.

4.2.2.3 PREPARATION OF SIM-LOADED BIODEGRADABLE MICROPARTICLES

The preparation of SIM-loaded microparticles was based on the solvent evaporation method described in Section 2.2.4.1. Both the polymer and the drug were dissolved in the organic solvent dichloromethane. Following that, the

organic phase was added dropwise to an aqueous phase, containing PVA as a surfactant, and a Silverson L5M homogeniser was used to form the primary emulsion. The concentration of PVA is depicted in Table 4.1, either 1%, 0.6 % and 0.06% w/v. This was then added to 200 ml of PVA solution and homogenized to form the secondary emulsion. The emulsion was subsequently stirred on a magnetic plate to aid the evaporation of dichloromethane. After solvent evaporation, the microparticles were recovered by vortex-mixing at 1400 rpm, sieved (40 μm) and washed twice with distilled water. All microspheres were freeze-dried using a Thermofisher Scientific FR-Drying Digital Unit for 48 hours and stored at -20°C until use.

4.2.2.4 EVALUATION OF PROCESS AND FORMULATIONS VARIABLES

In the emulsification-solvent evaporation process, several parameters govern the physicochemical properties of microparticles and these include the particle size, encapsulation efficiency and drug release kinetics. In this study, we aimed to investigate the effects of process variables, namely the homogenization speed, evaporation time and stir bar sizing, on the preparation of SIM-loaded biodegradable polymeric microparticles. The selection of homogenization speed and evaporation time in this chapter was crucial as to obtain reproducible range of particle sizes and high encapsulation efficiency of microparticles. We subsequently proceeded with further testing of the four following variables to further optimize the formulation: surfactant concentration, polymer type, magnetic stir bar size and drug amount (Table 4.1). Only one variable was altered at any one time while keeping all other variables of the system constant. All data was further analysed with two-way ANOVA, SPSS, version 24 in order to see the significant level of the parameters tested.

Table 4.1: Effect of formulation variables on the preparation of SIM-loaded biodegradable microparticles

code	homogenization speed (Primary)	evaporation time (Hour)	Surfactant concentration (w/v)	Polymer type	Polymer (mg)	magnetic stir bar sizes (cm)	Drug amount (mg)
Effect of homogenization speed							
H1	1000 rpm	4 hours	0.06%	IMW	1000	1.0	5
H2	2000 rpm	4 hours	0.06%	IMW	1000	1.0	5
H3	3000 rpm	4 hours	0.06%	IMW	1000	1.0	5
H4 *	4000 rpm	4 hours	0.06%	IMW	1000	1.0	5
Effect of evaporation time							
E1	4000 rpm	1 hour	0.06%	IMW	1000	1.0	5
E2	4000 rpm	2 hours	0.06%	IMW	1000	1.0	5
E3	4000 rpm	3 hours	0.06%	IMW	1000	1.0	5
E4 *	4000 rpm	4 hours	0.06%	IMW	1000	1.0	5
Effect of surfactant concentration							
A1	4000 rpm	4 hours	1%	IMW	1000	1.0	5
A2	4000 rpm	4 hours	0.6%	IMW	1000	1.0	5
A3 *	4000 rpm	4 hours	0.06%	IMW	1000	1.0	5
Effect of polymer type							
B1	4000 rpm	4 hours	0.06%	HMW	1000	1.0	5
B2 *	4000 rpm	4 hours	0.06%	IMW	1000	1.0	5

code	homogenization speed (Primary)	evaporation time (Hour)	Surfactant concentration (w/v)	Polymer type	Polymer (mg)	magnetic stir bar sizes (cm)	Drug amount (mg)
Effect of polymer concentration							
C1*	4000 rpm	4 hours	0.06%	IMW	1000	1.0	5
C2	4000 rpm	4 hours	0.06%	IMW	2000	1.0	5
C3	4000 rpm	4 hours	0.06%	IMW	3000	1.0	5
Effect of magnetic stir bar sizes							
D1	4000 rpm	4 hours	0.06%	IMW	1000	0.5	5
D2 *	4000 rpm	4 hours	0.06%	IMW	1000	1.0	5
D3	4000 rpm	4 hours	0.06%	IMW	1000	1.5	5
Effect of drug amount							
E1	4000 rpm	4 hours	0.06%	IMW	1000	1.0	1
E2	4000 rpm	4 hours	0.06%	IMW	1000	1.0	2
E3	4000 rpm	4 hours	0.06%	IMW	1000	1.0	3
E4	4000 rpm	4 hours	0.06%	IMW	1000	1.0	4
E5 *	4000 rpm	4 hours	0.06%	IMW	1000	1.0	5
E6	-	-	-	-	-	-	-
* Same formulation variables.							

4.2.2.4.1 EFFECT OF HOMOGENIZATION SPEED

Variations in high-pressure homogenization energy input has a direct effect on the size of the disperse phase during the emulsification process (Park *et al*., 2012). The size of the droplets of an emulsion is inversely related to the magnitude of shear stresses. Increasing the shear stress will typically result in reduced droplet size potentially down to the micro-scale. To investigate the effect of shear stress emulsification was performed at different homogenization speeds of 1000, 2000, 3000 or 4000 rpm for 2 minutes with the evaporation time of organic phase set to 4 hours.

4.2.2.4.2 EFFECT OF EVAPORATION TIME

In this study, PVA was selected as the organic solvent for dissolving the PLGA. This organic solvent was ultimately removed by evaporation to produce SIM-loaded microparticles. During solvent evaporation the microdroplets became solidified to produce microparticles and the drug was either adsorbed onto the surface and/or entrapped within the polymer matrix of these microparticles. The transition of microdroplets to microparticles could potentially have resulted in the drug diffusing out into the external aqueous phase. Therefore, controlling the solidification rate of the microparticles in order to achieve small particle size and high encapsulation efficiency was critical. The evaporation stage was carried out for 1, 2, 3 and 4 hours denoted as E1, E2, E3 and E4, with constant magnetic stirring at 3000 Hz on the multi-position magnetic stirrers.

4.2.2.4.3 EFFECT OF SURFACTANT CONCENTRATION

The effect of surfactant concentration plays a significant role because its presence at the aqueous/organic phase interface governs the effectiveness of emulsion formation and the stabilization of the oil microdroplets during the emulsification solvent evaporation process. PVA was employed as a surfactant and concentrations of 1%, 0.6 % and 0.006 % w/v were studied.

4.2.2.4.4 EFFECT OF POLYMER MOLECULAR WEIGHT

PLGA is a copolymer consisting of lactide and glycolide monomers. A multitude of factors influence the resulting drug release kinetics from PLGA microparticles and these include the lactide and glycolide content of the polymer. Two different PLGA will be used in this work, the intermediate molecular weight (IMW) PLGA (53kDa), which is formulation B1 and high (92–109 kDa) molecular weight (HMW) PLGA, which is formulation B2.

4.2.2.4.5 EFFECT OF POLYMER AMOUNT AND DIFFERENT SIZE OF STIR BAR

As explained in Section 3.1.5, increased amounts of hydrophobic polymer may result in greater encapsulation of hydrophobic drugs. This effect was explored by varying the amount of PLGA used: 1g, 2g and 3 g quantities were all employed. After emulsification has been achieved, the formulations containing SIM were transferred to 200 ml of PVA and stirred for 4 hours using magnetic stir bars of multiple sizes to facilitate the removal of the organic solvent. Thereafter, the mixture was filtered, washed three times with deionized water and freeze dried for 48 hours.

4.2.2.4.6 EFFECT OF DRUG AMOUNT

To achieve maximum encapsulation, variable drug amounts, ranging from 1 mg to 5 mg, were added to the organic phase to evaluate the effect of drug amount on microparticle synthesis.

4.2.2.5 CHARACTERIZATION OF SIM-LOADED MICROPARTICLES

Following the preparation of SIM-loaded biodegradable polymeric microparticles, the resultant formulations were characterised according to particle size, encapsulation efficiency and in-vitro drug release kinetics. All experiments were conducted in triplicate.

4.2.2.5.1 DETERMINATION OF ENCAPSULATION EFFICIENCY

The procedure used for analysing drug loading and encapsulation efficiency was as follows: 10 mg of microparticles were dissolved in 1 ml of methanol and centrifuged at 10 000 rpm using MiniSpin plus, Eppendorf for 15 minutes at room temperature. The supernatant was collected and subjected to HPLC analysis for the determination of SIM content as detailed in Section 2.2.1. SIM encapsulation efficiency was determined using Equation 4.1.

$$\text{Encapsulation Efficiency} = \frac{\text{Amount of drug in microparticles}}{\text{Theoretical drug added}} \times 100$$

……(Equation 4.1)

4.2.2.5.2 DETERMINATION OF IN-VITRO DRUG RELEASE KINETICS

The release profiles of SIM from the microspheres were studied using 50 mg of SIM-loaded microspheres which was added to 1.5 ml of PBS, pH 7.4 in a micro-centrifuge tube. The tubes were incubated at 37 °C in an incubator (Thermo Scientific™ Heratherm™ Compact Microbiological Incubator). from Day 1 to Day 30. At predetermined time intervals, all the PBS was removed and replaced with fresh buffer. Aliquots (150 µl) were withdrawn from the removed supernatant and assayed for their SIM content using HPLC as described in Section 4.2.2.1.

4.2.3 DATA ANALYSIS

Statistical analysis was done using Statistical Package for the Social Sciences (SPSS) version 24.0 (SPSS, Surrey, UK). All experiments were performed in triplicate. Microparticle characteristic data is represented as mean ± standard deviation (SD). A Student's T- test was used for the comparison of two groups. Differences were assessed using the independent samples T-test. The repeated measure ANOVA was used to assess relationship between groups and extent of encapsulation. Significance was accepted at the 5% level.

4.3 RESULTS AND DISCUSSION

4.3.1 CHARACTERIZATION OF SIM-LOADED BIODEGRADABLE POLYMERIC MICROPARTICLES

The comparisons of particle size, encapsulation efficiency and the cumulative amounts of drug released from SIM-loaded biodegradable polymeric microparticles prepared in this chapter are summarized in Table 4.2.

SIM is a hydrophobic drug and encapsulating hydrophobic or poorly water-soluble drugs with PLGA microparticles can be challenging. The solvent evaporation technique is frequently used due to its simplicity and the ease with which microparticles can typically be prepared. Critical factors which determine drug loading in microparticles are particle size, encapsulation efficiency and the cumulative amount of drug released from SIM-loaded biodegradable polymeric microparticles.

4.3.1.1 EFFECT OF HOMOGENIZATION SPEED

Homogenization speeds (1000, 2000, 3000 and 4000 rpm, i.e. formulations H1, H2, H3 and H4) had been used to see the impact on the resulting microparticles. Lower homogenization speed resulted in the formation of microparticles of larger particle sizes 40.13 ± 20.12 µm 38.87 ± 23.39 µm and 32.12 ± 19.45 µm, respectively, as compared to when stirred at 4000 rpm (formulation H4) where the particle size was 32.78 ± 21.45 µm (Table 4.2). These results showed that particle size is dependent on the stirring speed during solvent evaporation. During the process of emulsification, the force of the higher stirring speed distributes the internal phase into smaller droplets, resulting in the formation of smaller microparticles (Vyslouzil *et al*., 2014; Capan *et al*., 1999). The higher speed of homogenization causes a greater amount of energy to be released which in turn leads to a rapid dispersion of the polymer-containing organic phase, and it is for this reason that microparticles of smaller sizes and monomodal distribution were obtained (Figure 4.1).

The encapsulation efficiency increased from 41.5% to 89.5% when the speed of emulsification was increased from 3000 rpm (formulation H3) to 4000 rpm (formulation H4). This showed that increased encapsulation efficiency could be achieved with an increase in the homogenization speed. However, the encapsulation efficiency could not detect the SIM that had been encapsulated in both formulation H1 and H2. This could possibly be attributed to the usage of very low homogenization speeds and this meant that the SIM was unable to become incorporated into the microparticles. Conversely, the H3 and H4 formulations were prepared at higher homogenization speeds and this led to the incorporation of the drug.

The cumulative amount of drug released at 15 days increased in line with increasing homogenization speed (Figure 4.1). Formulations H1 and H2 were larger particle sizes and the encapsulation efficiency was low, as such, these formulations were not evaluated for drug release. The formulations consisting of larger particles exhibited a slower rate of drug release due to longer diffusion pathways. The same effect has been observed in other similar studies (Vyslouzil *et al.,* 2014; Lin *et al*., 2016). A two-way ANOVA was conducted to examine the effect of homogenization speed and time point. From the statistical analysis,

it was found that 4 hours homogenization speed has higher cumulative release than 3 hours homogenization speed with significant level of $p<0.0001$, $F(1.957, 19.572)=15.161$ was obtained.

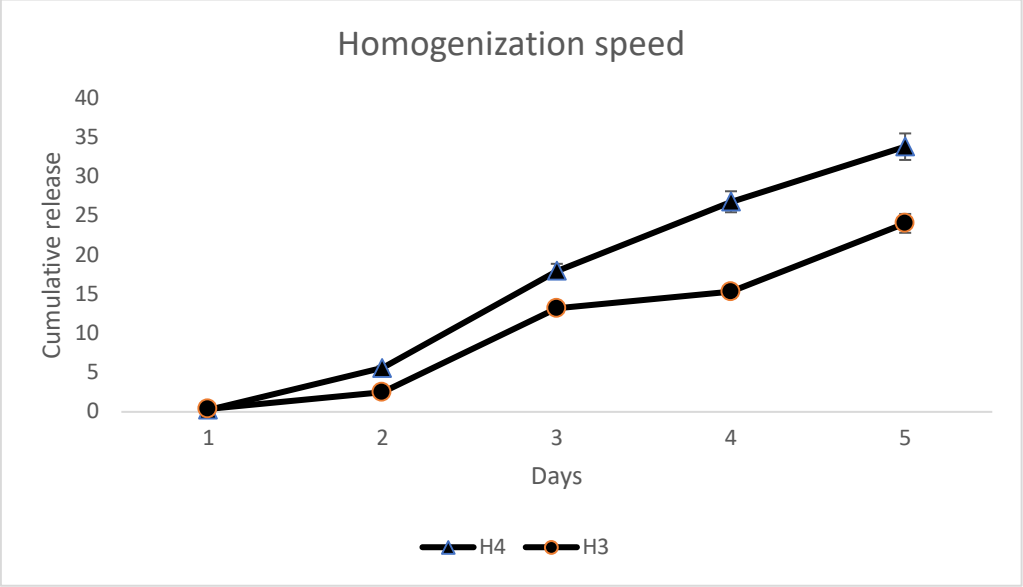


Figure 4.1: Effect of homogenization speed on in-vitro drug release kinetics of SIM-loaded biodegradable microparticles (data represent mean ± standard deviation, n = 3).

4.3.1.2 Effect of Evaporation Time

The double emulsion–solvent diffusion evaporation technique is one of the most commonly used in microparticle preparation, particularly for drug encapsulation. It involves two-step techniques i) the initial emulsification of polymer solution in a volatile organic solvent. followed by ii) the internal phase solvent evaporation or extraction that results in hardening and precipitation of microparticles. Solvent evaporation is generally carried out at atmospheric pressure (or sometimes under reduced pressure) to promote evaporation of the volatile solvent. The solvent extraction process, however, involves quenching in excess water or relevant quench medium, allowing for solvent diffusion through oil droplets. A critical process in microparticle synthesis is the diffusion of the organic solvent through the interface of the emulsion droplet (Izumikawa *et al.,* 1999). According to Asadi *et al*. (2011), the most commonly used approach to

stir the mixture during synthesis is with magnetic stirring plate. Increase in the stirring rate generally will results in a decrease in the particles size. This is due to the resulting high turbulence, caused frothing and adhesion to the container wall. Therefore, the mean particle size of microspheres decreased. As shown in Table 4.2, an increase in the evaporation time resulted in a decrease in particle size, an improved encapsulation efficiency and an increase in the cumulative amount of drug released at the end of the experiment. This result can be seen from formulation E1 to E4. When evaporation was carried out over a shorter period of time (i.e. at a faster evaporation rate), the diffusion of the organic solvent out of the oil droplets may have been incomplete when the droplets hardened, thus resulting in larger particles. During the evaporation process, the disperse phase volume gradually decreases and consequently there is an increase in the viscosity of the dispersed droplets.

Reduced encapsulation efficiency in the case of shorter evaporation time may be a result of the rapid replacement of the organic solvent with the aqueous medium before droplet hardening occurs. The formulations consisting of smaller size microparticles as seen in Table 4.2, exhibited faster drug release as denoted in formulation E3 and E4 (Table 4.2). It was presumed that the increased surface area of formulation E4, which had the smallest particle size, was the reason behind the greater release. It has been reported elsewhere that rapid solvent evaporation leads to a smoother surface of the particles as compared to the particles obtained by delayed solvent evaporation (Quintanar-Guerrero *et al*., 1996). Thus, the smoother surface of the polymer matrix could have resulted in a much slower release (Figure 4.2). Based on the results obtained, the variables used in the formulation of E4 were selected as optimal and used for the next evaluation of various formulation variables described below.

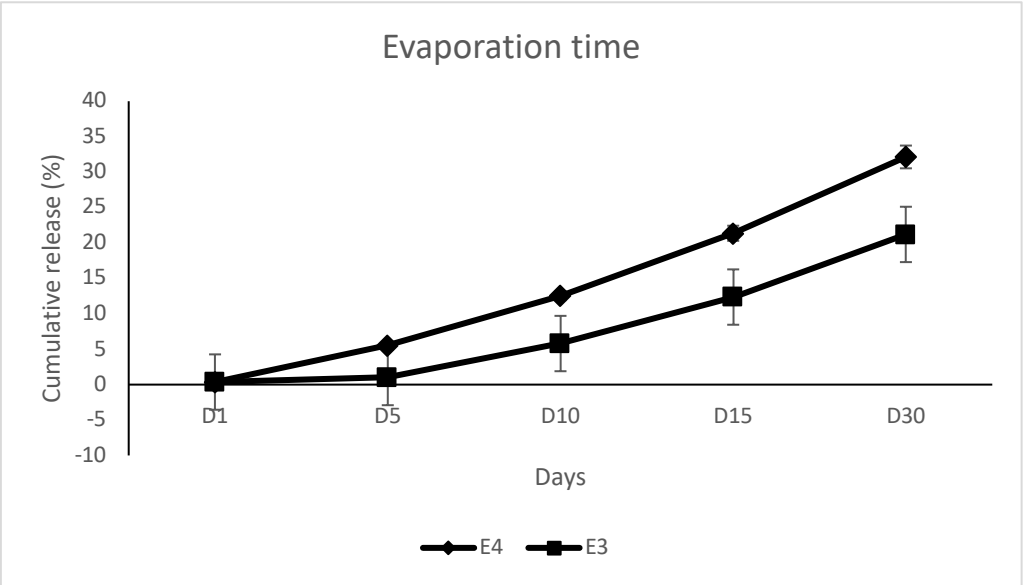
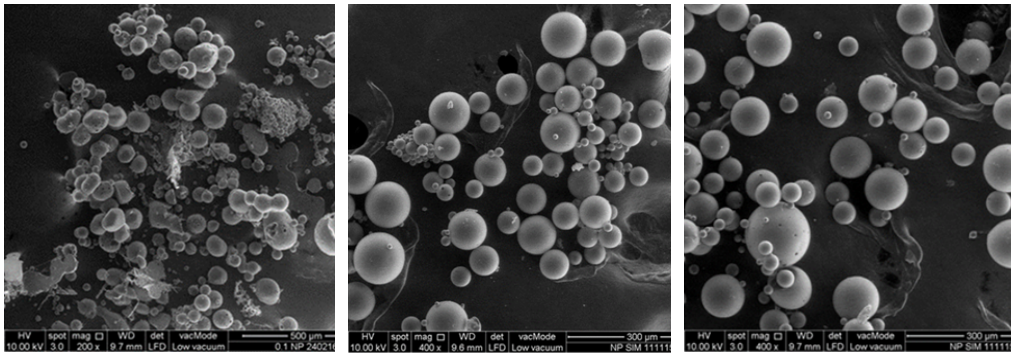


Figure 4.2: Effect of time on in-vitro drug release kinetics of SIM-loaded biodegradable microparticles (data represent mean ± standard deviation, n = 3).

A two-way ANOVA was conducted that examined the effect of evaporization time and time point. There was a statistically significant interaction between the effects of evaporation time and time point (Day 1, Day 5, Day 10, Day 15 and Day 30) on cumulative release of SIM with $F(1.682,16.822)=25.664$, $p < 0.0001$. The two way ANOVA is used in this study as to compare the evaporation time and the time point concurrently. When the $p < 0.0001$, it indicates that the E4 has higher cumulative release than E3 and the higher cumulative results is not happening by chance.

4.3.1.3 EFFECT OF SURFACTANT CONCENTRATION

In this investigation, PVA was selected and used as the aqueous phase in the SIM microparticles preparation. It was observed that at 1% PVA concentration (formulation A1), the emulsion which formed was not stable and aggregation occurred after a few hours of emulsification leaving polymer aggregates (Figure 4.3 a). Decreasing PVA concentration to 0.6% (formulation A2) and further to 0.06% (formulation A3) resulted in increased mean particle sizes of 18.65 ± 28.77μm and 32.78 ± 21.45 μm respectively (Fig 4.3b and Fig 4.3c). Overall cumulative release is shown in Figure 4.3 b. Results was statistically significant with F value (1.682, 16.822)=25.664, $p<0.000$.



a b c

Figure 4.3 a: Scanning electron micrographs of the SIM degraded biodegradable microparticles made with (a) 1 % PVA (b) 0.6 % PVA and (c) 0.06 % PVA**.**

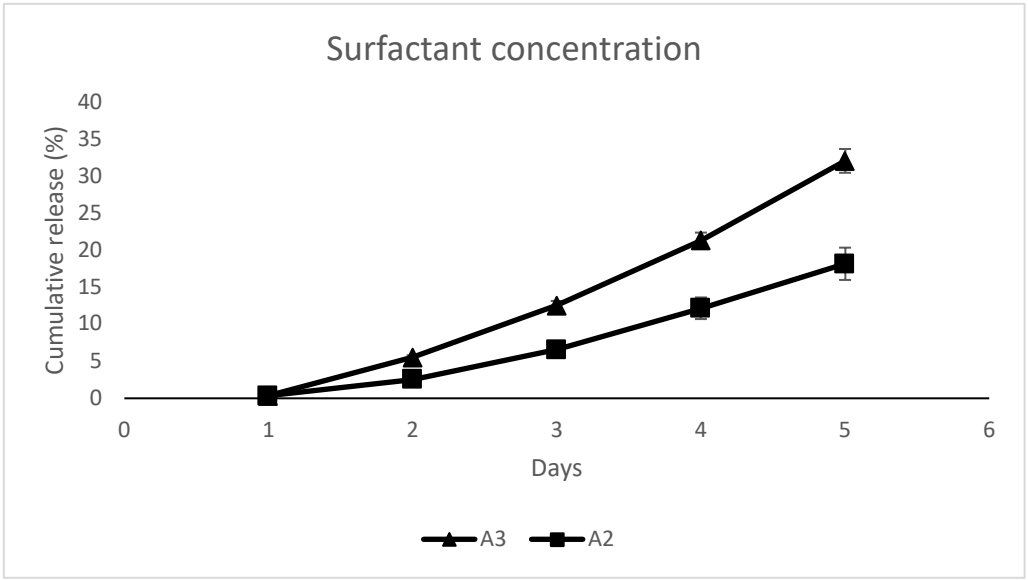


Figure 4.3b: Effect of surfactant concentration on in-vitro drug release kinetics of SIM loaded biodegradable polymeric microparticles (data represent mean ± standard deviation, n = 3).

In the water in oil in water (w/o/w) double emulsions, the internal and external aqueous phases are separated by an oil layer. In the synthesis of microparticles, the primary emulsion (W1/O) is dispersed in a second aqueous phase (external aqueous phase, W2) to form double emulsion (W1/O/W2). In this study, the SIM was dispersed in the primary emulsion containing DCM and subsequently was dispersed in the PVA which act as the external aqueous. The amount of

surfactant present, in this case, the PVA, plays a significant role because it prevents the solvent globules from coalescing. Coalescence is a separation process where the emulsified droplets unite to form larger droplets that will eventually be separated from the external phase (Viana *et al.,* 2014). The surfactant molecules tend to align themselves at the droplet surface lowering the free energy at the interface between two phases and resisting coalescence of the droplets (Murakami *et al*., 1997; McCall *et al*., 2013).

In general rule, the decrease of particle size can be observed with the increasing volume of organic phase. This is because an increase in solvent volume lowers the viscosity of the polymer concentration in the organic phase and results in a decrease in the resistance against shear forces during emulsification, resulting in the formation of smaller droplets. Here in our study however, we found that 0.06% PVA, i.e. the lowest concentration of surfactant used and increased volume of organic phase, led to the formation of larger particle size. Similar finding were observed by Allemann *et al*. (1992), Lemoine and Preat (1998), Vysloužil *et al.* (2014), whereby they witnessed marked increased in particle size with the decreased of PVA concentration. They suggested that at very low concentrations of PVA, the total amount of PVA, relative to PLGA, is insufficient to stabilize the emulsion droplets and causes larger particles. Apart from that, the amount of surfactant plays an important role, because it can avoid the coalescence of the oil globules. The surfactant molecules tend to align themselves at the droplet surface lowering the free energy at the interface between two phases and resisting coalescence of the droplets. Smaller microspheres have large surface area and thus need more surfactant to stabilize the emulsion containing the microspheres (Taghipour *et al*., 2014). Therefore, we anticipate the results in A1 and A2 was in accordance to this theory. Since the particle size prepared in these two formulation were much smaller than the microparticles prepared in A3, we assumed that more surfactants aligned themselves in the A1 and A2 formulation which further reduce the free energy between the droplets and further maintaining the particle size smaller than those prepared in A3. As we further increase the concentration of PVA in formulation A1 (i.e; 1% w/v), the sizes were further reduced. A decrease in PLGA microparticle size in response to an increase in PVA

concentration has also been reported in the literature (Zweers *et al*., 2003; Nandagiri *et al*., 2012; Vyslouzil *et al*, 2014; Liu *et al*., 2015). Increased PVA concentration ensured better system stabilization against coalescence of the emulsion and therefore led to formation of smaller microparticles however the agitation between microspheres in the solutions during homogenization process leads to formation of a larger number of aggregated microparticles during solidification (Nandagiri *et al.,* 2012). The encapsulation efficiency was observed to increase from 32.7 ± 1.8 µm (formulation A2) to 89.7± 2.4 µm (formulation A3) when the surfactant concentration decreased from 0.6% to 0.06% (Table 4.2). These results may be attributed from the viscosity of the PVA which leads to the ratio of the surface area that is contributed by the microparticles sizes

As explained earlier, when the viscosity of PVA concentration increased, it tends to make the PVA molecules to align themselves at the droplet surface lowering the free energy at the interface between two phases and this further reduced coalescence of the droplets. Therefore, production of smaller microparticles were observed. Smaller microparticles with large surface area can lead to particle–particle aggregation, limited drug loading and burst release (Talegaonkar *et al.,* 2017). The particle size observed in formulation A2 were smaller than the microparticles in formulation A3. This further explained the tendency of formulation A2 to have lower drug loading in contrast to formulation A3 which has larger particles and allow more drug to be encapsulated per particle (Singh *et al.,* 2009; Pal *et al.,* 2011; Caruso *et al*., 2017). Subsequently in total, this effect reduced the encapsulation efficiency in formulation A2. Whilst microparticles prepared in the formulation A1 were compromise due to agglutination, encapsulation efficiency was not observed here particularly due to drug lost during preparation. A secondary explanation could be due to gelatinization of the PVA molecules. Strong inter- or intra-molecular hydrogen bonding of the hydroxyl groups present on the PVA may have caused this gelatinization at the oil/water interface during the microparticle formation process (Murakami *et al*., 1997). PVA concentrations in the continuous phase may hinder the complete separation of nascent droplets due to a bridging effect at overly high PVA concentrations and may result in formation of a larger

number of aggregated microparticles during solidification. As a result, an increase in particle size and a reduction in encapsulation efficiency were observed at higher surfactant concentrations.

As mentioned in Table 4.2, the cumulative amount of drug released from formulations prepared using surfactant concentrations of 0.6% and 0.06% (formulations A2- A3) was 22.78 ± 0.28 % and 35.74 ± 0.8 % respectively ($p \leq 0.06$). However, the drug release profiles demonstrated no detectable release when 1% PVA concentration was used due to the agglomeration effect that was observed with formulation A1 (Figure 4.3d). This suggested SIM was not well encapsulated when a high concentration of PVA was used (Figure 4.3a). Drug diffusion through the microparticle matrix are governed by microparticle matrix erosion or degradation and the combination of erosion and diffusion processes. Smaller particles which can be seen in formulation A2 offer larger surface area. As a result, most of the drug loaded onto them will be exposed to the particle surface leading to fast drug release (Pal *et al.,* 2011). Because smaller particle size would also have limited drug encapsulated in it, the cumulative drug release was found lower in formulation A2 in contrast to the cumulative SIM release in formulation A3. On the contrary, drugs slowly diffuse inside formulation A3 leading to higher cumulative SIM release.

Table 4.2: Comparison of particle size, encapsulation efficiency, and cumulative amount of drug released from SIM loaded biodegradable polymeric microparticles using various process and formulation variables

Formulation code	Particle size (μm ± SD) [a]	Encapsulation efficiency (% ± SD) [a]	Cumulative drug released at 30 days (% ± SD) [a]
Effect of Homogenization speed (rpm)			
H1	40.13 ± 20.12	-	-
H2	38.87 ± 23.39	-	-
H3	36.12 ± 19.45	41.5 ± 5.3	15.67 ± 1.1
H4 *	32.78 ± 21.45	89.7± 2.4	35.74 ± 0.8
Effect of evaporation time (hour)			
E1	-	-	-
E2	68.7 ± 20.87	-	-
E3	35.11 ± 23.17	21.78 ± 9.5	21.98 ± 0.69
E4 *	32.78 ± 21.45	89.7 ± 2.4	35.74 ± 0.8
Effect of surfactant concentration (% w/v)			
A1	-	-	-
A2	18.65 ± 28.77	32.7 ± 1.8	22.78 ± 0.28
A3 *	32.78 ± 21.45	89.7± 2.4	35.74 ± 0.8
Effect of polymer type			
B1*	32.78 ± 21.45	89.7± 2.4	35.74 ± 0.8
B2	24.31 ± 26.21	92.89 ± 4.8	47.90 ± 1.3
Effect of polymer (g)			
C1*	32.78 ± 21.45	89.74 ± 2.4	35.74 ± 0.8
C2	38.76 ± 27.90	91.5 ± 7.3	21.6 ± 1.7
C3	45.89 ± 19.25	94.3 ± 0.78	5.9 ± 1.7
Effect of the stir bar size (cm)			
D1	22.73 ± 28.55	92.3 ± 1.8	22.67± 2.6
D2*	30.54 ± 29.86	89.7± 2.4	35.74 ± 0.8
D3	32.78 ± 21.45	77.54 ± 3.9	28.96 ± 1.77
Effect of drug amount (mg)			
E1	19.92 ± 24.87	-	-
E2	20.29 ± 27.56	-	-
E3	28.51 ± 29.23	65.67 ± 5.9	11.68 ± 0.5
E4	29.45 ± 30.17	68.7 ± 6.2	24.89 ± 0.3
E5 *	32.78 ± 21.45	89.7± 2.4	35.74 ± 0.8
E6	-	-	-

a Data represent mean ± standard deviation, n = 3.

* Same process variables as well as formulation variables

4.3.1.4 EFFECT OF POLYMER MOLECULAR WEIGHT

In this study, microparticles were successfully prepared from PLGA (85:15) polymers with two different molecular weight : IMW (53 kDa) and HMW (92–109 kDa). The mean particle diameter size of the microparticles prepared using IMW PLGA was 32.78 ± 21.45 µm, whereas with the HMW PLGA it was 24.31 ± 26.21 µm (Table 4.2). These results indicate that different molecular weight PLGA clearly influenced the particle size of the resultant microparticles. In a study conducted by Liu, R. *et al.,* 2016, they demonstrated varying molecular weights of poly(lactide-co-glycolide)(PLGA) to yield methoxy-poly(ethyleneglycol)-block-poly(lactide-co-glycolide)(mPEG-PLGA) nanocarriers: namely the mPEG-PLGA(3k), mPEG-PLGA(9k), mPEG-PLGA(11k) and mPEG-PLGA(16k). They observed increasing molecular weight of the hydrophobic block, reduced the size of nanocarrier. Similar finding was observed here whereby the microparticle size were reduced with the increasing polymer molecular weight. Another studied by Prakapenka, A. V. *et al.,* 2017 observed that the of E2 compared to the smaller sized particles. This correlation between increase particle sizes and increase PLGA molecular weight has been witnessed in study conducted by Enayati *et al.* (2012) and Xinteng *et al.* (2002). Taken together, these studies indicate that particle size can play a role in the release profile of SIM.

The difference between the drug release rates of the two polymer blends may be accounted for by the differing levels of immiscibility. In our study, SIM release was found to be significantly higher in terms of encapsulation efficiency from the microparticles prepared using HMW PLGA. The mean encapsulation efficiencies of the microparticles prepared using IMW PLGA was 89.7±2.4 % and with HMW PLGA it was 92.89 ± 4.8 %.

One possibility that could lead to higher encapsulation efficiency in HMW formulation is the increase in the hydrophobic interaction between the lipophilic drug. As discussed by Sharma *et al.* (2016), a higher molecular weight PLGA would resulted in higher encapsulation efficiency. The cumulative amount of drug released at 30 days was higher from the formulation prepared using the HMW PLGA, formulation B2 (47.90 ± 1.3) as compared to those made with IMW PLGA (Formulation B1) where the cumulative release was 35.74 ±

0.8 % (F value (1.682, 16.822)=25.664, p<0.0001). From the drug release profiles shown in Figure 4.4, formulation B2 resulted in higher release when compared to formulation B1. This could be due to the fact that SIM is a hydrophobic drug and it is incorporated into a hydrophobic polymer, which may result in the encapsulation of hydrophobic drug to a greater extent.

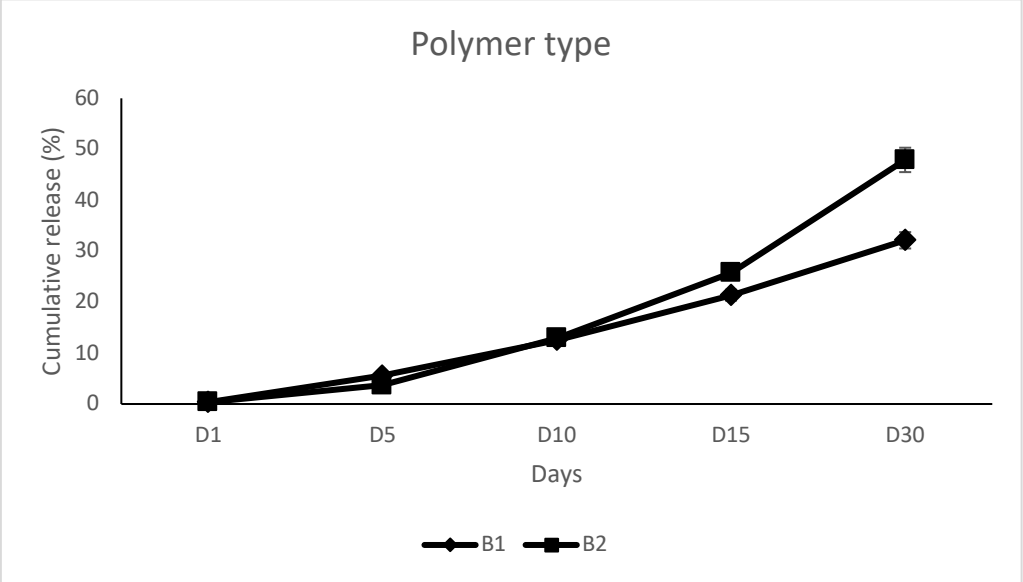


Figure 4.4: Effect of polymer type on in-vitro drug release kinetics of SIM loaded biodegradable polymeric microparticles (data represent mean ± standard deviation, n = 3).

4.3.1.5 EFFECT OF POLYMER CONCENTRATION

An increased amount of hydrophobic drug in the microparticle formulation may result in the encapsulation of the drug to a greater extent. Our study supports this and when the drug content was maintained at 5 mg for each formulation, the encapsulation efficiency was highest in formulation C3 (3000 mg PLGA) as compared to formulation C1 (1000 mg).

The mean ± SD particle size of formulations prepared using 1000 mg, 2000 mg and 3000 mg (formulations C1-C3) were distributed within 32.78 ± 21.45 µm, 38.76 ± 27.90 µm and 45.89 ± 19.25 µm (Table 4.2). As the polymer amount increased, the mean encapsulation efficiency increased from 89.7 ± 2.4%, 91.5 ± 7.3% and 94.3 ± 0.78% (Mean +/- SD) (F value (2.967, 22.249)=94.260,p<0.0001). An overall increase in the mean particle diameter of microspheres was observed as the amount of polymer in the formulation was

increased. The viscosity of the organic phase increased with greater polymer concentration, keeping the drug concentration and the volume of organic phase constant at 5 ml (Desgouilles *et al*., 2003; Zweers *et al*., 2003; Budhian *et al*. 2007; Song *et al*., 2008; Caruso *et al.,* 2017) The increase in polymer concentration in the inner phase led to an increase in the inner phase viscosity and droplet size, which in turn resulted in the formation of larger sized particles. Furthermore, the increase in polymer concentration increases the organic phase viscosity and this increases the diffusional resistance to drug molecules from the organic phase to the aqueous phase, thereby entrapping more drug in the polymer microparticles (Sharma *et al*., 2016).

Increase in the particle size correlated with a decrease in the cumulative release of SIM from the microparticles (Figure 4.5). This could be explained by considering the diffusional pathway aspect. The increased length of the diffusional pathways into the aqueous phase will reduce the amount of drug lost through diffusion and thereby increase the drug content. Moreover, the time available for polymer precipitation was lower at higher polymer concentrations, as such there was less time for drug molecules to diffuse from the microparticles, which in turn increased the drug content in the final formulation Liu *et al.* (2016). The other plausible explanation could be the availability of a greater amount of polymer present to facilitate drug encapsulation, thus preventing saturation of the encapsulation process (Krishnamachari *et al*., 2007). The decreased cumulative drug release could be due to the increased particle size and thus smaller surface area to volume ratios at the higher polymer concentrations. A further explanation for this could be due to the increased amount of polymer present which hinders drug release via diffusion (Sharma *et al.,* 2016). In general, the drug diffusion depends on several factors which are; drug solubility, desorption of the surface-bound or adsorbed drug, drug diffusion through the nanoparticle matrix, nanoparticle matrix erosion or degradation and finally the combination of erosion and diffusion processes. Hence, solubility, diffusion and biodegradation of the particle matrix govern the release process (Vyas *et al*., 2012).

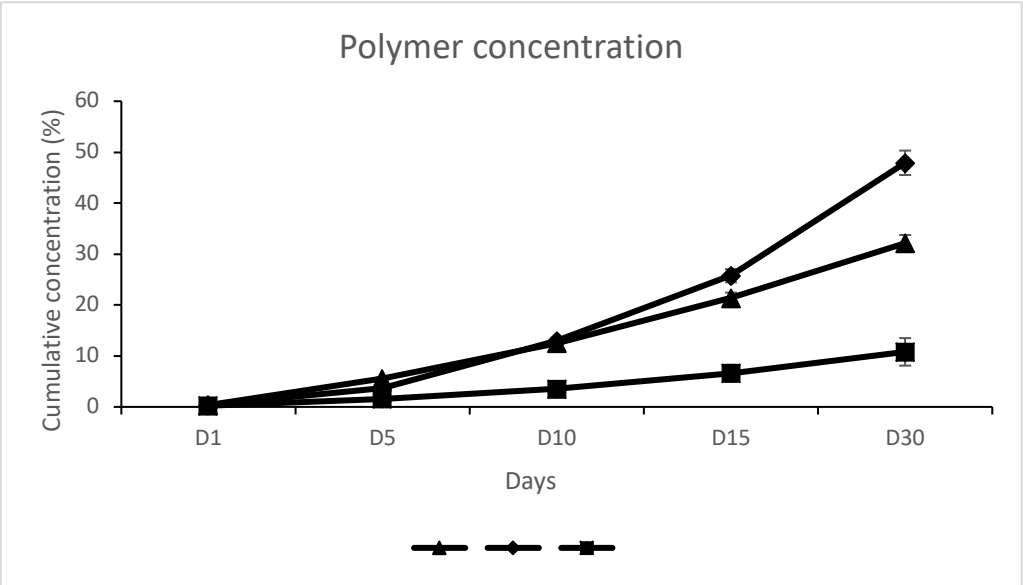


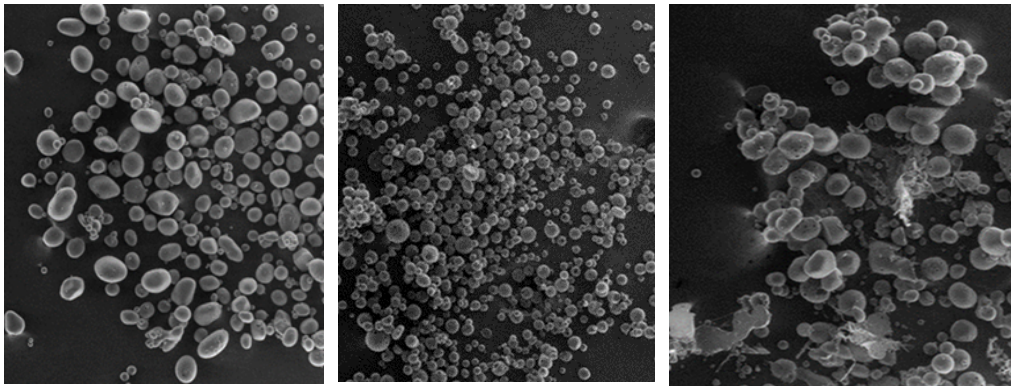
Figure 4.5: Effect of polymer concentration on in-vitro release kinetics of SIM-loaded biodegradable polymeric microparticles (data represent mean ± standard deviation, n = 3).

4.3.1.6 Effect of Stir Bar Size on the Emulsification Evaporation Process

The influence of stirring on different stir bar on microparticle morphology was demonstrated in this study while maintaining stirring speed at 4000 rpm. Stirring was performed using oval plastic-coated magnetic stir bars of three different lengths, 0.5 cm, 1.0 cm and 1.5 cm respectively. As conventional emulsification techniques typically rely on turbulent mixing for emulsifying the precursor solution, the resultant emulsion tends to be polydisperse in size. In our work, polydisperse PLGA microparticles were observed after magnetic stirring was applied to promote emulsification. The particle size and morphology changed from a hexagonal platelet, regular round shaped, to a poorly defined shape when the stir bar was varied. With the larger 1.5 cm stir bar, the shearing forces influenced the microparticle structure so that they became poorly defined in shape as compared to those microparticles produced using the 1.0 cm stir bar. SEM images of the microparticles produced using different stir bar are shown in Figure 4.7. Mainly agglomerates were observed in these images with the exception of the formulation prepared with the 1.0 cm stir bar.

Encapsulation efficiency was the highest in formulation D1 (Figure 4.6 a). However, this formulation also exhibited the lowest cumulative release of SIM (Table 4.2). In contrast, cumulative release was higher from formulation D2, despite the encapsulation efficiency being slightly lower than for formulation D1. Formulation D1 was prepared using a 0.5 cm magnetic stir bar, which produced the smallest average size 22.73 ± 28.55 µm and therefore the largest surface area to volume ratio. This is one of the possible reasons for the high encapsulation efficiency as compared to formulations D2 (89.74± 2.4 µm) (Figure 4.6b) and D3 (77.54 ± 3.9 µm) with F value (13.013, 22.597)=17.447, $p<0.0001$ (Figure 4.6c). This phenomenon in size differences could be explained by the force created by the two different magnetic stir bars. The shear introduced by the larger magnetic stir bar could have led to higher coalescence and break-up of droplets before particles can be formed, thus leading larger droplet sizes (Kong *et al*., 2012). Even though formulation D1 had the smallest average particle size, and also the highest encapsulation efficiency, surprisingly, the microparticles were irregularly shaped and was observed to produce agglomerated mass (Figure 4.7a). Both of these formulations attributes strongly influenced their cumulative release kinetics. The cumulative release was observed to be the highest from formulation D2 followed by formulation D3 and finally from formulation D1.

Formulation D3 (Figure 4.7c) had the largest microparticle sizes and the lowest encapsulation efficiency, however, we observed better cumulative release kinetics in this formulation as compared to formulation D1. This particle sizes observed in formulation D3 indicates that the average size and standard deviation of microparticles increase with the increase of stir bar length. This confirms that microparticles can be broken up into small fragments after minimal stir bar was used. The encapsulation of SIM in PLGA microparticles was also been influenced by different length of stir bars. Formulation D2 exhibited superior encapsulation efficiency, thus the 1.0 cm magnetic stir bar was chosen for the synthesis of microparticles which would ultimately be fabricated into scaffolds for the bone tissue-engineering study.



a b c

Figure 4.6: Scanning electron micrographs of SIM loaded degraded biodegradable microparticles for (a) Formulation D1 (0.5 cm) (b) Formulation D2 (1.0 cm) and (c) Formulation D3 (1.5 cm).

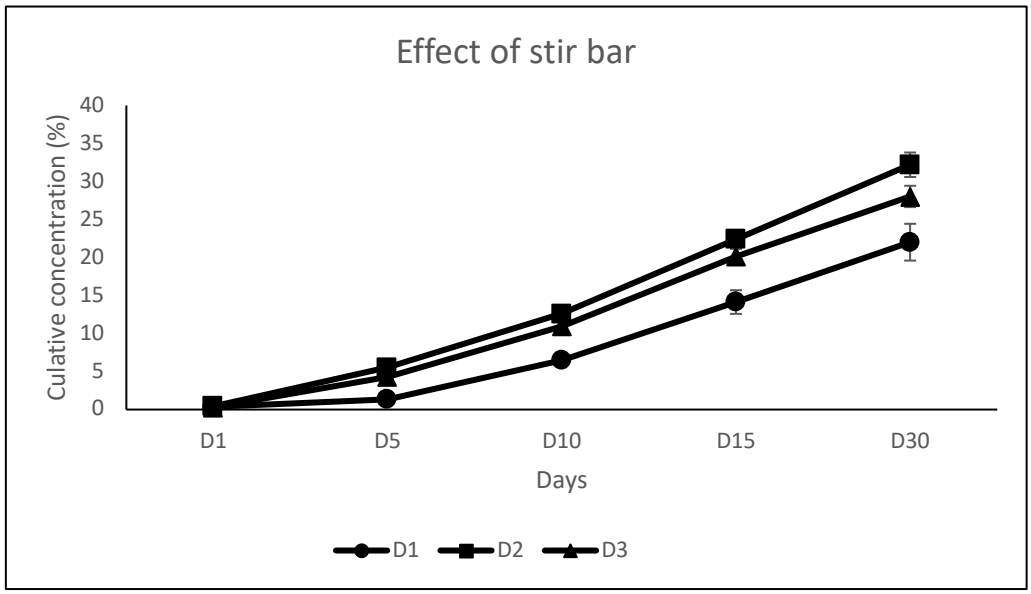


Figure 4.7: Effect of stir bar on in-vitro release kinetics of SIM-loaded biodegradable polymeric microparticles (data represent mean ± standard deviation; n = 3).

4.3.1.7 EFFECT OF DRUG AMOUNT

The mean particle size of formulations E1 and E2 prepared using 1 mg or 2 mg, respectively, with particle size ranges within 19.92 ± 24.87 µm for formulation E1 and 20.29 ± 27.56 for formulation E2 (Table 4.2). The particle size increased when the amount of drug was increased to 3 mg, 4 mg, or 5 mg (formulations E3–E5). This was attributed to the increased content of drug present. These results are in agreement with a previously published study from Sharma *et al.* (2016) where a 50% increase in particle size was observed when the drug concentration was increased from 0.2% to 1.0%.

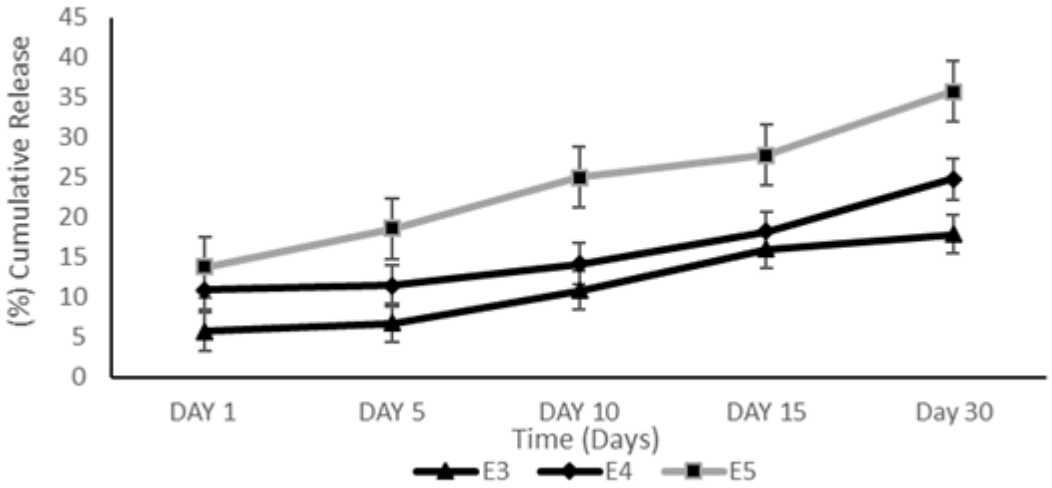


Figure 4.8: Effect of drug amount on in-vitro release kinetics of SIM-loaded biodegradable polymeric microparticles (data represent mean ± standard deviation, n = 3).

Negligible drug encapsulation was observed in Formulation E1 and E2. The drug added to these formulations was probably affected by the drug-polymer interactions and the drug miscibility in the polymer (Panyam *et al*., 2004). Lower drug miscibility led to lower drug incorporation and ultimately lower encapsulation of SIM in the formulation. Consequently, there is an implication that the amount of drug plays a very pivotal role in influencing the encapsulation efficiency of SIM-loaded PLGA microparticles. Studies show that the internal micro-morphology of the microparticles is not affected by an increase in drug loading (Mao *et al.,* 2008). On the contrary, our study showed the opposite pattern where the amount of drug had a significant impact on drug encapsulation

and cumulative kinetic release. SIM is a hydrophobic drug which has a low aqueous solubility and shows dissolution rate-limited absorption (Park, 2009). During the preparation of the microparticles, PLGA was dissolved in the organic phase that was emulsified with the assistance of a surfactant or stabilizer. SIM were added directly to the oil phase. The resulting emulsion was then added to a higher volume aqueous phase and this was stirred for several hours which allowed the DCM to evaporate. The loss of SIM might have occurred during the preparation stage, and this led to a low percentage of SIM ultimately being encapsulated. This is likely to be what was observed in the formulation of E1 and E2.

The encapsulation efficiency exhibited an upward trend (formulation E3 to E5) as amounts of drug included in the formulation were increased. It was observed that the cumulative amounts of drug released at 30 days from the formulations containing 3 mg, 4 mg or 5 mg of drug were 11.68 ± 0.5, 24.89 ± 0.3 and 35.74 ± 0.8, respectively (Table 4.2). The rate of drug release was lower from formulation E3 (drug content 3 mg) and higher when greater amounts of drug were included in the initial formulation (Figure 4.8). The slower rate of release, as well as cumulative amount released after 30 days, may be attributed to a relatively higher proportion of polymer in the formulation which in turn hindered the diffusion of drug from the microparticles. These results indicate that, when higher amounts of drug were included in the starting formulation, then drug release is independent of the amount of drug present in the formulation. Hence, it is assumed that formulation E6 with 6 mg of drug will also show a similar pattern. Therefore, formulation E6 was not characterized for drug release.

4.4 CONCLUSION

The key aim of this chapter was to optimise the production process to ensure successful drug loading with high encapsulation efficiencies. SIM was successfully incorporated into microparticles prepared using IMW and HMW PLGA. It was shown that process and formulation variables could be optimised to achieve the desired characteristics including appropriate particle size, entrapment efficiency and in vitro drug release kinetics.

Homogenization speed in the formulation preparation was found the best at 4,000 rpm (formulation E4). Although not linear, the increase in encapsulation efficiency was greater when the speed was increased. In this case, energy density, which is energy applied per unit total volume, had a direct effect on the size of the emulsion droplets produced. The evaporation time in the NPMP preparation was optimized to 4 hours as it was seen to successfully gave the highest encapsulation efficiency The inclusion of 0.06% PVA gave a stable aqueous phase as compared to other concentration of PVAs which leads to formation of microparticle dispersion without and agglomerated mass with increase encapsulation efficiency. This effect of surfactant concentration played a significant role in the prevention of coalescence of the oil globules between the microparticles. Effect of different polymer molecular weight showed HMW polymer has more capability in SIM encapsulation as compared to IMW polymer. Subsequently, we maintain 1 g of PLGA polymer for the microparticles formulation as this formulation was seen giving microsphere particles within the microsizes. In addition, this amount was successfully loaded with SIM. The encapsulation efficiency was seen highest too among the amount of polymer used. Since amount of polymer play a vital role in determining drug release, 1 g of polymer is sufficient enough to be selected as the model for the subsequent scaffold study as the amount of SIM was limited too. The more polymer is added in the formulation, the more amount of SIM is required to produce the cumulative release. In terms of size of stir bar, the size of the microparticles were affected by changes in the size of the stir bar, with the formulation prepared using the 1.0 cm bar providing the best range of microparticle diameter and demonstrating accelerated SIM encapsulation efficiency as compared to those prepared using the 1.5 and 0.5 cm stir bar. This effect was probably due to the difference in shearing forces produced as a result of two different sized stir bars, and this led to a lower droplet size in the microparticles prepared using the 1.0 cm bar as compared to 1.5 cm stir bar. With the optimal microparticle production parameters determined, the following work will examine the characterization of the microparticles and determine their suitability for 3D scaffold fabrication.

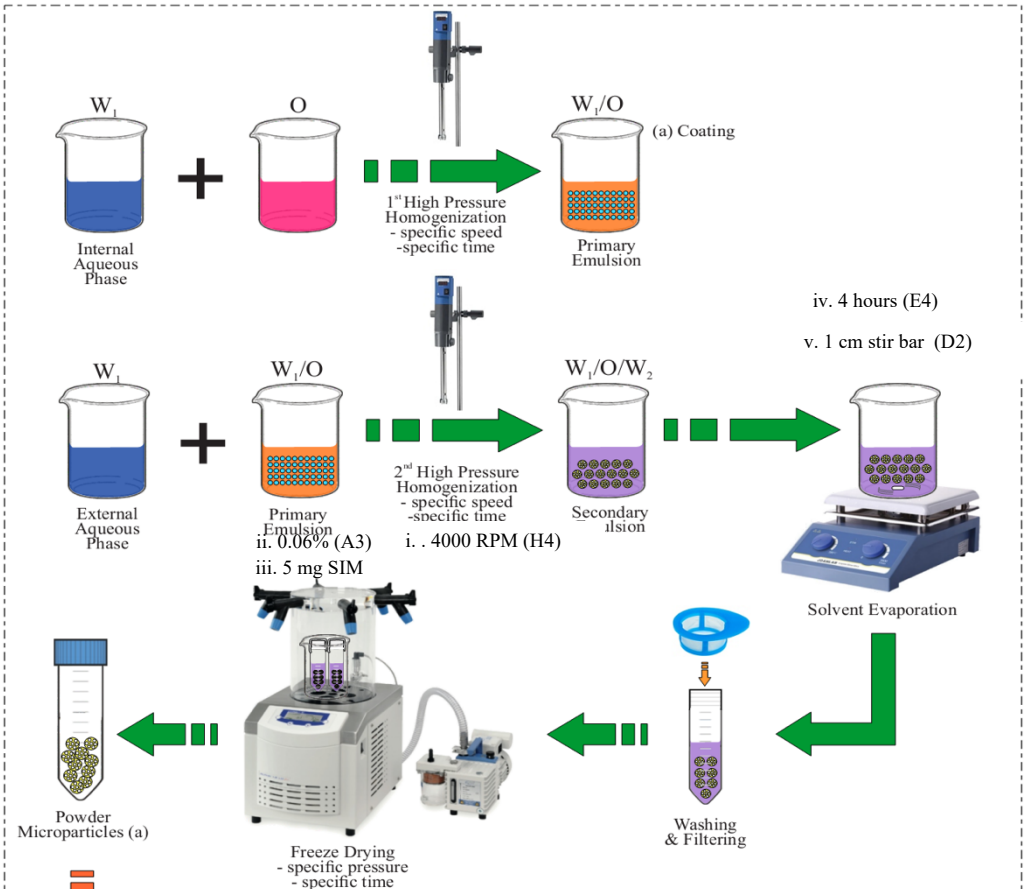


Figure 4.9 The flow chart of microparticles preparation after optimizing the process using different variables. i.Homogenization process at 4000 rpm, ii) surfactant concentration, iii). 5 mg of SIM, iv) 4 hours of evaporation process, v) 1 cm stir bar.

CHAPTER 5

PHYSICOCHEMICAL CHARACTERIZATION OF SIM-LOADED POLY(DL-LACTIC-CO-GLYCOLICACID) MICROSPHERES

5.1 INTRODUCTION

In this study, SIM was used as a drug which for release from the PLGA microspheres. Microspheres embedded within such a scaffold system have been shown capable of releasing therapeutic SIM and stimulating osteogenesis. As the scaffold and microspheres degrade the SIM-stimulated bone repair will gradually transfer the load on the fracture from the scaffold to the new bone. It is therefore crucial to characterise the composition of the SIM loaded polymer microspheres to understand their performance in such a complex scaffold therapeutic system.

The two principal characterization techniques employed here involve characterization within the microparticles and also surface characterization of the microparticles. It is well-known that, on heating or cooling, crystalline active pharmaceutical ingredients (API) can experience phase transitions which lead to the formation of polymorphs with significantly different physical properties. This, in turn, often has a considerable effect on the bioavailability of a drug from a different polymorphic form (Jin *et al*., 2014; Simões *et al.,* 2013). In terms of analytical analysis in chemical structure the crystalline phase (X-ray powder diffractometry (XRD), Differential Scanning Colorimetry (DSC), nuclear magnetic resonance (NMR), fourier-transform infrared spectroscopy (FTIR), near-infrared spectroscopy (NIR), and trace constituents such as High-performance liquid chromatography (HPLC), Liquid chromatography–mass spectrometry (LC/MS), Gas chromatography–mass spectrometry (GC/MS). These are among the instruments to measure the structure−energetics relationships between drug (in this case the SIM) and the polymers.

XRD is of interest to establish the effect of polymer on the kinetics of crystallization of a drug. A drug which is expected to show comparatively rapid

crystallization in pure form is expected to crystallize over an extended time period when it is dispersed in a suitable polymeric carrier (Thakral, 2018). However, some drugs loss their crystallization properties during fabrication process and becomes amorphous structure (for example during the mechanical treatment, heating (quench cooling or desolvation) and various solvent-based processes including rotary evaporation, double emulsion solvent evaporation, precipitation and spray-drying (Kavanagh *et al*., 2012). Crystallization structure in a freeze-dried formulation can also be determined using XRD. This analysis is important as to rule out the physical state of solutes in the final lyophile is a complex interplay of process and formulation variables.

Surface characterization, as the name implies, involves the analysis of various properties of the microparticle surface. The surface characterisation of a microparticle systems is crucial in understanding how composition and environment affect physicochemical character and performance. Surfaces may be characterised according to Brunauer–Emmett–Teller (BET) analysis, particle size (light scattering methods), and surface charge, i.e. zeta potential. Surface morphology on the hand can be characterized via scanning electron microscope (SEM) or atomic force microscope (AFM). SEM provides visualisation on the scale but offers no distinction of chemical constituents. AFM is a high-resolution scanning probe technique that allows visualization of the textures and shapes of material surfaces and their topographical features in three-dimensional maps. The sensitivity of the cantilever tip radius is very crucial since they will determine the precision of feedback signal in the AFM contact mode. There is an exceptionally good vertical resolution when a surface is scanned with a sharp tip attached to a sensitive cantilever and monitoring the force between the surface and the tip surface (Garg *et al.,* 2005; Yuana *et al*., 2010; Govedarica *et al*., 2010; Lal *et al*., 2010; Martins *et al*., 2014; D.A., 2014; Islam, *et al.,* 2014). This advance instrument is capable to visualise the material surfaces, their topographical features with resolution which further allow for measuring the surface physicochemical properties. This advantage belongs to AFM offers a unique capacity to complement broader chemical and visual analysis with nanometre resolution topographical, and simultaneous mechanical characterisation.

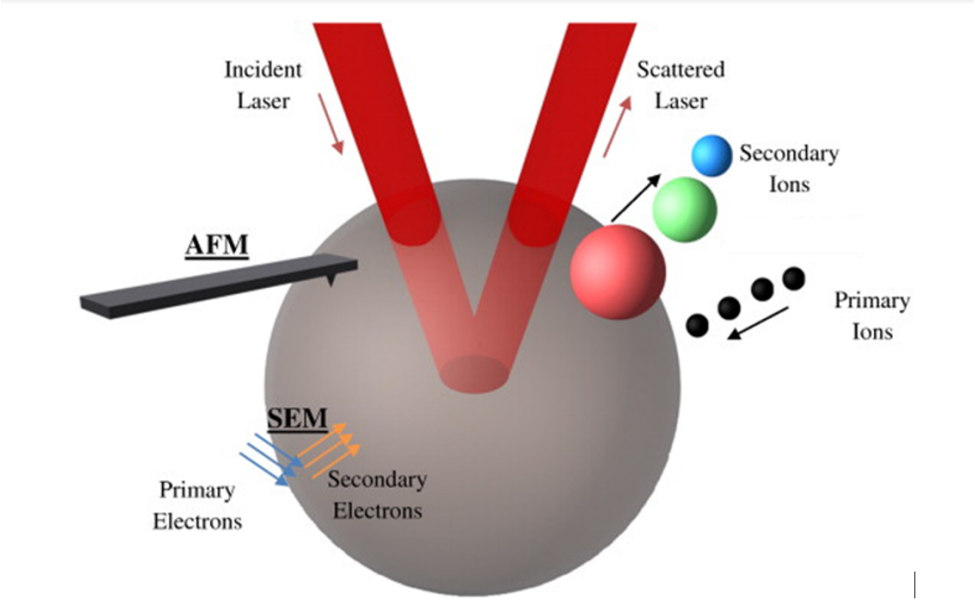


Figure 5.1: Analytical methods applied to the microsphere samples (Rafati *et al.*, 2012).

The work in Chapter 4 examined the incorporation of SIM in the microparticles and also particle size analysis. In Chapter 5, the aim was to:

i) characterize the structural-energetics of SIM-NPMP of two different molecular weight, the intermediate molecular weight (IMW) and HIGH molecular weight (HMW) with respect to the crystalline phase that belongs to SIM before it is encapsulated into the microparticles via XRD and DSC.

ii) investigate any possible interaction between SIM and the formulation components using FTIR and finally

iii) investigate the influence of different polymer molecular weight and SIM encapsulation on the surface phase behaviour and topography.

5.2 MATERIAL AND METHODS

5.2.1 MATERIALS

PLGA (lactic acid: glycolic acid ratio, 85:15) of intermediate (53 kDa) and high (92-109 kDa) molecular weight was purchased from Evonik (USA). Dichloromethane (DCM) was acquired from Fisher (UK) and phosphate buffered saline (PBS) was procured from Gibco (UK). Poly vinyl alcohol (PVA) 100% hydrolysed) and sodium hydroxide (NaOH) pellets were both obtained from Sigma Aldrich (UK). Dimethyl sulfoxide (DMSO) and sodium dodecyl sulfate (SDS) were bought from Fisher (UK). SIM was purchased from Merck (USA). Phosphate buffered saline tablets (0.01M phosphate buffer) was purchased from Sigma Aldrich.

5.2.2 METHODS

5.2.2.1 X-RAY POWDER DIFFRACTOMETRY (XRD)

The crystallinities of SIM, SIM-NPMP and blank NPMP microspheres were evaluated by X-ray diffractometry using a D8 Advance instrument (Bruker Optik GmbH, Ettlingen, Germany). Scanning was performed up to 2θ range between 2° and 90° using an Ni-filter.

5.2.2.2 DIFFERENTIAL SCANNING CALORIMETRY (DSC)

SIM, SIM-NPMP and blank NPMP samples were measured (3 gram per sample at each test) and sealed under air, in aluminium pans, and weighed to ± 0.1 µg on a Mettler UMT2 ultra-micro balance. A standard aluminium pan was used as the reference. The glass transition temperature (T_g) of the pure SIM, pure PLGA IMW and HMW and non-porous PLGA SIM-loaded microspheres were determined using a TA Q2000 DSC instrument equipped with an RCS40 cooler (TA Instruments Delaware, USA). Both the sample and the reference pan were heated from 0 ºC to 250 ºC at 10 ºC/min using nitrogen as the purging gas at 50 ml/min. The first heating cycle was used for the assessment.

5.2.2.3 FOURIER TRANSFORMATION INFRARED SPECTROSCOPY (FTIR)

The samples were mixed with solid potassium bromide (KBr) and then pressed into a very thin disc. The discs were placed into the holder onto which the IR laser beam was directed. Spectra were recorded using a Frontier™ is PerkinElmer model, loaded with IR solution software (version 1.2). IR spectra of the pure drug (SIM) and the polymer alone (IMW and HMW) were compared with the IR spectrum obtained for the SIM–loaded PLGA microspheres to look for any major features.

5.2.2.4 SCANNING ELECTRON MICROSCOPY (SEM) AND SIZE ANALYSIS

All three samples (SIM, SIM-NPMP and blank NPMP) were mounted on metal stubs and the surface morphology was viewed under a scanning electron microscope (FE-SEM, Quanta 400F, FEI, USA). The paticle sizes were measured by processing the image using Image J software (Java 1.8.0_172) to obtain the particle size diameter.

5.2.2.5 LASER DIFFRACTION ANALYSIS

All three samples (SIM, SIM-NPMP and blank NPMP) were analysed for its particle size and mean diameter distribution (polydispersity index) by laser diffraction analysis using a Mastersizer 2000 (Malvern, UK). The preparation of the sample was as follows: the microparticles were uniformly dispersed in distilled water with the aid of ultrasonic vibration. The samples were measured in triplicate to calculate the mean diameter and polydispersity index (PDI).

5.2.2.6 ATOMIC FORCE MICROSCOPY

Atomic force microscopy (AFM) was used to study the nanoscale topography and phase behaviour of the samples (SIM, SIM-NPMP and blank NPMP). Measurements were conducted at a temperature of 25 °C and a relative humidity of 20%. Commercial silicon AFM tips (BrukerNano, Germany) were used with spring constants from 20 to 80 N m and resonance frequencies between 347 and 393 kHz. Mica slides (Agar Scientific, Stansted, U.K.) were used as the sample substrate. NanoScope Analysis Version 1.70 (BrukerNano, Germany) was used for analysis. The following parameters were evaluated, root mean square

roughness (Rq) presented in Table 5.2, skewness of surface height distribution (Ssk) and kurtosis of surface height distribution (Sku) are presented in Table 5.3.

Roughness (Rq) is defined as the standard deviation of the elevation, z values, within the given area, is calculated from

$$R_q = \sqrt{\frac{\sum (Z_i)^2}{N}} \quad \text{..... Equation 5.1}$$

Measures the symmetry of surface data about a mean data profile, expressed as:

a. Skewness: is a non-dimensional quantity which is typically evaluated in terms of positive or negative.

$$Ssk = \frac{1}{R_q^{\,3}} \frac{1}{N} \sum_{j=1}^{N} Z_j^{\,3} \quad \text{..... Equation 5.2}$$

b. Kurtosis: is a non-dimensional quantity used to evaluate the shape of data about a central mean. It is calculated as:

$$Sku = \frac{1}{R_q^{\,4}} \frac{1}{N} \sum_{j=1}^{N} Z_j^{\,4} \quad \text{..... Equation 5.3}$$

Graphically, kurtosis indicates whether data are arranged flatly or sharply about the mean.

5.3 Results and Discussion

5.3.1 XRD Analysis

The XRD patterns of the samples were able to show whether a crystalline SIM phase was present in the complex of the SIM-microparticles. Figure 5.2a depicts several distinct peaks in the XRD of SIM at diffraction angles of 2°, 11°, 13°, 15.5°, 16.5°, 17.5°, 19°, 23.5° and 24.5° which indicate that SIM was present in

a crystalline form (Guan *et al*., 2015; Wu *et al*., 2016; Shid *et al.,* 2014). In contrast, these peaks were not observed in the XRD pattern of the SIM-NPMP (Figure 5.2b) suggesting that the crystallinity of SIM was not preserved in the a drug-microparticle complex. SIM may be either molecularly dispersed throughout the polymer or distributed in an amorphous form after its entrapment into the PLGA microspheres by freeze-drying. A change in the crystallinity of SIM when incorporated into microparticles has also been observed by other researchers (Pandya *et al*., 2011; Philip *et al*., 2012; Shid *et al*., 2014; Masaeli *et al.,* 2016; Wu *et al.,* 2016).

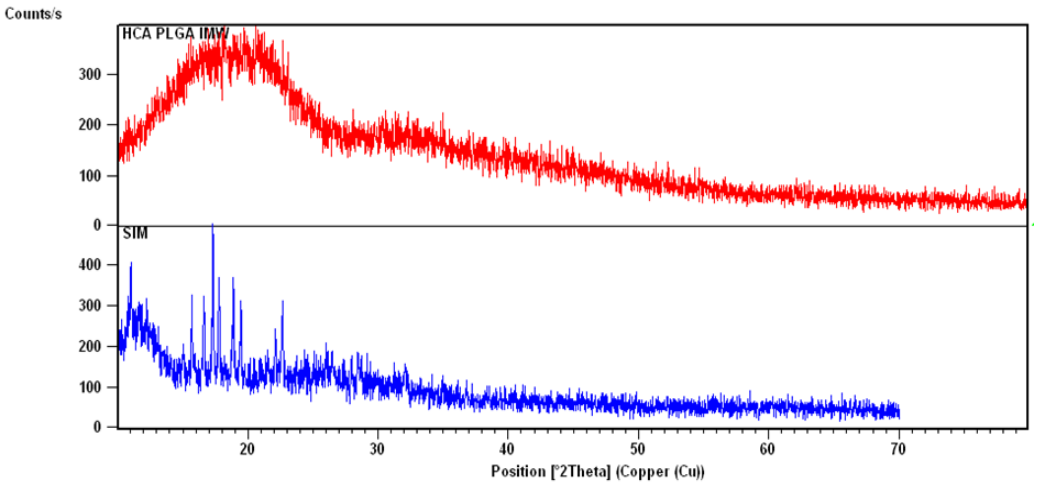


Figure 5.2a: X-ray diffraction spectra of (A) SIM; (B) blank microspheres.

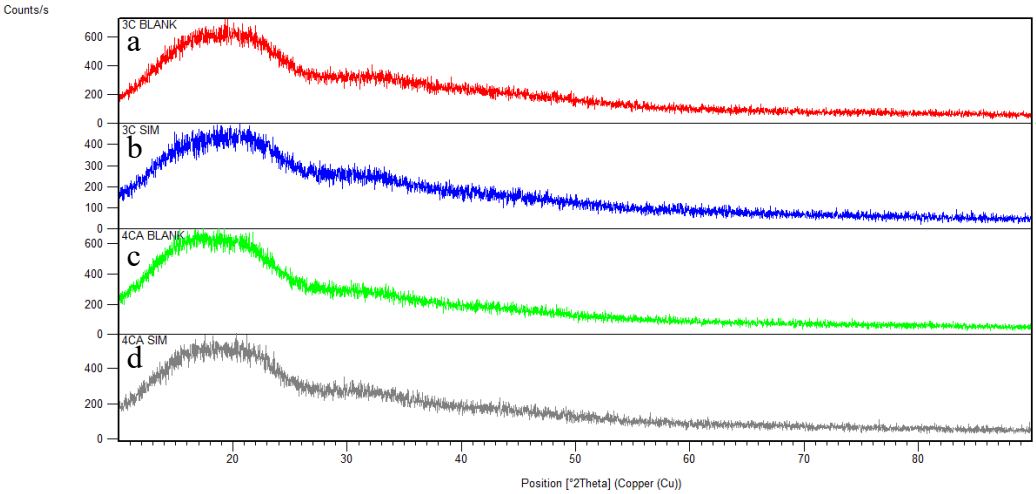


Figure 5.2b: X-ray diffraction spectra of (a) HMW blank microspheres; (b) HMW-SIM microspheres, (c) IMW blank microspheres and (d) IMW-SIM microspheres.

A solid material can exist in the crystalline state, an amorphous form or a mixture of the two different states. Whilst the crystalline form is characterised by regular and well-defined molecular packing, molecules in the amorphous state are arranged irregularly (Hancock *et al*., 1997; Antal *et al*., 2008; Kumar *et al*., 2012). The structure of an amorphous solid is usually described as having a crystal-like short-range molecular arrangement, but lacking a long-range order and have a disordered arrangement as depicted in Figure 5.2 c. (Einfal *et al*., 2013). Consequently, there exists more space between the molecules resulting in an increased specific volume compared to the crystalline composition (Yu, 2001; Jacob *et al*., 2012; Löbmann *et al.,* 2013). The transformation of a crystalline drug into the amorphous form is a widely employed technique for increasing aqueous solubility, however, drugs in the amorphous form are less thermodynamically stable, has more greater chemical instability due to its random arrangements and subsequently it is potential to alter the mechanical properties of a drug. (Wu *et al.,* 2016, Karagianni *et al*., 2018). Hence, in this work, co-precipitation of SIM within PLGA polymeric excipients was achieved via solvent evaporation process. The SIM presented in the polymeric microparticles was in an amorphous state as verified by the X-ray diffraction (XRD) patterns. Generally, amorphous drug co-existing in microparticles could provide a fine sustained release profiles with full release completeness (Li *et al.,*

2014). Therefore, solvent evaporation process is seen to be a useful method for developing a sustained drug release profile.

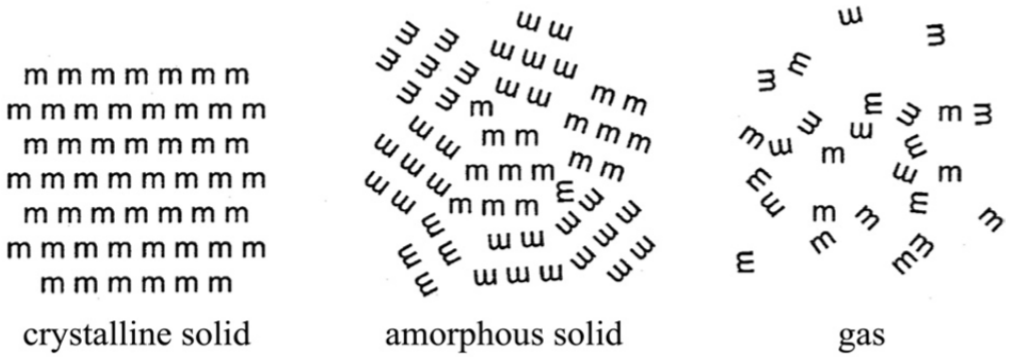


Figure 5.2 c: Schematic representation of the structure of an amorphous and a crystalline solid. Image adapted from Einfal *et al*., 2013.

5.3.2 FTIR Analysis

FTIR spectroscopy is widely used by researchers to verify the chemical characteristics of drugs and polymers used in the preparation of polymeric microspheres. FTIR spectroscopy was used to study the possible interactions between SIM and the polymer. Here as compared to FTIR analysis in Chapter 2, we compare the characteristic features of HMW and IMW NPMP with and without the SIM.

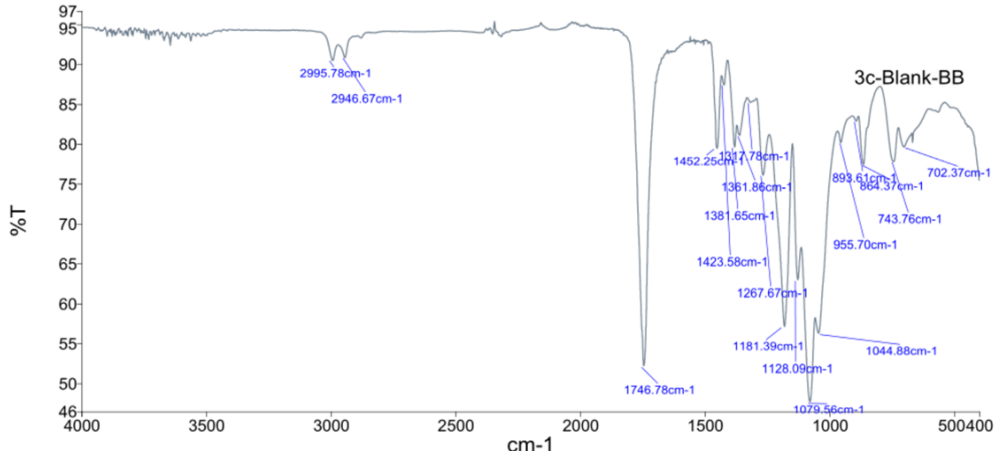


Figure 5.3a: FTIR of HMW-NPMP blank

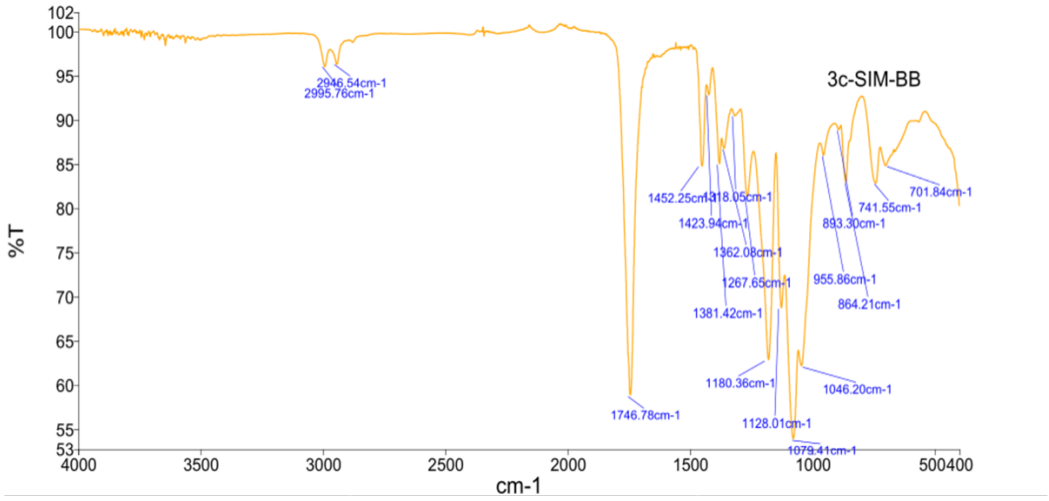


Figure 5.3 b: FTIR of HMW- NPMP with SIM.

As mentioned in chapter 2 (Section 2.3.5), the major peaks were observed in the mixture of SIM-NPMP and SIM-PMP however there was no

significant difference found in the FTIR spectra of pure drugs and PLGA. As in Chapter 2, the initial formulation of NPMP and PMP maintained its crystallinity as no bands broadening and shifted of peaks were observed. However, upon optimization of NPMP in chapter 4, the FTIR peaks were found shifted in both HMW and IMW formulation.

In this chapter, the FT-IR spectrum of the SIM-NPMP seemed to be the summation of drug and carrier. In the HMW formulation, the SIM-NPMP peaks were found to have shifted as compared to the peak in the spectrum from blank-NPMP particularly at the 700-1000cm-1 (Figure 5.3a and Figure 5.3b). It suggested that there were interactions between the drug and carrier in the SIM-loaded microparticles. As the drug and carrier interact, then the functional groups in the FT-IR spectra will show band shifts and broadening compared to the spectra of SIM and PLGA (Philip *et al*., 2012).

Similarly, in the IMW formulation, the bands were found shifting between 700-1050 cm-1. Although the peaks shifting is small, but it shows some peaks movement after SIM was added into the HMW and IMW PLGA for the NPMP preparation. Therefore, this implies structural changes of the microparticles upon adding the drug. In addition, based on the obtained results, the formulation with IMW shows multiple peaks shifting as compared to the HMW formulation.

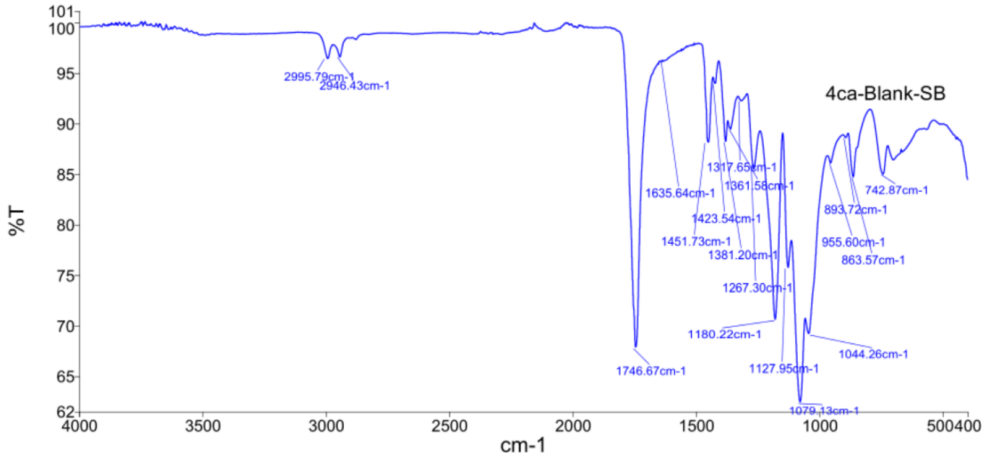


Figure 5.3c: FTIR of IMW- NPMP Blank.

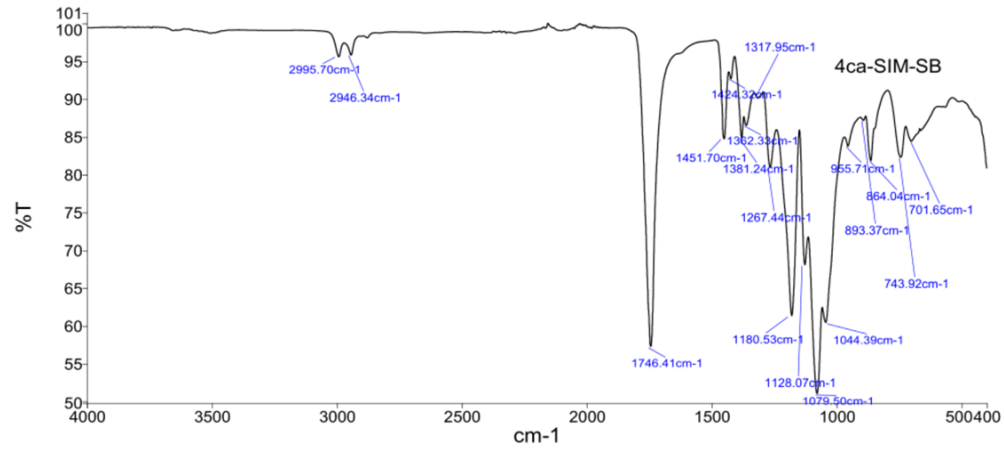


Figure 5.3d: FTIR of IMW- NPMP SIM.

The comparisons of the spectra suggest interaction between the drug and the polymer and the shifted bands observed in the SIM-NPMP spectrum during the preparation with double emulsion solvent evaporation indicate successful incorporation of SIM with the PLGA for both IMW and HMW respectively. The observations of peak broadening and shifting suggest that the drug-polymer complex was transformed into the amorphous state could be due to the mechanical agitation during the fabrication process as supported by Philip *et al*. (2012).

5.3.3 DIFFERENTIAL SCANNING CALORIMETRY (DSC) ANALYSIS

DSC analysis was carried out in order to determine the physical state of the drug in the microspheres. DSC as a technique quantifies heat transfer during physical and chemical processes. Figure 5.4 shows the DSC thermogram of SIM, pure PLGA and the optimized formulation of solid dispersion of IMW-SIM NPMP and HMW-SIM NPMP respectively. The DSC curve representing SIM, which exists naturally in the crystalline state, showed a sharp endothermic peak at 138.5 °C, indicative of the melting of a crystalline form. This is consistent with the SIM melting point which ranges from 136 °C to 140 °C (Sopyan *et al*., 2017; Gowda *et al*., 2014; Jagtap *et al*., 2012; Mandal, 2010; Silva *et al*., 2010). An endothermic peak for IMW PLGA was observed at 52.1 °C and for the HMW PLGA, this was seen at 52.7 °C.

It is also important to note that the endothermic peaks shifted and broadened for both PLGA, IMW and HMW, after encapsulated with SIM as compared to the blank formulation. The endothermic peaks shifted to 50.3 °C for IMW (Blank 54.8 °C) and to 51.5 °C for HMW (Blank 53.6 °C). Thermogram of IMW-SIM NPMP and HMW-SIM NPMP showed no such characteristic peak of SIM, indicating that the drug was uniformly dispersed at the molecular level in the microspheres (Jagtap *et al.,* 2013). The shift of the melting point also indicates a reduction in drug crystallinity in SIM-loaded PLGA microparticles. It indicates that the polymer used in the formulation had a significant effect on the thermal properties of drug. It might be due to the conversion of the crystalline form of SIM to the amorphous form or it may be as a result of the dissolution of crystalline SIM into the PLGA carrier (Gowda *et al*., 2014; Mandal, 2010). The absence of a peak in SIM in microparticles has also been observed in multiple other studies including where PLGA microspheres have been prepared using the electrospraying method (Nath *et al*., 2013). Similar results were seen with the DSC analysis of submicron particles of SIM prepared using spray drying method (Anzar *et al*., 2018), and also with SIM microcapsules made using the orifice gelation technique (Bal *et al*., 2012). These results are consistent with the XRD analysis, which revealed that SIM is crystalline while after encapsulated into the PLGA, it becomes amorphous (Pang *et al.,* 2011).

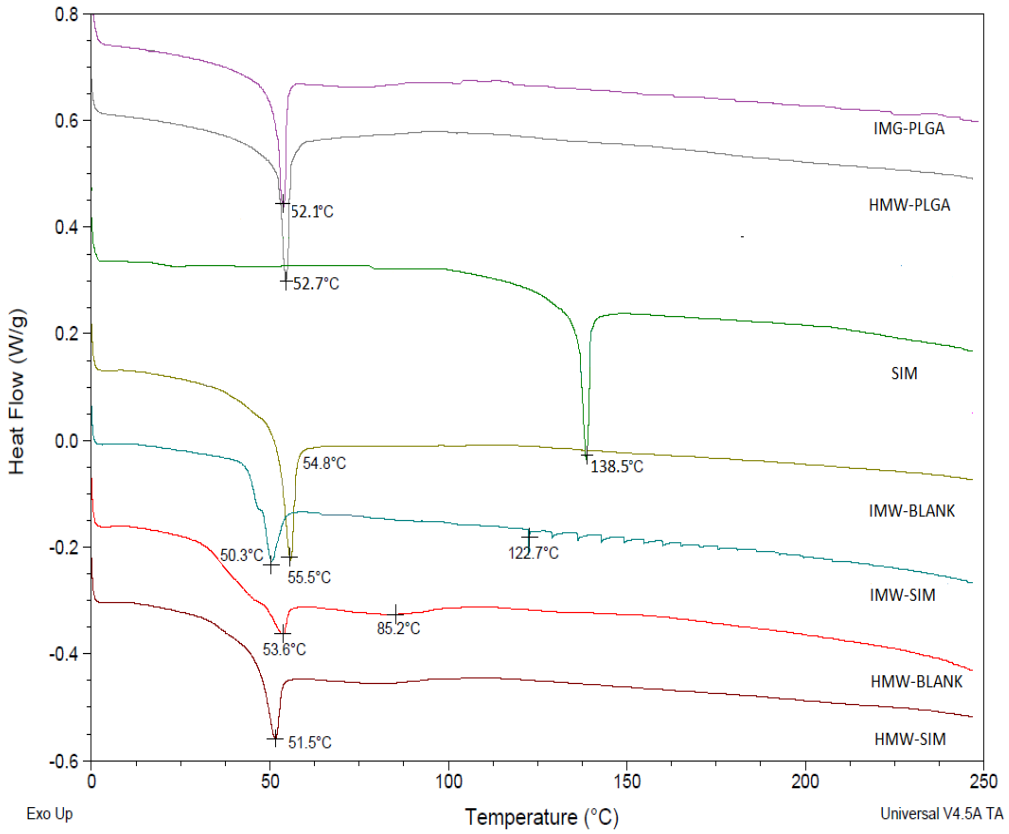


Figure 5.4: DSC thermogram of SIM, pure PLGA and optimized formulations of solid dispersions of IMW-NPMP and HMW-NPMP, pure IMW PLGA and HMW PLGA

5.3.4 Evaluation of Surface Characteristics Using Scanning Electron Microscopy (SEM) and Atomic Force Microscopy (AFM).

SEM and AFM have been extensively used to examine the morphology and size of polymer-based microspheres. The physical characteristics of drug carriers affects their response both *in-vivo* and *in-vitro*. In this section, we are focusing on the surface characteristics of the SIM-NPMP. Figure 5.5a shows the crystalline structure of SIM before the fabrication into the microspheres.

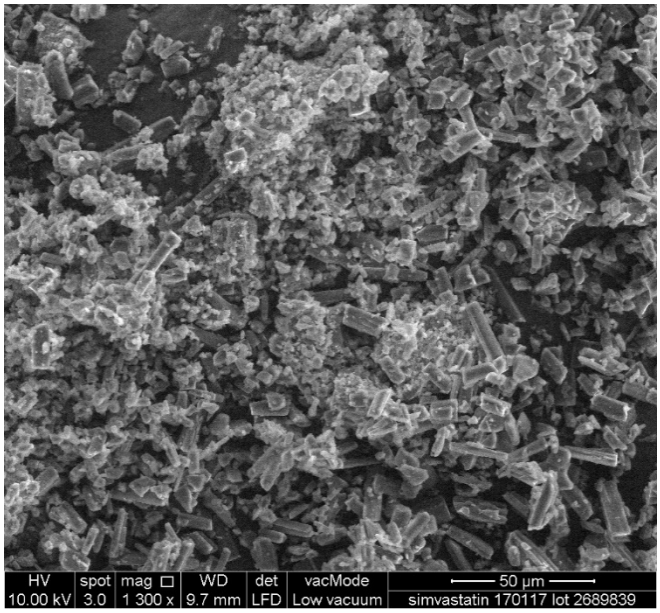
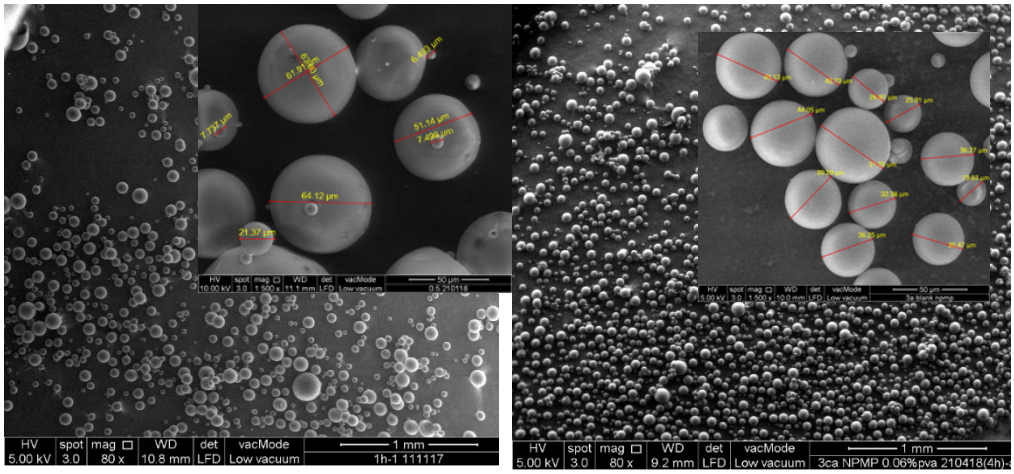


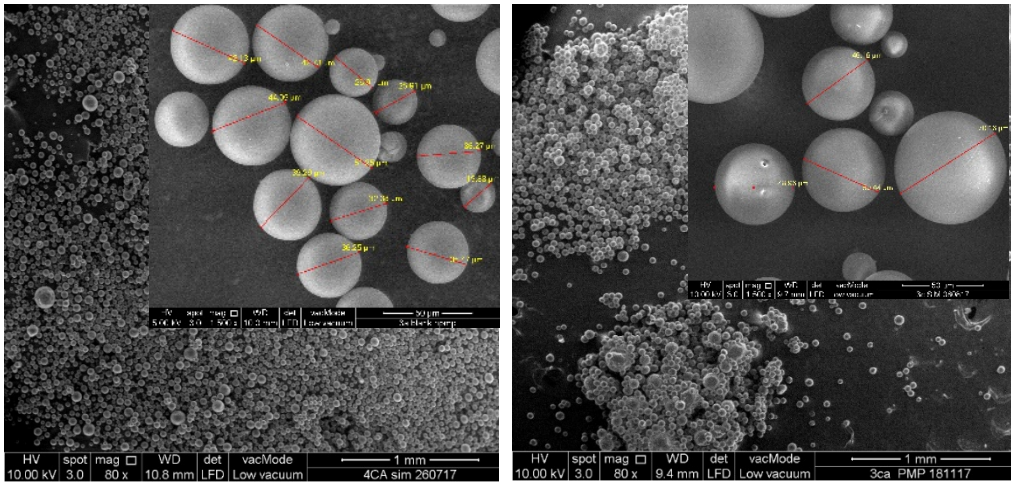
Figure 5.5a: The pure SIM crystalline structure observed under SEM.

5.3.4.1 SCANNING ELECTRON MICROSCOPY (SEM)

SEM was employed to gain an understanding of the size distribution and surface topography of the SIM-NPMP microspheres Figure. 5.5 b. In all cases, the microspheres were spherical, and no drug crystals were observed. The size of the microspheres varied between (Table 5.1). From the image obtained, no visible surface pores were observed on the microspheres. Rafati *et al.* (2012) suggested that formation of non-porous microparticles could be due to the inversion stage of the microemulsion where the PVA water phase is fully encapsulated in the PLGA-rich oil droplets and would not be expected to produce the surface pores. No microsphere agglomeration was observed following the optimization steps that were outlined in Chapter 4 and no deposition of debris was observed around the microparticles either. In the absence of SIM, the microparticles appear to possess a smooth surface and the average particle size is smaller than the microspheres containing SIM which were prepared with both IMW and HMW PLGA.



i iii



ii iv

Figure 5.5 b: SEM images of different preparations i=IMW-BLANK-NPMP, ii= IMW-SIM NPMP, iii =HMW-BLANK-NPMP, iv= HMW-SIM NPMP.

Table 5.1: Particle size of the various preparations of microparticles determined using Image J software

Type	Diameter (µm)
IMW-NPMP (Blank)	33.30 ± 22.53
IMW-NPMP (SIM)	42.91± 20.92
HMW-NPMP (Blank)	31.15 ± 16.78
HMW-NPMP (SIM)	40.74 ± 15.05

5.3.4.2 ATOMIC FORCE MICROSCOPY

In this study the influence of different polymer molecular weights on the topography and phase behaviour was investigated by AFM. AFM images illustrated that the surface morphology of the microparticles varied depending on their composition. The microparticles fabricated with HMW PLGA showed higher surface roughness in contrast to those prepared using IMW PLGA (Table 5.2). This behaviour can be attributed to the complexity of the crosslinking mechanism and also to the presence of the longer chain PLGA, and this that could lead to the synthesis of the microparticles with different surface structures (Lungan *et al.,* 2015). The rough surface is an important factor in cell adhesion to scaffolds (Kloczko *et al*., 2015) and modulates the biological response of tissues in contact with the implant (Chang *et al.,* 2011; Smith *et al*., 2011; Ghasemi-Mobarakeh *et al*., 2015; Mohanty *et al.,* 2015; Bružauskaitė *et al*., 2016). In this study, as mentioned earlier in 5.2.2.6, the analysis were focused only on these parameters; the roughness value, the surface skewness (Ssk) and coefficient of kurtosis (Sku). From the analysis of the different type of microparticles, the roughness were measured in 5 different points and the mean of the roughness are calculated. In this study, the AFM images were analysed with nanoscope analysis software.

Table 5.2: AFM mean roughness values for various preparations of microparticles. 5 different points were taken for the analysis.

Point measurement	IMW-NPMP (SIM) (µm)	IMW-NPMP (Blank) (µm)	HMW-NPMP (SIM) (µm)	HMW-NPMP (Blank) (µm)
Point 1	0.0356	0.0142	0.0589	0.0407
Point 2	0.0388	0.0134	0.0512	0.0301
Point 3	0.0402	0.0165	0.0501	0.0463
Point 4	0.0387	0.0199	0.0534	0.0378
Point 5	0.0359	0.0155	0.0523	0.0344
Mean ± SD	0.03784 ± 0.01	0.0159 ± 0.002	0.05318 ± 0.003	0.03786 ± 0.005

Based on Table 5.2, the particles has higher roughness values in SIM encapsulated microparticles as compared to the blank microparticles where the surface roughness is higher in HMW variants as compared to IMW variants. From the analysis of surface roughness, the incorporation of SIM into the IMW and HMW PLGA polymer leads to the increase of surface roughness from 0.03786 ± 0.005 (blank preparation) to 0.05318 ± 0.003 (HMW-SIM NPMP). Whilst for IMW microparticles the surface roughness was analysed as 0.0159 ± 0.002 (blank preparation) to 0.03784 ± 0.01 (IMW-SIM NPMP) respectively. Here in this AFM analysis, the surface roughness values and the dimension of pores are possibly influenced by the nature of the crosslinking agent interacting with the polymer. The surface roughness values are found in the following order: HMW-NPMP (SIM) > HMW-NPMP (Blank) > IMW-NPMP (SIM) > IMW-NPMP (Blank). The histograms of the topographical images were shown in image 5.6 (a-d) respectively. The histograms that contained SIM was found to be broadened as compared to blank microparticles.

Based on the high histograms of the topographical images, we then further evaluated the Ssk and Sku. The Ssk is an amplitude parameter that informs about the degree of asymmetry of surface height distribution. According to the values of Ssk, the surface with positive skewness value is characterized by high peaks and filled valleys, whereas the surface with negative skewness value is characterized by deep valleys and lack of peaks (De, R. R. L. *et al*., 2012, Hymavathi, B. *et al.,* 2015).

Table 5.3: AFM skewness of surface height distribution (Ssk) and kurtosis of surface height distribution (Sku).

Sample code	Ssk (µm)	Sku (µm)
IMW-NPMP (SIM)	0.837	10916
IMW-NPMP (Blank)	-66.2	4.56
HMW-NPMP (SIM)	232	56857
HMW-NPMP (Blank)	-0.174	2.71

Table 5.3 showed a summary obtained from the NanoScope analysis software. It can be observed that the presence of SIM leads to an increased surface roughness values. When the height distribution is symmetrical, the

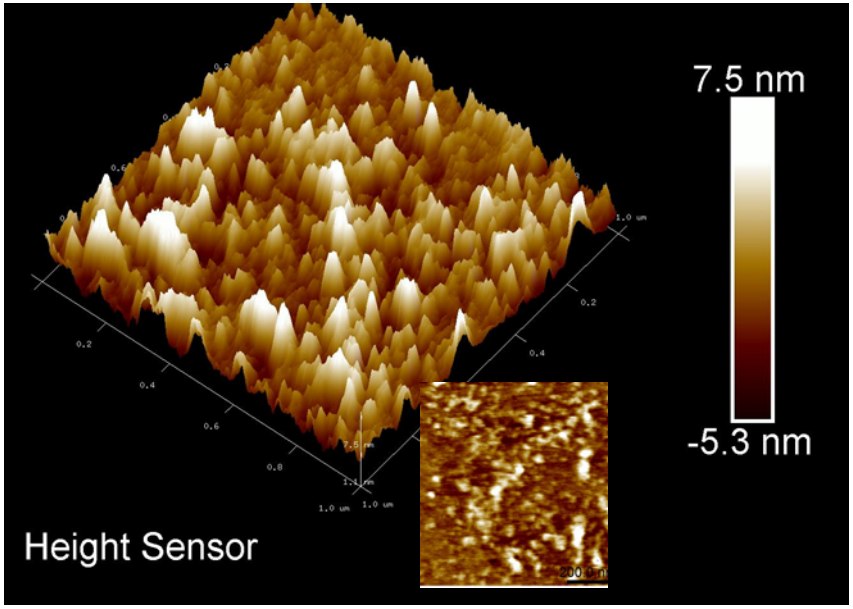
skewness is zero. If the height distribution is asymmetrical, and the surface has more peaks than valleys, the skewness moment is positive and if the surface is more planar and valleys are predominant, the skewness is negative (Bajpai *et al*., 2016).

In this analysis, the IMW-NPMP (SIM) and HMW-NPMP (SIM) have more protruding features as compared to blank microparticles (Fig. 5.6 b and Fig.5.6 d). The Sku for both type of microparticles were found positive. However, the skewness for blank microparticles were negative suggesting the surface is more planar and the valleys are predominant. A flat surface with protruding features would eventually lead to positive skewness, while pits of depression in the surface would lead to negative skewness. Therefore the SIM-encapsulated microparticles has more protruding features as compared to other materials.

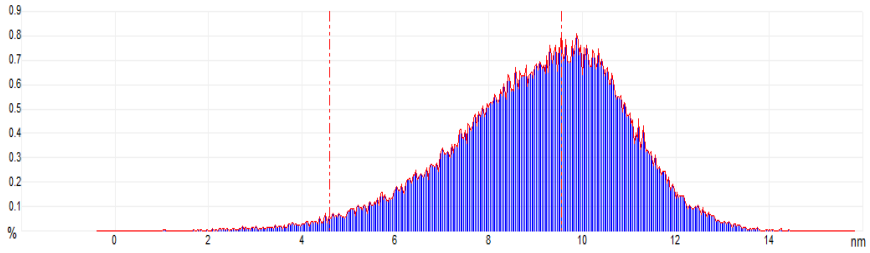
The surface kurtosis (Sku) on the other hand is a measure of the sharpness of surface height distribution. According to Sku formula as depicted in section 5.2.2.6, values may result the following situations (Sedlacek, Podgornik & Vizintin, 2012):

a. Sku = 3 for Gaussian surface;
b. Sku < 3 for surface that present bumpy morphology;
c. Sku > 3 for surface dominated by sharp peaks

For all types of microparticles, the values of Sku were higher than 3 which further suggested the present of sharp peaks except the HMW-NPMP (Blank) which had Sku lower than 3, indicating that the microparticles surfaces were presented with bumpy morphology. Here in this AFM analysis, the surface roughness values and the dimension of pores are possibly influenced by the nature of the crosslinking agent interacting with the polymer. As explained above, the presence of SIM further increased the surface roughness as compared to the blank preparations. Figure 5.6 (a-d) displays AFM images of each microparticles preparation.

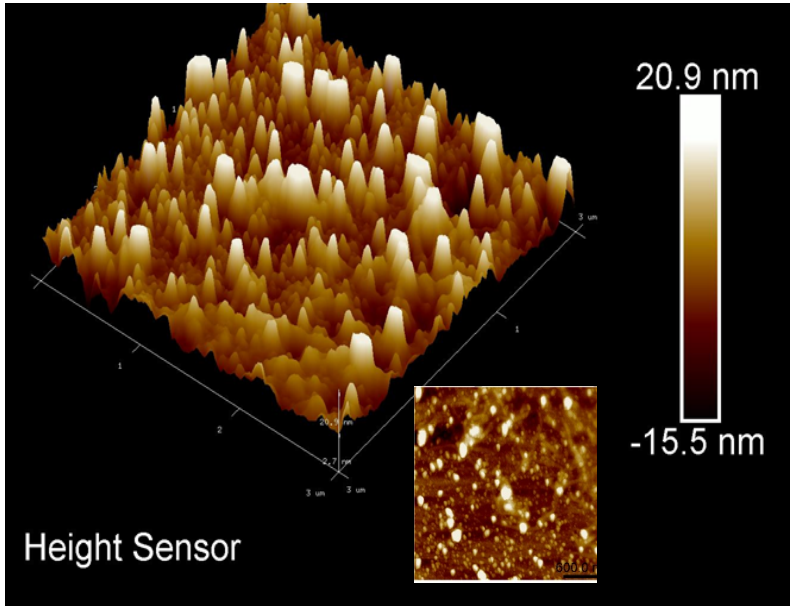


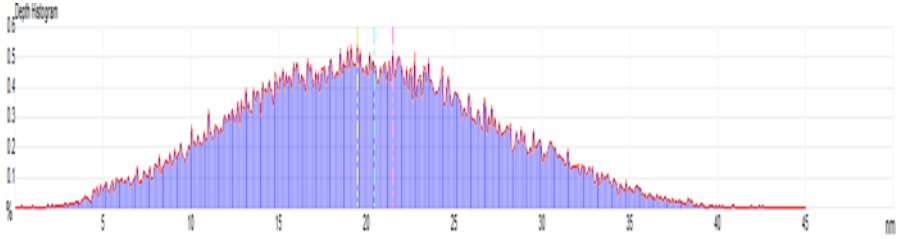
(a)



(b)

Figure 5.6 a: a) Atomic force microscopy (AFM) analysis of IMW-BLANK NPMP. b) the histograms of depth and surface roughness





a b

Figure 5.6 b: a) Atomic force microscopy (AFM) image of IMW-SIM NPMP. b) the histograms of depth and surface roughness.

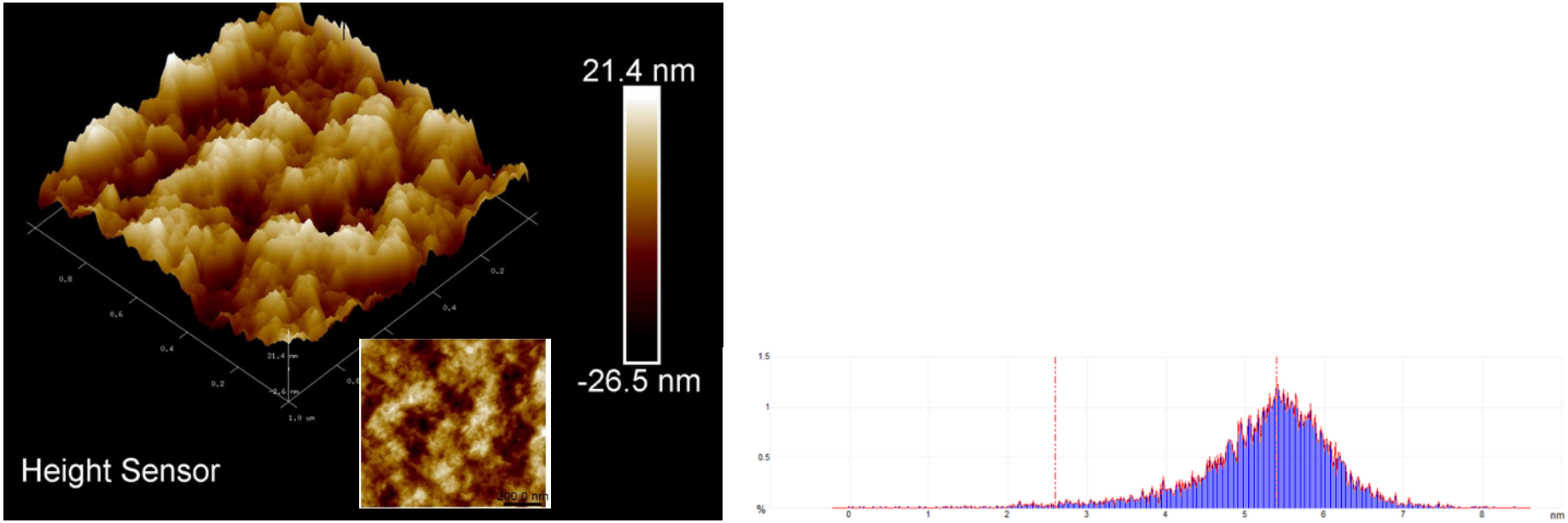


Figure 5.6 c: Atomic force microscopy (AFM) analysis of HMW-BLANK NPMP. b) the histograms of depth and surface roughness.

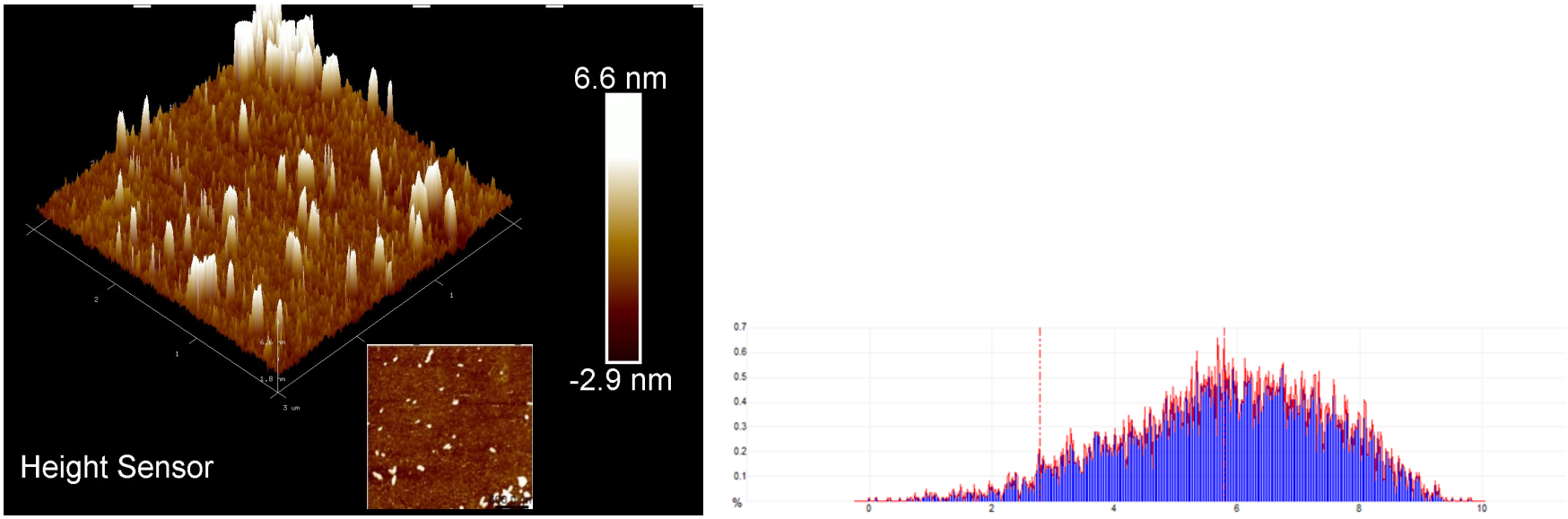


Figure 5.6 d: Atomic force microscopy (AFM) analysis of HMW-SIM NPMP . b) the histograms of depth and surface roughness.

5.4 CONCLUSION

The characteristics of the PLGA microparticles including the chemical characterization, phase behaviour, and topography were obtained using various instruments. From the DSC and XRD studies, SIM exhibited amorphous structure before it is encapsulated into the microparticles however, the crystal structure of SIM as observed in SEM (*Figure 5.5a*) were totally diminished during the fabrication process using the double emulsion solvent evaporation method. This could be due to drug degradation as a result of variations in the resonance structure, rotation of a portion with the possibility of granulation and mixing during the fabrication. However, the characteristics of amorphous structure of SIM in the microparticles may employed the solubilizing and stabilizing, commonly termed solid dispersions, provide avenues for exploiting the benefits of amorphous systems.

From the earlier SEM analysis, it was observed that the particle size increased when SIM was incorporated as depicted in Fig.5.5 (ii) and Fig.5.5b (iv). The increase in the chain length of PLGA, i.e. with HMW-microparticles, also caused an increase in the diameter of the microparticles (Fig.5.5b (iii) and Fig.5.5b (iv)). The AFM analysis observed that different polymer molecular weight affects the composition of the particle surface with the roughness increased in the HMW as compared to IMW. Presence of SIM encapsulated within the polymer matrix also increased the surface roughness which was observed by an increase of the peaks of both IMW and HMW polymers respectively whereby peaks were prominent in these microparticles as compared to blank.

Chapter 6 will review the use of IMW-NPMP and HMW-NPMP microparticles containing SIM particularly in controlled release delivery systems. It will also examine their carrier properties, mechanisms and kinetics of drug release with the aim of improving the predictability of performance in bone and tissue engineering.

CHAPTER 6

PHYSICO-MECHANICAL PROPERTIES OF SINTERED SCAFFOLDS FORMED FROM SIM-LOADED POLY (PLGA) MICROSPHERES FOR BONE TISSUE ENGINEERING.

6.1 INTRODUCTION

In chapter 4, different variables involving the formulation of the non-porous SIM microparticles were investigated. We also explained the outcome of changing each of the formulation variables and this eventually lead to the optimization of the method to fabricate SIM microparticles using the double emulsion solvent evaporation technique. We subsequently summarised the characterization studies of the SIM microparticles using various analytical techniques in Chapter 5. This enabled us to understand the drug-complex with regards to its physical and chemical interactions.

In this chapter, we aim to develop a novel dual-application scaffold system comprising of both porous and SIM-loaded microspheres. This formulation was designed to form porous scaffolds at body temperature which has potential for tissue regeneration purposes. Porous (PMP) and non-porous (SIM-loaded) PLGA microspheres (NPMP) were formulated with IMW PLGA (53 kDa) and HMW PLGA (84-109 kDa).

Scaffold design and fabrication are major subjects in tissue engineering and regenerative medicine research. The main objective of a bone tissue scaffold is to provide temporary mechanical integrity at the defect site until the bone tissue has been repaired and normal biomechanical function has been restored. Injectable scaffolds are of interest in the field of regenerative medicine because of their minimally invasive mode of delivery (O. Qutachi *et al*., 2013). Synthetic injectable scaffolds must be able to provide structural stability and mechanical support at the defect site. In addition, the injectable polymer scaffolds must be capable of fitting into any size and shape of bone defect compared to the 3D conventional (fixed size) scaffolds.

The main advantage of injectable polymeric materials compared to 3D scaffolds is that they can be delivered to the bone defect site using non-invasive

or minimally invasive surgeries (Ducheyne *et al*., 2011). The current study describes the development of an injectable, porous PLGA scaffold that solidifies *in situ* at 37 ºC (Qutachi *et al*., 2014).

Microspheres attract tremendous interest in regenerative medicine because they can be fabricated from various different natural and synthetic materials including chitosan, gelatin, nanohydroxyapatite, dextran, poly ε-caprolacton (Luciani *et al.,* 2008; Song *et al*., 2013). Different methods of sintering microspheres into scaffolds have also been investigated and strategies include the incorporation of plasticizers in order to reduce polymer glass transition temperatures the application of heat to the system (Luciani *et al*., 2008; Jiang *et al.,* 2008; Wang *et al*., 2009) and also the addition of organic solvents such as dichloromethane (Jaklenec *et al.,* 2008).

The 3D polymeric scaffolds with higher porosities and homogeneous interconnected pore network are very useful in tissue engineering. One way to achieve such a porous scaffold is to combine porous microspheres to form scaffold. Sufficient porosity is important in order to allow cells to proliferate. Scaffold structures can serve as a temporary extracellular matrix into which cells migrate and form functional tissues (Jaklenec *et al.,* 2008; Qutachi *et al*, 2013; Qutachi *et al*, 2014). Rahman and colleagues previously demonstrated that porous PLGA microspheres prepared using the double emulsion solvent evaporation method could form solid porous scaffolds at body temperature (Rahman, C. V. *et al.,* 2013, Boukhari Y. *et al*., 2017). Variations of this method have been tested in Chapter 2, these were largely attempts to induce porosity with the use of different type of porogens. In this context, appropriate mechanical properties are important in maintaining the integrity of the scaffolds *in vivo* whilst, at the same time, supporting the cell growth (Luciani *et al*., 2008; Bible *et al.,* 2009).

Along with scaffolds and cells, bioactive factors are one of the three components that make up the regenerative medicine triad and they are crucial in simulating the natural regrowth cascade (Luciani *et al*., 2008; Bible *et al*., 2009). Bone morphogenetic proteins (BMPs) have been studied for their use in non-union bone defects, spinal fusion and open tibial fractures (Makadia *et al.,* 2011; Lü *et al.,* 2009; Rahman *et al*., 2013). Such growth factors can be used to

simulate natural repair processes with great specificity and effectiveness, but disadvantages include their low stability, high cost and the requirement for high doses to illicit a response (Ryoo *et al.,* 2006). These problems can potentially be reduced by using a sustained/targeted delivery approach which includes the encapsulation of SIM within biodegradable PLGA microspheres prepared using the double emulsion solvent evaporation method (Putney *et al.,* 2006, Qutachi *et al*., 2013).

The aim of the current work was to combine porous PMP and SIM-loaded microspheres (NPMP formulation) and to see the potential of developing an injectable scaffold system for the purpose of bone regeneration. Whilst previous work has focused primarily on a single type of PLGA microsphere (with or without an additional biomaterial), we combine herein both porous and SIM-loaded microspheres into a single delivery system. The effects of PLGA molecular weight on scaffold microstructure, mechanical properties and SIM release were assessed.

6.2 MATERIALS AND METHODS

6.2.1 MATERIALS

PLGA (lactic acid:glycolic acid ratio, 85:15) of intermediate (53 kDa) and high (92-109 kDa) molecular weight was purchased from Evonik (USA). Dichloromethane (DCM) was purchased from Fisher (UK) and phosphate buffered saline (PBS), pH 7.0 was purchased from Gibco (UK). Poly vinyl alcohol (PVA) (87-89% hydrolysed) and sodium hydroxide (NaOH) pelletswere purchased from Sigma Aldrich (UK). Dimethyl sulfoxide (DMSO) and sodium dodecyl sulfate (SDS) were purchased from Fisher (UK). All sovents are chemically lab graded.

6.2.2 METHODS

6.2.2.1 FORMULATION OF MICROSPHERES

Porous PLGA microspheres of both IMW and HMW were prepared using the double emulsion solvent evaporation method as previously described in Section 2.3.3.2.2. Briefly, a 250 µl aliquot of PBS (pH 7.0) was added to a 20% w/v PLGA solution in DCM and homogenized at 9000 rpm using a Silverson L5M homogeniser to form the primary emulsion. This was then added to 200 ml of 0.3 % w/v PVA solution and homogenized at 4000 rpm to form the secondary emulsion, which was then stirred for 4 hours at 300 rpm to allow the DCM to evaporate and the microspheres to precipitate. The microspheres were washed with distilled water and then suspended in 10 ml of ethanolic-NaOH solution (70% ethanol: 30% 0.5 M NaOH; pH 13.62) to enhance the porosity of the microspheres. The above suspension was vortex-mixed at 1400 rpm for 1 minute, sieved (40 µm) and washed using distilled water. Non-porous microspheres were prepared in a similar way, with a 20 % w/v PLGA solution and 100 µl of distilled water being used instead of 250 µl of PBS; homogenization speeds of 4000 rpm and 2000 rpm were used for the primary and secondary emulsions respectively. All microspheres were freeze-dried using a Thermofisher Scientific FR-Drying Digital Unit for 48 hours and stored at -20º C until use. The SIM microparticles were prepared by adding 5 mg to the 200 ml 20 % w/v PLGA solution, prior to homogenization process.

6.2.2.2 SCANNING ELECTRON MICROSCOPY (SEM) AND SIZE ANALYSIS

The surface morphology of the microparticles were viewed using SEM. Samples were mounted on metal stubs and viewed using a FE-SEM, Quanta 400F instrument (FEI, USA). The particle size and mean diameter distribution (polydispersity index) of the microparticles were measured by two methods: (i) measurement of pore size in ImageJ; the scale of the image was set with bars of known distance. After that, with freehand selection, the outline of the pore was traced and the area measured; (ii) laser diffraction analysis using a Mastersizer 2000 (Malvern, UK). The preparation of the sample involved the microparticles being dispersed in distilled water, then a dilute solution of uniformly dispersed

microspheres was obtained by ultrasonic vibration. The samples were then measured three times to calculate the mean diameter and polydispersity index (PDI).

6.2.2.3 DIFFERENTIAL SCANNING CALORIMETRY (DSC)

The glass transition temperature (T_g) of the porous PLGA microspheres pre- and post-treatment with ethanolic-NaOH was determined using a TA Instruments Q2000 DSC equipped with a RCS40 cooler (Delaware, USA). Both the sample and the standard aluminium reference pan were heated from 0-250 ºC at 10 ºC/min using nitrogen as the purging gas at 50 ml/min. The first heating cycle was used for the assessment.

6.2.2.4 ENCAPSULATION EFFICIENCY OF SIM WITHIN MICROSPHERES.

The SIM content of 10 mg of PLGA microparticles was determined by using a suitably modified HPLC method as described by B.D Micheal *et al*, 2013. Briefly, the chromatographic procedure was as follows: HPLC analysis was performed using an Agilent Technologies Series 1120 HPLC (Wilmington. The chromatographic separations were performed using a ThermoScientific® 100 C18 column (5 µm, 150 mm × 4.6 mm) at 45 ºC, eluted with mobile phase at a flow rate of 1.0 ml/min. The mobile phase consisted of acetonitrile and 0.2 % acetic acid buffer pH 4.0 (70:30, v/v). This was filtered through a 0.45 µm nylon filter and degassed in an ultrasonic bath prior to use. The column was equilibrated for 30 minutes by using mobile phase after each run. Each sample was passed through a 0.22 µm polytetrafluoroethylene (PTFE) membrane filter before HPLC analysis; samples were analysed in triplicate and results were reported as an average of the three. The calibration curve for the quantification of SIM (0.001-100 µg/mL) had a correlation coefficient of $R^2 = 0.9994$.

Encapsulation efficiency is an expression of the amount of drug incorporated into the microparticles and is normally defined as the percentage of drug detected in the microparticles relative to the total amount of drug used. The procedure for analysing drug loading and encapsulation was as follows: 10 mg of microparticles was dissolved in 1 ml of methanol and this was centrifuged at 10,000 rpm for 15 minutes. The supernatant was collected and subjected to

HPLC analysis to determine the SIM content. The encapsulation efficiency was determined using Equation 6.1.

$$\text{Encapsulation Efficiency} = \frac{\text{Amount of drug in microparticles}}{\text{Drug added}} \times 10$$

……. (Equation 6.1)

6.2.2.5 PREPARATION OF 3D SCAFFOLDS

IMW and HMW PLGA scaffolds were formed by mixing a 1:1 mass ratio of porous to non-porous microspheres in a weighing boat. Each mixture contained an equivalent of 1, 2 or 3 mg of SIM per gram of total mixture. PBS (pH 7.4) was added to these microsphere mixtures at a ratio of 1:4(v/w) and they were then manually mixed to form a paste. The paste was packed into a 6 mm (diameter) × 12 mm (height) cylindrical PTFE mould of the using a spatula and then stored in a sealed de-humidifying chamber for 17 hours at 37 ºC.

6.2.2.6 CHARACTERIZATION OF 3D SCAFFOLDS

The compressive strength of the scaffolds was assessed using an Instron® electromechanical universal testing machine. To determine the stress-strain relationship and yield stress in the radial direction, an initial force of 0.005 N was applied to the sample ringlet, after which the rings were extended until failure at a rate of 5 mm/min. Dry IMW and HMW PLGA scaffolds for all three loadings of SIM (plus SIM-free control) were analysed in triplicate. The compressive strength was taken to be the stress at the maximum strain. The tensile strength was obtained from the Bluehill® Universal Software version 2.0.

The porosity of the scaffolds were calculated based on the relative density of the scaffold to PLGA using Equation 6.2.

$$\textbf{Porosity(\%)} = \left(1 - \frac{\rho_{scaffold}}{\rho_{PLGA}}\right) \times 100 \quad \text{.....(Equation 6.2)}$$

6.2.2.7 RELEASE OF SIM FROM MICROSPHERES AND SCAFFOLDS

In vitro SIM release from the optimized PLGA microparticles was determined by dispersing 10 mg of microparticles in 1 ml of PBS (100 mM, pH 7.4) and incubating at 37°C. At appropriate intervals, 200 µl were withdrawn and centrifuged at 10,000 rpm for 15 min. The supernatant was assayed for SIM release using the method described in Section 2.6. Each microparticle batch was analysed in triplicate and results were expressed as mean ±SD.

6.2.2.8 MECHANICAL TESTING

The compressive strength of scaffolds was tested with an INSTRON tensile testing machine (model 3365, Instron Corp., UK) using a cross-head speed of 1mm/min with a maximum load of 30N load cell. The resulting tensile stress was calculated using Bluehill2 software.

6.2.2.9 STATISTICAL ANALYSIS

Statistical analysis of the data was carried out using SPSS (version 21) software. The ANOVA procedure was performed with a Tukey-Kramer multiple comparison post-hoc test. A *P*-value of ≤ 0.05 was considered statistically significant. For comparing two or more means of differences, two-ways ANOVA was used as the statistical analysis.

6.3 RESULTS AND DISCUSSION

6.3.1 MICROSTRUCTURE AND SIZE ANALYSIS OF POROUS AND NON-POROUS PLGA MICROSPHERES

Shape and size are very important properties of particles since they affect the flow and packability of powders, which consequently affects the manufacturing process of solid dosage forms. In Chapter 2, we explained the importance of using chilled ethanolic-NaOH in the formation of porous microparticles (PMP). And in Chapter 4, we also analysed the variables that contributed to the variations in encapsulation efficiency among the NPMP with SIM incorporation in it. Thus, using all the information obtained, we formulated 3D scaffold consisting both NPMP and PMP microspheres in the last part of this chapter.

Figure 6.1 shows SEM images of porous microspheres (blank) treated with ethanolic-NaOH (a-b), and non-porous microspheres (c-d) prepared using various PLGA molecular weights that are loaded with SIM. As explained Section 2.3.3.2.1, longer treatment times with ethanolic-NaOH enhanced the porosity of the microspheres, but also compromised their structural integrity. The SEM images in Figure. 6.1 (a-b) represent optimal ethanolic NaOH exposure times for IMW and HMW which were 2 minutes. This optimal exposure time was based on qualitative examination of the microspheres, such that they retained their integrity and imposed maximum observable porosity. However, shorter treatment times did not yield sufficient porosity within the microspheres.

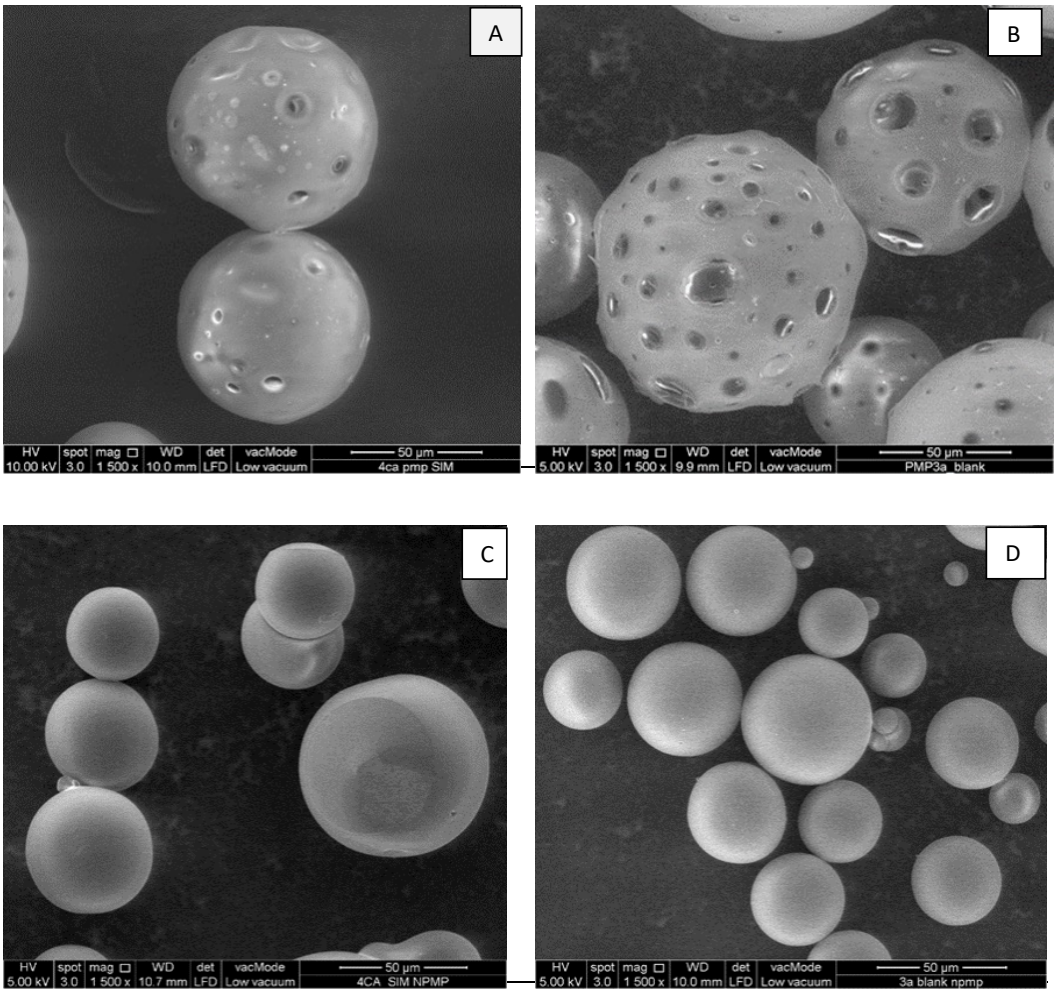


Figure 6.1: SEM images of porous (A-B) and non-porous microspheres (D-F) formulated with IMW (A,C) and HMW (B,D) PLGA

From the SEM images, the pore size distribution within the HMW microspheres was greater than the distribution in the IMW (Figure. 6.1 (a)) microspheres, which were more uniform in size. NPMP had a relatively smooth surface with no visible surface pores present (Figure. 6.1 (c-d)). There was no apparent difference in the surface topographies of the microspheres prepared from IMW and HMW PLGA. The size distribution for both types of microspheres (porous and non-porous) is shown in Figure. 6.2.

The blank PMP particle size was distributed over a range of 23.4 ± 12.89 μm to 20.49 ± 11.99 μm whilst the average diameter of the blank NPMP ranged from 27.55 ± 12.76 μm and 24.31 ± 8.69 μm for the IMW and HMW formulations respectively. The larger NPMP particle size can be attributed to the lower homogenisation speed used during the formation of the secondary emulsion (2000 rpm) as opposed to 4000 rpm used for the porous microspheres. We also postulated that surface erosion arising from the use of the ethanolic-NaOH on the porous microspheres contributed to the size reduction. Interestingly, the size of the IMW PLGS microparticles were larger than those prepared using HMW PLGA. We initially postulated that there was a direct relationship between PLGA molecular weight and the average microsphere diameter. This hypothesis was because the viscosity of polymer solutions increases in line with increasing polymer molecular weight. A more viscous polymer solution would present a greater barrier to the breakdown of droplets during the homogenisation of the primary emulsion and would hence result in the formation of larger microspheres (Mittal *et al.*, 2007; Biswal *et al*., 2011; Dangi *et al*., 2013). Therefore, we anticipated observing a higher range of particle sizes in microparticles formulated from HMW PLGA (Ansary *et al*., 2013). However, the results obtained clearly showed the opposite effect for both PMP and NPMP. Surprisingly, this characteristic have also been reported for microparticles prepared using PLGA where a low molecular weight polymer produces bigger microparticles compared to microparticles prepared from a HMW PLGA (Palacio *et al*., 2011). Nonetheless, all preparations were still observed to be in the micrometer size range.

When SIM was incorporated, the size of the NPMP were observed to increase: the average size for IMW PLGA microparticles after incorporation of

SIM was 42.91± 20.92 µm and it was 40.74 ± 15.65 µm for those prepared with HMW PLGA. When SIM in added into the internal aqueous phase, this would further increase the aqueous phase osmatic pressure/viscosity and result in difficult aqueous dispersion and larger partial size (Wu, G. et *al*.,2014).



Figure 6.2: Size distribution for NPMP (A) and blank (B), (C) and (D) with SIM, and PMP (E) and (F) as a function of PLGA molecular weight. Particle sizes were measured with Image J analysis.

In order to confirm the particle size range determined with ImageJ software, the size of microparticles prepared with IMW and HMW PLGA were further analysed via laser diffraction analysis using Malvern particle size analyser Mastersizer® 2000). Results observed are depicted in Table 6.1.

Table 6.1: Polydispersity index of different types of microparticles

Type	Size range (µm)	Average particle size (µm)
IMW NPMP (Blank)	67.989-188.472	113.803
IMW NPMP (SIM)	76.264- 236.499	135.275
IMW PMP (Blank)	53.709- 120.375	80.591
HMW NPMP (Blank)	46.102- 188.990	81.223
HMW NPMP (SIM)	43.001-158.959	88.495
HMW PMP (Blank)	45.380- 127.790	76.554

As to confirm further the particle size distribution, the laser diffraction analysis was carried out largely in agreement with the image J analysis. First, the size of the NPMP were also found to be higher than the PMP. Secondly, the microparticles that were fabricated with IMW PLGA were larger than those made with HMW. In addition, the particle size range were found to be close to the size of microparticles prepared in Chapter 4 for NPMP. High energy released from the homogenizer that was used during fabrication of PMP, which in turn would have led to a rapid dispersion of polymeric internal organic phase. This would have resulted in the small size and monomodal distribution that was observed (Sansdrap *et al.,* 1993; Mao *et al.*, 2008; Pal *et al*., 2013; Vysloužil *et al*., 2014). Particle size is probably the most important characteristic of microspheres, because of its effect on degradation rate, drug loading and the initial burst release of microspheres (Raman *et al.,* 2005; Yang *et al.,* 2013).

Note that the size of microparticles attributed from the particle analyser seems almost 3 times higher than the microparticles observed in the image J analysis. Laser diffraction measures particle size distributions through the measurement of scattering intensity as a function of scattering angle and wavelength of light as a laser beam passes through a dispersed particulate sample. Therefore, large particles will scatter light at small angles relative to the

laser beam whilst small particles scatter light at large angles (Retrieved from A guidebook to particle size analysis. Horiba Scientific instruments).

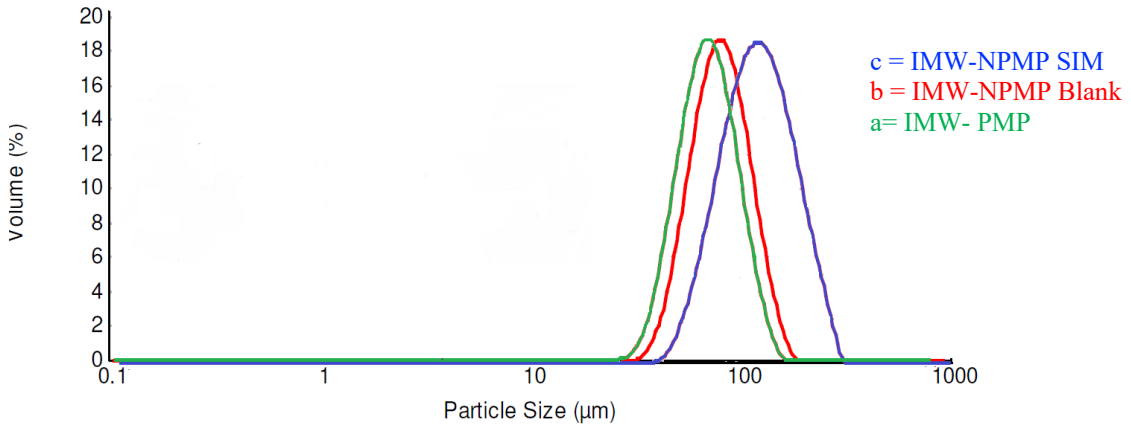


Figure 6.3 a: Analysis of size distribution for IMW of (a) IMW – PMP (b) IMW – NPMP Blank (c)IMW - NPMP SIM

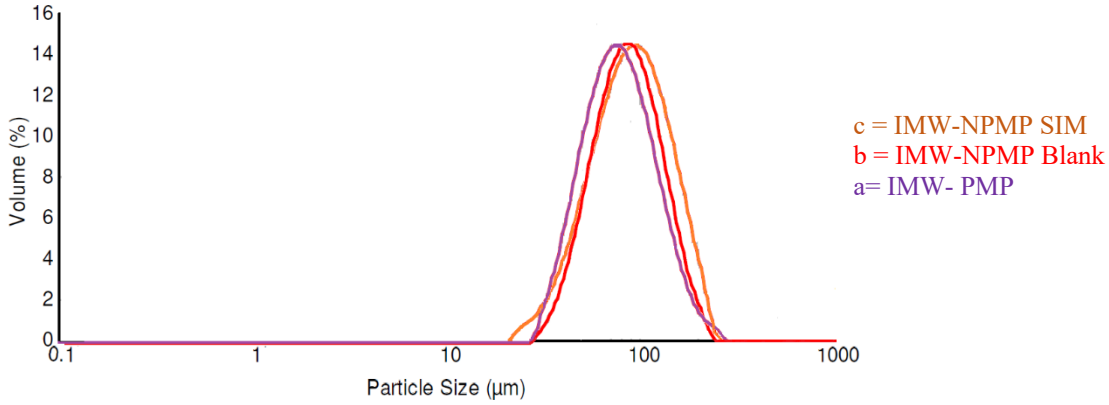


Figure 6.3 b: Analysis of size distribution for HMW. (a) HMW – PMP (b) HMW– NPMP Blank (c) HMW – NPMP SIM

For both porous and non-porous microspheres there was a direct positive relationship between the homogenization speed and the average microsphere diameter as shown in Table 6.1. Theoretically, a more viscous solution should have presented a greater barrier to the breakdown of droplets during the homogenisation of the primary emulsion and hence resulted in the formation of

larger microspheres. In this section, the shape of the bell-shaped curve of the IMW PLGA microparticles especially the SIM-NPMP was found shifted more to the right. This indicate the size range of IMW-SIM NPMP is much larger as compared to HMW-PMP. Here fabrication speed play roles. The broader size range of the IMW-NPMP could be due to high shear force applied to the dispersion. The NPMP shear force was 9000 rpm as compared to PMP which was 4000 rpm (Chapter 2).The size ranges of both the porous and non-porous microspheres were between 10 and 200 μm, which has been shown previously to be compatible with injection through a 22 G needle (Wang *et al*., 2009; Chen *et al.,* 2010; Hannink *et al*., 2011).

6.3.2 MICROSTRUCTURE AND POROSITY OF SCAFFOLDS

A previous study has reported that the ability of microspheres to sinter into scaffolds at body temperature may be due to local degradation of the polymer following treatment with ethanolic-NaOH (Qutachi *et al.,* 2013). In this regard, the degradation of the polymer is thought to result in a reduction in the T_g of PLGA at the surface of the microspheres, which allows the polymer to fuse more readily with neighbouring microspheres (Qutachi *et al*., 2013; Qutachi *et al*., 2014). In this study, the T_g of PLGA was found to fall by 1.9 ºC and 0.5 ºC respectively for the IMW and HMW formulations following treatment with ethanolic-NaOH (Table 6.2). It is apparent that for higher molecular weight PLGA treatment with ethanolic NaOH has less effect on the T_g. These findings were supported by the SEM observation that the surface of the IMW PLGA scaffold appeared to be extensively fused (Figure 6.5a) in contrast with the HMW PLGA scaffold (Figure. 6.5 b). Here, we predicted the presence of pores that were induced by ethanolic-NaOH in PLGA-based microparticles does not only increase the affinity to fuse with neighbouring microspheres, but it fundamentally alters the contributions of the involved physicochemical processes to the overall control of drug release from the NPMP-SIM in the scaffold. The NaOH-treated PLGA surfaces enhance the functions of osteoblasts (Park *et al*., 2004, Park e*t al*., 2005) which is advantageous in bone regeneration studies.

Table 6.2: Glass transition temperatures (T_g) of porous PLGA microspheres pre- and post-ethanolic-NaOH treatment.

Molecular weight of PLGA	IMW	HMW
T_g Porous microspheres pre-treatment (ºC)	53.7	51.8
T_g Porous microspheres ethanolic-NaOH treated (ºC)	51.8	51.3

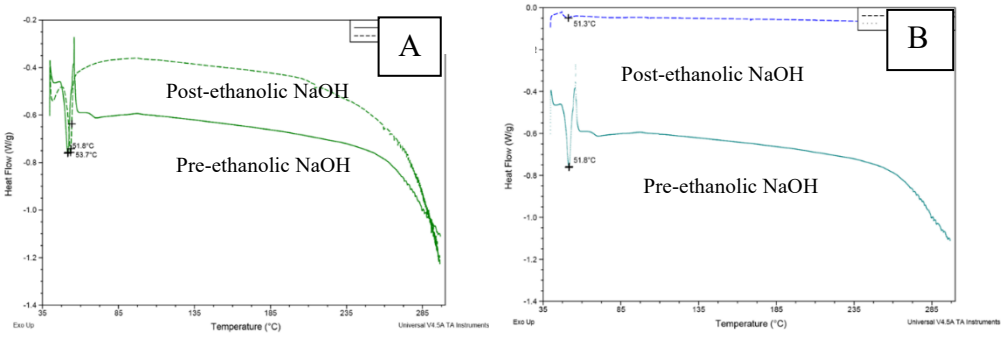


Figure 6.4: DSC thermal profiles of (A) IMW PLGA and (B) HMW PLGA porous microspheres pre- and post-ethanolic-NaOH treatment.

The DSC data are consistent with the SEM images of the scaffolds in Figure. 6.5, which show a more fused appearance for the IMW PLGA scaffolds compared to the HMW PLGA scaffolds.

The porosity of the scaffolds ranged from 80 to 90%, which is preferential as it has been previously shown *in vivo* that higher porosity results in improved bone ingrowth (Karageorgiou *et al.,* 2005). The HMW PLGA scaffolds were significantly less porous ($p<0.05$) in comparison to the IMW scaffolds, even though the latter appeared to be fused on the surface, as depicted in Figure 6.5. This observation is also supported by pore size data in Table 6.1. The IMW-PLGA variants possessing more pores as compared to HMW PLGA particles. This difference is believed to be related to the increase in internal porosity of the IMW PLGA scaffolds due to a slower solidification rate of the polymer in the microspheres (Kirby. *et al*., 2011). The IMW polymer is more soluble in the organic solvent and hence remains in solution longer than HMW polymers, which solidify more readily and precipitate out to form microspheres

(Jelvehgari *et al.,* 2010). This slower rate of solidification would result in a more porous internal structure due to the greater time available for the formation of channels.

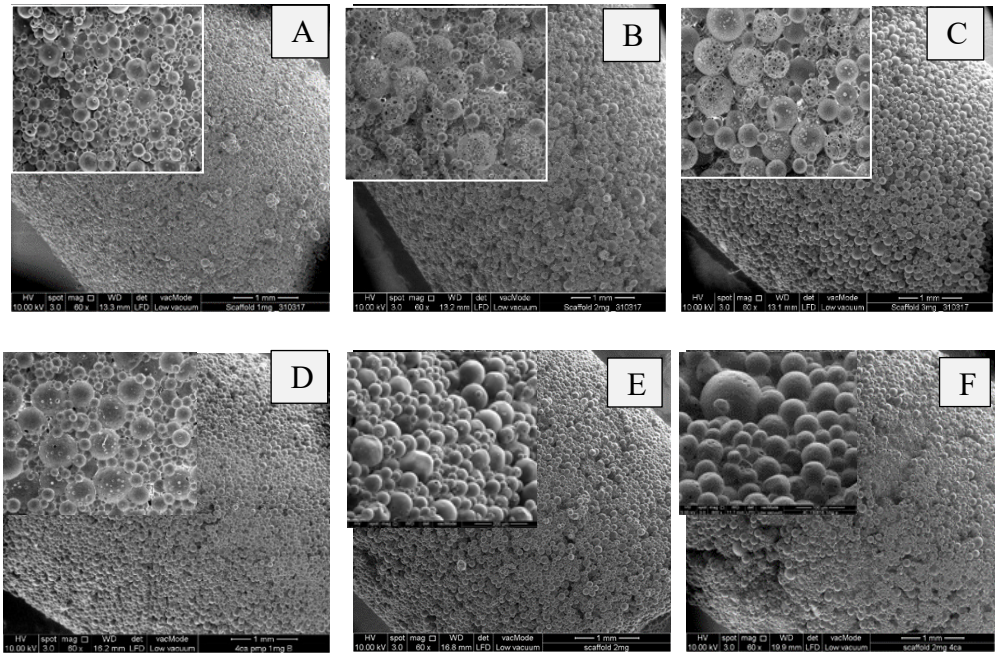


Figure 6.5: SEM images of sintered scaffolds with various SIM loadings A, B, C=IMW PLGA, D, E, F= HMW PLGA (1 mg/g, 2 mg/g and 3 mg/g)

It was found that porosity of the scaffold decreased as the SIM loading was increased from 1mg/g to 3 mg/g. This was partly due to the method that was used to prepare the scaffold. For 1 mg SIM loading, the amount of porous PMP-blank and NPMP-blank added were much higher than the amount of NPMP-SIM. Thus, structurally, the scaffold prepared containing 1 mg/sim had greater pore sizes as compared to 3 mg/sim. For the scaffold prepared with 3 mg/sim, the amount of NPMP-SIM is high with less amount of NPMP-Blank and PMP-blank in the prepared scaffold, therefore the pore sizes are less apparent in this scaffold preparation.

It is also worth mentioning here that the pore sizes for the IMW-PMP are larger than the pore sizes observed in the HMW-PMP variants (Figure 6.5 and Figure 6.6 a). This significant increase in pore sizes would indirectly increase the porosity and allow more permeability (Al-Munajjed *et al*., 2008). A porous surface to the microparticles is important as it improves mechanical interlocking (interdigitation) between the scaffold and the surrounding natural bone,

providing greater mechanical stability at this critical interface (Hannink *et al*., 2011; Meredith *et al,,* 2015). The minimum pore size is regarded to be 100 µm, any smaller and issues will arise due to cell size, migration requirements and nutrient transport (Murphy *et al.,* 2010; Meredith *et al*,, 2015; Nava *et al.,* 2016).

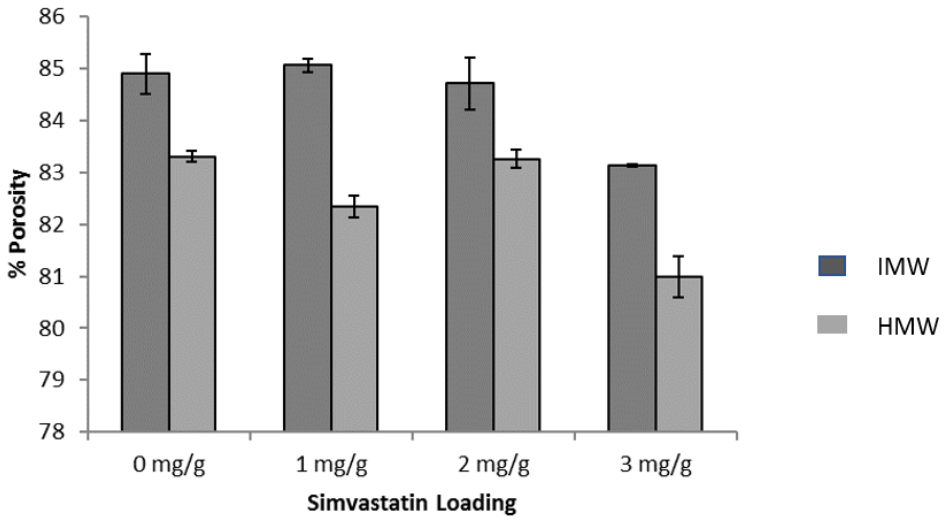


Figure 6.6a: Percentage of porosity of porous PLGA scaffolds loaded with various SIM concentrations;1 mg/g, 2 mg/g and 3 mg/g.

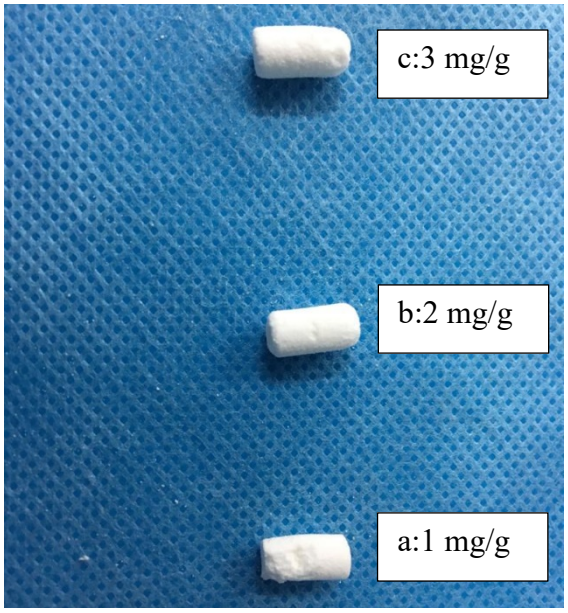


Figure 6.6 b: The scaffolds after 24 hours sintering. a: 1mg/g, b: 2mg/g and c: 3mg/g.

6.3.3 SINTERING OF MICROSPHERES INTO SCAFFOLDS AND COMPRESSIVE STRENGTH OF SCAFFOLDS

In order to study the effect of the scaffold preparation method on the subsequent morphology and mechanical strength, the composite scaffolds were prepared from a paste containing the microspheres, as previously reported (Boukari *et al*., 2015). Scaffolds that has been sintered are presented in Figure 6.6 b, respectively. The sintering process results in the expulsion of water from the scaffold and this leads to formation of components within close proximity. We believe that this close proximity structures favours 'fusion' and bond formation within the scaffolds. This approach to scaffold sintering at 37 ºC is superior to the methods employing elevated temperatures and reagents (Qutachi *et al.,* 2013; Rahman *et al*., 2013; Boukari *et al*., 2017).

The compressive strength of a material is a measure of its resistance to an applied stress. Figure 6.7 shows the average compressive strengths of the scaffolds at various SIM loadings (0, 1, 2 and 3 mg of SIM/g of scaffold). Both the control and SIM-loaded scaffolds exhibited an increase in mechanical strength when IMW PLGA were used. The HMW PLGA and IMW PLGA scaffolds exhibit a statistical difference in compressive strength after the incorporation of SIM ($p \leq 0.05$). Using one way ANOVA, There is a significant different of the mechanical strength in scaffold prepared in HMW for formulation in both 1mg/g and 2 mg/g as compared to 0 mg/g as depicted in Figure 6.7.

Overall, however, the scaffold fabricated with IMW PLGA microparticles possessed a higher compressive strength than the HMW PLGA scaffold. From the DSC thermogram it was found that the IMW PLGA microspheres had a higher T_g value in PMP which indicate crystallinity is slightly higher in the IMW formulation. Therefore, the compressive strength observed here is tailored with the results obtained in DSC with regards to the mechanical strength and crystallinity structure owned in IMW. The 'fusing' effect as anticipated from the DSC study was proven in the compressive strength study. Although some studies indicate that T_g increases with increasing molecular weight and increasing lactide content of the polymer, (Tsuji *et al*., 2000; Dorati. *et al*., 2010, Fu. *et al.,* 2011) we witnessed significant mechanical

strength in the IMW PLGA variants after treatment with NaOH-EtOH (Schliecker *et al*., 2003, Makadia *et al.,* 2011).

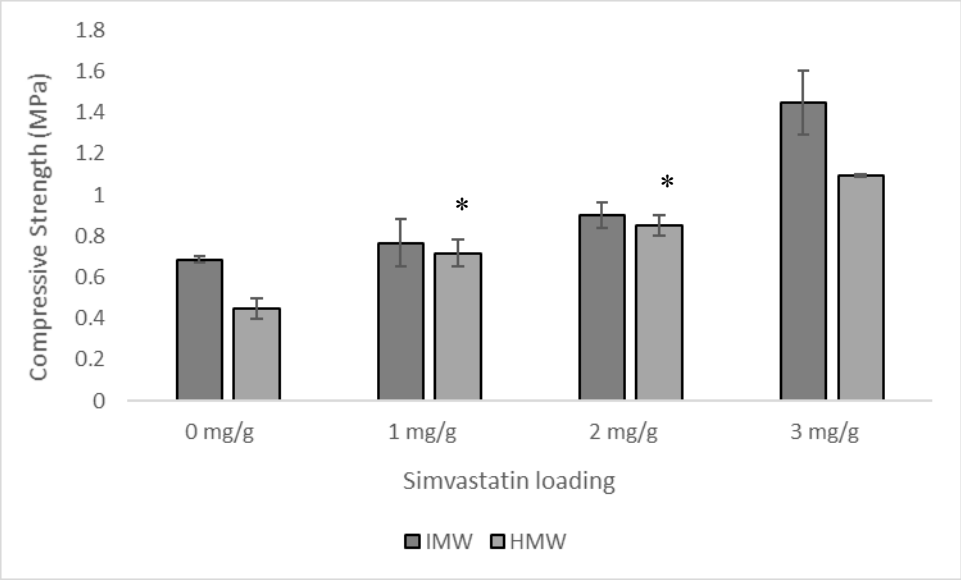


Figure 6.7: Compressive strengths of scaffolds of various SIM loadings: 1 mg/g, 2 mg/g and 3 mg/g; * indicate $p \leq 0.05$ with control group. Control represented by 0 mg/g formulation.

A previous study has reported the ultimate compressive strength of trabecular bone to be in the range of 0.22-10.44 MPa depending on the area of the body (Misch *et al.,* 1999; Boukari *et al*., 2015; Seyedmajidi *et al*., 2018). A further study has reported that cancellous bone has a compressive strength of 2 – 6 MPa (Lee *et al*., 2012). In this study, values of the compressive strength of the IMW and HMW PLGA scaffolds fell close to the range of compressive strength required for cancellous bone. In addition, the microparticle sizes which fell below 150 µm may suggest a possible dual-applicability of the system arising from the formulation's potential of two application modes. Firstly, a paste can be implanted within the degenerated bone tissue, that can take the shape of the defect area and then sinter at 37 °C. Secondly, there is the possibility of injecting the microsphere suspension directly into the defect area through a 19-G needle as the particle sizes obtained here is below 100 µm (Boukari *et al*., 2015; Boukari *et al*., 2017). The delivery of microparticles via needle is of crucial importance for therapeutic applications. Some of the parameters that need to be considered include the viscosity of the formulation, selection of an

appropriate needle, shear effects, and the concentration of additive such as the emulsifiers (Qutachi, O. *et al*., 2018). And most importantly, the drug release kinetics from the formulation post-injection would differ greatly compared to the paste formulation (Boukari Y., *et al*., 2017).

6.3.4 RELEASE OF SIM FROM NON-POROUS MICROSPHERES

Drug release *in vitro* for all formulations at low drug loading levels exhibited two different phases: an initial burst release followed by a slower release over a longer period. or a stable steady release on certain length of time is maintained (Huang *et al.,* 2014) depending on the drug target. For example, burst release phenomenon may be required in the delivery of anticancer via oral whilst in bone engineering, controlled drug release is preferable (Mouriño *et al*., 2010).

In this study, the release of SIM from microspheres formulated using IMW and HMW PLGA is shown in Figure 6.8. Both formulations showed gradual release in a sustained manner over a 30-day period. No burst release was observed in this experiment. This results was achieved after extensive investigation on different parameters that may affect the functions of microparticles in the release pattern which was reported in Chapter 4.

Following the release study, higher release was observed initially for HMW microspheres until Day 18. It is postulated that the drug diffuses from the polymer matrix as the matrix erodes. The process was slower for IMW PLGA particles at the beginning of the study, however, it started to increase from Day 18 onwards. The proportion of SIM released from the two types of microspheres at day 30 was 34.2 ± 0.5 % and 27.89 ± 0.22 %, respectively for IMW PLGA and HMW PLGA ($p \leq 0.049$). This indicates that a significant amount of SIM was retained within the microspheres even after 30 days. Looking at the pattern of the release, the release of SIM from HMW and IMW was observed to sustain for 30 days and started to be flattened after 30 days. We anticipate, the release of SIM after 30 days might has depleted hence the release of SIM is getting slower there.

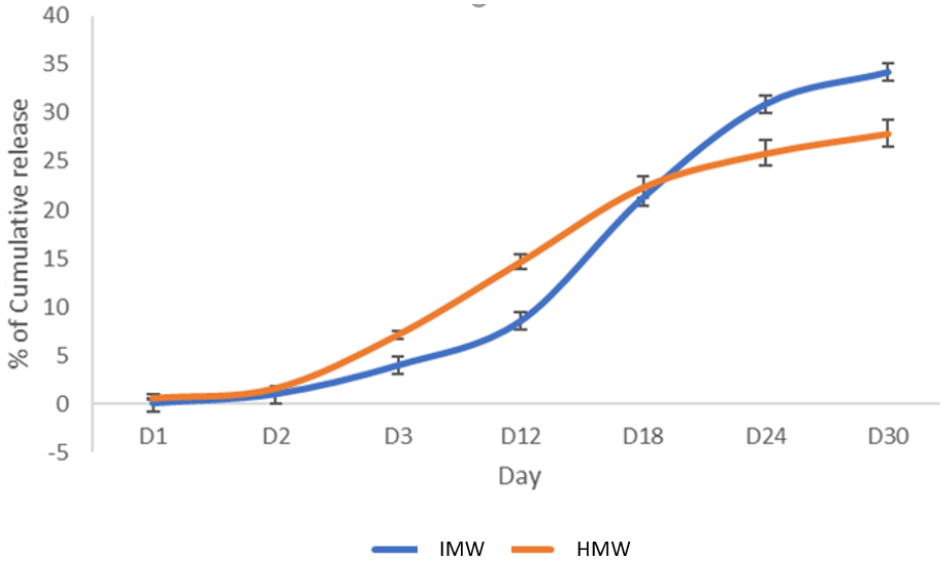


Figure 6.8: SIM release from microspheres as a function of PLGA molecular weight (IMW and HMW)

6.3.5 Release of SIM from Scaffolds

The cumulative release of SIM from scaffolds versus time is represented in Figure. 6.9. The release of SIM from the scaffolds is crucial in initiating and maintaining the cascade of reactions necessary for tissue regeneration (Ryoo *et al*., 2006; Putney *et al*., 1998). Drug release from all scaffolds started on day 1 and continued at a sustained rate for the remaining 35 days. Release of drug from scaffolds containing 1 mg SIM/g and 2 mg SIM/g was higher when prepared using HMW PLGA as compared to IMW PLGA. However, it appears at a higher SIM loading (3mg SIM/g), the rate of degradation of the IMW PLGA scaffolds was faster than the HMW scaffolds and this prompted a faster rate of SIM release from the IMW.

Table 6.3: Cumulative release of different scaffolds for 35 days

Scaffold drug loading	Cumulative drug release (%)		Significance level
	HMW PLGA scaffold	IMW PLGA scaffold	
1 mg SIM/g	17.23	13.74	0.08
2 mg SIM/g	23.14	15.66	0.021
3 mg SIM/g	31.07	38.94	0.047

Figure 6.9 a illustrates the initial slow release of SIM at Day 1 for both IMW and HMW of 1mg/g scaffolds. Due to hydrophobicity of SIM, it was found that the released of SIM from microparticulate carrier systems was via diffusion, down the concentration gradient. Hence, as SIM begins to release from the surface of the matrix, a concentration gradient is established to provide the driving force for drug diffusion from the interior of the matrix towards the surface for subsequent release (Panyam *et al*., 2004, Nandagiri *et al*., 2012). This possibly due to the interaction of SIM which is hydrophobic drug molecules within the polymer matrix. The interaction occur could be via hydrophobic binding forces with the polymer carboxyl groups in the HMW that might cause a trapping of the drug inside the particles and therefore, a slower release was observed.

A significantly lower release ($p<0.05$) was observed using two-ways ANOVA from the IMW PLGA scaffolds at the 1 mg SIM/g and 2 mg SIM/g loadings as compared to the same drug loading in HMW scaffolds (Table 6.3). This slower release of SIM from these scaffolds is believed to be due to the longer degradation time of IMW PLGA as compared to HMW PLGA (Makadia *et al.,* 2011). Incorporation of non-porous microparticles may have contributed to the release of SIM from the centre of the scaffold. Consequently, the rate of SIM release from the scaffolds was slower since the release of SIM from deep pockets within the microspheres is dependent on the surrounding polymer matrix degrading first in order to create conduits through which the drug can escape. The release profiles of SIM from the scaffolds loaded with 3mg/g however

showed slower release from HMW scaffold in comparison to IMW scaffold. This release mirror those from the microspheres in respect of molecular weight, i.e. HMW PLGA ≥ IMW PLGA as discussed in section 6.3.4. This trend, as explained earlier, can be attributed to the amount of SIM that was added rate of degradation of the polymer, which was highest for IMW PLGA at the higher SIM concentration.

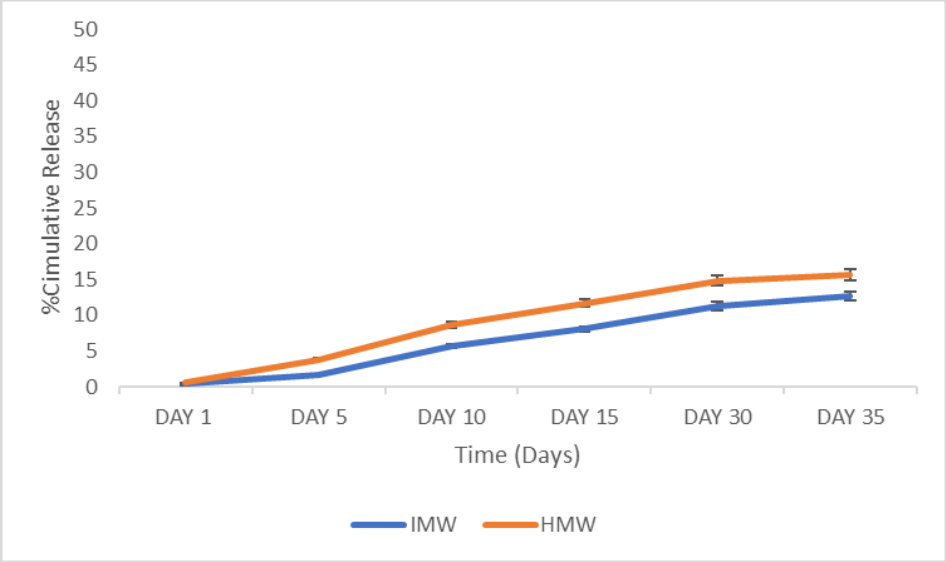


Figure 6.9 a: SIM release profiles from 1 mg SIM/g loadings. Data points represent the mean ± standard deviation. * $p < 0.05$.

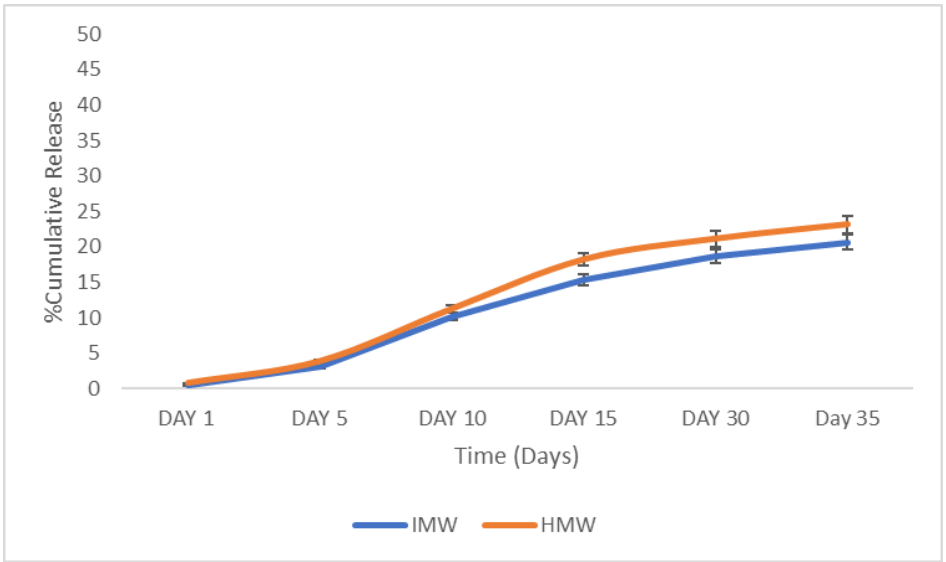


Figure 6.9 b: SIM release profiles from 2 mg SIM/g loadings. Data points represent the mean ± standard deviation. * $p < 0.05$.

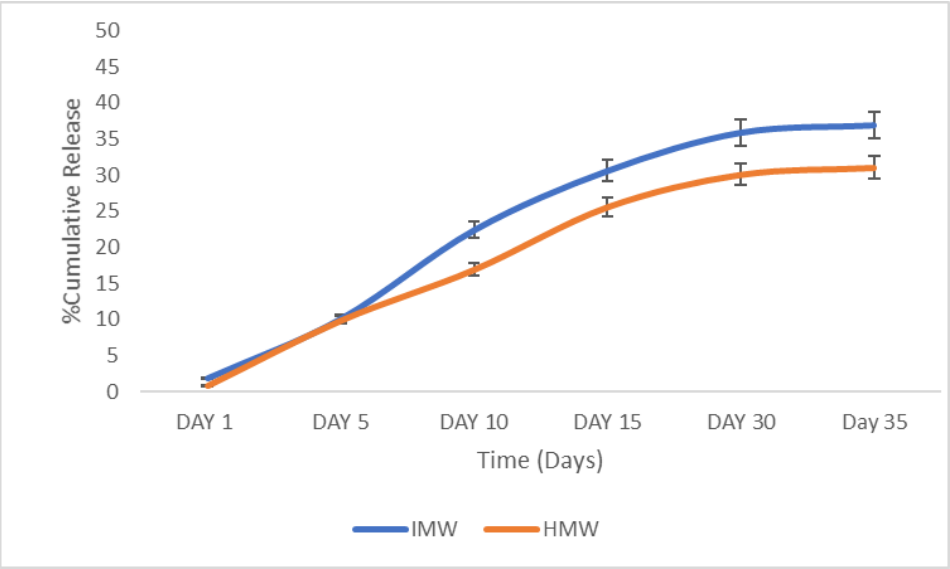


Figure 6.9 c: SIM release profiles from 3 mg SIM/g loadings. Data points represent the mean ± standard deviation. * $p < 0.05$.

Overall, the pattern of release of drug from both IMW and HMW scaffold fabricated from the microparticles shows a constant release. This is advantageous as it has been shown that when the release kinetics of SIM follows this pattern, it can provide a significant improvement to healing and regeneration of bone (White *et al*., 2013). This release pattern was also found in other studies and was shown to promote osteogenic differentiation and stimulated bone regeneration when it was locally released from the scaffolds into bone defects (Zhou *et al.,* 2010; Huang *et al*., 2014).

6.4 CONCLUSIONS

The average size of the microspheres was found to be directly related to the molecular weight of the PLGA from which they were produced. An initial release of SIM was observed from microspheres and scaffolds on day 1 during *in vitro* studies. In the case of the SIM-loaded microspheres, this release was inversely related to the polymer molecular weight, whereby release from the

HMW PLGA formulation was greater than the release from IMW PLGA formulation

Similarly, scaffolds loaded with 1 mg SIM/g exhibited an inverse release relationship between release and polymer molecular weight. The release was highest amongst HMW PLGA scaffolds loaded with 1 and 2 mg SIM/g. Sustained SIM release was observed after day 1 over 35 days for both microspheres and scaffolds. The compressive strengths of the scaffolds were found to be inversely proportional to PLGA molecular weight at each SIM concentration. Overall the data demonstrates the potential of the scaffolds for use in bone tissue regeneration.

CHAPTER 7

IN-VITRO TESTING OF PLGA COMPOSITE MICROSPHERES AND SCAFFOLDS

7.1 INTRODUCTION

In Chapter 6, we addressed the characterisation studies of SIM microparticles using the homogeniser and characterized the microparticles with SEM, DSC, particle size analyser and also mechanical testing via Instron Universal Testing Machine in order to determine the effect that the incorporation of SIM had on the physical properties of the microspheres and scaffolds. We also determine the release profiles of SIM from a prototype consisting of SIM microspheres that had been combined with porous microspheres. We subsequently studied the release profiles of SIM from scaffolds containing different SIM loadings fabricated with both NPMP and PMP.

In chapter 7, we extend the study to the biocompatibility of the scaffolds, which was ascertained through the use of MG-63 cell lines. A number of different cell lines have been used in bone tissue engineering research and these are shown in Table 7.1. The MG-63 osteosarcoma cell line is a common choice for evaluating a biomaterial's compatibility for use in bone tissue engineering (Lee *et al*., 2003; Vitale-Brovarone *et al*., 2007; Lee *et al*., 2013; Wang *et al.*, 2013). These cells proliferate more rapidly than other non-cancerous human-derived bone cells; therefore, they are an economical cell-line for use in biocompatibility tests. They also possess osteoblastic traits and are considered to be immature osteoblasts (Bächle *et al*., 2004) therefore, some studies still using this cell line as the model to study drug release in bone tissue regeneration (Nath *et al.,* 2013) or these reasons, MG-63 cells were selected for the preliminary screening of the PLGA/SIM composite scaffold biocompatibility studies.

As to ascertain functional porous scaffold containing SIM, first, we evaluate the effects of SIM alone on MG-63 cell lines. Subsequently we tested

the SIM-NPMP effects on the MG-63 viability by adding 1: 1 ratio of PMP and SIM-NPMP. We then aimed to evaluate the cells-scaffold constructs using environmental scanning electron microscopy (ESEM) as to see the interconnection effects of the scaffolds within the neighbouring cells.

Table 7.1: Previous studies on pleotropic effects of SIM with various cell lines

Title	Authors	Year	Cell line/cell viability studies
Melatonin releasing PLGA micro/nanoparticles and their effect on osteosarcoma cells.	Altindal, D. Ç. *et al.*	2016	MG63
SIM protects human osteosarcoma cells from oxidative stress-induced apoptosis through mitochondrial-mediated signalling.	Zhao, X. H. *et al.*	2012	MG63
Localised controlled release of SIM from porous chitosan-gelatin scaffolds engrafted with SIM loaded PLGA-microparticles for bone tissue engineering application.	Gentile, P. *et al.*	2016	MG63
Preparation and characterization of PLGA microspheres by the electrospraying method for delivering SIM for bone regeneration.	Nath, S. D. *et al.*	2013	MG63
SIM and atorvastatin enhance gene expression of collagen type 1 and osteocalcin in primary human osteoblasts and MG-63 cultures	Ruiz-Gaspa, S. *et al*.	2007	MG63
Preparation and Characterization of SIM, Loaded PLGA Microparticles for Tissue, Engineering Applications	Nath, S. D. *et al.*	2013	hFOB cells
Microparticle-embedded fibroin/alginate beads for prolonged local release of SIM hydroxyacid to mesenchymal stem cells	Ungaro, F. *et al.*	2017	Mesenchymal stem cells
Study of mesenchymal stem cells cultured on a poly(lactic-co-glycolic acid) scaffold containing SIM for bone healing.	Mendes Junior D. *et al*.	2017	Mesenchymal stem cells
Enhanced osteogenesis and angiogenesis by mesoporous hydroxyapatite microspheres-derived SIM sustained release system for superior bone regeneration.	Yu, W. L. *et al.*	2017	EA.hy926 cells
Enhancement of osteoinduction by continual SIM release from poly(lactic-co-glycolic acid)-hydroxyapatite-SIM nano-fibrous scaffold	Jiang, L. *et al.*	2013	MC3T3-E1

Poly(L-lactic acid)/hydroxyapatite nanocylinders as nanofibrous structure for bone tissue engineering scaffolds		2013	MC3T3-E1
Localised controlled release of SIM from porous chitosan-gelatin scaffolds engrafted with SIM loaded PLGA-microparticles for bone tissue engineering application	Gentile, P. *et al*.	2016	hFOB cells
Enhanced in vitro osteoblast differentiation on TiO2scaffold coated with alginate hydrogel containing SIM	Pullisaar, H. *et al.*	2013	Primary human osteoblasts (hOBs)
SIM and atorvastatin enhance gene expression of collagen type 1 and osteocalcin in primary human osteoblasts and MG-63 cultures			SIM and atorvastatin enhance gene expression of collagen type 1 and osteocalcin in primary human osteoblasts and MG-63 cultures

7.2 MATERIALS AND METHODS

7.2.1 MATERIAL

For MG-63 cell culture, Eagle's minimum essential medium (EMEM) was purchased from ATCC (USA). Foetal bovine serum (FBS), trypsin EDTA and antibiotic antimycotic (×100) were purchased from Gibco, Life Technologies (USA). Dulbecco's phosphate-buffered saline liquid was purchased from Sigma-Aldrich, USA. For SEM biological sample viewing, the materials include: PBS tablet, Glutaraldehyde (Grade I, 70% in H2O, specially purified for use as an electron microscopy fixative), Osmium oxide, Sodium cacodylate, absolute ethanol, hexamethyldisilazane (HMDS) (All purchased from Sigma-Aldrich, USA).

7.2.2 METHODS

7.2.2.1 PREPARATION OF NON-POROUS AND POROUS MICROSPHERES

IMW-SIM NPMP and IMW-NPMP were prepared as detailed in the previous chapters (Section 4.2.3 and 6.2.2).

7.2.2.2 CELL CULTURE AND SEEDING ONTO SCAFFOLDS

MG-63 osteosarcoma cells were cultured in EMEM supplemented with 10% FBS and 1% antibiotic anti-mycotic. The cells were maintained in a humidified tissue-culture incubator at 37 °C and 5% CO_2. Scaffolds were prepared directly into a 24-well plate as described next. A 1:1 porous to non-porous microsphere mixture was UV-sterilised for 80 minutes and then transferred to the wells. Basal growth media was then added at a ratio of 1:4 media to microspheres, respectively. After 17 hours of sintering, each scaffold/well was seeded with 2×10^5 MG-63 cells and incubated for 2 hours, followed by the addition of 1 ml of media to each scaffold/well. The cell-seeded scaffolds were then maintained at 37 °C and 5% CO^2. For all the cell experiments, either 5 replicates or 2 independent repeats, each comprising at least 3 replicates, were carried out.

7.2.2.3 CELL VIABILITY ASSAY

After incubation for 24 hours under culture conditions, MG 63 cells in the 96-well plates were incubated and treated differently; a) with SIM b) 1:1 ratio of PMP and NPMP for both IMW and HMW PLGA as this represent the scaffold containing SIM for 24, 48 and 72 hours. The amount of SIM was calculated based on the SIM concentration in the IMW-SIM NPMP and HMW-SIM-NPMP in a dose-dependent (0.1, 0.2, 0.4, 0.8, 1.6, 3.2, 6.25, 12.5, 25 mg/ml). The cytotoxicity of this treatment was then evaluated in triplicate by the 3-(4,5-dimethylthiazol-2-yl)-2,5- diphenyltetrazolium bromide (MTT) proliferation assay. Plating was performed in a 96-well plate and treated with test compounds for 24, 48 and 72 hours. MTT solution was added following incubation and further incubated for 4 hours. Supernatant was removed, and DMSO was added to dissolve the formed formazan crystal. The plate was further incubated for 15 minutes prior to measurement at 570 nm with an ELISA plate reader (BioTek,USA).

7.2.2

.4 INVERTED MICROSCOPY IMAGING

Microscopic examination of MG-63 was performed using an inverted microscopy (Olympus, German). Briefly, MG-63 cells were plated onto a 24-well plate and treated 1:1 ratio of PMP and NPMP. The amount of SIM was calculated based on the SIM concentration in the IMW-SIM NPMP and HMW-SIM-NPMP in a dose-dependent (0.1, 0.4, 1.0 mg/ml) for 24, 48 and 72 hours. The cells were wash once with PBS and subjected to image capturing under inverted microscope.

7.2.2.5 ENVIRONMENTAL SCANNING ELECTRON MICROSCOPE (ESEM) IMAGING

Three different scaffolds which differ in SIM-NPMP amount were studied at each separate time point. The scaffold preparation followed the same protocol described in Section 6.2.7. After day 3, Samples were pre-fixed with 3% glutaraldehyde for 30 min, and were dehydrated with a serial of dehydration

solutions consisting of ethanol and hexamethyldisilazane. The dehydrated specimens were observed by ESEM (Quanta 200, FEI, USA).

7.3 Results and Discussion

7.3.1 Viability Assay

Cell viability was determined using the MTT assay. The antiproliferative effects of SIM were determined following 24 to 72 hours of exposure to SIM. We first observed the effect of SIM on MG 63. Here, we observed the absorbance decreased with the increased amount of SIM concentration within the cells (Figure 7.1). The effects seen here clearly suggests that SIM exerts anti proliferative effects on MG 63 cultured cells which is also seen in Magan-Fernandez, A. *et al*., 2018. Their studies show that, after 72 hours of SIM treatment, the highest dose of 0.01 µmol/L was observed not giving any effects on cell proliferation. Instead at 0.01 µmol/L, the proliferation of MG 63 started to decrease. In our study however 0.04 mg/l was seen as the concentration that started to decrease the cell proliferation after it was exposed with SIM within 24 hours and drastically decreased when the cells exposed for 48 hours.

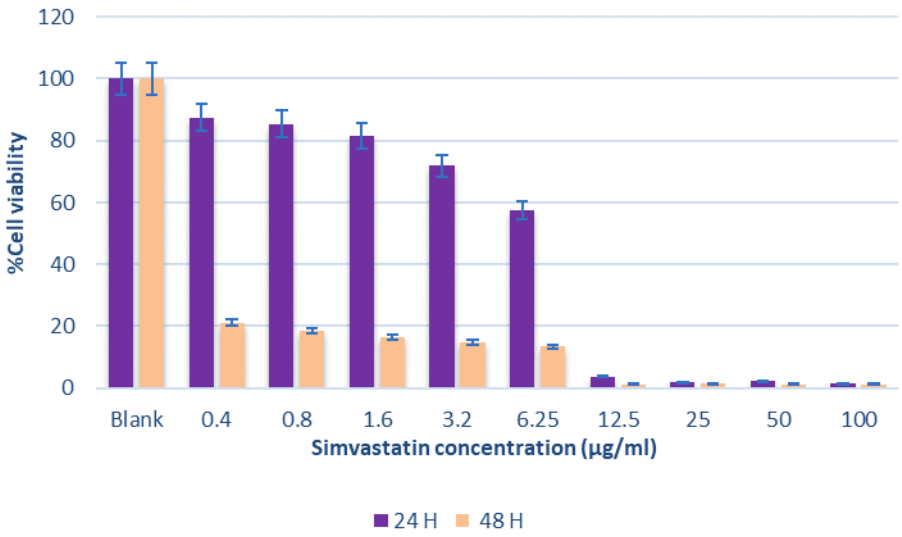


Figure 7.1: In-vitro toxicity of SIM in MG 63 cell line. Growth of MG 63cell was valuated after 48 hours exposure to a wide range of SIM concentrations (0.4-

100 µg/ml) in comparison to control cell (blank) which was treated with solvent alone. Data expressed as the mean ± SD of triplicate cultures.

Following the treatment of MG-63 cells with SIM alone, we further investigated the viability effects of MG-63 towards SIM encapsulated in the scaffold which was represented using 1: 1 ratio of PMP and SIM-NPMP for both IMW and HMW polymers.

This cell culture study was conducted using different concentrations of IMW-SIM NPMP and HMW-SIM NPMP; 0, 0.1, 0.2, 0.4, 0.8, 1.6, 3.2, 6.25, 12.5, 25 mg/ml for three consecutive days and the viability of the cells were analysed using MTT. Results obtained for 24, 48 and 72 hours are given in Figure7.2 a, Figure 7.2 b and Figure 7.2 c.

In 24 hours treatment, it was observed that the absorbance of the cells for MTT decreased with increasing concentrations of SIM-NPMP. This further indicate antiproliferative effects for all treated groups however showing a proliferative effect beginning at 0.4 µg/ml. The proliferation effects of MG 63 increased considerably as the concentration of the SIM-NPMP increased. The same pattern was clearly seen for both cells treated with IMW SIM-NPMP and HMW SIM-NPMP respectively. At a higher dose (25 µg/ml), the proliferative capacity of these cells completely diminished in comparison to control cell including at the 24 hours exposure to SIM. This result is obvious especially when the cells were treated with HMW-SIM NPMP. This could be due to several reasons. First, higher concentration of scaffold may generally block the absorbance of MTT to the cells thus it gives false-negative results. Secondly, it could be due to the presence of artifacts that contributed to the reducing the capacity of absorbace in the well plate Therefore MTT might not be a suitable analysis tool in this study. An option for this could be via fluorescent imaging study.

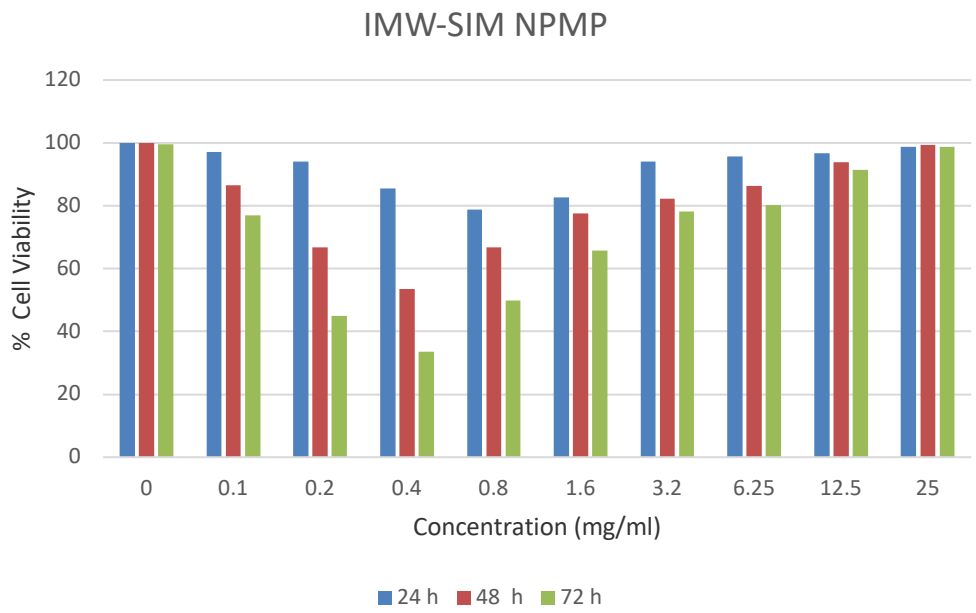


Figure 7.2a: Viability of MG-63 responding to different concentrations IMW-SIM scaffold for different days. Values are the mean ± SE (three parallel samples for each concentration). Blank PLGA microparticles were used as a control group.

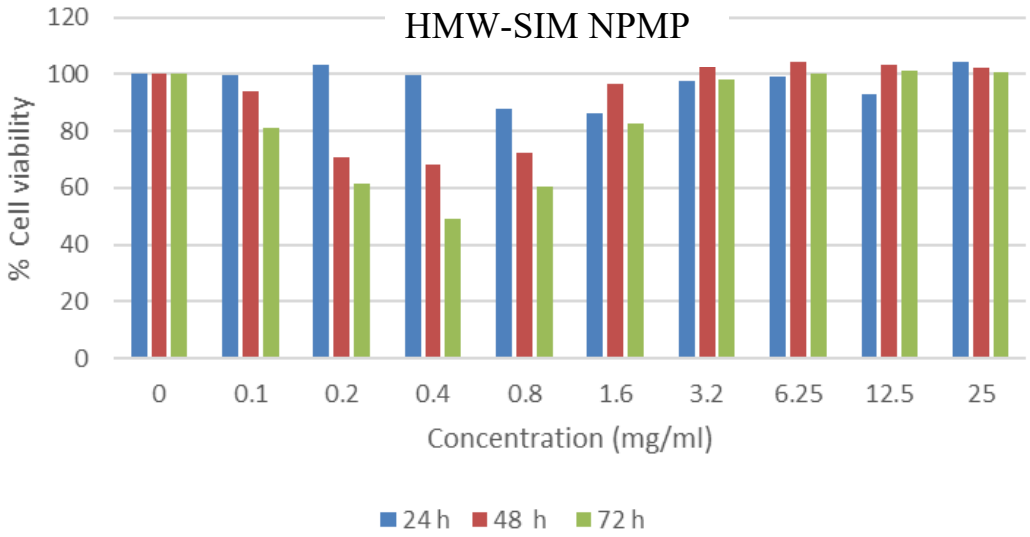


Figure 7.2b: Viability of MG-63 responding to different concentrations HMW-SIM scaffold for different days. Values are the mean ± SE (three parallel samples for each concentration). Blank PLGA microparticles were used as a control group.

In comparison between different SIM- NPMP cells viability study, the cells treated with HMW-SIM NPMP showed higher percentage of viability as compared to cells treated with IMW SIM-NPMP. That means, treatment with IMW-SIM NPMP scaffold showed higher anti-proliferation as compared to treatment with HMW-SIM NPMP. This can be seen when the MG-63 cells were exposed with the microparticles for 72 hours. The viability cells were found 44.8% in cells treated with HMW-SIM NPMP whilst 33.6% with IMW-SIM NPMP. Over a 24-hour period the MG-63 cells showed a significant decrease in cell proliferation when they were treated with both IMW and HMW scaffolds. Similarly goes for 48 hours exposure. It was previously observed that SIM can induce antiproliferation in MG-63 cells (Figure 7.1) and these results shown in both Figure 7.2 a and 7.2 b confirmed that SIM was released from the NPMP and giving antiproliferation pattern from 0.1 to 0.4 mg/ml .

Interestingly, above certain concentrations, the antiproliferation effects were not seen. In addition to that, more cells were proliferated as the concentration of the SIM-NPMP increased regardless for both IMW or HMW scaffold. Over a 24-hour treatment period, the concentration of 0.8 μg/ml was observed to give the highest antiproliferation effects in cells treated with IMW SIM scaffold, however, the cell viability further increased as the concentration of IMW SIM-NPMP was further increased beyond 0.8 mg/ml. Similar observation was seen for cells treated with HMW-SIM scaffolds where the antiproliferative effect stopped at 0.8 mg/ml and thereafter the cells started to proliferate above this concentration. Again here, the presence of artifacts might interfere the results.

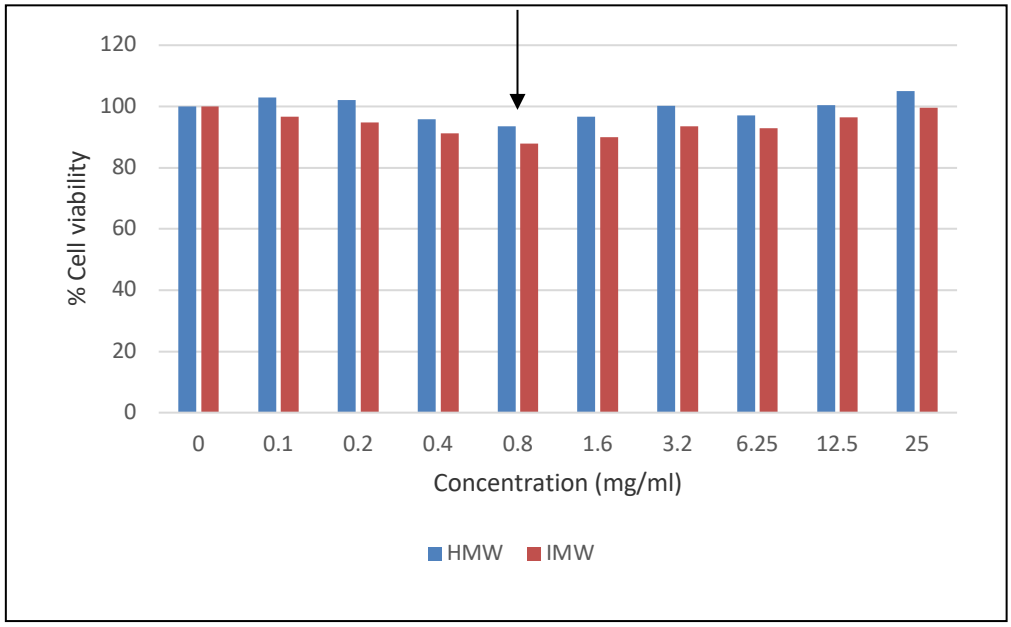


Figure 7.3 a: Comparison between IMW and HMW MG 63 viability responding to different concentrations for 24 hours treatment. Values are the mean ± SE (three parallel samples for each concentration). Blank PLGA microparticles were used as a control group. Arrow indicates the lowest antiproliferation of the scaffold.

In order to make better comparison, we compare IMW-SIM scaffold with the HMW-SIM scaffold on MG-63 cells over a 24-hour incubation period (Figure 7.3 a). As explained earlier, the antiproliferation effects can be clearly seen in IMW-SIM scaffold rather than the HMW SIM scaffold.

The cells were further treated for 48 hours in order to see the effect of SIM from encapsulated microparticles. In cell treated with IMW-SIM and HMW-SIM scaffold, the antiproliferation were observed from 0.1 to 0.4 mg/ml and started to lose the antiproliferation effects beyond 0.4 mg/ml concentration. However, previous treatment within 24 hours shown antiproliferative effects at 0.8 mg/ml.

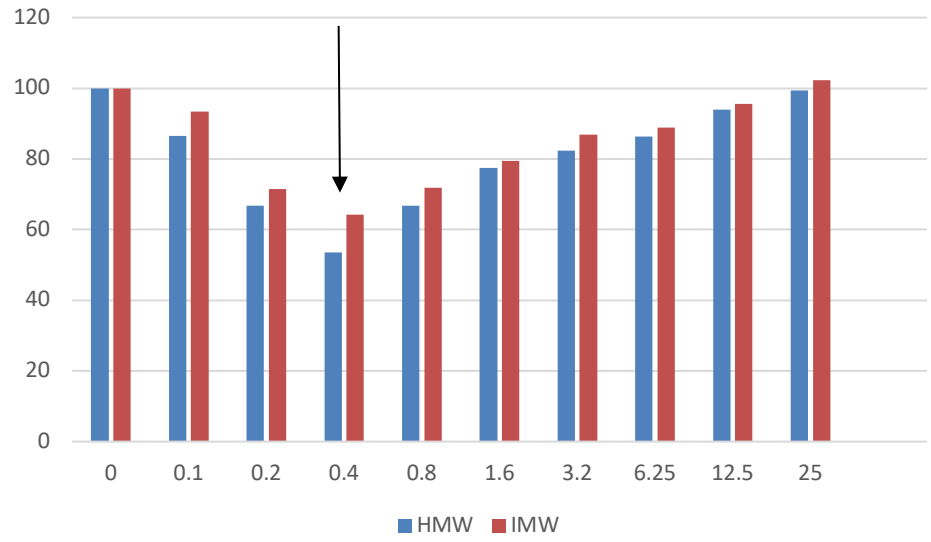


Figure 7.3 b: Comparison between IMW and HMW MG63 viability responding to different concentrations for 48 hours treatment. Values are the mean ± SE (three parallel samples for each concentration). Blank PLGA microparticles were used as a control group. Arrow indicates the lowest antiproliferation of the scaffold.

The cells then were investigated for 72 hours exposure and it was observed that the antiproliferation effect followed similar trend as in 24- and 48-hours proliferation effects. In addition, the cells treated with the IMW SIM-NPMP has similar cut-off concentration at 0.4 mg/ml for the antiproliferation, before the cells started to actively increase in their proliferation rate. Moreover, the effect was more suppressive in cells treated for 72 hours as compared to 48 hours (Figure 7.3 b) treatment where the percentage of viable cells were reduced at the concentration of 0.4 µg/ml.

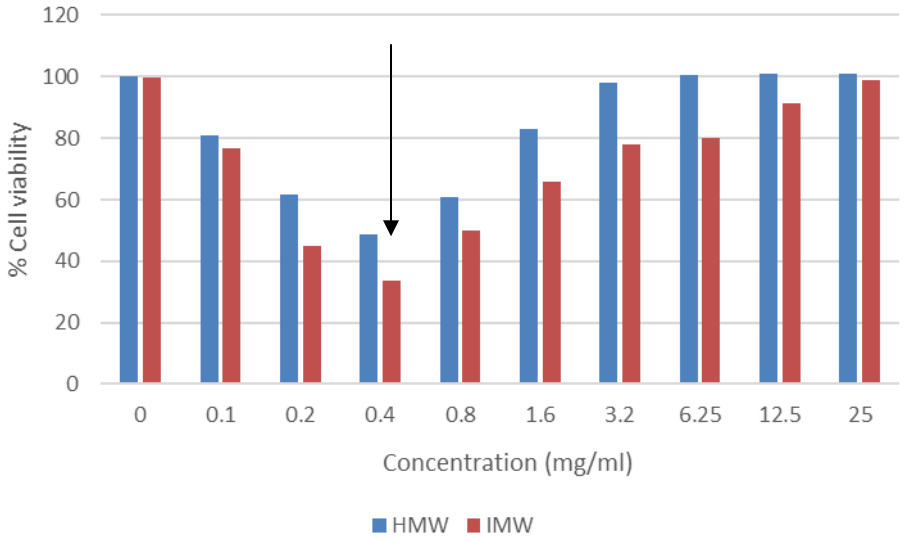


Figure 7.3 c: Comparison between IMW and HMW MG 63 viability responding to different concentrations for 72 hours treatment. Values are the mean ± SE (three parallel samples for each concentration). Blank PLGA microparticles were used as a control group. Arrow indicates the lowest antiproliferation of the scaffold.

Following the viability assay, SIM-loaded scaffolds in different concentration were interacted with MG-63 cells. Blank microparticles were used as a control. In the first day, the viability of the cells interacting with both SIM-loaded PLGA scaffold for all groups were significantly decreased. The interesting point in this assay was that the ability of MG-63 cells to start proliferating at certain concentration which was 0.8 mg/ml in 24 hours whilst 0.4 mg/ml in 48 and 72 hours exposure. The loss of the toxic effects were observed as the concentration increased in the treatment. Based on these results, it was postulated that, the SIM- loaded scaffold have the dose-dependent effect on MG-63 cells. This dose-dependent effect changed the proliferation of cells across different concentrations of SIM-NPMP.

SIM was previously reported to produce accumulation of cytosolic lipid droplets in non-malignant and also malignant cells which inversely mirrored the marginal anti-proliferative effects in a dose and time-dependent manner to their antiproliferative effects (Lettiero, B. *et al*., 2018). However, Martinet *et al*, 2018 found little cytoplasm vacuolization of mesenchymal stem cells (MSC) after treated with 0.01 µmol/L SIM. These two different effects further suggested that

effect of SIM may be attributable to the difference in baseline differentiation between MSC and MG-63 cells, which means the action of SIM may be dependent on the degree of differentiation of different two cells type (the MSC and MG-63 cells). According to Magan-Fernandez *et al.,* 2018, the degree of differentiation was supported by immunohistochemical analysis of CD56 and Musahi-1 expression in MG 63 cells. From their study, they found that the expression of CD56 and Musahi-1 expression was greatly reduced in the SIM-treated MG-63. When the expression of CD56 and Musahi-1 reduced, these effects consequently related to the improve of MG-63 differentiation which in their study, they observed the MG-63 with special staining, suggesting a possible involvement of this factor in bone regeneration. Due to cost constraint, we could not analyse the expression of CD 56, Musahi-1 and also Ki-67 which these are the markers for cell proliferation index.

Fabrication of microparticles from PLGA has previously shown to be capable of controlling the release of drugs (Zheng *et al.,* 2010; Malavia *et al.* 2015), with excellent biocompatibility (Barrow, 2004; Kapoor *et al.,* 2015). One of the characteristics of PLGA degradation is surface erosion (Anderson *et al.,* 2012, Fredenberg *et al.,* 2011) which have the feature of being biodegraded only at their surfaces and further release the entrapped drugs. This characteristic eventually led to the development of three-dimensional scaffolds and formation of controlled-release scaffold in our work. Therefore in this study, the scaffold was found to release the SIM however the effects of antiproliferation stops at 0.4 or 0.8 mg/ml depending on the time the MG-63 cells exposure to the scaffold.

As observed in Figure 7.2 and 7.3, the antiproliferative effects stopped at a few concentration beginning at 0.4 mg/ml in 24 hours cells exposure to the scaffolds and 0.8 mg/ml for 48 and 72 hours cells exposure scaffolds. These phenomenon could be due to several reasons. Firstly, it might be due to the amount of SIM that was encapsulated in the NPMP. Since the loading amount of SIM was low in NPMP preparations (section 2.3.4), the effects of SIM arresting the cell proliferation might be impeded as the microparticles might have small amount of SIM encapsulated in it. Secondly, it might be due to amount of PMP microparticles used in the scaffold preparation. As the scaffold contained PMP, the cells has the capability to proliferate rather than arrested and

this effect subsequently increased in cells proliferation. This is due to cell attachment at the pores that facilitate the proliferation of the cells as the amount of PMP increased alongside with the increased of SIM-NPMP.

In terms of bone proliferation, our findings are in accordance with research conducted by Magan-Fernandez *et al*. (2018). To our knowledge, this research was the latest research using an MG 63 cell model to reveal SIM as a stabilizing agent in osteogenic cell renewal processes. Their study described the ultrastructural and immunocytochemical changes observed *in vitro* using SIM as the antiproliferative agent and consequently relates the finding of SIM as modulator of osteoclastogenesis and osteogenesis. Such a treatment could potentially provide a pathway to recovery of the normal morphological and functional status of bone tissue and enhancing the differentiation of the normal cells following an injury.

7.3.2 Cell Morphology and Proliferation

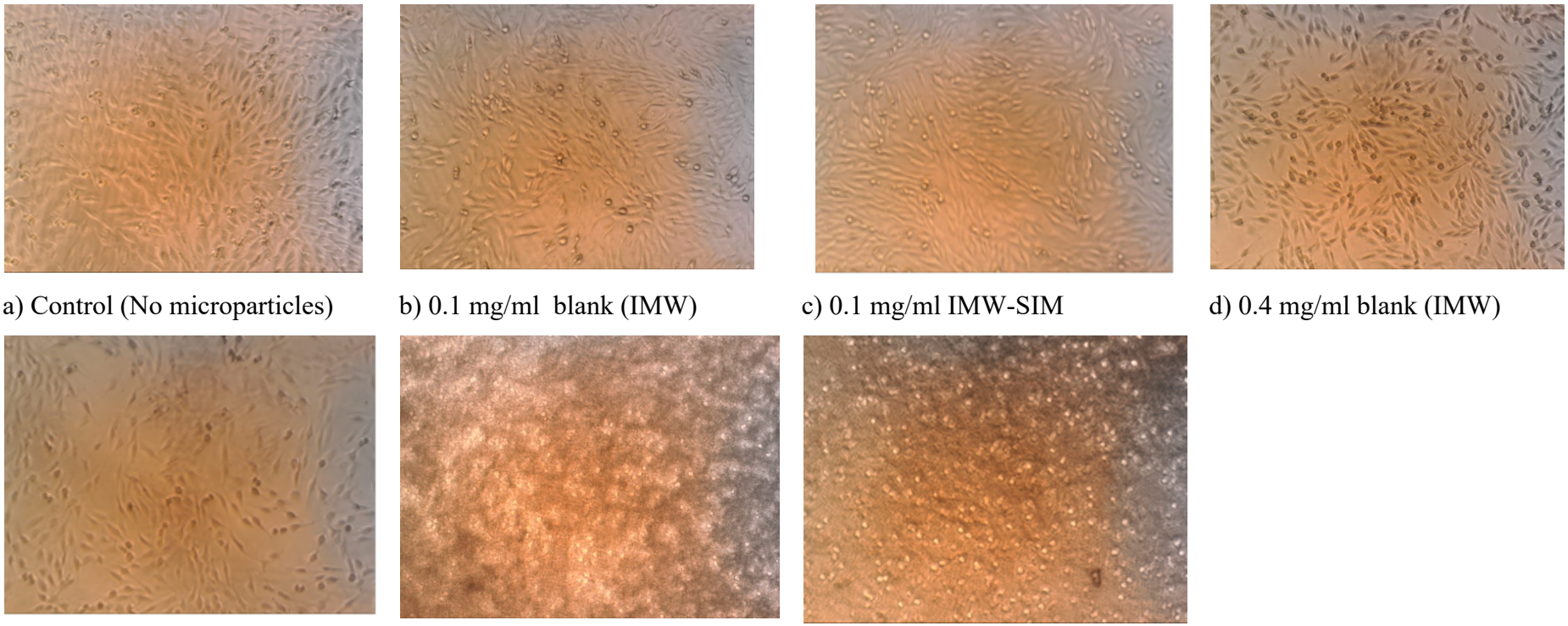
7.3.2.1 Observation of MG 63 Cells with Scaffold using inverted Microscope

The ability of cells to attach and grow on a scaffold is paramount in the development of drug delivery systems in tissue regenerative medicine. The biocompatibility of the scaffolds with a human osteoblast cell-line, MG-63 cells, was observed with an inverted microscope (Figure 7.4 a-d). Cells proliferation reduced over time on both scaffold types. Theoretically, other literature has shown that the doubling time of MG 63 cells was approximately 24-30 hours (Billiau *et al*., 1977; Altindal *et al*., 2016). However, as explained in section7.3.1, SIM was giving antiproliferation effects against MG-63 cells. Therefore, we anticipated cells reduction upon treatment with SIM-scaffolds, Here in this section, we observed morphological changes whereby SIM inhibited the MG-63 cell proliferation in a dose- and time-dependent manner and this supported the results obtained in the viability study. At different concentrations (0.1, 0.4 and 1.0 mg/ml scaffold), the control group of cells showed a typical polygonal and intact appearance for both 24 and 48 hours. However, the blank scaffold containing no SIM displayed dose-dependent changes in cell counts and

started to shrink as the scaffold concentration increased. The IMW-SIM scaffold showed slightly slimmer spindle shapes but did not totally differ from the control and cells treated with blank microparticles. At the concentration of 1mg/ml, the cells completely died upon treatment with both blank and SIM-scaffolds. Similar trend was also observed for the 48-hour treatment time whereby we observed loss of cell-to-cell contact, poor adherence and floating shapes especially in 0.4 mg/ml (Figure 7.4 b, magnification, x100) and completely burst when treated with 1 mg/ml.

For HMW-SIM scaffold, the trends observed were similar to those seen with IMW except that the number of cells that was suppressed by the drug was slightly lower than those cell that were interacting with IMW-SIM scaffolds, as more cells were seen to have lost it morphologically when treated with IMW-SIM scaffold. HMW-SIM scaffold induced suppression and showed better morphology in terms of the cell appearance with less shrinkage and the number is higher than the cells observed with IMW-SIM scaffold. In order to compare the cytoplasmic destruction, the control cells were compared with the cells treated with 1 mg/ml. The MG-63 cells were morphologically reverted by SIM treatment which significantly reduced the amount of cytoplasmic destruction and reduced the number of cytoplasmic vacuoles containing cell material. Similar results were observed in a study conducted by Magan-Fernandez, A. *et al*. (2018) and Wang, H. *et al*., 2016. According to that study, SIM acted against the cell stress, which further stabilized the osteogenic cell renewal processes (Wang *et al.,* 2016; Magan-Fernandez *et al.,* 2018). In the context of bone production, preservation and remodeling, we postulated that SIM may therefore act as a modulator of osteoclastogenesis/osteogenesis.

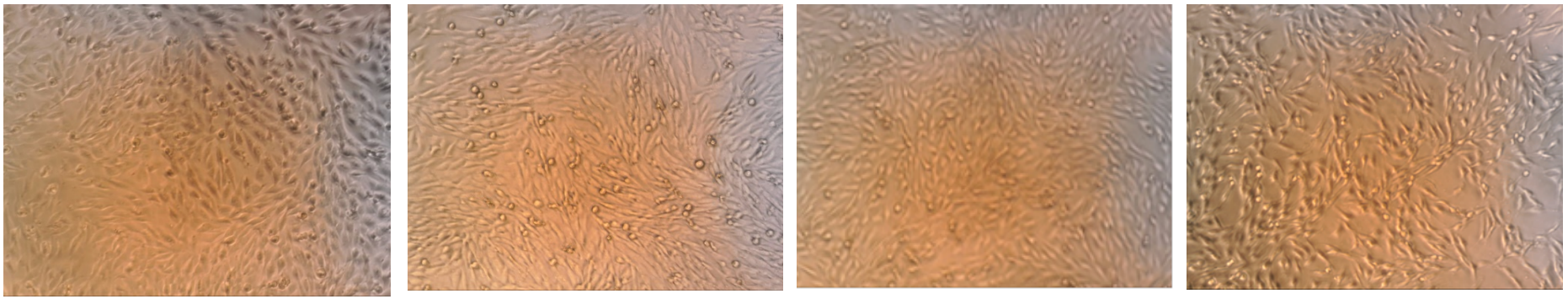
The viability of MG 63 cells were totally diminished following the treatment of microparticles at 3 µg/ml for both IMW-SIM NPMP and HMW-SIM NPMP , irrespective of whether SIM was present. This further suggest that the microparticles may have had a toxic effect on MG 63 cells due to the amount added into the MG 63 cells.



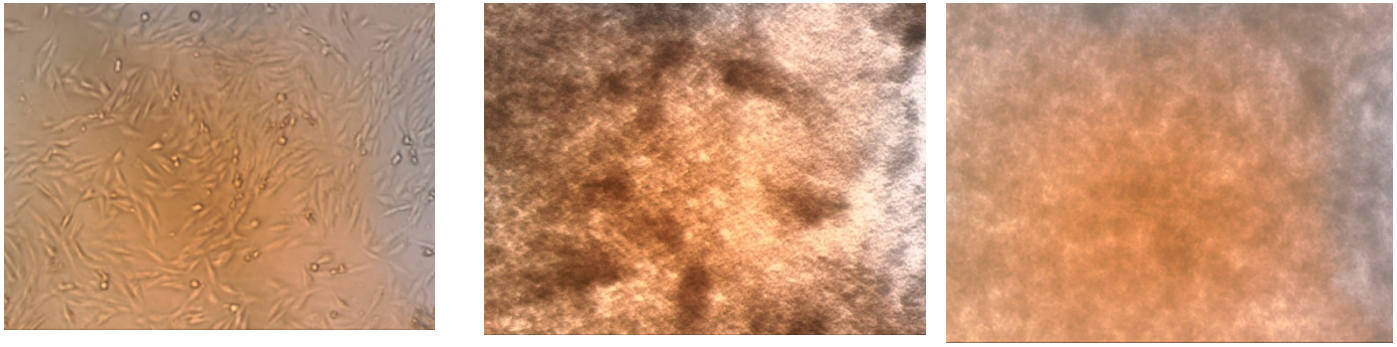
a) Control (No microparticles) b) 0.1 mg/ml blank (IMW) c) 0.1 mg/ml IMW-SIM d) 0.4 mg/ml blank (IMW)

e) 0.4 mg/ml IMW-SIM f) 1.0 mg/ml blank (IMW) g) 1.0 mg/ml IMW-SIM

Figure 7. 4 a: Inverted microscope image of MG-63 cells treated with different concentration of IMW scaffold for 24 hours incubation; a) Control (No scaffold) b) 0.1 mg/ml blank IMW c) 0.1 mg/ml IMW-SIM d) 0.4 mg/ml IMW-BLANK , e) 0.4 mg/ml IMW- SIM f)1.0 mg/ml IMW-BLANK and g)1.0 mg/ml IMW- SIM.

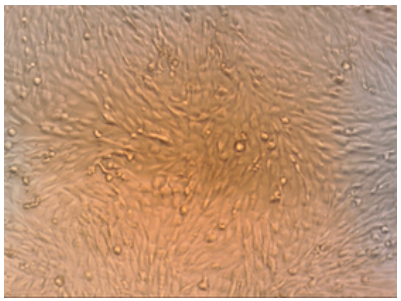


a) Control (No microparticles) b) 0.1 mg/ml blank (HMW) c) 0.1 mg/ml HMW-SIM d) 0.4 mg/ml blank (HMW)

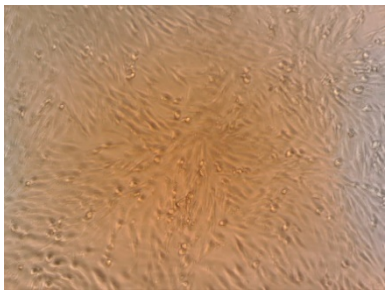


e) 0.4 mg/ml HMW-SIM f) 1.0 mg/ml blank (HMW) g) 1.0 mg/ml HMW-SIM

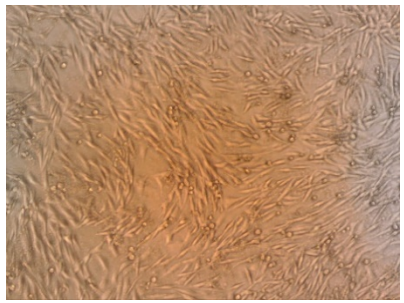
Figure 7.4 b: Inverted microscope image of MG-63 cells treated with different concentration of HMW scaffold for 24 hours incubation; a) Control (No scaffold) b) 0.1 mg/ml blank HMW c) 0.1 mg/ml HMW-SIM d) 0.4 mg/ml HMW-BLANK , e) 0.4 mg/ml HMW- SIM f)1.0 mg/ml HMW-BLANK and g)1.0 mg/ml HMW- SIM.



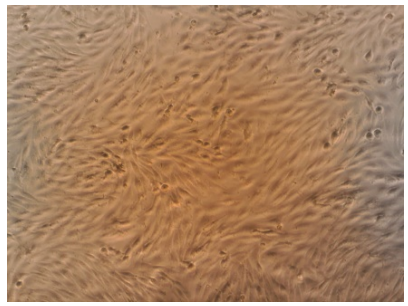
a) Control (No microparticles)



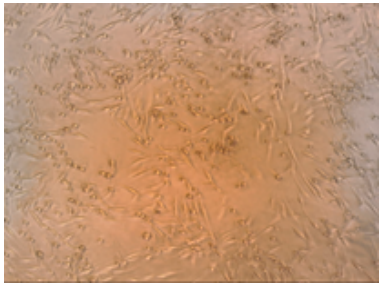
b) 0.1 mg/ml blank (IMW)



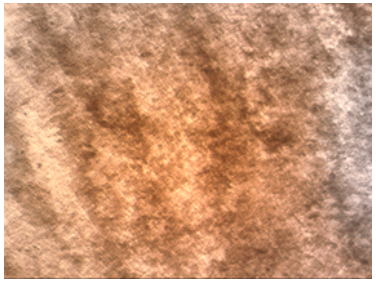
c) 0.1 mg/ml IMW-SIM



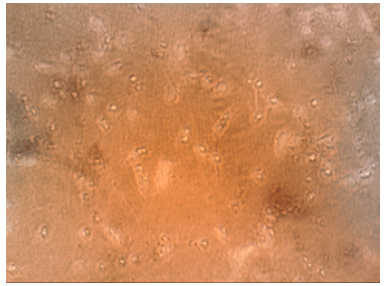
d) 0.4 mg/ml blank (IMW)



e) 0.4 mg/ml IMW-SIM

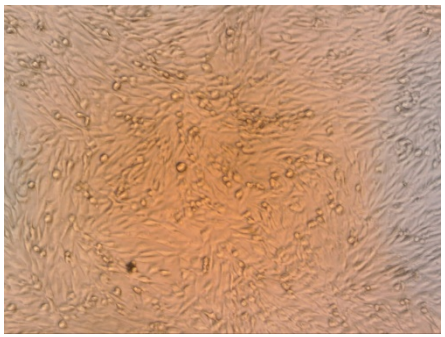


f) 1.0 mg/ml blank (IMW)

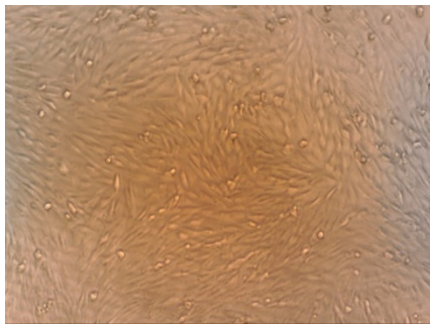


g) 1.0 mg/ml IMW-SIM

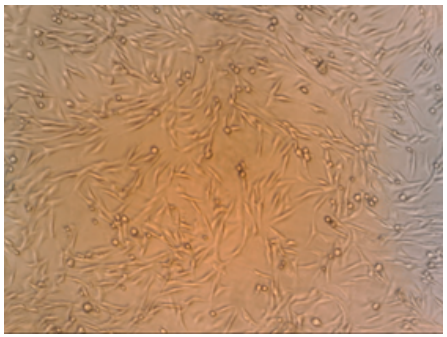
Figure 7.4 c: Inverted microscope image of MG-63 cells treated with different concentration of IMW scaffold for 48 hours incubation; a) Control (No scaffold) b) 0.1 mg/ml blank IMW c) 0.1 mg/ml IMW-SIM d) 0.4 mg/ml IMW-BLANK , e) 0.4 mg/ml IMW- SIM f)1.0 mg/ml IMW-BLANK and g)1.0 mg/ml IMW- SIM.



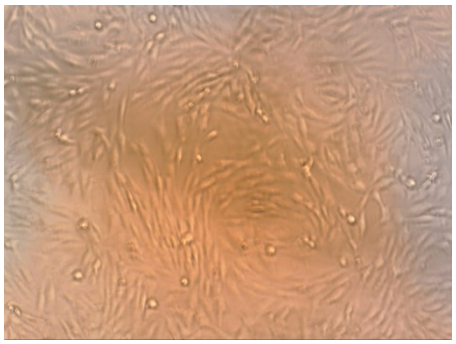
a) Control (No microparticles)



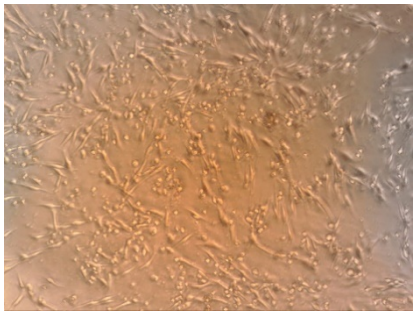
b) 0.1 mg/ml blank (HMW)



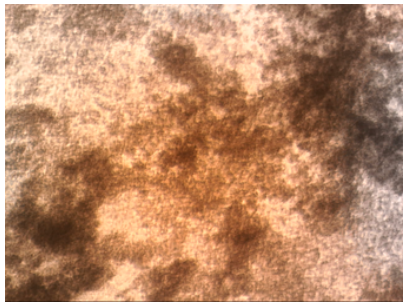
c) 0.1 mg/ml HMW-SIM



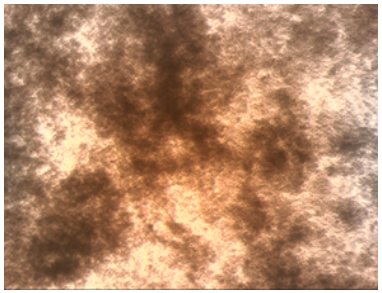
d) 0.4 mg/ml blank (HMW)



e) 0.4 mg/ml HMW-SIM



f) 1.0 mg/ml blank (HMW)



g) 1.0 mg/ml HMW-SIM

Figure 7.4 d: Inverted microscope image of MG-63 cells treated with different concentration of HMW scaffold for 24 hours incubation; a) Control (No scaffold) b) 0.1 mg/ml blank HMW c) 0.1 mg/ml HMW-SIM d) 0.4 mg/ml HMW-BLANK , e) 0.4 mg/ml HMW- SIM f)1.0 mg/ml HMW-BLANK and g)1.0 mg/ml HMW- SIM.

A major disadvantage of using an inverted light microscope to study the cells was the lack of clarity in the images. In addition, the light microscope only provides 2-dimensional information only i.e. the surface features (Bibi *et al*., 2011; Robson *et al*., 2018). Therefore, we subsequently investigate the interaction of MG-63 with scaffolds fabricated from both PMP and SIM NPMP (Section 7.3.2.2) and SIM-NPP. Electron microscopy is a method for the visualization of vesicles under very high magnification (Adler, 1985). Scanning electron microscopy (SEM) utilizes an electron beam that is scanned across or over a sample (rather than through a sample) to produce a magnified image of an object (Ruozi *et al*., 2011; Hua *et al*., 2015).

7.3.2.2 OBSERVATION OF MG 63 CELLS WITH SCAFFOLD VIA ENVIRONMENTAL SCANNING ELECTRON MICROSCOPY (ESEM*)*

ESEM is a unique system in which a biological material can be examined in the presence of water vapour in the microscope chamber (Bibi *et al*., 2011; Robson *et al*., 2018). Because of this, ESEM permits wet and insulating samples to be imaged without prior specimen preparation (Muscariello *et al*., 2005).

ESEM images of the cell-scaffold constructs on day 3 confirm MG 63 growth on the scaffolds (Figure 7.5). Figure 7.5 a shows very few visible cells on the scaffolds prepared with the blank microspheres (1:1 from PMP and NPMP of HMW) whilst figure 7.5 b (1: 1 from PMP and SIM-NPMP of IMW) shows more cells and microfilaments covering the microparticles. In contrast to IMW PLGA variants, scaffolds prepared with Blank-HMW PLGA was observed to have fewer cells interconnected to the surface of the scaffold. With the presence of SIM in the HMW particles, the cells were seen to have improved interconnective effects with neighbouring particles, however, the effect occurred was not as much as seen with the cells treated with the IMW scaffolds. This comparison mainly derived from the cells attachment observed in the IMW and HMW scaffolds depicted in Figure 7.5 b and d.

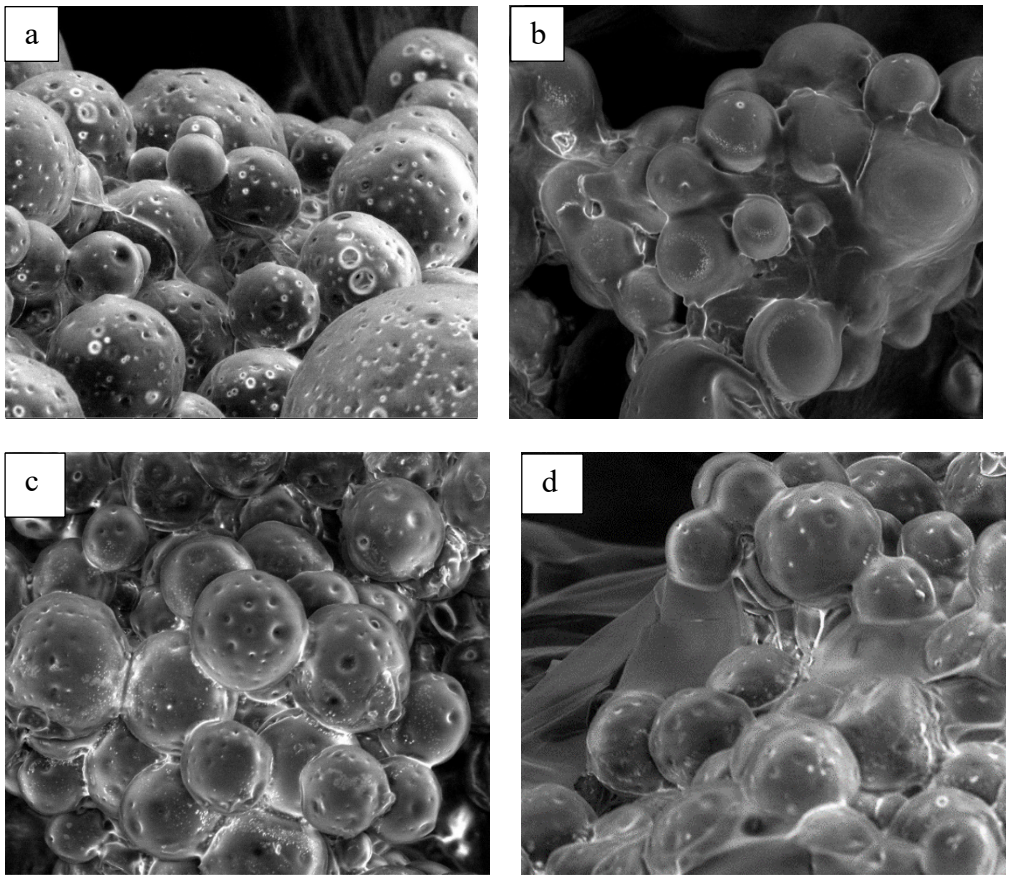


Figure 7.5: ESEM images after cell MG 63 proliferation on a) IMW-BLANK b) IMW porous, c) IMW SIM-NPMP, d) HMW BLANK and HMW SIM-NPMP scaffold after 3 days.

The results from the inverted microscope suggested that SIM significantly suppressed the proliferation ability in a dose dependent manner as compared to the control group. Despite that knowledge that SIM act as antiproliferation to MG-63 cells (Ruiz-Gaspa *et al*., 2007; Czekanska *et al*., 2012; Liu *et al*., 2013; Nath *et al*., 2013; Magan-Fernandez *et al.,* 2018), we suggested that the arrangement of suppressed cells indicate that SIM acts as a cell stressor which further stabilizes the osteogenic process. The ESEM observations indicated that the process of cell stabilization could be attributed to the release of SIM. The presence of lamellapodia and an interlaced microsphere bed network demonstrated good cell proliferation. Images of each sample were taken at the same magnification to assess cell

proliferation on the surfaces of the microspheres. Cell proliferation was higher on the SIM-loaded microspheres than that of the blank. The cells had completely covered the microsphere mats with IMW-SIM scaffold treatment.

Although SIM played a suppressive role in MG 63 cells, it has been established that MG-63 cells treated by SIM can still initiate osteogenic differentiation (Magan-Fernandez *et al.,* 2018). This osteogenic differentiation indicates the function of SIM as a modulator of osteoclastogenesis and osteogenesis. Osteoclast is a type of cells that break bone cell (Teitelbaum, S. L. (2007, Florencio-Silva, R. *et al.,* 2015). SIM was previously found to potentially act as the agent to revert the osteoclastogenesis via increasing the expression of BMP-2 (bone morphogenetic protein-2) mRNA and protein in HOS (human osteosarcoma) cells. (Yamashita, M. *et al*., 2010, Roy, A *et al*., 2016).As describe in section 7.3.2.1, SIM acted against the cell stress, which further stabilized the osteogenic cell renewal processes (Wang et al., 2016; Magan-Fernandez et al., 2018).

7.4 CONCLUSION

The effect of statins on bone metabolism was first reported by Mundy *et al*., 1999 in an *in-vitro* animal model, which revealed higher BMP-2 expression in the cell culture and increased medullar bone formation in rodents. Since then, more studies have been conducted particularly to investigate the significant relationship between SIM and bone tissue regeneration.

In this chapter, we presented and compared the two approaches of combining SIM with IMW and HMW PLGA in non-porous microparticles. MG 63 cells were used in this study because it has signified its role in bone tissue proliferation based on other studies as presented in Table 7.1. In addition, the doubling time and specific growth rate are high for MG-63 cells, thus they are a useful model.

In this study, we found SIM was able to supress MG-63 in a dose-dependent and time-dependent manner. The images from the inverted microscope further support the notion that SIM is released from the encapsulated microparticles. Overall studies indicate IMW-SIM scaffolds have higher release and increase MG-

63 suppression in the viability studies, whilst the HMW-SIM-scaffold showed a delay of suppression. This is mainly due to the surface erosion taking longer for the higher molecular weight polymer, and therefore there is a slower release of drug. The investigation using inverted microscopy follow similar trends as observed in the viability test in terms of the antiproliferation effects. The ESEM showed biocompatibility test with regards to the effects of SIM in the scaffolds and the neighbouring cells whereby he IMW-SIM scaffold showed better interconnection activity with the neighbouring MG-63 cells.

There are some limitations to this work. To generate a more specific outcome with regards to bone proliferation, further investigation is needed, particularly with the incorporation of immunohistochemical, gene and protein expression, as well as using ultramicroscopy imaging to elucidate the SIM encapsulated scaffold in bone tissue engineering. Optimizing the result in bone proliferation can be collectively supported by other studies for example the usage of normal bone cell line, different immunohistochemical studies using MG 63 cell line, gene and protein expressions in both normal and MG 63 cell line.

CHAPTER 8

FINAL CONCLUSIONS AND FUTURE WORK

8.1 FINAL CONCLUSIONS

The focus of this work was on the formulation and in vitro characterisation of an injectable microparticulate system with the ability to deliver SIM in a controlled manner. The first phase of work resulted in the fabrication of porous and non-porous of PLGA microspheres through the adjustment of the formulation and processing variables. We started the investigation with background study by elaborating the significant of this study as described in Chapter 1.

Following the literature search, we embarked the work by investigating different protocols for fabrication of encapsulating SIM in microspheres. With tourer justification, we adapted the protocol outlined by Yamina *et al*., 2016. We made some changes to the original protocol and observed the outcome of the modified methods. The adapted version with modifications were finally achieved after series of testing and validation. All the modification and adapted methods were explained thoroughly in Chapter 2.

We then noticed the importance to have a validated HPLC protocol as this instrument is the anchor to study the encapsulation efficiency, drug loading, percentage of yield and most importantly the release profiles of the SIM encapsulated microspheres of different preparation. We presented the entire HPLC validation process in Chapter 3.

We then went on to study the effect of the PLGA molecular weight on the properties of non-porous SIM-loaded microspheres. We observed that the molecular weight of the PLGA had a profound effect on the release profiles of the drug release study. The release corresponding profile between the SIM and the PLGA molecular weight are peculiar whereby the encapsulation efficiency was observed higher in the

high molecular weight PLGA. Variations in the reaction parameters during the synthesis of SIM encapsulated microparticles synthesis from different processing variables were analysed and summarised in Chapter 4.

In order to confirm the influence of SIM impacting the physicochemical properties, we investigate the structure-energetics within the microparticles and the surface characterization of the microparticles using different analysis instruments as summarised in Chapter 5. The surface characteristics including the chemical composition, phase behaviour, and topography of the PLGA microparticles. Here we conclude the amorphous structure of SIM in the microparticles may employed the solubilizing and stabilizing the systems and the surface roughness observed in the microspheres enhances attachment, proliferation and differentiation of anchorage dependent bone forming cells.

The SIM-loaded NPMP and PMP were sintered into scaffolds and then physically characterised in Chapter 6. Both IMW and HMW scaffolds were observed to have sufficient compressive strength respectively. The size range of both NPMP and PMP fell between 10-200 μm, which shown to be compatible with injection through a 22 G and 19 G needle. These results highlight a method for fabricating porous PLGA microspheres that form solid porous scaffolds at body temperature, creating an injectable system capable of supporting cell attachment and proliferation in vitro. However, due to the weaknesses and fragility of the scaffold delivery across a range of clinically relevant needle gauges, we did not perform this investigation.

Subsequently, we focused on addressing the biocompatibility and osteogenic potential on the microparticles and scaffolds. Here in this chapter 7, we have various limitations of study as outlined in the section 8.2. These limitations are the main challenges as to proof the successful of the SIM- encapsulated microspheres in bone tissue regeneration study. Overall, the microspheres composite in combination with porous PLGA microspheres show some degree of great potential for use in bone tissue engineering. As motioned in Chapter 7, proliferation and cell functions exhibited by osteosarcoma cells may not fully representative of those in human

primary osteoblasts, nevertheless, the MG 63 cell line has been extensively used as an in vitro model for bone research and finding on the proliferation of these cels have proven comparable to observation particularly in primary human osteoblasts.

8.2 LIMITATION OF THE WORK

The limitations of the work are mainly focusing on the investigation of proliferation and cell functions exhibited by osteosarcoma cells. The investigation will be more significant with the incorporation of the following studies.

Immunohistochemical studies using several monoclonal antibodies and proliferation markers such as Musashi-1, Ki-67, CD56 and CD44 whereby this proliferation markers may attribute to the differences in baseline differentiation between different range of SIM fabrication, either the microparticles or the scaffold.

The information obtained from the study can also be more elusive with the incorporation of mesenchymal stem cell. The incorporation of primary cells which are derived directly from the human tissue of a specific person is another aspect that can be considered as it will increase the clinical relevance in comparison with the use of immortalized cells, which may have slight differences to their primary counterparts. The primary cells are one step closer to in vivo testing conditions than an immortalized cell line would be too.

The gene expression studies is also an important tool to investigate related molecular pathway that eventually promoted osteoblasts proliferation and differentiation, reduce osteoclastogenesis by inhibiting osteolclastic differentiation and also to protect osteoblasts. Some of the important gene expression are upregulating the BMP-2 ad Runx 2 expression, upregulating MAPK phosphatase-1 (MAPK-1) via the MAPK/BMP-2 signalling pathway, the TGFβ/Smad3 signalling pathway and also OPG/RANKL/RANK signalling pathway through the stimulation of Erα expression.

Imaging studies may reveal number of importance parameters with regards to the successful of fabricated microparticles and scaffolds. Not only we can visualize the morphology feature of the cells treated, the cell-permeant dye that can

be used to determine cell viability in most eukaryotic cells for example Calcein AM. Analysing cellular events in real time can lead to new biological discoveries once unachievable using traditional cellular analysis techniques for example PCR, flow cytometry and antibody immunocytochemistry staining as these methods were limited by analyzing cellular events as a snapshot rather than in real-time. Fluorescent cell labeling technologies used for cell tracking might be another option.

8.3 FUTURE WORK

Further work is required before this system could be considered for animal studies. Suggestions for the further work are described below.

1. Further investigation to understand the delivery of microspheres via injectable method, as described in Chapter 6 (section 6.3.3), is required. Following to that, investigation mist be carried out in a scenario where the formulation is injected in combination with cells. This would involve combining the microsphere mixtures with primary hMSCs and determining the cell activity post injection through a needle.
2. In this study the lactic acid to glycolic acid ratio of PLGA was fixed at 85:15; however, other ratios could be studied, which would result in a formulation with variable release properties depending on the ratio used i.e. a higher proportion of lactic acid in the polymer results in a slower degradation time.
3. In this study, other analysis as to investigate the role of the SIM scaffold were not carried out due t to the cost implications. Therefore, the next step would involve the limitations as outlined in section 8.2 and then further characterization and cell-line studies will be conducted.

It is a well-accepted paradigm in the formulation of tissue engineering scaffolds that after the characterisation and optimisation in vitro, the next step is the study of the system in an in vivo biological model. These studies will allow the use of complex biochemical and biomechanical environments that are key in the development of bone. Therefore, it is very important to determine the capability of the SIM scaffold to sustain and promote bone growth in such an environment. In

vivo tests would be undertaken in rats or rabbit models, as these are well-established for the investigation of factors that affect bone healing. At this point, we have successfully fabricated the SIM encapsulated microspheres which can be sintered for scaffold. Addition of porous microspheres in the scaffold will further enhance the regeneration process in the bone microenvironment.

REFERENCES

Abdal-Hay, A., Hussein, K. H., Casettari, L., Khalil, K. A., & Hamdy, A. S. (2016). Fabrication of novel high performance ductile poly(lactic acid) nanofiber scaffold coated with poly(vinyl alcohol) for tissue engineering applications. *Materials Science and Engineering C*, *60*, 143–150. Retrieved from https://doi.org/10.1016/j.msec.2015.11.024

Abdal-Hay, A., Sheikh, F. A., & Lim, J. K. (2013). Air jet spinning of hydroxyapatite/poly(lactic acid) hybrid nanocomposite membrane mats for bone tissue engineering. *Colloids and Surfaces B: Biointerfaces*, *102*, 635–643. Retrieved from https://doi.org/10.1016/j.colsurfb.2012.09.017

Aceves-Hernández, J. M., Hinojosa-Torres, J., Nicolás-Vázquez, I., Ruvalcaba, R. M., & García, R. M. L. (2011). Solubility of SIM: A theoretical and experimental study. *Journal of Molecular Structure*, *995*(1–3), 41–50. Retrieved from https://doi.org/10.1016/j.molstruc.2011.03.048

Adham, S., Miranda, S., Doucet, J., Lévesque, H., & Benhamou, Y. (2018). Statins in primary prevention of cardiovascular disease. *Revue de Medecine Interne*. Paris, France: Elsevier Masson SAS. Retrieved from https://doi.org/10.1016/j.revmed.2017.08.002

Adler K., & Schiemann J. (1985). Characterization of liposomes by scanning electron microscopy and the freeze-fracture technique. *Micron Microsc. Acta, 16,* 109–113. Retrieved from https://doi.org/10.1016/0739-6260(85)90039-5

Agarwal, R., & García, A. J. (2015). Biomaterial strategies for engineering implants for enhanced osseointegration and bone repair. *Advanced Drug Delivery Reviews*. Amsterdam, Netherlands: Elsevier B.V. Retrieved from https://doi.org/10.1016/j.addr.2015.03.013

Agrawal, V., & Badylak, S. F. (2015). *Biological scaffolds for regenerative medicine.* In Biomaterials and Regenerative Medicine (pp. 133–150). Retrieved from https://www.cambridge.org/core/books/biomaterials-and-

regenerative-medicine/biological-scaffolds-for-regenerative-medicine/A67B3200D4DA92C08DF6EDE540A70CBC

Ahmed, A. R., & Bodmeier, R. (2009). Preparation of preformed porous PLGA microparticles and antisense oligonucleotides loading. *European Journal of Pharmaceutics and Biopharmaceutics*, *71*(2), 264–270. Retrieved from https://doi.org/10.1016/j.ejpb.2008.09.007

Akter, F., & Ibanez, J. (2016). Bone and cartilage tissue engineering. *In Tissue Engineering Made Easy* (pp. 77–97). Retrieved from https://doi.org/10.1016/B978-0-12-805361-4.00008-4

Albertsson, A. C. (1993). Degradable polymers. *Journal of Macromolecular Science, Part A, 30*(9–10), 757–765. Retrieved from https://doi.org/10.1080/10601329308021261

Alessandrino A., Marelli B., Arosio C., Fare S., & Tanzi M. G. (2008). Electrospun silk fibroin mats for tissue engineering. *Engineering in Life Sciences. 8*(3), 219–225. Retrieved from https://doi.org/10.1002/elsc.200700067

Alhosseini, S. N., Moztarzadeh, F., Mozafari, M., Asgari, S., Dodel, M., Samadikuchaksaraei, A., … & Jalali, N. (2012). Synthesis and characterization of electrospun polyvinyl alcohol nanofibrous scaffolds modified by blending with chitosan for neural tissue engineering. *International Journal of Nanomedicine*, *7*, 25–34.

Ali, H., & Nazzal, S. (2009). Development and validation of a reversed-phase HPLC method for the simultaneous analysis of SIM and tocotrienols in combined dosage forms. *Journal of Pharmaceutical and Biomedical Analysis, 49*(4), 950–956. Retrieved from https://doi.org/10.1016/j.jpba.2009.02.009

Al-Munajjed, A. A., Hien, M., Kujat, R., Gleeson, J. P., & Hammer, J. (2008). Influence of pore size on tensile strength, permeability and porosity of hyaluronan-collagen scaffolds. *Journal of Materials Science: Materials in Medicine, 19*(8), 2859–2864. Retrieved from https://doi.org/10.1007/s10856-008-3422-5

Altindal, D. Ç., & Gumusderelioglu, M. (2016). Melatonin releasing PLGA micro/nanoparticles and their effect on osteosarcoma cells. *Journal of Microencapsulation, 33(*1), 53–63. Retrieved from https://doi.org/10.3109/02652048.2015.1115901

Altman, G. H., Diaz, F., Jakuba, C., Calabro, T., Horan, R. L., Chen, J., … & Kaplan, D. L. (2003). Silk-based biomaterials. *Biomaterials*, *24*(3), 401–16. Retrieved from http://www.ncbi.nlm.nih.gov/pubmed/12423595

Amini, A. A., & Nair, L. S. (2012). Injectable hydrogels for bone and cartilage repair. *Biomedical Materials*. Bristol, UK: Institute of Physics Publishing. Retrieved from https://doi.org/10.1088/1748-6041/7/2/024105

Amini, A. R., Laurencin, C. T., & Nukavarapu, S. P. (2012). Bone tissue engineering: recent advances and challenges. *Critical Reviews in Biomedical Engineering*, *40*(5), 363–408. Retrieved from http://www.ncbi.nlm.nih.gov/pubmed/23339648

Amsa, P., Tamizharasi, S., Jagadeeswaran, M., & Sivakumar, T. (2014). Preparation and solid state characterization of SIM nanosuspensions for enhanced solubility and dissolution. *International Journal of Pharmacy and Pharmaceutical Sciences*, *6*(1), 265–269.

Anderson, J. M., & Shive, M. S. (2012). Biodegradation and biocompatibility of PLA and PLGA microspheres. *Advanced Drug Delivery Reviews*. Retrieved from https://doi.org/10.1016/j.addr.2012.09.004

Ansary, R. H., Awang, M. B., & Rahman, M. M. (2014). Biodegradable poly(D,L-lactic-co-glycolic acid)-based micro/nanoparticles for sustained release of protein drugs - A review. *Tropical Journal of Pharmaceutical Research. University of Benin*. Retrieved from https://doi.org/10.4314/tjpr.v13i7.24

Antal, I., & Zelkó, R. (2008). Pharmaceutical significance of amorphous materials. *Acta Pharmaceutica Hungarica, 78*(3), 121—133. Retrieved from http://europepmc.org/abstract/MED/18986089

Anzar, N., Mirza, M. A., Anwer, K., Khuroo, T., Alshetaili, A. S., Alshahrani, S. M., … & Iqbal, Z. (2018). Preparation, evaluation and pharmacokinetic studies of spray dried PLGA polymeric submicron particles of SIM for the effective treatment of breast cancer. *Journal of Molecular Liquids, 249,* 609–616. Retrieved from https://doi.org/10.1016/j.molliq.2017.11.081

Aravamudhan, A., Ramos, D., Nip, J., Subramanian, A., James, R., Harmon, M., … & Kumbar, S. (2013). Osteoinductive small molecules: Growth factor alternatives for bone tissue engineering. *Current Pharmaceutical Design*, *19*(19), 3420–3428. Retrieved from https://doi.org/10.2174/1381612811319190008

Asadi, H., Rostamizadeh, K., Salari, D., & Hamidi, M. (2011). Preparation of biodegradable nanoparticles of tri-block PLA-PEG-PLA copolymer and determination of factors controlling the particle size using artificial neural network. *Journal of Microencapsulation, 28*(5), 406–416. Retrieved from https://doi.org/10.3109/02652048.2011.576784

Avgoustakis, K. (2015). Polylactic-co-glycolic acid (PLGA). In *Encyclopedia of Biomaterials and Biomedical Engineering, Second Edition - Four Volume Set* (pp. 2259–2269). Florida: CRC Press. Retrieved from https://doi.org/10.1201/b18990-216

Bächle, M., & Kohal, R. J. (2004). A systematic review of the influence of different titanium surfaces on proliferation, differentiation and protein synthesis of osteoblast-like MG63 cells. *Clinical Oral Implants Research*. Retrieved from https://doi.org/10.1111/j.1600-0501.2004.0105

Bae, S. E., Son, J. S., Park, K., & Han, D. K. (2009). Fabrication of covered porous PLGA microspheres using hydrogen peroxide for controlled drug delivery and regenerative medicine. *Journal of Controlled Release, 133*(1), 37–43. Retrieved from https://doi.org/10.1016/j.jconrel.2008.09.006

Bal, T., Murthy, P., & Sengupta, S. (2012). Preparation and evaluation of mucoadhesive SIM microcapsules using orifice gelation technique. *Asian*

Journal of Pharmaceutics, *6*(1), 74. Retrieved from https://doi.org/10.4103/0973-8398.100152

Baptista, J. G. C., Rodrigues, S. P. J., Matsushita, A. F. Y., Vitorino, C., Maria, T. M. R., Burrows, H. D., … & Valente, A. J. M. (2016). Does poly(vinyl alcohol) act as an amphiphilic polymer? An interaction study with SIM. *Journal of Molecular Liquids*, *222*, 287–294. Retrieved from https://doi.org/10.1016/j.molliq.2016.07.025

Baron, R. (2000). *Anatomy and ultrastructure of bone: Histogenesis, growth and remodeling*. Endotext. Retrieved from http://www.ncbi.nlm.nih.gov/pubmed/25905372

Barrère, F., Mahmood, T. A., de Groot, K., & van Blitterswijk, C. A. (2008). Advanced biomaterials for skeletal tissue regeneration: Instructive and smart functions. *Materials Science and Engineering R: Reports*. Retrieved from https://doi.org/10.1016/j.mser.2007.12.001

Barrow, W. W. (2004). Microsphere technology for chemotherapy of mycobacterial infections. *Current Pharmaceutical Design, 10*(26), 3275–84. Retrieved from https://doi.org/10.2174/1381612043383197

Benoit DSW, Nuttelman CR, Collins SD, et al. Synthesis and characterization of a fluvastatin-releasing hydrogel delivery system to modulate hMSC differentiation and function for bone regeneration. Biomaterials. 2006;27:6102–10.

Berchane, N. S., Jebrail, F. F., Carson, K. H., Rice-Ficht, A. C., & Andrews, M. J. (2006). About mean diameter and size distributions of poly(lactide-co-glycolide) (PLG) microspheres. *Journal of Microencapsulation*, *23*(5), 539–552. Retrieved from https://doi.org/10.1080/02652040600776440

Bhadra, S., Das, S. C., Roy, S., Arefeen, S., & Rouf, A. S. S. (2011). Development and validation of RP-HPLC method for quantitative estimation of vinpocetine in pure and pharmaceutical dosage forms. *Chromatography Research*

International, *2011*, 1–7. Retrieved from https://doi.org/10.4061/2011/801656

Bhardwaj, S. K., Dwivedi, K., & Agarwal, D. D. (2015). A review: HPLC method development and validation. *International Journal of Analytical and Bioanalytical Chemistry, 5*(4), 76–81. Retrieved from https://www.researchgate.net/publication/284717827_A_Review_HPLC_Method_Development_and_Validation

Bibi, S., Kaur, R., Henriksen-Lacey, M., McNeil, S. E., Wilkhu, J., Lattmann, E., … & Perrie, Y. (2011). Microscopy imaging of liposomes: From coverslips to environmental SEM. *International Journal of Pharmaceutics, 417*(1–2), 138–150. Retrieved from https://doi.org/10.1016/j.ijpharm.2010.12.021

Bible, E., Chau, D. Y. S., Alexander, M. R., Price, J., Shakesheff, K. M., & Modo, M. (2009). Attachment of stem cells to scaffold particles for intra-cerebral transplantation. *Nature Protocols*, *4*(10), 1440–1453. Retrieved from https://doi.org/10.1038/nprot.2009.156

Bible, E., Chau, D. Y. S., Alexander, M. R., Price, J., Shakesheff, K. M., & Modo, M. (2009). The support of neural stem cells transplanted into stroke-induced brain cavities by PLGA particles. *Biomaterials, 30*(16), 2985–2994. Retrieved from https://doi.org/10.1016/j.biomaterials.2009.02.012

Billiau, A., Edy, V. G., Heremans, H., Van Damme, J., Desmyter, J., Georgiades, J. A., & De Somer, P. (1977). Human interferon: Mass production in a newly established cell line, MG 63. *Antimicrobial Agents and Chemotherapy, 12(*1), 11–15. Retrieved from https://doi.org/10.1128/AAC.12.1.11

Black, C. R. M., Goriainov, V., Gibbs, D., Kanczler, J., Tare, R. S., & Oreffo, R. O. C. (2015). Bone tissue engineering. *Current Molecular Biology Reports, 1(3),* 132–140. Retrieved from https//doi: 10.1007/s40610-015-0022-2

Bock, N., Woodruff, M. A., Hutmacher, D. W., & Dargaville, T. R. (2011). Electrospraying, a reproducible method for production of polymeric

microspheres for biomedical applications. *Polymers*, *3*(1), 131–149. Retrieved from https://doi.org/10.3390/polym3010131

Bolourchian, N., Mahboobian, M. M., & Dadashzadeh, S. (2013). The effect of PEG molecular weights on dissolution behavior of SIM in solid dispersions. *Iranian Journal of Pharmaceutical Research*, *12*(SUPPL.), 9–18. Retrieved from https://www.ncbi.nlm.nih.gov/pubmed/24250667

Bone, H. (2012). Future directions in osteoporosis therapeutics. *Endocrinology and Metabolism Clinics of North America*. Retrieved from https://doi.org/10.1016/j.ecl.2012.05.003

Bose, S., Roy, M., & Bandyopadhyay, A. (2012). Recent advances in bone tissue engineering scaffolds. *Trends in Biotechnology*. Retrieved from https://doi.org/10.1016/j.tibtech.2012.07.005

Boukari, Y., Qutachi, O., Scurr, D. J., Morris, A. P., Doughty, S. W., & Billa, N. (2017). A dual-application poly (dl-lactic-co-glycolic) acid (PLGA)-chitosan composite scaffold for potential use in bone tissue engineering. *Journal of Biomaterials Science, Polymer Edition, 28*(16), 1966–1983. Retrieved from https://doi.org/10.1080/09205063.2017.1364100

Boukari, Y., Scurr, D. J., Qutachi, O., Morris, A. P., Doughty, S. W., Rahman, C. V., & Billa, N. (2015). Physicomechanical properties of sintered scaffolds formed from porous and protein-loaded poly(DL-lactic-co-glycolic acid) microspheres for potential use in bone tissue engineering. *Journal of Biomaterials Science, Polymer Edition*, *26*(12), 796–811. Retrieved from https://doi.org/10.1080/09205063.2015.1058696

Boyle, W. J., Simonet, W. S., & Lacey, D. L. (2003). Osteoclast differentiation and activation. *Nature*. Retrieved from https://doi.org/10.1038/nature01658

Boyne, P. J., & Shabahang, S. (2001). An evaluation of bone induction delivery materials in conjunction with root-form implant placement. *International Journal of Periodontics Restorative Dent*, *21*(4), 333–343. Retrieved from

http://www.ncbi.nlm.nih.gov/entrez/query.fcgi?cmd=Retrieve&db=PubMed&dopt=Citation&list_uids=11519702

Boyne, P. J., Marx, R. E., Nevins, M., Triplett, G., Lazaro, E., Lilly, L. C., … & Nummikoski, P. (1997). A feasibility study evaluating rhBMP-2/absorbable collagen sponge for maxillary sinus floor augmentation. *The International Journal of Periodontics & Restorative Dentistry*, *17*(1), 11–25. Retrieved from http://www.ncbi.nlm.nih.gov/pubmed/10332250

Bret, U. D., Lakshmi, N. S., & Laurencin, C. T. (2011). Biomedical applications of biodegradable polymers. *Journal of Polymer Science Part B: Polymer Physics, 3(49*), 832–864. Retrieved from https://doi.org/10.1002/polb.22259

Brittain, H. G. (1999). *Polymorphism in pharmaceutical solids* (2nd ed.). New York: Marcel Dekker.

Burr, D. B., & Akkus, O. (2013). Bone morphology and organization. In *Basic and Applied Bone Biology* (pp. 3–25). Amsterdam, Netherlands: Elsevier Inc. Retrieved from https://doi.org/10.1016/B978-0-12-416015-6.00001-0

Caetano-Lopes, J., Canhão, H., & Fonseca, J. E. (2007). Osteoblasts and bone formation. *Acta Reumatológica Portuguesa*. Retrieved from http://www.actareumatologica.pt/oldsite/conteudo/pdfs/ARP_2007_2_103_AR_-_Osteoblasts_and_bone_formation.pdf

Cai, Y., Chen, Y., Hong, X., Liu, Z., & Yuan, W. (2013). Porous microsphere and its applications. *International Journal of Nanomedicine, 8,* 1111. Retrieved from https://doi.org/10.2147/IJN.S41271

Capan, Y., Woo, B. H., Gebrekidan, S., Ahmed, S., & DeLuca, P. P. (1999). Influence of formulation parameters on the characteristics of poly(D, L-lactide-co-glycolide) microspheres containing poly(L-lysine) complexed plasmid DNA. *Journal of Control Release, 60*(2–3), 279–286. Retrieved from https://doi.org/10.1016/s0168-3659(99)00076-0

Chan, B. P., & Leong, K. W. (2008). Scaffolding in tissue engineering: General approaches and tissue-specific considerations. In *European Spine*

Journal (Vol. 17). Retrieved from https://doi.org/10.1007/s00586-008-0745-3

Chang, H.-I., & Wang, Y. (2011). Cell responses to surface and architecture of tissue engineering scaffolds. In *Regenerative Medicine and Tissue Engineering - Cells and Biomaterials*. InTech. Retrieved from https://doi.org/10.5772/21983

Chen, F. M., Zhang, M., & Wu, Z. F. (2010). Toward delivery of multiple growth factors in tissue engineering. *Biomaterials*. Retrieved from https://doi.org/10.1016/j.biomaterials.2010.04.053

Chen, G. & Kawazoe, N. (2016). *Preparation of polymer-based porous scaffolds for tissue engineering*. Retrieved from https://www.sciencedirect.com/science/article/pii/B9781782420873000055

Chen, H., Huang, X., Zhang, M., Damanik, F., Baker, M. B., Leferink, A., … & Moroni, L. (2017). Tailoring surface nanoroughness of electrospun scaffolds for skeletal tissue engineering. *Acta Biomaterialia*, *59*, 82–93. Retrieved from https://doi.org/10.1016/j.actbio.2017.07.003

Chiou, W. L., & Riegelman, S. (1971). Pharmaceutical applications of solid dispersion systems. *Journal of Pharmaceutical Sciences*, *60*(9), 1281–1302. Retrieved from https://doi.org/10.1002/jps.2600600902

Choi, Y., Faccio, R., Teitelbaum, S. L., & Takayanagi, H. (2015). Osteoclast biology: Regulation of formation and function. *In Osteoimmunology: Interactions of the Immune and Skeletal Systems* (2nd ed.) (pp. 41–70). Amsterdam, Netherlands: Elsevier Inc. Retrieved from https://www.sciencedirect.com/book/9780128005712/osteoimmunology

Clockaerts S, Van Osch GJ, Bastiaansen-Jenniskens YM, Verhaar JA, Van Glabbeek F, Van Meurs JB, et al. Statin use is associated with reduced incidence and progression of knee osteoarthritis in the Rotterdam study. Ann Rheum Dis. 2012;71:642–7. doi: 10.1136/annrheumdis-2011-200092.

Chromacademy. (2010). The theory of HPLC: Gradient HPLC. *Chromacademy*, 1–23. Retrieved from https://doi.org/10.1016/S0075-7535(08)70364-4

Chung, H. J., Kim, H. K., Yoon, J. J., & Park, T. G. (2006). Heparin immobilized porous PLGA microspheres for angiogenic growth factor delivery. *Pharmaceutical Research*, *23*(8), 1835–1841. Retrieved from https://doi.org/10.1007/s11095-006-9039-9

Clarke, B. (2008). Normal bone anatomy and physiology. *Clinical Journal of the American Society of Nephrology : CJASN*, *3 Suppl 3*, S131-9. Retrieved from https://doi.org/10.2215/CJN.04151206

Clas, S. D., Dalton, C. R., & Hancock, B. C. (1999). Differential scanning calorimetry: Applications in drug development. *Pharmaceutical Science and Technology Today*. Retrieved from https://doi.org/10.1016/S1461-5347(99)00181-9

Clementino, A., & Sonvico, F. (2018). Development and validation of a RP-HPLC method for the simultaneous detection and quantification of SIM's isoforms and coenzyme Q10 in lecithin/chitosan nanoparticles. *Journal of Pharmaceutical and Biomedical Analysis*, *155*, 33–41. Retrieved from https://doi.org/10.1016/j.jpba.2018.03.046

Cochran, D. L., Schenk, R., Buser, D., Wozney, J. M., & Jones, A. A. (2005). Recombinant human bone morphogenetic protein-2 stimulation of bone formation around endosseous dental implants. *Journal of Periodontology*, *70*(2), 139–150. Retrieved from https://doi.org/10.1902/jop.1999.70.2.139

Cooper, D. L., & Harirforoosh, S. (2014). Effect of formulation variables on preparation of celecoxib loaded polylactide-co-glycolide nanoparticles. *PLoS ONE, 9*(12). Retrieved from https://doi.org/10.1371/journal.pone.0113558

Corrigan, O. I. (1985). Mechanisms of dissolution of fast release solid dispersions. *Drug Development and Industrial Pharmacy*, *11*(2–3), 697–724. Retrieved from https://doi.org/10.3109/03639048509056896

Costa, P. F. (2015). Bone tissue engineering drug delivery. *Current Molecular Biology Reports, 1*(2), 87–93. Retrieved from https://doi.org/10.1007/s40610-015-0016-0.

Craig, M. (2006). *Thermal analysis of pharmaceuticals.* Boca Raton, FL: CRC Press. Retrieved from https://www.crcpress.com/Thermal-Analysis-of-Pharmaceuticals/Craig-Reading/p/book/9780824758141

Crawford Scientific (2015). *Quantitative & qualitative HPLC*. Retrieved from http://www.chromacademy.com/lms/sco9/Theory_Of_HPLC_Quantitative_and_Qualitative_HPLC.pdf

Cui, W., Wang, Q., Chen, G., Zhou, S., Chang, Q., Zuo, Q., … & Fan, W. (2011). Repair of articular cartilage defects with tissue-engineered osteochondral composites in pigs. *Journal of Bioscience and Bioengineering*, *111*(4), 493–500. Retrieved from https://doi.org/10.1016/j.jbiosc.2010.11.023

Cuijpers, V. M. J. I., Walboomers, X. F., & Jansen, J. A. (2011). Scanning electron microscopy stereoimaging for three-dimensional visualization and analysis of cells in tissue-engineered constructs: Technical note. *Tissue Engineering Part C: Methods*, *17*(6), 663–668. Retrieved from https://doi.org/10.1089/ten.tec.2010.0455

Czekanska, E. M., Stoddart, M. J., Richards, R. G., & Hayes, J. S. (2012). In search of an osteoblast cell model for in vitro research. European Cells and Materials. *AO Research Institute Davos*. Retrieved from https://doi.org/10.22203/eCM.v024a01

D'Avila Carvalho Erbetta, C. (2012). Synthesis and characterization of poly(d,l-lactide-co-glycolide) copolymer. *Journal of Biomaterials and Nanobiotechnology, 3*(02), 208–225. Retrieved from https://doi.org/10.4236/jbnb.2012.32027.

Dahlberg, C. (2010). Drugs and polymers in dissolving solid dispersions: NMR imaging and spectroscopy. *Technology*. Retrieved from http://kth.diva-portal.org/smash/record.jsf?pid=diva2:281756

Dai, W., Kawazoe, N., Lin, X., Dong, J., & Chen, G. (2010). The influence of structural design of PLGA/collagen hybrid scaffolds in cartilage tissue engineering. *Biomaterials*, *31*(8), 2141–2152. Retrieved from https://doi.org/10.1016/j.biomaterials.2009.11.070

Danhier, F., Ansorena, E., Silva, J. M., Coco, R., Le Breton, A., & Préat, V. (2012, July 20). PLGA-based nanoparticles: An overview of biomedical applications. *Journal of Controlled Release*. Retrieved from https://doi.org/10.1016/j.jconrel.2012.01.043

Danilevicius, P., Georgiadi, L., Pateman, C. J., Claeyssens, F., Chatzinikolaidou, M., & Farsari, M. (2015). The effect of porosity on cell ingrowth into accurately defined, laser-made, polylactide-based 3D scaffolds. In *Applied Surface Science* (Vol. 336, pp. 2–10). Elsevier B.V. Retrieved from https://doi.org/10.1016/j.apsusc.2014.06.012

Danley, R. L. (2003). New heat flux DSC measurement technique. *Thermochimica Acta*, *395*(1–2), 201–208. Retrieved from https://doi.org/10.1016/S0040-6031(02)00212-5

De Vera, M. A., Bhole, V., Burns, L. C., & Lacaille, D. (2014). Impact of statin adherence on cardiovascular disease and mortality outcomes: A systematic review. *British Journal of Clinical Pharmacology*, *78*(4), 684–698. Retrieved from https://doi.org/10.1111/bcp.12339

De, R. R. L., Albuquerque, D. A. C., Cruz, T. G. S., Yamaji, F. M., & Leite, F. L. (2012). Measurement of the Nanoscale Roughness by Atomic Force Microscopy: Basic Principles and Applications. In *Atomic Force Microscopy - Imaging, Measuring and Manipulating Surfaces at the Atomic Scale*. Retrieved from https://doi.org/10.5772/37583

Deligkaris, K., Tadele, T. S., Olthuis, W., & van den Berg, A. (2010, June 3). Hydrogel-based devices for biomedical applications. *Sensors and Actuators, B: Chemical*. https://doi.org/10.1016/j.snb.2010.03.083

Devescovi, V., Leonardi, E., Ciapetti, G., & Cenni, E. (2008). Growth factors in bone repair. *La Chirurgia Degli Organi Di Movimento*. Retrieved from https://doi.org/10.1007/s12306-008-0064-1

Dhillon, A., Schneider, P., Kuhn, G., Reinwald, Y., White, L. J., Levchuk, A., … & Rahman, C. V. (2011). Analysis of sintered polymer scaffolds using concomitant synchrotron computed tomography and in situ mechanical testing. *Journal of Materials Science: Materials in Medicine, 22*(12), 2599–2605. Retrieved from https://doi.org/10.1007/s10856-011-4443-z

Dirckx, N., Van Hul, M., & Maes, C. (2013). Osteoblast recruitment to sites of bone formation in skeletal development, homeostasis, and regeneration. *Birth Defects Research Part C - Embryo Today: Reviews*. Retrieved from https://doi.org/10.1002/bdrc.21047

Donald, A. M. (2003). The use of environmental scanning electron microscopy for imaging wet and insulating materials. *Nature Materials, 2*(8), 511–516. Retrieved from https://doi.org/10.1038/nmat898

Dorati, R., Colonna, C., Genta, I., Modena, T., & Conti, B. (2010). Effect of porogen on the physico-chemical properties and degradation performance of PLGA scaffolds. *Polymer Degradation and Stability, 95*(4), 694–701. Retrieved from https://doi.org/10.1016/j.polymdegradstab.2009.11.039

Downey, P. A., & Siegel, M. I. (2006). Bone biology and the clinical implications for osteoporosis. *Physical Therapy, 86*(1), 77–91. Retrieved from https://doi.org/10.1093/ptj/86.1.77

Ducheyne, P., Healy, K. E., Grainger, D. W., Hutmacher, D. W., & Kirkpatrick, C. J. (2011). Comprehensive biomaterials. *Comprehensive Biomaterials* (Vol. 1, pp. 1–3363). Retrieved from https://doi.org/10.1016/C2009-1-28384-5

Duncanson, W. J., Zieringer, M., Wagner, O., Wilking, J. N., Abbaspourrad, A., Haag, R., & Weitz, D. A. (2012). Microfluidic synthesis of monodisperse porous microspheres with size-tunable pores. *Soft Matter, 8(41),* 10636–10640. Retrieved from https://doi.org/10.1039/c2sm25694k

E. J., Bray, G., Hamid, O. A., Rose, F. R. A. J., Shakesheff, K. M., & Delcassian, D. (2018). Improved delivery of PLGA microparticles and microparticle-cell scaffolds in clinical needle gauges using modified viscosity formulations. International *Journal of Pharmaceutics, 546*(1–2), 272–278. Retrieved from https://doi.org/10.1016/j.ijpharm.2018.05.025

Edalat, F. (2012). *NIH public access*, 40(6), 1301–1315. Retrieved from https://doi.org/10.1007/s10439-011-0452-9.Engineering

El Sayed, S. A., & Bhimji, S. S. (2017). *Physiology, bone*. Treasure Island, FL: StatPearls Publishing. Retrieved from https://www.ncbi.nlm.nih.gov/books/NBK441968/

Ezirganli, Ş., Kazancioğlu, H. O., Mihmanli, A., Aydin, M. Ş., Sharifov, R., & Alkan, A. (2014). The effect of local SIM application on critical size defects in the diabetic rats. *Clinical Oral Implants Research*, *25*(8), 969–976. Retrieved from https://doi.org/10.1111/clr.12177

Ezirganli, Ş., Kazancioğlu, H. O., Mihmanli, A., Aydin, M. Ş., Sharifov, R., & Alkan, A. (2014). The effect of local SIM application on critical size defects in the diabetic rats. *Clinical Oral Implants Research, 25*(8), 969–976. Retrieved from https://doi.org/10.1111/clr.12177

Florencio-Silva, R., Sasso, G. R. D. S., Sasso-Cerri, E., Simões, M. J., & Cerri, P. S. (2015). Biology of bone tissue: Structure, function, and factors that influence bone cells. *BioMed Research International*. Hindawi Publishing Corporation. Retrieved from https://doi.org/10.1155/2015/421746

Fredenberg, S., Wahlgren, M., Reslow, M., & Axelsson, A. (2011). The mechanisms of drug release in poly(lactic-co-glycolic acid)-based drug delivery systems - A review. *International Journal of Pharmaceutics, 30;415*(1-2), 34-52. Retrieved from https://doi.org/10.1016/j.ijpharm.2011.05.049

Freyman, T. M., Yannas, I. V., & Gibson, L. J. (2001). Cellular materials as porous scaffolds for tissue engineering. *Progress in Materials Science*. Retrieved from https://doi.org/10.1016/S0079-6425(00)00018-9

Freyman, T. M., Yannas, I. V., & Gibson, L. J. (2001). Cellular materials as porous scaffolds for tissue engineering. *Progress in Materials Science, 46*(3–4), 273–282. Retrieved from https://doi.org/10.1016/S0079-6425(00)00018-9

Fu, Q., Saiz, E., Rahaman, M. N., & Tomsia, A. P. (2011). Bioactive glass scaffolds for bone tissue engineering: State of the art and future perspectives. Materials *Science and Engineering C*. Retrieved from https://doi.org/10.1016/j.msec.2011.04.022

Furman, C., Carpentier, R., Barczyk, A., Chavatte, P., Betbeder, D., & Lipka, E. (2017). Development and validation of a reversed-phase HPLC method for the quantification of paclitaxel in different PLGA nanocarriers. *Electrophoresis*, *38*(19), 2536–2541. Retrieved from https://doi.org/10.1002/elps.201600552

Fuster, J., Negro, S., Salama, A., Fernández-Carballido, A., Marcianes, P., Boeva, L., & Barcia, E. (2015). HPLC-UV method development and validation for the quantification of ropinirole in new PLGA multiparticulate systems: Microspheres and nanoparticles. *International Journal of Pharmaceutics*, *491*(1–2), 310–317. Retrieved from https://doi.org/10.1016/j.ijpharm.2015.06.035

Gaihre, B., Uswatta, S., & Jayasuriya, A. (2017). Reconstruction of Craniomaxillofacial Bone Defects Using Tissue-Engineering Strategies with Injectable and Non-Injectable Scaffolds. *Journal of Functional Biomaterials*, *8*(4), 49. Retrieved from https://doi.org/10.3390/jfb8040049

Garbuz, D. S., Masri, B. A., & Czitrom, A. A. (1998). Biology of allografting. *Orthopedic Clinics of North America*, *29*(2), 199–204. Retrieved from https://doi.org/10.1016/S0030-5898(05)70318-7

Garg, A., & Kokkoli, E. (2005, January). Characterizing particulate drug-delivery carriers with atomic force microscopy. IEEE Engineering in Medicine and Biology Magazine. Retrieved from https://doi.org/10.1109/MEMB.2005.1384106

Garrett, I. R., & Mundy, G. R. (2002). The role of statins as potential targets for bone formation. *Arthritis Research*, *4*(4), 237–240. Retrieved from https://doi.org/10.1186/ar413

Gasser, J. A., & Kneissel, M. (2017). *Bone physiology and biology* (pp. 27–94). Retrieved from https://doi.org/10.1007/978-3-319-56192-9_2

Gentile, P., Chiono, V., Carmagnola, I., & Hatton, P. V. (2014). An overview of poly(lactic-co-glycolic) Acid (PLGA)-based biomaterials for bone tissue engineering. *International Journal of Molecular Sciences*. Molecular Diversity Preservation International. Retrieved from https://doi.org/10.3390/ijms15033640

Gentile, P., Nandagiri, V. K., Daly, J., Chiono, V., Mattu, C., Tonda-Turo, C., … & Ramtoola, Z. (2016). Localised controlled release of SIM from porous chitosan-gelatin scaffolds engrafted with SIM loaded PLGA-microparticles for bone tissue engineering application. *Materials Science and Engineering C*, *59*, 249–257. Retrieved from https://doi.org/10.1016/j.msec.2015.10.014

Gerstenfeld, L. C., Cullinane, D. M., Barnes, G. L., Graves, D. T., & Einhorn, T. A. (2003). Fracture healing as a post-natal developmental process: Molecular, spatial, and temporal aspects of its regulation. *Journal of Cellular Biochemistry*, *88*(5), 873–884. Retrieved from https://doi.org/10.1002/jcb.10435

Gilbert, S. (2016). Osteogenesis: The development of bones. In *Developmental Biology* (pp. 572–575). Retrieved from https://doi.org/10: 0-87893-243-7

Glowacki, J., & Mizuno, S. (2008). Collagen scaffolds for tissue engineering. *Biopolymers*, *89*(5), 338–344. Retrieved from https://doi.org/10.1002/bip.20871

Goff, L. A., Boucher, S., Ricupero, C. L., Fenstermacher, S., Swerdel, M., Chase, L. G., … & Hart, R. P. (2008). Differentiating human multipotent mesenchymal stromal cells regulate microRNAs: Prediction of microRNA regulation by PDGF during osteogenesis. *Experimental Hematology*, *36*(10). Retrieved from https://doi.org/10.1016/j.exphem.2008.05.004

Gotoh, M., Mizuno, K., Ono, Y., & Takahashi, M. (2011). Fluvastatin increases bone mineral density in postmenopausal women. *Fukushima Journal of Medical Science*, *57*(1), 19–27. https://doi.org/10.5387/fms.57.19

Govedarica, B., Teskač, K., Pajk, S., Pečar, S., Srčič, S., & Kristl, J. (2010). Probing the surface properties of solid lipid nanoparticles by atomic force microscopy. *Toxicol Appl Pharmacol, 78,* 61–69. Retrieved from https://doi.org/10.3797/scipharm.cespt.8.PDD14

Gowda, D. V., Deshpande, R. D., Keerthy, H. S., & Datta, V. (2014). Fabrication and evaluation of solid dispersion containing SIM. *International Journal of Pharmaceutical Sciences Review and Research*, *27*(2), 403–407. Retrieved from https://doi.org/http://dx.doi.org/10.1001/jama.2014.9405

Guan, Q., Chen, W., & Hu, X. (2015). Development of lovastatin-loaded poly(lactic acid) microspheres for sustained oral delivery: In vitro and ex vivo evaluation. *Drug Design, Development and Therapy, 9*, 791–798. Retrieved from https://doi.org/10.2147/DDDT.S76676

Gupta, M., Aina, A., Boukari, Y., Doughty, S., Morris, A., & Billa, N. (2018, February 7). Effect of volume of porogens on the porosity of PLGA scaffolds in pH-controlled environment. *Pharmaceutical Development and Technology*. Routledge: Taylor and Francis Ltd. Retrieved from https://doi.org/10.1080/10837450.2017.1304415

Haines, P. (2002). *Principles of thermal analysis and calorimetry*. Cambridge: Royal Society of Chemistry. Retrieved from https://doi.org/10.1039/9781847551764

Han, F. Y., Thurecht, K. J., Whittaker, A. K., & Smith, M. T. (2016). Bioerodable PLGA-based microparticles for producing sustained-release drug formulations and strategies for improving drug loading. *Frontiers in Pharmacology*. Frontiers Research Foundation. Retrieved from https://doi.org/10.3389/fphar.2016.00185

Han, X.-Q., Dong, Z.-H., Yu, X.-R., Guo, C.-C., Gu, X., & Wu, Z. (2014). Experimental study of tissue-engineered bone constructed with SIM carried by PLGA/CPC and bone marrow stromal cells. *Shanghai Kou Qiang Yi Xue = Shanghai Journal of Stomatology*, *23*(1), 7–14. Retrieved from http://www.ncbi.nlm.nih.gov/pubmed/24608605

Hancock, B. C., & Zografi, G. (1997). Characteristics and significance of the amorphous state in pharmaceutical systems. *Journal of Pharmaceutical Sciences, 86*(1), 1–12. Retrieved from https://doi.org/10.1021/js9601896

Hannink, G., & Arts, J. J. C. (2011). Bioresorbability, porosity and mechanical strength of bone substitutes: What is optimal for bone regeneration? *Injury, 42(SUPPL. 2).* Retrieved from https://doi.org/10.1016/j.injury.2011.06.008

Heidorn, M. (2016). *The role of temperature and column thermostatting in liquid chromatography*. Retrieved from http://tools.thermofisher.com/content/sfs/brochures/WP-71499-LC-Temperature-Column-Thermostatting-WP71499-EN.pdf

Hench, L. L. (1997). Sol-gel materials for bioceramic applications. *Current Opinion in Solid State and Materials Science,* 2(5), 604–610. Retrieved from https://doi.org/10.1016/S1359-0286(97)80053-8

Hing, K. A. (2005). Bioceramic bone graft substitutes: Influence of porosity and chemistry. *International Journal of Applied Ceramic Technology*. Retrieved from https://doi.org/10.1111/j.1744-7402.2005.02020.x

Hoffman, A. S. (2012, December). Hydrogels for biomedical applications. *Advanced Drug Delivery Reviews*. https://doi.org/10.1016/j.addr.2012.09.010

Hollister, S. J. (2005). Porous scaffold design for tissue engineering. *Nature Materials*, *4*(7), 518–24. https://doi.org/10.1038/nmat1421.

Hong, L., Han, D., Li, M. X., Zhang, P., & Liu, C. G. (2017). Development and validation of an ultraviolet–visible spectrophotometric method for determination of phenylethyl resorcinol in new topical nanoemulsions. *International Journal of Cosmetic Science*, *39*(3), 337–343. Retrieved from https://doi.org/10.1111/ics.12381

Horiba Scientific (n.d.). *A guidebook to particle size analysis: Horiba Scientific instruments*. Retrieved from http://www.horiba.com/us/en/scientific/products/particle-characterization/.

Hou, Q., De Bank, P. A., & Shakesheff, K. M. (2004). Injectable scaffolds for tissue regeneration. *Journal of Materials Chemistry*. Retrieved from https://doi.org/10.1039/b401791a

Hrafnkelsson, H., Sigrudsson, G., Magnusson, K. T., Johannsson, E., & Sigurdsson, E. L. (2010). Factors associated with bone mineral density and content in 7-year-old children. *Bone*, *46*(4), 1058–1062. https://doi.org/10.1016/j.bone.2009.11.035

Hsia, J., Morse, M., & Levin, V. (2002). Effect of SIM on bone markers in osteopenic women: Aplacebo-controlled, dose-ranging trial [ISRCTN85429598]. *BMC Musculoskeletal Disorders*, *3*, 1–5. Retrieved from https://doi.org/10.1186/1471-2474-3-7

Hu, R., Sharma, S. M., Bronisz, A., Srinivasan, R., Sankar, U., & Ostrowski, M. C. (2007). Eos, MITF, and PU.1 recruit corepressors to osteoclast-specific genes in committed myeloid progenitors. *Molecular and Cellular Biology, 27*(11), 4018–4027. Retrieved from https://doi.org/10.1128/MCB.01839-06

Hua, S., Marks, E., Schneider, J. J., & Keely, S. (2015). Advances in oral nano-delivery systems for colon targeted drug delivery in inflammatory bowel disease: Selective targeting to diseased versus healthy tissue. *Nanomedicine:*

Nanotechnology, Biology, and Medicine. Amsterdam, Netherlands: Elsevier Inc. Retrieved from https://doi.org/10.1016/j.nano.2015.02.018

Huang, C. L., Lee, W. L., & Loo, J. S. C. (2014). Drug-eluting scaffolds for bone and cartilage regeneration. *Drug Discovery Today*. Amsterdam, Netherlands: Elsevier Ltd. Retrieved from https://doi.org/10.1016/j.drudis.2013.11.007

Huang, X., Huang, Z., & Li, W. (2014). Highly efficient release of SIM from SIM-loaded calcium sulphate scaffolds enhances segmental bone regeneration in rabbits. *Molecular Medicine Reports, 9*(6), 2152–2158. Retrieved from https://doi.org/10.3892/mmr.2014.2101

Hunt, D. R., Jovanovic, S. A., Wikesjö, U. M. E., Wozney, J. M., & Bernard, G. W. (2005). Hyaluronan supports recombinant human bone morphogenetic protein-2 induced bone reconstruction of advanced alveolar ridge defects in dogs: A pilot study. *Journal of Periodontology*, *72*(5), 651–658. Retrieved from https://doi.org/10.1902/jop.2001.72.5.651

Huss, F. R. M., Nyman, E., Bolin, J. S. C., & Kratz, G. (2010). Use of macroporous gelatine spheres as a biodegradable scaffold for guided tissue regeneration of healthy dermis in humans: An in vivo study. *Journal of Plastic, Reconstructive and Aesthetic Surgery*, *63*(5), 848–857. https://doi.org/10.1016/j.bjps.2009.01.068

Hutmacher, D. W., Schantz, J. T., Lam, C. X. F., Tan, K. C., & Lim, T. C. (2007). State of the art and future directions of scaffold-based bone engineering from a biomaterials perspective. *Journal of Tissue Engineering and Regenerative Medicine, 1*(4), 245–260. Retrieved from https://doi.org/10.1002/term.24

Hymavathi, B., Kumar, B. R., & Rao, T. S. (2015). Investigations on physical properties of nanostructured Cr doped CdO thin films for optoelectronic applications. *Procedia Materials Science*, *10*, 285–291. Retrieved from https://doi.org/10.1016/j.mspro.2015.06.052

ICH (2005). *ICH harmonised tripartite guideline: Validation of analytical procedures: text and methodology, Q2(R1).* ICH, Geneva, Switzerland:

International Conference on Harmonization of Technical Requirements for Registration of Pharmaceuticals for Human Use. Retrieved from http://www.ich.org/fileadmin/Public_Web_Site/ICH_Products/Guidelines/Quality/Q2_R1/Step4/Q2_R1__Guideline.pdf

Iqbal, M., Zafar, N., Fessi, H., & Elaissari, A. (2015). Double emulsion solvent evaporation techniques used for drug encapsulation. *International Journal of Pharmaceutics*. Retrieved from Elsevier. https://doi.org/10.1016/j.ijpharm.2015.10.057

IR Spectrum Table by Frequency Range (n.d.). Retrieved from https://www.sigmaaldrich.com/technical-documents/articles/biology/ir-spectrum-table.html

Islam, N., Tuli, R. A., George, G. A., & Dargaville, T. R. (2014). Colloidal drug probe: Method development and validation for adhesion force measurement using atomic force microscopy. In *Advanced Powder Technology* (Vol. 25, pp. 1240–1248). Amsterdam: Netherlands: Elsevier B.V. Retrieved from https://doi.org/10.1016/j.apt.2014.06.021

Izumikawa, S., Yoshioka, S., Aso, Y., & Takeda, Y. (1991). Preparation of poly(l-lactide) microspheres of different crystalline morphology and effect of crystalline morphology on drug release rate. *Journal of Controlled Release, 15*(2), 133–140. Retrieved from https://doi.org/10.1016/0168-3659(91)90071-K

J Deng, H., Liu, Y., Guo, C., Di Chen, Li, X. J., & Jee, W. S. S. (2010). Integrated Bone Tissue Anatomy And Physiology. In *Current Topics in Bone Biology* (pp. 11–56). Singapore: World Scientific. https://doi.org/10.1142/9789812701176_0002

Jacob, S., Nair, A. B., Patil, P. N., & Panda, B. P. (2011). Solid state crystallinity, amorphous state, and its implications in the pharmaceutical process. *International Journal of Pharmaceutical Sciences and Research, 2*(3), 472–482. Retrieved from http://www.ijpsr.com/V2I3/1

Jagtap, Y., Ranade, A., Ranpise, N., & Bhujbal, R. (2012). Effect of various polymers concentrations on physicochemical properties of floating microspheres. *Indian Journal of Pharmaceutical Sciences, 74*(6), 512. Retrieved from https://doi.org/10.4103/0250-474X.110578

Jaiswal, A. K., Kadam, S. S., Soni, V. P., & Bellare, J. R. (2013). Improved functionalization of electrospun PLLA/gelatin scaffold by alternate soaking method for bone tissue engineering. *Applied Surface Science*, *268*, 477–488. Retrieved from https://doi.org/10.1016/j.apsusc.2012.12.152

Jaklenec, A., Hinckfuss, A., Bilgen, B., Ciombor, D. M., Aaron, R., & Mathiowitz, E. (2008). Sequential release of bioactive IGF-I and TGF-β1from PLGA microsphere-based scaffolds. *Biomaterials, 29(*10), 1518–1525. Retrieved from https://doi.org/10.1016/j.biomaterials.2007.12.004

Jaklenec, A., Wan, E., Murray, M. E., & Mathiowitz, E. (2008). Novel scaffolds fabricated from protein-loaded microspheres for tissue engineering. *Biomaterials, 29*(2), 185–192. Retrieved from https://doi.org/10.1016/j.biomaterials.2007.09.017

Jeon, O., Krebs, M., & Alsberg, E. (2011). Controlled and sustained gene delivery from injectable, porous PLGA scaffolds. *Journal of Biomedical Materials Research - Part A*, *98 A*(1), 72–79. Retrieved from https://doi.org/10.1002/jbm.a.33098

Jiang, T., Abdel-Fattah, W. I., & Laurencin, C. T. (2006). In vitro evaluation of chitosan/poly(lactic acid-glycolic acid) sintered microsphere scaffolds for bone tissue engineering. *Biomaterials, 27*(28), 4894–4903. Retrieved from https://doi.org/10.1016/j.biomaterials.2006.05.025

Jin, L., Ball, J., Bremner, T., & Sue, H. J. (2014). Crystallization behavior and morphological characterization of poly(ether ether ketone). *Polymer*, *55*(20), 5255–5265. Retrieved from https://doi.org/10.1016/j.polymer.2014.08.045

Jung, R. E., Glauser, R., Schärer, P., Hàmmerle, C. H. F., Sailer, H. F., & Weber, F. E. (2003). Effect of rhBMP-2 on guided bone regeneration in humans: A

randomized, controlled clinical and histomorphometric study. *Clinical Oral Implants Research*, *14*(5), 556–568. Retrieved from https://doi.org/10.1034/j.1600-0501.2003.00921.x

Kadajji, V. G., & Betageri, G. V. (2011). Water soluble polymers for pharmaceutical applications. *Polymers*, *3*(4), 1972-2009. Retrieved from https://doi.org/10.3390/polym3041972

Kajita, T., Ariyoshi, W., Okinaga, T., Mitsugi, S., Tominaga, K., & Nishihara, T. (2018). Mechanisms involved in enhancement of osteoclast formation by activin-A. *Journal of Cellular Biochemistry*, *119*(8), 6974–6985. Retrieved from https://doi.org/10.1002/jcb.26906

Kapoor, D. N., Bhatia, A., Kaur, R., Sharma, R., Kaur, G., & Dhawan, S. (2015, January 1). PLGA: A unique polymer for drug delivery. *Therapeutic Delivery. Future Science Ltd.* Retrieved from https://doi.org/10.4155/tde.14.91

Karageorgiou, V., & Kaplan, D. (2005). Porosity of 3D biomaterial scaffolds and osteogenesis. *Biomaterials*. Amsterdam, Netherlands: Elsevier BV. Retrieved from https://doi.org/10.1016/j.biomaterials.2005.02.002

Karagianni, A., Kachrimanis, K., & Nikolakakis, I. (2018). Co-amorphous solid dispersions for solubility and absorption improvement of drugs: Composition, preparation, characterization and formulations for oral delivery. *Pharmaceutics. MDPI AG*. Retrieved from https://doi.org/10.3390/pharmaceutics10030098

Katou, H., Wandrey, A. J., & Gander, B. (2008). Kinetics of solvent extraction/evaporation process for PLGA microparticle fabrication. *International Journal of Pharmaceutics*, *364*(1), 45–53. Retrieved from https://doi.org/10.1016/j.ijpharm.2008.08.015

Kaushal, A. M., Gupta, P., & Bansal, A. K. (2004). Amorphous drug delivery systems: molecular aspects, design, and performance. *Critical Reviews in Therapeutic Drug Carrier Systems, 21*(3), 133–193. Retrieved from https://doi.org/10.1615/CritRevTherDrugCarrierSyst.v21.i3.10

Kavanagh, A., McConvey, I., McCabe, J., Blade, H., & Cosgrove, S. (2012). Developing amorphous pharmaceuticals: Opportunity and necessity. *American Pharmaceutical Review*, *15*(5). Retrieved from https://www.americanpharmaceuticalreview.com/Featured-Articles/119521-Developing-Amorphous-Pharmaceuticals-Opportunity-and-Necessity/

Kavitha, R., & Abdul Hasan Sathali, A. (2012). Enhancement of solubility of repaglinide by solid dispersion technique. *International Journal of Chemical Sciences*, *10*(1), 377–390.

Keiser, M. J., Irwin, J. J., & Shoichet, B. K. (2010). The chemical basis of pharmacology. *Biochemistry*, *49*(48), 10267–10276. Retrieved from https://doi.org/10.1021/bi101540g

Khan, S. N., Cammisa, F. P., Sandhu, H. S., Diwan, A. D., Girardi, F. P., & Lane, J. M. (2005). The biology of bone grafting. *The Journal of the American Academy of Orthopaedic Surgeons*. Retrieved from https://doi.org/10.5435/00124635-200501000-00010\

Kheirallah, M., & Almeshaly, H. (2016). SIM, dosage and delivery system for supporting bone regeneration, an update review. *Journal of Oral and Maxillofacial Surgery, Medicine, and Pathology*. Amsterdam: Elsevier Ltd. Retrieved from https://doi.org/10.1016/j.ajoms.2015.10.005

Khoda, A. K. M. B. (2010). Engineered tissue scaffolds with variational porous architecture. *Journal of Biomechanical Engineering*, *133*(1), 011001. Retrieved from https://doi.org/10.1115/1.4002933

Kim, H. K., Chung, H. J., & Park, T. G. (2006). Biodegradable polymeric microspheres with "open/closed" pores for sustained release of human growth hormone. *Journal of Controlled Release, 112*(2), 167–174. Retrieved from https://doi.org/10.1016/j.jconrel.2006.02.004

Kini, U., & Nandeesh, B. N. (2012). Physiology of bone formation, remodeling, and metabolism. In *Radionuclide and Hybrid Bone Imaging* (Vol.

9783642024009, pp. 29–57). Springer-Verlag Berlin Heidelberg. Retrieved from https://doi.org/10.1007/978-3-642-02400-9_2

Klee, D., & Ho, H. (2007). Synthesis and characterization of poly (vinyl alcohol) -graft- [poly (D, L-lactide)/ poly (D, L-lactide-co-glycolide)] hydrogels. *Polymer, 47(*13), 4536–4544. Retrieved from https://doi.org/10.1002/pola

Kloczko, E., Nikkhah, D., & Yildirimer, L. (2015). Scaffolds for hand tissue engineering: The importance of surface topography. *Journal of Hand Surgery: European Volume*. Thousand Oaks, CA: SAGE Publications Ltd. Retrieved from https://doi.org/10.1177/1753193415571308

Knopp, M. M., Löbmann, K., Elder, D. P., Rades, T., & Holm, R. (2016). Recent advances and potential applications of modulated differential scanning calorimetry (mDSC) in drug development. *European Journal of Pharmaceutical Sciences*. Amsterdam: Elsevier B.V. Retrieved from https://doi.org/10.1016/j.ejps.2015.12.024

Koempel, J. A., Patt, B. S., O'Grady, K., Wozney, J., & Toriumi, D. M. (1998). The effect of recombinant human bone morphogenetic protein-2 on the integration of porous hydroxyapatite implants with bone. *Journal of Biomedical Materials Research*, *41*(3), 359–363. https://doi.org/10.1002/(SICI)1097-4636(19980905)41:3<359::AID-JBM3>3.0.CO;2-B

Kong, T., Wu, J., To, M., Wai Kwok Yeung, K., Cheung Shum, H., & Wang, L. (2012). Droplet based microfluidic fabrication of designer microparticles for encapsulation applications. *Biomicrofluidics, 6*(3). Retrieved from https://doi.org/10.1063/1.4738586

Krebs, M. D., Sutter, K. A., Lin, A. S. P., Guldberg, R. E., & Alsberg, E. (2009). Injectable poly(lactic-co-glycolic) acid scaffolds with in situ pore formation for tissue engineering. *Acta Biomaterialia*, *5*(8), 2847–2859. Retrieved from https://doi.org/10.1016/j.actbio.2009.04.035

Kretlow, J. D., Klouda, L., & Mikos, A. G. (2007). Injectable matrices and scaffolds for drug delivery in tissue engineering. *Advanced Drug Delivery Reviews, 59*(4–5), 263–273. Retrieved from https://doi.org/10.1016/j.addr.2007.03.013

Krishnamachari, Y., Madan, P., & Lin, S. (2007). Development of pH- and time-dependent oral microparticles to optimize budesonide delivery to ileum and colon. *International Journal of Pharmaceutics, 338*(1–2), 238–247. Retrieved from https://doi.org/10.1016/j.ijpharm.2007.02.015

Kumar, G. P., & Kumar, B. S. (2012). Current challenges in the development and formulation of amorphous solids. *Indonesian Journal of Pharmacy, 23*(2), 66–83.

Lal, R., Ramachandran, S., & Arnsdorf, M. F. (2010). Multidimensional atomic force microscopy: A versatile novel technology for nanopharmacology research. *The AAPS Journal, 12*(4), 716–728. Retrieved from https://doi.org/10.1208/s12248-010-9232-y

Lamprou, D. A. (2014). The atomic force microscopy (AFM) in nanomedicine. An overview. *Anticancer Research, 34*(10), 6021. Retrieved from http://www.embase.com/search/results?subaction=viewrecord&from=export&id=L71807812

Lee, S. J., Choi, J. S., Park, K. S., Khang, G., Lee, Y. M., & Lee, H. B. (2004). Response of MG63 osteoblast-like cells onto polycarbonate membrane surfaces with different micropore sizes. *Biomaterials, 25*(19), 4699–4707. Retrieved from https://doi.org/10.1016/j.biomaterials.2003.11.034

Lee, S., Porter, M., Wasko, S., Lau, G., Chen, P. Y., Novitskaya, E. E., … & McKittrick, J. (2012). Potential bone replacement materials prepared by two methods. In *Materials Research Society Symposium Proceedings* (Vol. 1418, pp. 177–188). Retrieved from https://doi.org/10.1557/opl.2012.671

Lee, W. H., Loo, C. Y., Zavgorodniy, A. V., Ghadiri, M., & Rohanizadeh, R. (2013). A novel approach to enhance protein adsorption and cell proliferation on

hydroxyapatite: Citric acid treatment. *RSC Advances, 3*(12), 4040–4051. Retrieved from https://doi.org/10.1039/c3ra22966a

Lee, Y., Schmid, M. J., Marx, D. B., Beatty, M. W., Cullen, D. M., Collins, M. E., & Reinhardt, R. A. (2008). The effect of local SIM delivery strategies on mandibular bone formation in vivo. *Biomaterials*, *29*(12), 1940–1949. https://doi.org/10.1016/j.biomaterials.2007.12.045

Lennernäs, H., & Fager, G. (1997). Pharmacodynamics and pharmacokinetics of the HMG-CoA reductase inhibitors. Similarities and differences. *Clinical Pharmacokinetics*. Basel, Switzerland: Springer International Publishing. Retrieved from https://doi.org/10.2165/00003088-199732050-00005

Lettiero, B., Inasu, M., Kimbung, S., & Borgquist, S. (2018). Insensitivity to atorvastatin is associated with increased accumulation of intracellular lipid droplets and fatty acid metabolism in breast cancer cells. *Scientific Reports, 8*(1). Retrieved from https://doi.org/10.1038/s41598-018-23726-3

Levengood, S. K. L., & Zhang, M. (2014). Chitosan-based scaffolds for bone tissue engineering. *Journal of Materials Chemistry B*, *2*(21), 3161–3184. https://doi.org/10.1039/c4tb00027g

Li, M., Rouaud, O., & Poncelet, D. (2008). Microencapsulation by solvent evaporation: State of the art for process engineering approaches. *International Journal of Pharmaceutics*. Retrieved from https://doi.org/10.1016/j.ijpharm.2008.07.018

Li, Y., & Ju, D. (2016). The application, neurotoxicity, and related mechanism of cationic polymers. In *Neurotoxicity of Nanomaterials and Nanomedicine* (pp. 285–329). Amsterdam: Elsevier Inc. Retrieved from https://doi.org/10.1016/B978-0-12-804598-5.00012-X

Li, Y., Zhang, Z., & Zhang, Z. (2018). Porous chitosan/nano-hydroxyapatite composite scaffolds incorporating SIM-loaded PLGA microspheres for bone repair. *Cells Tissues Organs, 205*(1), 20–31. Retrieved from https://doi.org/10.1159/000485502

Liao, J. K., & Laufs, U. (2009). Pleiotropic effects of statins. *Annual Reviews of Pharmacology and Toxicology, 45*(8), 89–118. Retrieved from http://www.ijp-online.com/article.asp?issn=02537613;year=2005;volume=37;issue=2;spage=77;epage=85;aulast=Tandon

Liechty, W. B., Kryscio, D. R., Slaughter, B. V., & Peppas, N. A. (2010). Polymers for drug delivery systems. *Annual Review of Chemical and Biomolecular Engineering*, *1*(1), 149–173. Retrieved from https://doi.org/10.1146/annurev-chembioeng-073009-100847

Lin, H. R., Kuo, C. J., Yang, C. Y., Shaw, S. Y., & Wu, Y. J. (2002). Preparation of macroporous biodegradable PLGA scaffolds for cell attachment with the use of mixed salts as porogen additives. *Journal of Biomedical Materials Research, 63*(3), 271–279. Retrieved from https://doi.org/10.1002/jbm.10183

Lin, X., Wang, J., Xu, Y., Tang, X., Chen, J., Zhang, Y., … & Yang, Z. (2016). Tracking the effect of microspheres size on the drug release from a microsphere/sucrose acetate isobutyrate (SAIB) hybrid depot in vitro and in vivo. *Drug Development and Industrial Pharmacy, 42*(9), 1455–1465. Retrieved from https://doi.org/10.3109/03639045.2016.1143952

Lindholm, J. (2004). Development and validation of HPLC methods for analytical and preparative purposes. *Acta Universitatis Upsaliensis*, 87. Retrieved from http://www.diva-portal.org/smash/get/diva2:164877/fulltext01

Liu, J., Zhu, L. P., Yang, X. L., Huang, H. L., & Ye, D. Q. (2013). HMG-CoA reductase inhibitors (statins) and bone mineral density: A meta-analysis. *Bone*, *54*(1), 151–156. https://doi.org/10.1016/j.bone.2013.01.044

Liu, M., Zeng, X., Ma, C., Yi, H., Ali, Z., Mou, X., … He, N. (2017, May 30). Injectable hydrogels for cartilage and bone tissue engineering. *Bone Research*. Sichuan University. https://doi.org/10.1038/boneres.2017.14

Liu Y, Hou S, Wang L, Yang S. (2010). Development and validation of a liquid chromatography method for the analysis of paromomycin sulfate and its impurities. *Analytical and Bioanalytical Techniques,* 1(102). Retrieved from https://www.omicsonline.org/development-and-validation-of-a-liquid-chromatography-method-for-the-analysis-of-paromomycin-sulfate-and-its-impurities-2155-9872.1000102.php?aid=84

Liu, C., Wu, Z., & Sun, H. (2009). The effect of SIM on mRNA expression of transforming growth factor β1, Bone morphogenetic protein 2 and vascular endothelial growth factor in tooth extraction socket. *International Journal of Oral Science*, *1*(2), 90–98. https://doi.org/10.4248/ijos.08011

Liu, M., Wang, K., Tang, T., Dai, K., & Zhu, Z. (2009). The effect of SIM on the differentiation of marrow stromal cells from aging rats. *Pharmazie*, *64*(1), 43–48. Retrieved from https://doi.org/10.1691/ph.2008.8671

Liu, X., Holzwarth, J. M., & Ma, P. X. (2012). Functionalized synthetic biodegradable polymer scaffolds for tissue engineering. *Macromolecular Bioscience*. Retrieved from https://doi.org/10.1002/mabi.201100466

Liu, X., Li, X., Zhou, L., Li, S., Sun, J., Wang, Z., … Dai, J. (2013). Effects of SIM-loaded polymeric micelles on human osteoblast-like MG-63 cells. Colloids and Surfaces B: *Biointerfaces, 102*, 420–427. Retrieved from https://doi.org/10.1016/j.colsurfb.2012.06.037

Liu, Z. P., Cui, L., Yu, D. G., Zhao, Z. X., & Chen, L. (2014). Electrosprayed core-shell solid dispersions of acyclovir fabricated using an epoxy-coated concentric spray head. *International Journal of Nanomedicine*, *9*(1), 1967–1977. Retrieved from https://doi.org/10.2147/IJN.S59516

Lupattelli, G., Scarponi, A. M., Vaudo, G., Siepi, D., Roscini, A. R., Gemelli, F., … Mannarino, E. (2004). SIM increases bone mineral density in hypercholesterolemic postmenopausal women. *Metabolism: Clinical and Experimental*, *53*(6), 744–748. https://doi.org/10.1016/j.metabol.2004.01.010

Löbmann, K., Grohganz, H., Laitinen, R., Strachan, C., & Rades, T. (2013). Amino acids as co-amorphous stabilizers for poorly water soluble drugs - Part 1: Preparation, stability and dissolution enhancement. *European Journal of Pharmaceutics and Biopharmaceutics, 85*(3 PART B), 873–881. Retrieved from https://doi.org/10.1016/j.ejpb.2013.03.014

Low, S. P., Voelcker, N. H., Canham, L. T., & Williams, K. A. (2009). The biocompatibility of porous silicon in tissues of the eye. *Biomaterials*, *30*(15), 2873–2880. Retrieved from https://doi.org/10.1016/j.biomaterials.2009.02.008

Lu, H., Kawazoe, N., Kitajima, T., Myoken, Y., Tomita, M., Umezawa, A., … & Ito, Y. (2012). Spatial immobilization of bone morphogenetic protein-4 in a collagen-PLGA hybrid scaffold for enhanced osteoinductivity. *Biomaterials*, *33*(26), 6140–6146. Retrieved from https://doi.org/10.1016/j.biomaterials.2012.05.038

Lü, J. M., Wang, X., Marin-Muller, C., Wang, H., Lin, P. H., Yao, Q., & Chen, C. (2009, May). Current advances in research and clinical applications of PLGA-based nanotechnology. *Expert Review of Molecular Diagnostics*. Retrieved from https://doi.org/10.1586/erm.09.15

Luan, X., Skupin, M., Siepmann, J., & Bodmeier, R. (2006). Key parameters affecting the initial release (burst) and encapsulation efficiency of peptide-containing poly(lactide-co-glycolide) microparticles. *International Journal of Pharmaceutics*, *324*(2), 168–175. https://doi.org/10.1016/j.ijpharm.2006.06.004

Luchin, A., Suchting, S., Merson, T., Rosol, T. J., Hume, D. A., Cassady, A. I., & Ostrowski, M. C. (2001). Genetic and physical interactions between microphthalmia transcription factor and PU.1 are necessary for osteoclast gene expression and differentiation. *Journal of Biological Chemistry*, *276*(39), 36703–36710. Retrieved from https://doi.org/10.1074/jbc.M106418200

Luciani, A., Coccoli, V., Orsi, S., Ambrosio, L., & Netti, P. A. (2008). PCL microspheres based functional scaffolds by bottom-up approach with predefined microstructural properties and release profiles. *Biomaterials, 29*(36), 4800–4807. Retrieved from https://doi.org/10.1016/j.biomaterials.2008.09.007

Luginbuehl, V., Meinel, L., Merkle, H. P., & Gander, B. (2004, September). Localized delivery of growth factors for bone repair. *European Journal of Pharmaceutics and Biopharmaceutics*. Retrieved from https://doi.org/10.1016/j.ejpb.2004.03.004

Lungan, M. A., Popa, M., Racovita, S., Hitruc, G., Doroftei, F., Desbrieres, J., & Vasiliu, S. (2015). Surface characterization and drug release from porous microparticles based on methacrylic monomers and xanthan. *Carbohydrate Polymers, 125,* 323–333. Retrieved from https://doi.org/10.1016/j.carbpol.2015.02.058

Luo, N., Lu, Y., & Jiang, Y. (2011). Solubility of paclitaxel in mixtures of dichloromethane and supercritical carbon dioxide. *Chinese Journal of Chemical Engineering, 19*(4), 558–564. Retrieved from https://doi.org/10.1016/S1004-9541(11)60021-9

Lyles, M. B., Hu, J. C., Varanasi, V. G., Hollinger, J. O., & Athanasiou, K. A. (2015). Bone tissue engineering. In *Regenerative Engineering of Musculoskeletal Tissues and Interfaces* (pp. 97–134). Amsterdam: Elsevier Inc. https://doi.org/10.1016/B978-1-78242-301-0.00005-7

Ma, B., Clarke, S. A., Brooks, R. A., & Rushton, N. (2008). The effect of SIM on bone formation and ceramic resorption in a peri-implant defect model. *Acta Biomaterialia*, *4*(1), 149–155. https://doi.org/10.1016/j.actbio.2007.05.004

Ma, G., Liu, Y., Peng, C., Fang, D., He, B., & Nie, J. (2011). Paclitaxel loaded electrospun porous nanofibers as mat potential application for chemotherapy against prostate cancer. *Carbohydrate Polymers*, *86*(2), 505–512. Retrieved from https://doi.org/10.1016/j.carbpol.2011.04.082

Ma, L., Gao, C., Mao, Z., Zhou, J., Shen, J., Hu, X., & Han, C. (2003). Collagen/chitosan porous scaffolds with improved biostability for skin tissue engineering. *Biomaterials*, *24*(26), 4833–4841. Retrieved from http://www.ncbi.nlm.nih.gov/pubmed/14530080

Ma, P. X., & Choi, J.-W. (2001). Biodegradable polymer scaffolds with well-defined interconnected spherical pore network. *Tissue Engineering, 7*(1), 23–33. Retrieved from https://doi.org/10.1089/107632701300003269

Maeda T, Matsunuma A, Kawane T, Horiuchi N. SIM promotes osteoblast differentiation and mineralization in MC3T3-E1 cells. Biochem Biophys Res Commun 2001;280:874–7

Maeda, T., Matsunuma, A., Kurahashi, I., Yanagawa, T., Yoshida, H., & Horiuchi, N. (2004). Induction of osteoblast differentiation indices by statins in MC3T3-E1 cells. *Journal of Cellular Biochemistry*, *92*(3), 458–471. https://doi.org/10.1002/jcb.20074

Magan-Fernandez, A., Fernández-Barbero, J. E., O' Valle, F., Ortiz, R., Galindo-Moreno, P., & Mesa, F. (2018). SIM exerts antiproliferative and differentiating effects on MG63 osteoblast-like cells: Morphological and immunocytochemical study. *Journal of Periodontal Research, 53*(1), 91–97. Retrieved from https://doi.org/10.1111/jre.12491

Makadia, H. K., & Siegel, S. J. (2011). Poly lactic-co-glycolic acid (PLGA) as biodegradable controlled drug delivery carrier. *Polymers, 3*(3), 1377–1397. Retrieved from https://doi.org/10.3390/polym3031377

Malafaya, P. B., Silva, G. A., & Reis, R. L. (2007, May 30). Natural-origin polymers as carriers and scaffolds for biomolecules and cell delivery in tissue engineering applications. *Advanced Drug Delivery Reviews*. Retrieved from https://doi.org/10.1016/j.addr.2007.03.012

Malavia, N., Reddy, L., Szinai, I., Betty, N., Pi, J., Kanagaraj, J., E. (2015). Biodegradable sustained-release drug deliverysystems fabricated using a dissolvable hydrogel template technology for the treatment of ocular

indications. *IOVS, 56,* 1296. Retrieved from https://doi.org/10.1136/heartjnl-2013-305402

Mallick, K. K., & Cox, S. C. (2013). Biomaterial scaffolds for tissue engineering. *Frontiers in Bioscience*. Retrieved from https://pdfs.semanticscholar.org/d028/e0ca69ee2041edd061dd5d72a76563a0877d.pdf

Mandal, D. (2010). Effect of carriers on solid dispersions of simvasta tin (sim): Physico-chemical characterizations and dissolution studies. *Der Pharmacia Lettre, 2*(4), 47–56. Retrieved from https://www.ajol.info/index.php/tjpr/article/view/107479

Manoochehri, S., Darvishi, B., Kamalinia, G., Amini, M., Fallah, M., Ostad, S. N., … & Dinarvand, R. (2013). Surface modification of PLGA nanoparticles via human serum albumin conjugation for controlled delivery of docetaxel. *DARU, Journal of Pharmaceutical Sciences*, *21*(1). Retrieved from https://doi.org/10.1186/2008-2231-21-58

Mao, S., Shi, Y., Li, L., Xu, J., Schaper, A., & Kissel, T. (2008). Effects of process and formulation parameters on characteristics and internal morphology of poly(d,l-lactide-co-glycolide) microspheres formed by the solvent evaporation method. *European Journal of Pharmaceutics and Biopharmaceutics, 68*(2), 214–223. Retrieved from https://doi.org/10.1016/j.ejpb.2007.06.008

Marelli, B., Alessandrino, A., Farè, S., Freddi, G., Mantovani, D., & Tanzi, M. C. (2010). Compliant electrospun silk fibroin tubes for small vessel bypass grafting. *Acta Biomaterialia*, *6*(10), 4019–4026. Retrieved from https://doi.org/10.1016/j.actbio.2010.05.008

Marin, E., Rojas, J., & Ciro, Y. (2014). A review of polyvinilalcohol derivates: Promising materials for pharmaceutical and biomedical applications. *African Journal of Pharmacy and Pharmacology*, *8*(24), 674–684. Retrieved from https://doi.org/10.5897/AJPP2013.3906

Maritz, F. J., Conradie, M. M., Hulley, P. A., Gopal, R., & Hough, S. (2001). Effect of statins on bone mineral density and bone histomorphometry in rodents. *Arteriosclerosis, Thrombosis, and Vascular Biology*, *21*(10), 1636–1641. Retrieved from https://doi.org/10.1161/hq1001.097781

Martin, T. J., & Takahashi, N. (1992). Modulation of osteoclast differentiation. *Endocrine Reviews*, *13*(1), 316–328. Retrieved from https://doi.org/10.1210/edrv-13-1-66

Martins, C., Sousa, F., Araújo, F., & Sarmento, B. (2018). Functionalizing PLGA and PLGA derivatives for drug delivery and tissue regeneration applications. advanced healthcare materials. Wiley-VCH Verlag. Retrieved from https://doi.org/10.1002/adhm.201701035

Martins, K. F., Messias, A. D., Leite, F. L., & Duek, E. A. R. (2014). Preparation and characterization of paclitaxel-loaded PLDLA microspheres. *Materials Research, 17*(3), 650–656. Retrieved from https://doi.org/10.1590/S1516-14392014005000028

Masaeli, R., Kashi, T. S. J., Dinarvand, R., Tahriri, M., Rakhshan, V., & Esfandyari-Manesh, M. (2016). Preparation, characterization and evaluation of drug release properties of SIM-loaded PLGA microspheres. *Iranian Journal of Pharmaceutical Research*, *15*, 205–211. Retrieved from https://www.ncbi.nlm.nih.gov/pubmed/28228818

Masaeli, R., Kashi, T. S. J., Dinarvand, R., Tahriri, M., Rakhshan, V., & Esfandyari-Manesh, M. (2016). Preparation, characterization and evaluation of drug release properties of SIM-loaded PLGA microspheres. *Iranian Journal of Pharmaceutical Research, 15,* 205–211. Retrieved from https://www.ncbi.nlm.nih.gov/pubmed/28228818

Mathews, S., Gupta, P. K., Bhonde, R., & Totey, S. (2011). Chitosan enhances mineralization during osteoblast differentiation of human bone marrow-derived mesenchymal stem cells, by upregulating the associated genes. *Cell Proliferation*, *44*(6), 537–549. Retrieved from https://doi.org/10.1111/j.1365-2184.2011.00788.x

Matsumoto, M., Kogawa, M., Wada, S., Takayanagi, H., Tsujimoto, M., Katayama, S., … & Nogi, Y. (2004). Essential role of p38 mitogen-activated protein kinase in cathepsin K gene expression during osteoclastogenesis through association of NFATc1 and PU.1. *Journal of Biological Chemistry*, *279*(44), 45969–45979. Retrieved from https://doi.org/10.1074/jbc.M408795200

McCall, R. L., & Sirianni, R. W. (2013). PLGA nanoparticles formed by single- or double-emulsion with vitamin E-TPGS. *Journal of Visualized Experiments,* 82. Retrieved from https://doi.org/10.3791/51015

Meredith, J., & Mallick, K. K. (2015). High-strength scaffolds for bone regeneration. *Bioinspired, Biomimetic and Nanobiomaterials, 4*(1), 48–58. Retrieved from https://doi.org/10.1680/bbn.14.00019

Milella, E., Barra, G., Ramires, P. A., Leo, G., Aversa, P., & Romito, A. (2001). Poly(L-lactide)acid/alginate composite membranes for guided tissue regeneration. *Journal of Biomedical Materials Research*, *57*(2), 248–257. Retrieved from https://doi.org/10.1002/1097-4636(200111)57:2<248::AID-JBM1165>3.0.CO;2-X

Misra, A. (2017). Tissue engineering. In *Biotechnology: Recent Trends and Emerging Dimensions* (pp. 123–140). Boca Raton, FL: CRC Press. Retrieved from https://doi.org/10.1201/9780203711033

Mittal, A., Negi, P., Garkhal, K., Verma, S., & Kumar, N. (2010). Integration of porosity and bio-functionalization to form a 3D scaffold: Cell culture studies and in vitro degradation. *Biomedical Materials*, *5*(4). Retrieved from https://doi.org/10.1088/1748-6041/5/4/045001

Mittal, G., Sahana, D. K., Bhardwaj, V., & Ravi Kumar, M. N. V. (2007). Estradiol loaded PLGA nanoparticles for oral administration: Effect of polymer molecular weight and copolymer composition on release behavior in vitro and in vivo. *Journal of Controlled Release, 119(*1). Retrieved from 77–85. Retrieved from https://doi.org/10.1016/j.jconrel.2007.01.016

Mondal, D., & Tiwari, A. (2012). Electrospun nanomatrix for tissue regeneration. In *Biomedical Materials and Diagnostic Devices*. Retrieved from https://onlinelibrary.wiley.com/doi/10.1002/9781118523025.ch18

Moon, H. J., Kim, S. E., Yun, Y. P., Hwang, Y. S., Bang, J. B., Park, J. H., & Kwon, I. K. (2011). SIM inhibits osteoclast differentiation by scavenging reactive oxygen species. *Experimental and Molecular Medicine*, *43*(11), 605–612. Retrieved from https://doi.org/10.3858/emm.2011.43.11.067

Montagnani A, Gonnelli S, Cepollaro C, Pacini S, Campagna MS, Franci MB, et al. Effect of SIM treatment on bone mineral density and bone turnover in hypercholesterolemic postmenopausal women: a 1-year longitudinal study. Bone 2003; 32(4):427–33. [PubMed: 12689687]

Montero, J., Manzano, G., & Albaladejo, A. (2014). The role of topical SIM on bone regeneration: A systematic review. *Journal of Clinical and Experimental Dentistry*, *6*(3). https://doi.org/10.4317/jced.51415

Moriyama, Y., Ayukawa, Y., Ogino, Y., Atsuta, I., & Koyano, K. (2008). Topical application of statin affects bone healing around implants. *Clinical Oral Implants Research*, *19*(6), 600–605. Retrieved from https://doi.org/10.1111/j.1600-0501.2007.01508.x

Morse, L. R., Coker, J., & Battaglino, R. A. (2018, January 1). Statins and bone health: A mini review. *Actualizaciones En Osteologia*. Asociacion Argentina de Osteologia y Metabolismo Mineral.

Moshiri, A., Sharifi, A. M., & Oryan, A. (2016). Role of SIM on fracture healing and osteoporosis: a systematic review on in vivo investigations. *Clinical and Experimental Pharmacology and Physiology*. Hoboken, NJ: Blackwell Publishing. Retrieved from https://doi.org/10.1111/1440-1681.1257

Mouriño, V., & Boccaccini, A. R. (2010). Bone tissue engineering therapeutics: controlled drug delivery in three-dimensional scaffolds. *Journal of the Royal Society, Interface / the Royal Society, 7*(43), 209–27. Retrieved from https://doi.org/10.1098/rsif.2009.0379

Mundy, G. R. (2001). Statins and their potential for osteoporosis. *Bone*, *29*(6), 495–497. Retrieved from https://doi.org/10.1016/s8756-3282(01)00606-8

Mundy, G., Garrett, R., Harris, S., Chan, J., Chen, D., Rossini, G., … & Gutierrez, G. (1999). Stimulation of bone formation in vitro and in rodents by statins. *Science, 286*(5446), 1946–1949. Retrieved from https://doi.org/10.1126/science.286.5446.1946

Munir, A., Ahmad, M., Malik, M. Z., & Minhas, M. U. (2014). Analysis of SIM using a simple and fast high performance liquid chromatography-ultra violet method: Development, validation and application in solubility studies. *Tropical Journal of Pharmaceutical Research*, *13*(1), 135–139. Retrieved from https://doi.org/10.4314/tjpr.v13i1.19

Murakami, H., Kawashima, Y., Niwa, T., Hino, T., Takeuchi, H., & Kobayashi, M. (1997). Influence of the degrees of hydrolyzation and polymerization of poly(vinylalcohol) on the preparation and properties of poly(DL-lactide-co-glycolide) nanoparticle. *International Journal of Pharmaceutics, 149*(1), 43–49. Retrieved from https://doi.org/10.1016/S0378-5173(96)04854-5

Murphy, C. M., & O'Brien, F. J. (2010). Understanding the effect of mean pore size on cell activity in collagen-glycosaminoglycan scaffolds. *Cell Adhesion and Migration*. Abingdon: Taylor and Francis Inc. Retrieved from https://doi.org/10.4161/cam.4.3.11747

Murphy, C. M., Haugh, M. G., & O'Brien, F. J. (2010). The effect of mean pore size on cell attachment, proliferation and migration in collagen-glycosaminoglycan scaffolds for bone tissue engineering. *Biomaterials, 31*(3), 461–466. Retrieved from https://doi.org/10.1016/j.biomaterials.2009.09.063

Murtaza, G. (2012). Solubility enhancement of SIM: A review. *Acta Poloniae Pharmaceutica - Drug Research*, *69*(4), 581-590.

Muscariello, L., Rosso, F., Marino, G., Giordano, A., Barbarisi, M., Cafiero, G., & Barbarisi, A. (2005). A critical overview of ESEM applications in the

biological field. *Journal of Cellular Physiology*. Retrieved from https://doi.org/10.1002/jcp.20444

Naga, S. M., El-Maghraby, H. F., Mahmoud, E. M., Talaat, M. S., & Ibrhim, A. M. (2015). Preparation and characterization of highly porous ceramic scaffolds based on thermally treated fish bone. *Ceramics International*, *41*(10), 15010–15016. Retrieved from https://doi.org/10.1016/j.ceramint.2015.08.057

Naito, Y., Terukina, T., Galli, S., Kozai, Y., Vandeweghe, S., Tagami, T., … & Jimbo, R. (2014). The effect of SIM-loaded polymeric microspheres in a critical size bone defect in the rabbit calvaria. *International Journal of Pharmaceutics*, *461*(1–2), 157–162. Retrieved from https://doi.org/10.1016/j.ijpharm.2013.11.046

Nandagiri, V. K., Muttu, C., Daly, J., Ramtoola, Z., Ciardelli, G., & Montevecchi, F. M. (2012). Preparation and characterization of SIM loaded PLGA microparticles for tissue engineering applications. *Current Research in Pharmaceutical Sciences*, *2*, 81–90. Retrieved from https://epubs.rcsi.ie/biolart/15/

Nath, S. D., Linh, N. T. B., Sadiasa, A., & Lee, B. T. (2014). Encapsulation of SIM in PLGA microspheres loaded into hydrogel loaded BCP porous spongy scaffold as a controlled drug delivery system for bone tissue regeneration. *Journal of Biomaterials Applications, 28*(8), 1151–1163. Retrieved from https://doi.org/10.1177/0885328213499272

Nath, S. D., Son, S., Sadiasa, A., Min, Y. K., & Lee, B. T. (2013). Preparation and characterization of PLGA microspheres by the electrospraying method for delivering SIM for bone regeneration. *International Journal of Pharmaceutics*, *443*(1–2), 87–94. Retrieved from https://doi.org/10.1016/j.ijpharm.2012.12.037

Nava, M. M., Draghi, L., Giordano, C., & Pietrabissa, R. (2016). The effect of scaffold pore size in cartilage tissue engineering. *Journal of Applied Biomaterials & Functional Materials, 14*(3), 0–0. Retrieved from https://doi.org/10.5301/jabfm.5000302

Nishant T., Kumar A., Kumar S & Bheemidi V.S. (2011). Development and validation of analytical methods for pharmaceuticals. *Analytical and Bioanalytical Techniques, 2*(5), 1000127-1000132. Retrieved from https://www.omicsonline.org/development-and-validation-of-analytical-methods-for-pharmaceuticals-2155-9872.1000127.php?aid=3153

Niu, X., Luo, Y., Li, Y., Fu, C., Chen, J., & Wang, Y. (2008). Design of bioinspired polymeric materials based on poly(D,L-lactic acid) modifications towards improving its cytocompatibility. *Journal of Biomedical Materials Research - Part A*, *84*(4), 908–916. Retrieved from https://doi.org/10.1002/jbm.a.31360

Nyan, M., Sato, D., Kihara, H., MacHida, T., Ohya, K., & Kasugai, S. (2009). Effects of the combination with α-tricalcium phosphate and SIM on bone regeneration. *Clinical Oral Implants Research*, *20*(3), 280–287. Retrieved from https://doi.org/10.1111/j.1600-0501.2008.01639.x

O'Brien, F. J. (2011). Biomaterials & scaffolds for tissue engineering. *Materials Today*. Amsterdam: Elsevier B.V. https://doi.org/10.1016/S1369-7021(11)70058-X

Oh, D. J., Lee, B. C., & Hwang, S. J. (2007). Solubility of SIM and lovastatin in mixtures of dichloromethane and supercritical carbon dioxide. *Journal of Chemical and Engineering Data*, *52*(4), 1273–1279. Retrieved from https://doi.org/10.1021/je700019h

Ohba, S., Hojo, H., & Chung, U.-I. (2012). Bioactive factors for tissue regeneration: state of the art. *Muscles, Ligaments and Tendons Journal*, *2*(3), 193–203. Retrieved from http://www.ncbi.nlm.nih.gov/pubmed/23738297

Oliveira, A. R., Caland, L. B., Oliveira, E. G., Egito, E. S. T., Pedrosa, M. F. F., & Silva, A. A. (2015). HPLC-DAD and UV-vis spectrophotometric methods for methotrexate assay in different biodegradable Microparticles. *Journal of the Brazilian Chemical Society*, *26*(4), 649–659. Retrieved from https://doi.org/10.5935/0103-5053.20150022

Olsen B. R. (1990). *Bone embryology*. Retrieved from https://pdfs.semanticscholar.org/7b23/4ba3d4a3858cbcf949cac934d78833ce05af.pdf

Omenetto, F. G., & Kaplan, D. L. (2010). New opportunities for an ancient material. *Science*. Retrieved from https://doi.org/10.1126/science.1188936

Pal, S., Mohanta, U., & Manna, P. (2013). Antihypertensive drug loaded PLGA nanoparticles: Impact of formulation variables on particle size distribution. *Der Pharmacia Sinica, 4*(1), 40–46. Retrieved from http://search.ebscohost.com/login.aspx?direct=true&profile=ehost&scope=site&authtype=crawler&jrnl=09768688&AN=86859010&h=2tscfvXGqZ58NpUHO%2BMzjsqxs36a5wukjemfYs1WG0QH2JkNn7AAp%2BQwPxR%2B1Jy7JXYJHCXiBi7vYW2x9ocibg%3D%3D&crl=c

Palacio, J., Orozco, V. H., & Lopez, B. L. (2011). Effect of the molecular weight on the physicochemical properties of poly(lactic acid) nanoparticles and on the amount of ovalbumin adsorption. *Journal of the Brazilian Chemical Society, 22*(12), 2304–2311. Retrieved from <Go to ISI>://WOS:000299000600009

Pan, Z., & Ding, J. (2012). Poly(lactide-co-glycolide) porous scaffolds for tissue engineering and regenerative medicine. *Interface Focus*. Royal Society. Retrieved from https://doi.org/10.1098/rsfs.2011.0123

Pandya, V. M., Patel, J. K., & Patel, D. J. (2011). Formulation, optimization and characterization of SIM nanosuspension prepared by nanoprecipitation technique. *Der Pharmacia Lettre, 3*(2), 129–140. Retrieved from https://www.researchgate.net/publication/265185723_Formulation_Optimization_and_characterization_of_SIM_Nanosuspension_prepared_by_nanoprecipitation_technique

Pang, J., Luan, Y., Li, F., Cai, X., Du, J., & Li, Z. (2011). Ibuprofen-loaded poly(lactic-co-glycolic acid) films for controlled drug release. International *Journal of Nanomedicine, 6,* 659–665. Retrieved from https://doi.org/10.2147/IJN.S17011

Panyam, J., William, D., Dash, A., Leslie-Pelecky, D., & Labhasetwar, V. (2004). Solid-state solubility influences encapsulation and release of hydrophobic drugs from PLGA/PLA nanoparticles. *Journal of Pharmaceutical Sciences, 93*(7), 1804–1814. Retrieved from https://doi.org/10.1002/jps.20094

Panyam, J., William, D., Dash, A., Leslie-Pelecky, D., & Labhasetwar, V. (2004). Solid-state solubility influences encapsulation and release of hydrophobic drugs from PLGA/PLA nanoparticles. *Journal of Pharmaceutical Sciences, 93*(7), 1804–1814. Retrieved from https://doi.org/10.1002/jps.20094

Park, J. B. (2009). *The use of SIM in bone regeneration*. Medicina Oral: Patologia Oral y Cirugia Bucal.

Park, P. I. P., & Jonnalagadda, S. (2006). Predictors of glass transition in the biodegradable polylactide and poly-lactide-co-glycolide polymers. *Journal of Applied Polymer Science*, *100*(3), 1983–1987. Retrieved from https://doi.org/10.1002/app.22135

Park, S. H., Park, D. S., Shin, J. W., Kang, Y. G., Kim, H. K., Yoon, T. R., & Shin, J. W. (2012). Scaffolds for bone tissue engineering fabricated from two different materials by the rapid prototyping technique: PCL versus PLGA. *Journal of Materials Science: Materials in Medicine*, *23*(11), 2671–2678. Retrieved from https://doi.org/10.1007/s10856-012-4738-8

Park, S. H., Park, D. S., Shin, J. W., Kang, Y. G., Kim, H. K., Yoon, T. R., & Shin, J. W. (2012). Scaffolds for bone tissue engineering fabricated from two different materials by the rapid prototyping technique: PCL versus PLGA. *Journal of Materials Science: Materials in Medicine, 23*(11), 2671–2678. Retrieved from https://doi.org/10.1007/s10856-012-4738-8

PDQ Cancer Information Summaries Paediatric Treatment Editorial Board. (2017). *Childhood acute myeloid leukemia, other myeloid malignancies treatment*. Retrieved from http://www.ncbi.nlm.nih.gov/pubmed/26389454.

Pillai, O., & Panchagnula, R. (2001, August 1). Polymers in drug delivery. *Current Opinion in Chemical Biology*. Elsevier Ltd. https://doi.org/10.1016/S1367-5931(00)00227-1

Pişkin, E. (2002). Biodegradable polymers in medicine. In *Degradable Polymers*. Dordrecht: Springer Netherlands. Retrieved from https://link.springer.com/chapter/10.1007/978-94-017-1217-0_10

Pradeep AR, Rao NS, Bajaj P, Kumari M. Efficacy of subgingivally delivered SIM in the treatment of patients with type 2 diabetes and chronic periodontitis: a randomized double-masked controlled clinical trial. Journal of Periodontology. 2013;84:24–31.

Pradeep, A. R., & Thorat, M. S. (2010). Clinical effect of subgingivally delivered SIM in the treatment of patients with chronic periodontitis: A randomized clinical trial. *Journal of Periodontology*, *81*(2), 214–222. Retrieved from https://doi.org/10.1902/jop.2009.090429

Pradeep, A. R., Priyanka, N., Kalra, N., Naik, S. B., Singh, S. P., & Martande, S. (2012). Clinical efficacy of subgingivally delivered 1.2-mg SIM in the treatment of individuals with class II furcation defects: A randomized controlled clinical trial. *Journal of Periodontology*, *83*(12), 1472–1479. Retrieved from https://doi.org/10.1902/jop.2012.110716

Puppi, D., Chiellini, F., Piras, A. M., & Chiellini, E. (2010, April). Polymeric materials for bone and cartilage repair. *Progress in Polymer Science (Oxford)*. Retrieved from https://doi.org/10.1016/j.progpolymsci.2010.01.006

Putney, S. D., & Burke, P. A. (1998). Improving protein therapeutics with sustained-release formulations. *Nature Biotechnology*. Retrieved from https://doi.org/10.1038/nbt0298-153

Quintanar-Guerrero, D., Fessi, H., All6mann, E., & Doelker, E. (1996). international journal of pharmaceutics Influence of stabilizing agents and preparative variables on the formation of poly(D,L-lactic acid) nanoparticles by an emulsification-diffusion technique. *International Journal of Pharmaceutics,*

143(143), 133–141. Retrieved from https://doi.org/10.1016/S0378-5173(96)04697-2

Qutachi, O., Shakesheff, K. M., & Buttery, L. D. K. (2013). Delivery of definable number of drug or growth factor loaded poly(dl-lactic acid-co-glycolic acid) microparticles within human embryonic stem cell derived aggregates. *Journal of Controlled Release, 168*(1), 18–27. Retrieved from https://doi.org/10.1016/j.jconrel.2013.02.029

Qutachi, O., Vetsch, J. R., Gill, D., Cox, H., Scurr, D. J., Hofmann, S., … & Rahman, C. V. (2014). Injectable and porous PLGA microspheres that form highly porous scaffolds at body temperature. *Acta Biomaterialia*, *10*(12), 5090–5098. Retrieved from https://doi.org/10.1016/j.actbio.2014.08.015

Rafati, A., Boussahel, A., Shakesheff, K. M., Shard, A. G., Roberts, C. J., Chen, X., … Davies, M. C. (2012). Chemical and spatial analysis of protein loaded PLGA microspheres for drug delivery applications. *Journal of Controlled Release, 162*(2), 321–329. Retrieved from https://doi.org/10.1016/j.jconrel.2012.05.008

Raftery, R., O'Brien, F. J., & Cryan, S. A. (2013). Chitosan for gene delivery and orthopedic tissue engineering applications. *Molecules*. Retrieved from https://doi.org/10.3390/molecules18055611

Rahman, C. V., Kuhn, G., White, L. J., Kirby, G. T., Varghese, O. P., McLaren, J. S., ... & Shakesheff, K. M. (2013). PLGA/PEG-hydrogel composite scaffolds with controllable mechanical properties. *Journal of Biomedical Materials Research Part B: Applied Biomaterials, 101*(4), 648-655. Retrieved from https://doi.org/10.1002/jbm.b.32867

Rai, B., Lin, J. L., Lim, Z. X. H., Guldberg, R. E., Hutmacher, D. W., & Cool, S. M. (2010). Differences between in vitro viability and differentiation and in vivo bone-forming efficacy of human mesenchymal stem cells cultured on PCL-TCP scaffolds. *Biomaterials*, *31*(31), 7960–7970. Retrieved from https://doi.org/10.1016/j.biomaterials.2010.07.001

Rao NS, Pradeep AR, Bajaj P, Kumari M, Naik SB. SIM local drug delivery in smokers with chronic periodontitis: a randomized controlled clinical trial. Aust Dent J. 2013;58:156–62.

Raju, K. N., Babu, I. S., Jyothi, R., & Prathyusha, S. (2012). Spectrophotometric methods for estimation of SIM in bulk drug and its dosage form. *Int J Pharma Chem Biol Sci, 2*(2), 124–129. Retrieved from https://www.tsijournals.com/articles/spectrophotometric-methods-for-estimation-of-SIM-in-bulk-drug-and-its-dosage-form.pdf

Ralston, S. H. (2004). Structure and metabolism of bone. *Medicine*, *29*(12), 60–66. Retrieved from https://doi.org/10.1383/medc.29.12.60.28510

Ralston, S. H. (2017). Bone structure and metabolism. *Medicine (United Kingdom)*. Amsterdam: Elsevier Ltd. Retrieved from https://doi.org/10.1016/j.mpmed.2017.06.008.

Raman, C., Berkland, C., Kim, K., & Pack, D. W. (2005). Modeling small-molecule release from PLG microspheres: Effects of polymer degradation and nonuniform drug distribution. *Journal of Controlled Release, 103*(1), 149–158. Retrieved from https://doi.org/10.1016/j.jconrel.2004.11.012

Rambhia, K. J., & Ma, P. X. (2015). Controlled drug release for tissue engineering. *Journal of Controlled Release*, *219*, 119–128. Retrieved from https://doi.org/10.1016/j.jconrel.2015.08.049

Reichert, J. C., Saifzadeh, S., Wullschleger, M. E., Epari, D. R., Schütz, M. A., Duda, G. N., … & Hutmacher, D. W. (2009). The challenge of establishing preclinical models for segmental bone defect research. *Biomaterials*, *30*(12), 2149–2163. Retrieved from https://doi.org/10.1016/j.biomaterials.2008.12.050

Ribani, M., Grespan Bottoli, C. B., Collins, C. H., Fontes Jardim, I. C. S., & Costa Melo, L. F. (2004). Validação em métodos cromatográficos e eletroforéticos. *Quimica Nova. Sociedade Brasileira de Quimica*. Retrieved from https://doi.org/10.1590/S0100-40422004000500017

Rice, J. J., Martino, M. M., De Laporte, L., Tortelli, F., Briquez, P. S., & Hubbell, J. A. (2013). Engineering the regenerative microenvironment with biomaterials. *Advanced Healthcare Materials*, *2*(1), 57–71. Retrieved from https://doi.org/10.1002/adhm.201200197

Roberts, T. T., & Rosenbaum, A. J. (2012). Bone grafts, bone substitutes and orthobiologics the bridge between basic science and clinical advancements in fracture healing. *Organogenesis*, *8*(4), 114–124. Retrieved from https://doi.org/10.4161/org.23306

Robson, A. L., Dastoor, P. C., Flynn, J., Palmer, W., Martin, A., Smith, D. W., … Hua, S. (2018). Advantages and limitations of current imaging techniques for characterizing liposome morphology. *Frontiers in Pharmacology. Frontiers Media S.A*. Retrieved from https://doi.org/10.3389/fphar.2018.00080

Rojas, A., Aguilar, R., Henriquez, B., Lian, J. B., Stein, J. L., Stein, G. S., … & Montecino, M. (2015). Epigenetic control of the bone-master Runx2 gene during osteoblast-lineage commitment by the histone demethylase JARID1B/KDM5B. *Journal of Biological Chemistry*, *290*(47), 28329–28342. Retrieved from https://doi.org/10.1074/jbc.M115.657825

Roodman, G. D. (1999). Cell biology of the osteoclast. *Experimental Hematology*. Retrieved from https://doi.org/10.1016/S0301-472X(99)00061-2

Rosyida, N. F., Ariyanto, T., Pudyani, P. S., & Ana, I. D. (2018). Preparation of SIM Hydrogel through arginine addition for drug delivery system. In *MATEC Web of Conferences* (Vol. 156). Retrieved from https://doi.org/10.1051/matecconf/201815601002

Rouwkema, J., Rivron, N. C., & van Blitterswijk, C. A. (2008). Vascularization in tissue engineering. *Trends in Biotechnology*, *26*(8), 434-441. https://doi.org/10.1016/j.tibtech.2008.04.009

Roy, A., Jhunjhunwala, S., Bayer, E., Fedorchak, M., Little, S. R., & Kumta, P. N. (2016). Porous calcium phosphate-poly (lactic-co-glycolic) acid composite bone cement: A viable tunable drug delivery system. *Materials Science and*

Engineering C, *59*, 92–101. Retrieved from https://doi.org/10.1016/j.msec.2015.09.081

Ruan, F., Zheng, Q., & Wang, J. (2012, December). Mechanisms of bone anabolism regulated by statiretrieved from ns. *Bioscience Reports*. https://doi.org/10.1042/BSR20110118.

Ruiz-Gaspa, S., Nogues, X., Enjuanes, A., Monllau, J. C., Blanch, J., Carreras, R., … Pedro-Botet, J. (2007). SIM and atorvastatin enhance gene expression of collagen type 1 and osteocalcin in primary human osteoblasts and MG-63 cultures. *Journal of Cellular Biochemistry, 101*(6), 1430–1438. Retrieved from https://doi.org/10.1002/jcb.21259

Ruozi, B., Belletti, D., Tombesi, A., Tosi, G., Bondioli, L., Forni, F., & Vandelli, M. A. (2011). AFM, ESEM, TEM, and CLSM in liposomal characterization: a comparative study. *International Journal of Nanomedicine, 6*, 557–563. Retrieved from https://doi.org/10.2147/IJN.S14615

Ryoo, H. M., Lee, M. H., & Kim, Y. J. (2006, January 17). Critical molecular switches involved in BMP-2-induced osteogenic differentiation of mesenchymal cells. *Gene*. Retrieved from https://doi.org/10.1016/j.gene.2005.10.011

Sansdrap, P., & Moës, A. J. (1993). Influence of manufacturing parameters on the size characteristics and the release profiles of nifedipine from poly(DL-lactide-co-glycolide) microspheres. *International Journal of Pharmaceutics, 98*(1–3), 157–164. Retrieved from https://doi.org/10.1016/0378-5173(93)90052-H

Sarapirom, S., Yu, L. D., Boonyawan, D., & Chaiwong, C. (2014). Effect of surface modification of poly(lactic acid) by low-pressure ammonia plasma on adsorption of human serum albumin. *Applied Surface Science*, *310*, 42–50. Retrieved from https://doi.org/10.1016/j.apsusc.2014.03.141

Scanning, D., & Dsc, C. (2006). Characterizing protein/ligand binding by DSC. *Life Sciences*, (20111020706), 4.

Schachter, M. (2005). Chemical, pharmacokinetic and pharmacodynamic properties of statins: An update. *Fundamental and Clinical Pharmacology*. Retrieved from https://doi.org/10.1111/j.1472-8206.2004.00299.x

Schellinger, A. P., & Carr, P. W. (2006). Isocratic and gradient elution chromatography: A comparison in terms of speed, retention reproducibility and quantitation. *Journal of Chromatography A, 1109,* 253–266. Retrieved from https://doi.org/10.1016/j.chroma.2006.01.047

Schliecker, G., Schmidt, C., Fuchs, S., Wombacher, R., & Kissel, T. (2003). Hydrolytic degradation of poly(lactide-co-glycolide) films: Effect of oligomers on degradation rate and crystallinity. *International Journal of Pharmaceutics, 266*(1–2), 39–49. https://doi.org/10.1016/S0378-5173(03)00379-X

Sedlaček, M., Podgornik, B., & Vižintin, J. (2012). Correlation between standard roughness parameters skewness and kurtosis and tribological behaviour of contact surfaces. In *Tribology International* (Vol. 48, pp. 102–112). Retrieved from https://doi.org/10.1016/j.triboint.2011.11.008

Sethia, S., & Squillante, E. (2004). Solid dispersion of carbamazepine in PVP K30 by conventional solvent evaporation and supercritical methods. *International Journal of Pharmaceutics, 272*(1–2), 1–10. Retrieved from https://doi.org/10.1016/j.ijpharm.2003.11.025

Seyedmajidi, S., Seyedmajidi, S., Alaghehmand, H., Hajian-Tilaki, K., Haghanifar, S., Zabihi, E., … & Seyedmajidi, M. (2018). Synthesis and characterization of hydroxyapatite/bioactive glass nanocomposite foam and fluorapatite/bioactive glass nanocomposite foam by gel casting method as cell scaffold for bone tissue. *Eurasian Journal of Analytical Chemistry, 13*(3). Retrieved from https://doi.org/10.29333/ejac/85078

Shabir, G. A. (2003). Validation of high-performance liquid chromatography methods for pharmaceutical analysis: Understanding the differences and similarities between validation requirements of the US Food and Drug Administration, the US Pharmacopeia and the International Conference on

Harmonization. In *Journal of Chromatography A, 987,* 57–66.Retrieved from https://doi.org/10.1016/S0021-9673(02)01536-4.

Shah, S. R., Werlang, C. A., Kasper, F. K., & Mikos, A. G. (2015). Novel applications of statins for bone regeneration. *National Science Review*. Oxford University Press. https://doi.org/10.1093/nsr/nwu028

Shah, P. V, Midha, K. K., Dighe, S., McGilveray, J. I, Skelly, P. J, Yacobi, A., Layloff, T., Viswanathan, C. T., Cook, E. C., Mcdowall, R. D., Pittman, A. K. & Spector S. (1992). Analytical method validation: Bioavailability, bioequivalence and pharmacokinetics studies. *Journal of Pharmaceutical Sciences, 81*, 309-312. Retrieved from https://www.sciencedirect.com/science/article/pii/037851739290065A

Sharma, N., Madan, P., & Lin, S. (2016). Effect of process and formulation variables on the preparation of parenteral paclitaxel-loaded biodegradable polymeric nanoparticles: A co-surfactant study. *Asian Journal of Pharmaceutical Sciences, 11*(3), 404–416. https://doi.org/10.1016/j.ajps.2015.09.004

Shid, R. L., Dhole, S. N., Kulkarni, N., & Shid, S. L. (2014). Formulation and evaluation of nanosuspension formulation for drug delivery of SIM. *International Journal of Pharmaceutical Sciences and Nanotechnology, 7*(2), 2459–2475. Retrieved from https://doi.org/10.1016/j.jconrel.2016.03.023

Shinde, A. J., & More, H. N. (2011). Design and evaluation of polylactic-CO-Glycolic acid nanoparticles containing SIM. *International Journal of Drug Development and Research*, *3*(2), 280–289. Retrieved from https://www.researchgate.net/publication/261880332_Design_and_Evaluation_of_Polylactic-co-glycolic_acid_Nanoparticles_containing_SIM

Shinde, A. J., & More, H. N. (2014). Formulation, development and characterization of SIM nanoparticles by solvent displacement method. *Der Pharmacia Lettre*, *6*(2), 145–155. Retrieved from https://www.scholarsresearchlibrary.com/articles/formulation-development-

and-characterization-of-SIMnanoparticles-by-solvent-displacement-method.pdf

Sibik, J., Löbmann, K., Rades, T., & Zeitler, J. A. (2015). Predicting crystallization of amorphous drugs with terahertz spectroscopy. *Molecular Pharmaceutics*, *12*(8), 3062–3068. Retrieved from https://doi.org/10.1021/acs.molpharmaceut.5b0033

Sigurdsson, T. J., Nygaard, L., Tatakis, D. N., Fu, E., Turek, T. J., Jin, L., … & Wikesjö, U. M. (1996). Periodontal repair in dogs: evaluation of rhBMP-2 carriers. *The International Journal of Periodontics & Restorative Dentistry*, *16*(6), 524–37. Retrieved from http://www.ncbi.nlm.nih.gov/pubmed/9242091

Silva, T. D., Arantes, V. T., Resende, J. A. L. C., Speziali, N. L., De Oliveira, R. B., & Vianna-Soares, C. D. (2010). Preparation and characterization of solid dispersion of SIM Preparation and characterization of solid dispersion. *Drug Development and Industrial Pharmacy, 36*(11), 1348–1355. Retrieved from https://doi.org/10.3109/03639041003801901

Silva, T. D., Oliveira, M. A., De Oliveira, R. B., & Vianna-Soares, C. D. (2012). Development and validation of a simple and fast HPLC method for determination of lovastatin, pravastatin and SIM. *Journal of Chromatographic Science*, *50*(9), 831–838. Retrieved from https://doi.org/10.1093/chromsci/bms079

Simões, R. G., Bernardes, C. E. S., Diogo, H. P., Agapito, F., & Minas Da Piedade, M. E. (2013). Energetics and structure of SIM. *Molecular Pharmaceutics, 10*(7), 2713–2722. Retrieved from https://doi.org/10.1021/mp400132r

Sims, N. A., & Martin, T. J. (2014). Coupling the activities of bone formation and resorption: a multitude of signals within the basic multicellular unit. *BoneKEy Reports*, *3*. Retrieved from https://doi.org/10.1038/bonekey.2013.215

Sims, N. A., Martin, T. J., & Quinn, J. M. W. (2015). *Coupling: The influences of immune and bone cells.* In *Osteoimmunology: Interactions of the Immune and*

Skeletal Systems (2nd ed.). Retrieved from https://www.sciencedirect.com/science/article/pii/B9780128005712000104

Smith, I. O., & Ma, P. X. (2011). Biomimetic scaffolds in tissue engineering. *Tissue Engineering: From Lab to Clinic, 9783642028243,* 31–39. Springer-Verlag Berlin Heidelberg. Retrieved from https://doi.org/10.1007/978-3-642-02824-3_2

Song, C., Guo, Z., Ma, Q., Chen, Z., Liu, Z., Jia, H., & Dang, G. (2003). SIM induces osteoblastic differentiation and inhibits adipocytic differentiation in mouse bone marrow stromal cells. *Biochemical and Biophysical Research Communications*, *308*(3), 458–462. Retrieved from https://doi.org/10.1016/S0006-291X(03)01408-6

Song, K., Liu, Y., MacEdo, H. M., Jiang, L., Li, C., Mei, G., & Liu, T. (2013). Fabrication and evaluation of a sustained-release chitosan-based scaffold embedded with PLGA microspheres. *Materials Science and Engineering C, 33(*3), 1506–1513. Retrieved from https://doi.org/10.1016/j.msec.2012.12.054

Sopyan, I., Fudholi, A., Muchtaridi, M., & Sari, I. P. (2017). SIM-nicotinamide co-crystal: Design, preparation and preliminary characterization. *Tropical Journal of Pharmaceutical Research, 16*(2), 297–303. Retrieved from https://doi.org/10.4314/tjpr.v16i2.6

Spiller, K. L., Liu, Y., Holloway, J. L., Maher, S. A., Cao, Y., Liu, W., … & Lowman, A. M. (2012). A novel method for the direct fabrication of growth factor-loaded microspheres within porous nondegradable hydrogels: Controlled release for cartilage tissue engineering. *Journal of Controlled Release*, *157*(1), 39–45. Retrieved from https://doi.org/10.1016/j.jconrel.2011.09.057

Stancu, C., & Sima, A. (2001). Statins: Mechanism of action and effects. *Journal of Cellular and Molecular Medicine*, *5*(4), 378–387. Retrieved from https://doi.org/10.1111/j.1582-4934.2001.tb00172.x

Stevens, J. S., Byard, S. J., Zlotnikov, E., & Schroeder, S. L. M. (2011). Detection of free base surface enrichment of a pharmaceutical salt by X-ray photoelectron spectroscopy (XPS). *Journal of Pharmaceutical Sciences*, *100*(3), 942–948. Retrieved from https://doi.org/10.1002/jps.22334

Stokes, D. J. (2003). Recent advances in electron imaging, image interpretation and applications: Environmental scanning electron microscopy. *Philosophical Transactions of the Royal Society A: Mathematical, Physical and Engineering Sciences.* Retrieved from https://doi.org/10.1098/rsta.2003.1279

Sui, G., Yang, X., Mei, F., Hu, X., Chen, G., Deng, X., & Ryu, S. (2007). Poly-L-lactic acid/hydroxyapatite hybrid membrane for bone tissue regeneration. *Journal of Biomedical Materials Research - Part A*, *82*(2), 445–454. Retrieved from https://doi.org/10.1002/jbm.a.31166

Sui, G., Yang, X., Mei, F., Hu, X., Chen, G., Deng, X., & Ryu, S. (2007). Poly-L-lactic acid/hydroxyapatite hybrid membrane for bone tissue regeneration. *Journal of Biomedical Materials Research - Part A, 82*(2), 445–454. Retrieved from https://doi.org/10.1002/jbm.a.31166

Sultana, N. (2017). Mechanical and biological properties of scaffold materials. In *Functional 3D Tissue Engineering Scaffolds*: *Materials, Technologies, and Applications.* Retrieved from https://www.sciencedirect.com/science/article/pii/B978008100979600001X

Sun, L., Zhou, S., Wang, W., Li, X., Wang, J., & Weng, J. (2009). Preparation and characterization of porous biodegradable microspheres used for controlled protein delivery. *Colloids and Surfaces A: Physicochemical and Engineering Aspects*, *345*(1–3), 173–181. Retrieved from https://doi.org/10.1016/j.colsurfa.2009.04.053

Taek, K. K., Jun, J. Y., Doo, S. L., & Park, T. G. (2006). Gas foamed open porous biodegradable polymeric microspheres. *Biomaterials, 27*(2), 152–159. Retrieved from https://doi.org/10.1016/j.biomaterials.2005.05.081

Tai, I. C., Fu, Y. C., Wang, C. K., Chang, J. K., & Ho, M. L. (2013). Local delivery of controlled-release SIM/PLGA /HA p microspheres enhances bone repair. *International Journal of Nanomedicine*, *8*, 3895–3905. Retrieved from https://doi.org/10.2147/IJN.S48694

Tai, I. C., Fu, Y. C., Wang, C. K., Chang, J. K., & Ho, M. L. (2013). Local delivery of controlled-release SIM/PLGA /HA p microspheres enhances bone repair. *International Journal of Nanomedicine*, *8*, 3895–3905. Retrieved from https://doi.org/10.2147/IJN.S48694

Tandale, P., Joshi, D., & Gaud, R. S. (2011). Formulation and evaluation of extended release solid dispersions containing SIM. *Asian Journal of Biomedical and Pharmaceutical Sciences, 1*(4), 13–19. Retrieved from https://pdfs.semanticscholar.org/f464/1b6455b4f3b2694c035346d4f5654014bf91.pdf

Tayebi, L., Nozari, A., Vashaee, D., & Mozafari, M. (2012). Current opinion in tissue engineering microscopy techniques. *Current Microscopy Contributions to Advances in Science and Technology*, 591–601.

Teitelbaum, S. L. (2007). Osteoclasts: What do they do and how do they do it? In *American Journal of Pathology* (Vol. 170, pp. 427–435). American Society for Investigative Pathology Inc. https://doi.org/10.2353/ajpath.2007.060834. Retrieved from https://www.ncbi.nlm.nih.gov/pmc/articles/PMC1851862/pdf/7126.pdf

Terukina, T., Numaguchi, T., Hattori, Y., & Otsuka, M. (2017). Development of controllable SIM-releasing PLGA/β-TCP composite microspheres sintered scaffolds as synthetic bone substitutes. In *Bioceramics 29* (Vol. 758, pp. 126–131). Trans Tech Publications. Retrieved from https://doi.org/10.4028/www.scientific.net/KEM.758.126

Terukina, T., Saito, H., Tomita, Y., Hattori, Y., & Otsuka, M. (2017). Development and effect of a sustainable and controllable SIM-releasing device based on PLGA microspheres/carbonate apatite cement composite: In vitro evaluation for use as a drug delivery system from bone-like biomaterial. *Journal of Drug*

Delivery Science and Technology, 37, 74–80. Retrieved from https://doi.org/10.1016/j.jddst.2016.10.007

Tevlin, R., McArdle, A., Atashroo, D., Walmsley, G. G., Senarath-Yapa, K., Zielins, E. R., … & Wan, D. C. (2014). Biomaterials for craniofacial bone engineering. *Journal of Dental Research*. Thousand Oaks, CA: SAGE Publications Inc. Retrieved from https://doi.org/10.1177/0022034514547271

Thylin, M. R., McConnell, J. C., Schmid, M. J., Reckling, R. R., Ojha, J., Bhattacharyya, I., … & Reinhardt, R. A. (2005). Effects of SIM gels on murine calvarial bone. *Journal of Periodontology*, *73*(10), 1141–1148. Retrieved from https://doi.org/10.1902/jop.2002.73.10.1141

Todd, P. A., & Goa, K. L. (1990). SIM: A review of its pharmacological properties and therapeutic potential in hypercholesterolaemia. *Drugs*, *40*(4), 583–607. Retrieved from https://doi.org/10.2165/00003495-199040040-00007

Toriumi, D. M., Kotler, H. S., Luxenberg, D. P., Holtrop, M. E., & Wang, E. A. (1991). Mandibular reconstruction with a recombinant bone-inducing factor: functional, histologic, and biomechanical evaluation. *Archives of Otolaryngology--Head and Neck Surgery*, *117*(10), 1101–1112. Retrieved from https://doi.org/10.1001/archotol.1991.01870220049009

Tran, R. T., Naseri, E., Kolasnikov, A., Bai, X., & Yang, J. (2011). A new generation of sodium chloride porogen for tissue engineering. *Biotechnology and Applied Biochemistry*, *58*(5), 335–344. Retrieved from https://doi.org/10.1002/bab.44

Tsuji, H., & Ikada, Y. (2000). Properties and morphology of poly(L-lactide) 4. Effects of structural parameters on long-term hydrolysis of poly(L-lactide) in phosphate-buffered solution. *Polymer Degradation and Stability, 67(*1), 179–189. Retrieved from https://doi.org/10.1016/S0141-3910(99)00111-1

Tuszynski, M. H., Yang, J. H., Barba, D., Hoi-Sang, U., Bakay, R. A. E., Pay, M. M., … Nagahara, A. H. (2015). Nerve growth factor gene therapy activation of neuronal responses in Alzheimer disease. *JAMA Neurology*, *72*(10), 1139–1147. Retrieved from https://doi.org/10.1001/jamaneurol.2015.1807

Ungaro, F., Catanzano, O., d'Angelo, I., Diaz-Gomez, L., Concheiro, A., Miro, A., … Quaglia, F. (2017). Microparticle-embedded fibroin/alginate beads for prolonged local release of SIM hydroxyacid to mesenchymal stem cells. *Carbohydrate Polymers*, *175*, 645–653. Retrieved from https://doi.org/10.1016/j.carbpol.2017.08.045

Urban, M. C. C., Mainardes, R. M., & Gremião, M. P. D. (2009). Development and validation of HPLC method for analysis of dexamethasone acetate in microemulsions. *Brazilian Journal of Pharmaceutical Sciences*, *45*(1), 87–92. https://doi.org/10.1590/s1984-82502009000100010

Uzzan, B., Cohen, R., Nicolas, P., Cucherat, M., & Perret, G. Y. (2007). Effects of statins on bone mineral density: A meta-analysis of clinical studies. *Bone*, *40*(6), 1581–1587. https://doi.org/10.1016/j.bone.2007.02.019

Väänänen, H. K., & Laitala-Leinonen, T. (2008, May 15). Osteoclast lineage and function. *Archives of Biochemistry and Biophysics*. Retrieved from https://doi.org/10.1016/j.abb.2008.03.037

Vikingsson, L., Claessens, B., Gómez-Tejedor, J. A., Gallego Ferrer, G., & Gómez Ribelles, J. L. (2015). Relationship between micro-porosity, water permeability and mechanical behavior in scaffolds for cartilage engineering. *Journal of the Mechanical Behavior of Biomedical Materials*, *48*, 60–69. Retrieved from https://doi.org/10.1016/j.jmbbm.2015.03.021

Vitale-Brovarone, C., Verné, E., Robiglio, L., Appendino, P., Bassi, F., Martinasso, G., … & Canuto, R. (2007). Development of glass-ceramic scaffolds for bone tissue engineering: Characterisation, proliferation of human osteoblasts and nodule formation. *Acta Biomaterialia, 3*(2), 199–208. Retrieved from https://doi.org/10.1016/j.actbio.2006.07.012

Von Stechow, D., Fish, S., Yahalom, D., Bab, I., Chorev, M., Müller, R., & Alexander, J. M. (2003). Does SIM stimulate bone formation in vivo? *BMC Musculoskeletal Disorders*, *4*, 1–10. Retrieved from https://doi.org/10.1186/1471-2474-4-8

Vysloužil, J., Doležel, P., Kejdušová, M., Mašková, E., Mašek, J., Lukáč, R., … Dvorackova, K. (2014). Influence of different formulations and process parameters during the preparation of drug-loaded PLGA microspheres evaluated by multivariate data analysis. *Acta Pharmaceutica, 64*(4), 403–417. Retrieved from https://doi.org/10.2478/acph-2014-0032

Wan, F., & Yang, M. (2016). Design of PLGA-based depot delivery systems for biopharmaceuticals prepared by spray drying. *International Journal of Pharmaceutics*. Thousand Oaks, CA: Elsevier B.V. Retrieved from https://doi.org/10.1016/j.ijpharm.2015.12.025

Wang, C. Z., Chen, S. M., Chen, C. H., Wang, C. K., Wang, G. J., Chang, J. K., & Ho, M. L. (2010). The effect of the local delivery of alendronate on human adipose-derived stem cell-based bone regeneration. *Biomaterials*, *31*(33), 8674–8683. Retrieved from https://doi.org/10.1016/j.biomaterials.2010.07.096

Wang, H., Sun, N., Li, X., Li, K., Tian, J., & Li, J. (2016). SIM suppresses cell migration and invasion, induces G0/G1 cell cycle arrest and apoptosis in osteosarcoma cells. *International Journal of Clinical and Experimental Pathology*, *9*(6), 5837–5848. Retrieved from https://www.researchgate.net/publication/310445939_SIM_suppresses_cell_migration_and_invasion_induces_G0G1_cell_cycle_arrest_and_apoptosis_in_osteosarcoma_cells

Wang, J., Yang, Q., Cheng, N., Tao, X., Zhang, Z., Sun, X., & Zhang, Q. (2016). Collagen/silk fibroin composite scaffold incorporated with PLGA microsphere for cartilage repair. *Materials Science and Engineering C*, *61*, 705–711. Retrieved from https://doi.org/10.1016/j.msec.2015.12.097

Wang, L., Li, C., Chen, Y., Dong, S., Chen, X., & Zhou, Y. (2013). Poly(lactic-co-glycolic) acid/nanohydroxyapatite scaffold containing chitosan microspheres with adrenomedullin delivery for modulation activity of osteoblasts and vascular endothelial cells. *BioMed Research International*. Retrieved from https://doi.org/10.1155/2013/530712

Wang, N., Wu, X. S., Li, C., & Feng, M. F. (2000). Synthesis, characterization, biodegradation, and drug delivery application of biodegradable lactic/glycolic acid polymers I: Synthesis and characterization. *Journal of Biomaterials Science, Polymer Edition*, *11*(3), 301–318.

Wang, N., Ma, M., Luo, Y., Liu, T., Zhou, P., Qi, S., … Chen, H. (2018). Mesoporous Silica Nanoparticles-Reinforced Hydrogel Scaffold together with Pinacidil Loading to Improve Stem Cell Adhesion. *ChemNanoMat*, *4*(7), 631–641. https://doi.org/10.1002/cnma.201800026

Wang, W., Nyman, J. S., Moss, H. E., Gutierrez, G., Mundy, G. R., Yang, X., & Elefteriou, F. (2010). Local low-dose lovastatin delivery improves the bone-healing defect caused by Nf1 loss of function in osteoblasts. *Journal of Bone and Mineral Research*, *25*(7), 1658–1667. Retrieved from https://doi.org/10.1002/jbmr.42

Wang, Y., Blasioli, D. J., Kim, H. J., Kim, H. S., & Kaplan, D. L. (2006). Cartilage tissue engineering with silk scaffolds and human articular chondrocytes. *Biomaterials*, *27*(25), 4434–4442. Retrieved from https://doi.org/10.1016/j.biomaterials.2006.03.050

Wang, Y., Shi, X., Ren, L., Wang, C., & Wang, D. A. (2009). Porous poly (lactic-co-glycolide) microsphere sintered scaffolds for tissue repair applications. *Materials Science and Engineering C*, *29*(8), 2502–2507. Retrieved from https://doi.org/10.1016/j.msec.2009.07.018

Wang, Y., Shi, X., Ren, L., Yao, Y., Zhang, F., & Wang, D. A. (2010). Poly(lactide-co-glycolide)/titania composite microsphere-sintered scaffolds for bone tissue engineering applications. *Journal of Biomedical Materials Research - Part B Applied Biomaterials*, *93*(1), 84–92. Retrieved from https://doi.org/10.1002/jbm.b.31561

Whitaker, M. J., Quirk, R. A., Howdle, S. M., & Shakesheff, K. M. (2001). Growth factor release from tissue engineering scaffolds. *Journal of Pharmacy and Pharmacology*, *53*(11), 1427–1437. Retrieved from https://doi.org/10.1211/0022357011777963

Whitten, R. A., & Bhimji, S. S. (2018). *Statin medications*. Retrieved from http://www.ncbi.nlm.nih.gov/pubmed/28613690.

Wichitnithad, W., Jongaroonngamsang, N., Pummangura, S., & Rojsitthisak, P. (2009). A simple isocratic HPLC method for the simultaneous determination of curcuminoids in commercial turmeric extracts. *Phytochemical Analysis*, *20*(4), 314–319. Retrieved from https://doi.org/10.1002/pca.1129

Wikesjoö, U. M. E., Sorensen, R. G., Kinoshita, A., & Wozney, J. M. (2002). RhBMP-2/alphaBSM induces significant vertical alveolar ridge augmentation and dental implant osseointegration. *Clinical Implant Dentistry and Related Research*, *4*(4), 174–182. Retrieved from https://doi.org/10.1111/j.1708-8208.2002.tb00169.x

Wong, R. W. K., & Rabie, A. B. M. (2005). Histologic and ultrastructural study on statin graft in rabbit skulls. *Journal of Oral and Maxillofacial Surgery*, *63*(10), 1515–1521. Retrieved from https://doi.org/10.1016/j.joms.2005.06.009

Woodard, J. R., Hilldore, A. J., Lan, S. K., Park, C. J., Morgan, A. W., Eurell, J. A. C., … Wagoner Johnson, A. J. (2007). The mechanical properties and osteoconductivity of hydroxyapatite bone scaffolds with multi-scale porosity. *Biomaterials*, *28*(1), 45–54. Retrieved from https://doi.org/10.1016/j.biomaterials.2006.08.021

World Health Organization (1998). *World health report, report of the director-general.* Geneva, Switzerland: World Health Organization.

Wu, C., Sun, X., Zhao, Z., Zhao, Y., Hao, Y., Liu, Y., & Gao, Y. (2014). Synthesis of novel core-shell structured dual-mesoporous silica nanospheres and their application for enhancing the dissolution rate of poorly water-soluble drugs. *Materials Science and Engineering C, 44,* 262–267. Retrieved from https://doi.org/10.1016/j.msec.2014.08.040

Wu, G., Chen, L., Li, H., Deng, C. L., & Chen, X. F. (2014). Comparing microspheres with different internal phase of polyelectrolyte as local drug

delivery system for bone tuberculosis therapy. *BioMed Research International*, *2014*. Retrieved from https://doi.org/10.1155/2014/297808

Wu S., Liu X., Yeung K.W.K., Liu C., Yang X. Biomimetic porous scaffolds for bone tissue engineering. Mater. Sci. Eng. R Rep. 2014;80:1–36.

Wu, Z., Liu, C., Zang, G., & Sun, H. (2008). The effect of SIM on remodelling of the alveolar bone following tooth extraction. *International Journal of Oral and Maxillofacial Surgery*, *37*(2), 170–176. Retrieved from https://doi.org/10.1016/j.ijom.2007.06.018

Wu, Z., Liu, C., Zang, G., & Sun, H. (2008). The effect of SIM on remodelling of the alveolar bone following tooth extraction. *International Journal of Oral and Maxillofacial Surgery, 37*(2), 170–176. Retrieved from https://doi.org/10.1016/j.ijom.2007.06.018

Wunderlich, B. (1990). *Thermal analysis*. Cambridge: Academic Press. Retrieved from https://www.elsevier.com/books/thermal-analysis/wunderlich/978-0-12-765605-2

Würzler, K. K., DeWeese, T. L., Sebald, W., & Reddi, A. H. (1998). Radiation-induced impairment of bone healing can be overcome by recombinant human bone morphogenetic protein-2. *Journal of Craniofacial Surgery*, *9*(2), 131–137. Retrieved from https://doi.org/10.1097/00001665-199803000-00009

Yamashita, M., Otsuka, F., Mukai, T., Otani, H., Inagaki, K., Miyoshi, T., … & Makino, H. (2008). SIM antagonizes tumor necrosis factor-α ihibition of bone morphogenetic proteins-2-induced osteoblast differentiation by regulating Smad signaling and Ras/Rho-mitogen-activated protein kinase pathway. *Journal of Endocrinology*, *196*(3), 601–613. Retrieved from https://doi.org/10.1677/JOE-07-0532

Yamashita, M., Otsuka, F., Mukai, T., Yamanaka, R., Otani, H., Matsumoto, Y., … & Makino, H. (2010). SIM inhibits osteoclast differentiation induced by bone morphogenetic protein-2 and RANKL through regulating MAPK, AKT and

Src signaling. *Regulatory Peptides*, *162*(1–3), 99–108. Retrieved from https://doi.org/10.1016/j.regpep.2010.03.003

Yang, C. Y., Tsay, S. Y., & Tsiang, R. C. (2000). An enhanced process for encapsulating aspirin in ethyl cellulose microcapsules by solvent evaporation in an O/W emulsion. *Journal of Microencapsulation, 17*(3), 269-277. Retrieved from https://doi.org/10.1080/026520400288256

Yang, D. J., & Hwang, L. S. (2006). Study on the conversion of three natural statins from lactone forms to their corresponding hydroxy acid forms and their determination in Pu-Erh tea. *Journal of Chromatography A*, *1119*(1–2), 277–284. Retrieved from https://doi.org/10.1016/j.chroma.2005.12.031

Yang, Y. Y., Chung, T. S., & Ping Ng, N. (2001). Morphology, drug distribution, and in vitro release profiles of biodegradable polymeric microspheres containing protein fabricated by double-emulsion solvent extraction/evaporation method. *Biomaterials, 22*(3), 231–241. Retrieved from https://doi.org/10.1016/S0142-9612(00)00178-2

Yang, Y. Y., Chung, T. S., Bai, X. L., & Chan, W. K. (2000). Effect of preparation conditions on morphology and release profiles of biodegradable polymeric microspheres containing protein fabricated by double-emulsion method. *Chemical Engineering Science*, *55*(12), 2223–2236. Retrieved from https://doi.org/10.1016/S0009-2509(99)00503-5

Yang, Y., Bajaj, N., Xu, P., Ohn, K., Tsifansky, M. D., & Yeo, Y. (2009). Development of highly porous large PLGA microparticles for pulmonary drug delivery. *Biomaterials*, *30*(10), 1947–1953. Retrieved from https://doi.org/10.1016/j.biomaterials.2008.12.044

Yang, Y., Gao, Y., & Mei, X. (2013). Effects of formulation parameters on encapsulation efficiency and release behavior of thienorphine loaded PLGA microspheres. *Pharmaceutical Development and Technology, 18(*5), 1169–1174. Retrieved from https://doi.org/10.3109/10837450.2011.618948

Yasasvini, S., Anusa, R., VedhaHari, B., Prabhu, P., & RamyaDevi, D. (2017). Topical hydrogel matrix loaded with SIM microparticles for enhanced wound healing activity. *Materials Science and Engineering C, 72,* 160–167. Retrieved from https://doi.org/10.1016/J.MSEC.2016.11.038

Ye, M., Kim, S., & Park, K. (2010). Issues in long-term protein delivery using biodegradable microparticles. *Journal of Controlled Release, 146*(2), 241-260. Retrieved from https://doi.org/10.1016/j.jconrel.2010.05.011

Yoo, N. Y., Youn, Y. S., Oh, N. M., Oh, K. T., Lee, D. K., Cha, K. H., … & Lee, E. S. (2011). Antioxidant encapsulated porous poly(lactide-co-glycolide) microparticles for developing long acting inhalation system. *Colloids and Surfaces B: Biointerfaces*, *88*(1), 419–424. Retrieved from https://doi.org/10.1016/j.colsurfb.2011.07.024

Yu, L. (2001). Amorphous pharmaceutical solids: Preparation, characterization and stabilization. *Advanced Drug Delivery Reviews, 48*(1), 27–42. Retrieved from https://doi.org/10.1016/S0169-409X(01)00098-9

Yu, W. L., Sun, T. W., Qi, C., Zhao, H. K., Ding, Z. Y., Zhang, Z. W., … & He, Y. H. (2017). Enhanced osteogenesis and angiogenesis by mesoporous hydroxyapatite microspheres-derived SIM sustained release system for superior bone regeneration. *Scientific Reports*, *7*. Retrieved from https://doi.org/10.1038/srep44129

Yu, W. L., Sun, T. W., Qi, C., Zhao, H. K., Ding, Z. Y., Zhang, Z. W., … He, Y. H. (2017). Enhanced osteogenesis and angiogenesis by mesoporous hydroxyapatite microspheres-derived SIM sustained release system for superior bone regeneration. *Scientific Reports,* 7. Retrieved from https://doi.org/10.1038/srep44129

Yuan, F. L., Wu, Q. Y., Miao, Z. N., Xu, M. H., Xu, R. S., Jiang, D. L., … & Li, X. (2018). Osteoclast-derived Extracellular vesicles: Novel regulators of osteoclastogenesis and osteoclast-osteoblasts communication in bone remodeling. *Frontiers in Physiology*. Frontiers Media S.A. Retrieved from https://doi.org/10.3389/fphys.2018.00628

Yuana, Y., Oosterkamp, T. H., Bahatyrova, S., Ashcroft, B., Garcia Rodriguez, P., Bertina, R. M., & Osanto, S. (2010). Atomic force microscopy: A novel approach to the detection of nanosized blood microparticles. *Journal of Thrombosis and Haemostasis, 8*(2), 315–323. Retrieved from https://doi.org/10.1111/j.1538-7836.2009.03654.x

Zamani, M., Prabhakaran, M. P., & Ramakrishna, S. (2013). Advances in drug delivery via electrospun and electrosprayed nanomaterials. *International Journal of Nanomedicine*. Retrieved from https://doi.org/10.2147/IJN.S43575

Zareidoost, A., Yousefpour, M., Ghasemi, B., & Amanzadeh, A. (2012). The relationship of surface roughness and cell response of chemical surface modification of titanium. *Journal of Materials Science: Materials in Medicine*, *23*(6), 1479–1488. Retrieved from https://doi.org/10.1007/s10856-012-4611-9

Zhang, H. X., Xiao, G. Y., Wang, X., Dong, Z. G., Ma, Z. Y., Li, L., … Nie, L. (2015). Biocompatibility and osteogenesis of calcium phosphate composite scaffolds containing SIM loaded PLGA microspheres for bone tissue engineering. *Journal of Biomedical Materials Research - Part A*, *103*(10), 3250–3258. Retrieved from https://doi.org/10.1002/jbm.a.35463

Zhang, R., Lee, P., Lui, V. C. H., Chen, Y., Liu, X., Lok, C. N., … Wong, K. K. Y. (2015). Silver nanoparticles promote osteogenesis of mesenchymal stem cells and improve bone fracture healing in osteogenesis mechanism mouse model. *Nanomedicine: Nanotechnology, Biology, and Medicine*, *11*(8), 1949–1959. Retrieved from https://doi.org/10.1016/j.nano.2015.07.016

Zhang, Y., Fan, W., Ma, Z., Wu, C., Fang, W., Liu, G., & Xiao, Y. (2010). The effects of pore architecture in silk fibroin scaffolds on the growth and differentiation of mesenchymal stem cells expressing BMP7. *Acta Biomaterialia*, *6*(8), 3021–3028. Retrieved from https://doi.org/10.1016/j.actbio.2010.02.030

Zhang, Y., Wang, H., Gao, C., Li, X., & Li, L. (2013). Highly ordered mesoporous carbon nanomatrix as a new approach to improve the oral absorption of the

water-insoluble drug, SIM. *European Journal of Pharmaceutical Sciences*, *49*(5), 864–872. Retrieved from https://doi.org/10.1016/j.ejps.2013.05.031

Zhao, X. H., Xu, Z. R., Zhang, Q., & Yang, Y. M. (2012). SIM protects human osteosarcoma cells from oxidative stress-induced apoptosis through mitochondrial-mediated signaling. *Molecular Medicine Reports, 5*(2), 483–488. Retrieved from https://doi.org/10.3892/mmr.2011.641

Zheng, C., & Liang, W. (2010). A one-step modified method to reduce the burst initial release from PLGA microspheres. *Drug Delivery, 17*(2), 77–82. Retrieved from https://doi.org/10.3109/10717540903509001

Zhou, Q. T., Denman, J. A., Gengenbach, T., Das, S., Qu, L., Zhang, H., … & Morton, D. A. V. (2011). Characterization of the surface properties of a model pharmaceutical fine powder modified with a pharmaceutical lubricant to improve flow via a mechanical dry coating approach. *Journal of Pharmaceutical Sciences*, *100*(8), 3421–3430. Retrieved from https://doi.org/10.1002/jps.22547

Zhou, Y., Ni, Y., Liu, Y., Zeng, B., Xu, Y., & Ge, W. (2010). The role of SIM in the osteogenesis of injectable tissue-engineered bone based on human adipose-derived stromal cells and platelet-rich plasma. *Biomaterials, 31*(20), 5325–5335. Retrieved from https://doi.org/10.1016/j.biomaterials.2010.03.037

Zweers, M. L. T., Grijpma, D. W., Engbers, G. H. M., & Feijen, J. (2003). The preparation of monodisperse biodegradable polyester nanoparticles with a controlled size. *Journal of Biomedical Materials Research, 66B*(2), 559–566. Retrieved from https://doi.org/10.1002/jbm.b.10046